Docket No. 71-9330, Model No. ATR FFSC Package

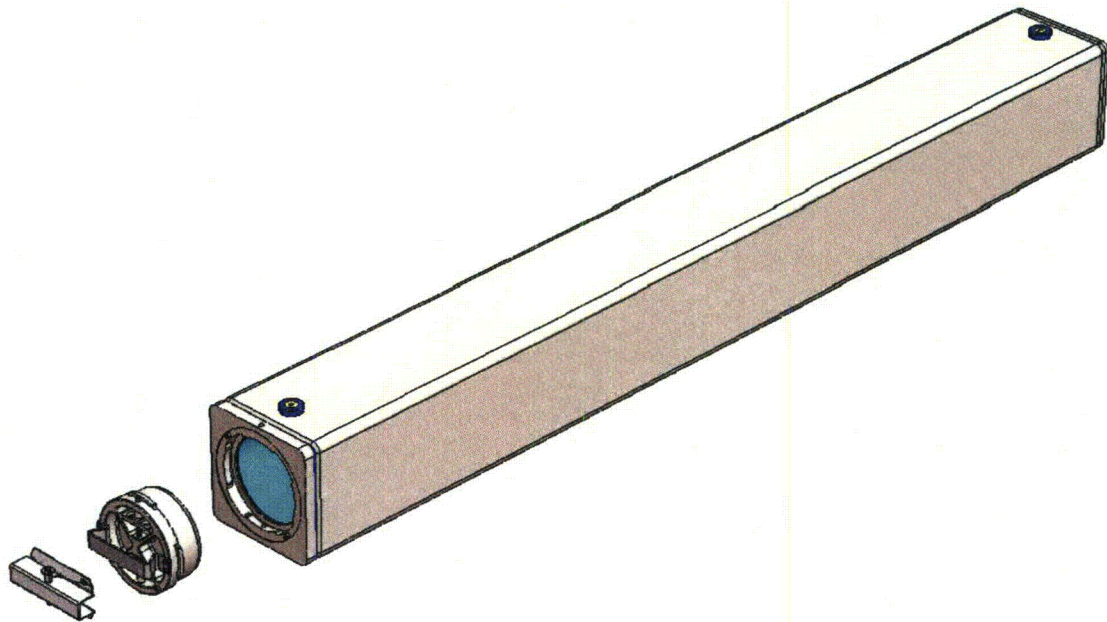## Changes Included in Revision 9 of the SAR

The following list summarizes the changes made to the ATR FFSC SAR in Revision 9.

1. The U-Mo demonstration element has been added as an allowable content.

2. A minor error was corrected in Chapter 3 that resulted in small temperature changes during hypothetical accident conditions. In addition, editorial errors in Chapter 3 (e.g., misspellings) have been corrected, and sequential footnote numbering has been incorporated.

Guidelines for updating the SAR are provided below.

Remove Rev. 8 pages:	Add Rev. 9 pages:
Cover page	Cover page
Table of Contents, pages i through v	Table of Contents, pages i through vi
Chapter 1 (entire chapter)	Chapter 1 (entire chapter)
Chapter 2, pages 2-1 through 2-5	Chapter 2, pages 2-1 through 2-5
Chapter 3 (entire chapter)	Chapter 3 (entire chapter)
Chapter 4 (entire chapter)	Chapter 4 (entire chapter)
Chapter 6, pages 6-1 and 6-2	Chapter 6, pages 6-1 and 6-2
--	Chapter 6, pages 6-177 through 6-214
Chapter 7, page 7-2	Chapter 7, page 7-2

Safety Analysis Report

Advanced Test Reactor Fresh Fuel Shipping Container (ATR FFSC)

Revision 9, December 2012

Docket 71-9330

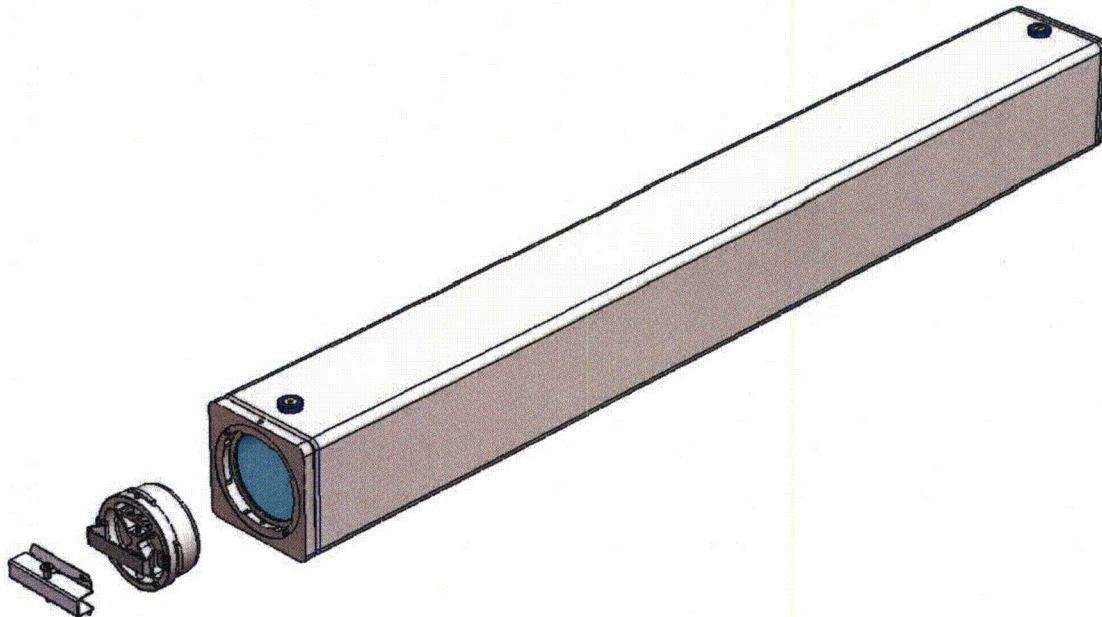| Prepared by:	Prepared for:
AREVA **AREVA Federal Services LLC**	**INL** Idaho National Laboratory **Battelle Energy Alliance, LLC** **(BEA)**

Safety Analysis Report

Advanced Test Reactor Fresh Fuel Shipping Container
(ATR FFSC)

Revision 9, December 2012

Docket 71-9330

Prepared by:	Prepared for:
AREVA	**iNL** Idaho National Laboratory
AREVA Federal Services LLC	**Battelle Energy Alliance, LLC (BEA)**

AREVA

iNL
Idaho National Laboratory

ATR FFSC

Safety
Analysis
Report

Docket
71-9330

Revision 9
Dec 2012

TABLE OF CONTENTS

1.0 GENERAL INFORMATION

This chapter of the Safety Analysis Report (SAR) presents a general introduction and description of the Advanced Test Reactor (ATR) Fresh Fuel Shipping Container (FFSC).[1] This application seeks validation of the ATR FFSC as a Type AF fissile materials shipping container in accordance with Title 10, Part 71 of the Code of Federal Regulations (10CFR71).

The major components comprising the package are discussed in Section 1.2.1, *Packaging*, and illustrated in Figure 1.2-1 through Figure 1.2-9. Detailed drawings of the package design are presented in Appendix 1.3.2, *Packaging General Arrangement Drawings*. A glossary of terms is presented in Appendix 1.3.1, *Glossary of Terms*.

1.1 Introduction

The single ATR FFSC has been designed to transport unirradiated fuel. The payload consists of a fresh fuel element for use in either the Advanced Test Reactor located in Idaho Falls, Idaho, the Massachusetts Institute of Technology (MIT) research reactor, or the University of Missouri Research Reactor (MURR). The package is designed to transport fuel element plates that have either not yet been assembled into a fuel element or have been removed from an unirradiated fuel element. The fuel plates may be either flat or rolled to the geometry required for assembly into a fuel element. The package is also designed for small quantity payloads, which is defined as fuel with a U-235 loading ≤ 400 g, and U-235 enrichment $\leq 94\%$. Fuel that qualifies as small quantity includes Rhode Island Nuclear Science Center (RINSC) fuel, MIT or MURR fuel plates, ATR Full-size plate In Flux trap Position (AFIP) elements, uranium-molybdenum (U-Mo) foils, and design demonstration elements (DDEs).

The fuel elements are all fabricated in a similar manner using aluminum-clad fuel plates. The ATR, MURR, and MIT plates consist of a uranium aluminide (UAl_x) core containing high-enriched uranium (HEU) enriched to a maximum of 94% U-235. The ATR U-Mo demonstration element contains a mixture of HEU UAl_x fueled plates and low-enriched uranium (LEU) U-Mo fueled plates. The LEU U-Mo fuel plates are enriched to a maximum of 20% U-235. The RINSC plates consist of a uranium silicide core containing LEU enriched to a maximum of 20% U-235. The AFIP elements, U-Mo foils, and DDEs use U-Mo either as a monolithic alloy or dispersed in a matrix of aluminum and silicon. Enrichments typically range from 20% to 94% U-235. The fuel plates vary in size and number between the ATR, MIT, MURR, RINSC, AFIP, and DDE fuel elements, with the ATR fuel plates being the longest. Further details of the fuel elements are provided in Section 1.2.2, *Contents*.

Since the A_2 value of the payloads is low and radiation is negligible, the only safety function performed by the package is criticality control. This function is achieved, in the case of a transport accident, by confining the fuel element within the package and by maintaining separation of fuel in multiple packages. The fuel itself is robust and inherently resists

---

[1] In the remainder of this Safety Analysis Report, *Advanced Test Reactor Fresh Fuel Shipping Container* will be abbreviated as *ATR FFSC*. In addition, the term 'packaging' will refer to the assembly of components necessary to ensure compliance with the regulatory requirements, but does not include the payload. The term 'package' includes both the packaging components and the fresh fuel payload.

unfavorable geometry reconfiguration while contained within the package. For ease of handling and property protection purposes, each fuel element is contained within a lightweight aluminum housing referred to as the fuel handling enclosure. The loose ATR fuel plates are contained in a loose plate basket which prevents the fuel from reconfiguring into an unfavorable geometry. The loose MIT and MURR fuel plates qualify as a small quantity payload, and while these plates will be transported in the small quantity fuel handling enclosure, the enclosure is not required for criticality control purposes.

For the fuel elements, the criticality control function is demonstrated via full-scale testing of a prototypic package followed by a criticality analysis using a model which bounds the test results, ensuring that the calculated $k_{eff} + 2\sigma$ is below the upper subcritical limit (USL) in the most limiting case. Two full-scale prototype models are used to perform a number of performance tests including normal conditions of transport (NCT) free drop and hypothetical accident condition (HAC) free drop and puncture tests.

Authorization is sought for a Type A(F)-96, fissile material package per the definitions delineated in 10 CFR §71.4[2]. Each ATR fuel element contains up to 1,200 grams of U-235 enriched to a maximum of 94% U-235. The ATR U-Mo demonstration element contains up to 1,240 g U-235 and is a mixture of HEU and LEU fuel plates. The MIT fuel element contains up to 515 grams of U-235 enriched to a maximum of 94% U-235, the MURR fuel element contains up to 785 grams of U-235 enriched to a maximum of 94% U-235, and the small quantity payload fuel contains up to 400 grams of U-235 enriched to a maximum of 94% U-235. When shipping loose ATR fuel plates, the package is limited to a maximum fissile payload of 600 grams U-235.

The Criticality Safety Index (CSI) for the package, determined in accordance with the definitions of 10 CFR §71.59, is dependent upon the contents. For ATR, MIT, and MURR fuel elements, as well as loose ATR fuel plates, the CSI is 4.0. For the small quantity payload, which includes RINSC fuel elements, AFIP elements, U-Mo foils, DDEs, and loose MIT and MURR plates, the CSI is 25.0. The CSI for the various payloads is summarized in Table 1.1-1. The CSI is based on the number of packages for criticality control purposes (the method and the CSI determination are given in Chapter 6.0, *Criticality Evaluation*).

---

[2] Title 10, Code of Federal Regulations, Part 71 (10 CFR 71), *Packaging and Transportation of Radioactive Material*, 1-1-06 Edition.

Table 1.1-1 – Criticality Safety Index per Content

Content	U-235 Mass Limit (g)	CSI
1 ATR Fuel Element	1200	4.0
1 ATR U-Mo demonstration element	1240	4.0
1 MIT Fuel Element	515	4.0
1 MURR Fuel Element	785	4.0
ATR fuel plates in the loose plate basket	600	4.0
Small quantity payload	400	25.0

1.2 Package Description

This section presents a basic description of the ATR FFSC. General arrangement drawings are presented in Appendix 1.3.2, *Packaging General Arrangement Drawings.*

1.2.1 Packaging

1.2.1.1 Packaging Description

The ATR FFSC is designed as Type AF packaging for transportation of the following payload types: ATR fuel elements, ATR U-Mo demonstration elements, MIT fuel elements, MURR fuel elements, unassembled ATR fuel element plates, and small quantity payloads. The packaging is rectangular in shape and is designed to be handled singly with slings, or by fork truck when racked. Package components are shown in Figure 1.2-1. Transport of the package is by highway truck. The maximum gross weight of the package in any loaded configuration is 290 lbs.

The ATR FFSC is a two part packaging consisting of the body and the closure. The body is a single weldment that features square tubing as an outer shell and round tubing for the payload cavity. Three 1-inch thick ribs maintain spacing between the inner and outer shells. The components of the packaging are shown in Figures 1.2-2, 1.2-3, 1.2-4, and 1.2-5 and are described in more detail in the sections which follow. With the exception of several minor components, all steel used in the ATR FFSC is ASTM Type 304 stainless steel. Components are joined using full-thickness fillet welds (i.e., fillet welds whose leg size is nominally equal to the lesser thickness of the parts joined) and full and partial penetration groove welds.

1.2.1.1.1 ATR FFSC Body

The ATR FFSC body is a stainless steel weldment 73 inches long and 8 inches square weighing (empty) approximately 230 lbs. It consists of two nested shells; the outer shell a square stainless steel tube with a 3/16 inch wall thickness and the inner shell a 6 inch diameter, 0.120 inch wall, stainless steel round tube. There are three 1 inch thick stiffening plates secured to the round tube by fillet welds at equally spaced intervals. The tube is wrapped with thermal insulation and the insulation is overlaid with 28 gauge stainless steel sheet. The stainless steel sheet maintains the insulation around the inner shell. This insulated weldment is then slid into the outer square tube shell and secured at both ends by groove welds. Thermal insulation is built into the bottom end of the package as shown in Figure 1.2-3, and the closure provides thermal insulation at the closure end of the package as shown in Figure 1.2-4.

1.2.1.1.2 ATR FFSC Closure

The closure is a small component designed to be easily handled by one person. It weighs approximately 10 lbs and is equipped with a handle to facilitate use with gloved hands. The closure engages with the body using a bayonet style design. There are four lugs, uniformly spaced on the closure, that engage with four slots in the mating body feature. The closure is secured by retracting two spring loaded pins, rotating the closure through approximately 45°, and releasing the spring loaded pins such that the pins engage with mating holes in the body. When the pins are properly engaged with the mating holes the closure is locked.

A small post on the closure is drilled to receive a tamper indicating device (TID) wire. An identical post is located on the body and is also drilled for the TID wire. For ease in operation, there are two TID posts on the body. There are only two possible angular orientations for the closure installation and the duplicate TID post on the body enables TID installation in both positions.

A cover is placed over the closure handle during transport to render the handle inoperable for inadvertent lifting or tiedown. Figure 1.2-5 illustrates the placement of the handle cover. The profile of the cover depicted in Appendix 1.3.2, *Packaging General Arrangement Drawings*, is optional and may be modified to fit other handle profiles to ensure lifting and tiedown features are disabled as required by 10 CFR §71.45. As an option, the closure handle may be removed for transport rather than installing the handle cover.

1.2.1.1.3 ATR Fuel Handling Enclosure

The ATR Fuel Handling Enclosure (FHE) is a hinged thin gauge aluminum weldment used with the ATR fuel element or ATR U-Mo demonstration element, as illustrated in Figure 1.2-1. The ATR FHE is a cover used to protect the fuel from handling damage during ATR FFSC loading and unloading operations. It is a thin walled aluminum fabrication featuring a hinged lid and neoprene rub strips to minimize fretting of the fuel element side plates where they are in contact with the container.

During transport the ATR FHE is not relied upon to add strength to the package, or satisfy any safety requirement. For purposes of determining worst case reactivity, the ATR FHE is assumed to be not present.

1.2.1.1.4 MIT Fuel Handling Enclosure

The MIT FHE is comprised of two identical machined segments which surround the MIT fuel element secured by two end spacers and locked together using ball lock pins (see Figure 1.2-6). The primary purpose of end spacers is to secure the two sections of the FHE prior to loading the FHE into the package. The location of the hole in the end plate of the spacer also facilitates easy removal of the FHE from the package. The MIT FHE is a cover used to protect the fuel from handling damage during ATR FFSC loading and unloading operations. It is an aluminum fabrication featuring machined segments and neoprene rub strips to minimize fretting of the fuel element side plates where they are in contact with the container.

During transport the MIT FHE, including the end spacers, is not relied upon to add strength to the package; however the enclosure does maintain the fuel element within a defined dimensional envelope.

1.2.1.1.5 MURR Fuel Handling Enclosure

The MURR FHE is very similar to the MIT FHE and is comprised of two identical machined segments which surround the MURR fuel element secured by two end spacers and locked together using ball lock pins (see Figure 1.2-7). The primary purpose of end spacers is to secure the two sections of the FHE prior to loading the FHE into the package. The location of the hole in the end plate of the spacer also facilitates easy removal of the FHE from the package. The MURR FHE is a cover used to protect the fuel from handling damage during ATR FFSC loading and unloading operations. It is an aluminum fabrication featuring machined segments and neoprene rub strips to minimize fretting of the fuel element side plates where they are in contact with the container.

During transport the MURR FHE, including the end spacers, is not relied upon to add strength to the package; however the enclosure does maintain the fuel element within a defined dimensional envelope.

1.2.1.1.6 RINSC Fuel Handling Enclosure

The RINSC fuel, although classified as a small quantity payload, has its own dedicated FHE. The RINSC FHE is very similar to the MURR and MIT FHEs and is comprised of two identical machined segments which surround the RINSC fuel element and are secured by two end spacers and locked together using ball lock pins (see Figure 1.2-8). The primary purpose of end spacers is to secure the two sections of the FHE prior to loading the FHE into the package. The location of the hole in the end plate of the spacer also facilitates easy removal of the FHE from the package. The RINSC FHE is a cover used to protect the fuel from handling damage during ATR FFSC loading and unloading operations. It is an aluminum fabrication featuring machined segments and neoprene rub strips to minimize fretting of the fuel element side plates where they are in contact with the container.

During transport the RINSC FHE does not add strength to the package nor satisfy any safety requirement. For purposes of determining worst case reactivity, the RINSC FHE is assumed to be not present.

1.2.1.1.7 ATR FFSC Loose Fuel Plate Basket

The Loose Plate Fuel Basket (LFPB) is comprised of four identical machined segments joined by threaded fasteners (reference Figure 1.2-15). The fasteners joining the segments in the lengthwise direction are permanently installed. The basket is opened/closed using the 8 hand tightened fasteners. For criticality control purposes during transport the loose fuel plate basket maintains the fuel plates within a defined dimensional envelope.

Additional aluminum plates may be used as dunnage to fill gaps between the fuel plates and the basket payload cavity. The dunnage is used for property protection purposes only.

1.2.1.1.8 Small Quantity Payload FHE

The small quantity payload FHE (SQFHE) is very similar to the RINSC, MURR, and MIT FHEs. The SQFHE is comprised of two identical machined segments which surround the small quantity payloads and are secured by two end spacers and locked together using ball lock pins (see Figure 1.2-9). The primary purpose of end spacers is to secure the two sections of the FHE

prior to loading the FHE into the package. The location of the hole in the end plate of the spacer also facilitates easy removal of the FHE from the package. The SQFHE is a cover used to protect the fuel from handling damage during ATR FFSC loading and unloading operations. It is an aluminum fabrication featuring machined components.

During transport the SQFHE does not add strength to the package nor satisfy any safety requirement. For purposes of determining worst case reactivity, the SQFHE is assumed to be not present.

Aluminum plates, shapes, and sheets may be used as dunnage to fill gaps between the small quantity payloads and SQFHE. Miscellaneous steel or aluminum fasteners may be used with the optional dunnage. The SQFHE does not come with neoprene rub strips like the RINSC FHE, however 1/8 inch thick neoprene rub strips may be used in the SQFHE to minimize fretting of the small quantity payloads where there may be contact with the SQFHE or optional aluminum dunnage. Neoprene rub strips may be used between the SQFHE and the small quantity payloads and/or between the optional aluminum dunnage and the small quantity payloads. The 1/8 inch neoprene rub strips shall not be stacked in more than two layers between the small quantity payload and any interior face of the SQFHE.

1.2.1.2 Gross Weight

The maximum shipped weight of the ATR FFSC (gross weight) with the specified payload is 290 lbs for all payload configurations. Further discussion of the gross weight is presented in Section 2.1.3, *Weights and Centers of Gravity*.

1.2.1.3 Neutron Moderator/Absorption

There are no moderator or neutron absorption materials in this package.

1.2.1.4 Heat Dissipation

The uranium payload produces a negligible thermal heat load. Therefore, no special devices or features are needed or utilized in the ATR FFSC to dissipate heat. A more detailed discussion of the package thermal characteristics is provided in Chapter 3.0, *Thermal*.

1.2.1.5 Protrusions

The closure handle protrudes 1 3/8-inches from the face of the closure. The handle is secured to the closure by means of four 10-24 UNC screws. The screws will fail prior to presenting any significant loading to either the closure engagement lugs or the locking pins.

On one face of the package body, two index lugs are secured to the package to facilitate stacking of the packages. The opposite face of the package has pockets into which the index lugs nest as illustrated in Figure 1.2-10. Each index lug is secured to the package by means of a 3/8-16 socket flat head cap screw. Under any load condition, the screw will fail prior to degrading the safety function of the package.

1.2.1.6 Lifting and Tiedown Devices

The ATR FFSC may be lifted from beneath utilizing a standard forklift truck when the package is secured to a fork pocket equipped pallet, or in a package rack. Swivel lift eyes may be installed in the package to enable package handling with overhead lifting equipment. The swivel eyes are installed after removing the 3/8-16 socket flat head cap screws and index lugs.

The threaded holes into which the swivel lift eyes are installed for the lifting the package are fitted with a 3/8-16 UNC screw and an index lug (see Figure 1.2-10) during transport. When the packages are stacked and the index lugs are nested in the mating pockets of the stacked packages, the index lugs can serve to carry shear loads between stacked packages.

1.2.1.7 Pressure Relief System

There are no pressure relief systems included in the ATR FFSC design. There are no out-gassing materials in any location of the package that are not directly vented to atmosphere. The package insulation, located in the enclosed volumes of the package, is a ceramic fiber. The insulation does not off-gas under normal or hypothetical accident conditions. The closure is not equipped with either seals or gaskets so that potential out-gassing of the FHE neoprene material and fuel element plastic bag material will readily vent without significant pressure build-up in the payload cavity.

1.2.1.8 Shielding

Due to the nature of the uranium payload, no biological shielding is necessary or specifically provided by the ATR FFSC.

1.2.2 Contents

The ATR FFSC is loaded with contents consisting of unirradiated fuel elements (ATR, ATR U-Mo, MIT, and MURR), small quantity payloads (RINSC element, AFIP element, U-Mo foils, DDEs, MIT loose fuel element plates, and MURR loose fuel element plates), and ATR loose fuel element plates. The total mass of polyethylene in the packaging shall not exceed 100g. The total mass of neoprene in the packaging is not limited, however the neoprene thickness and arrangement shall be as directed by the drawings in Appendix 1.3.2, *Packaging General Arrangement Drawings*, or as dictated throughout this Chapter.

1.2.2.1 ATR Fuel Element and ATR U-Mo Demonstration Element

Standard ATR Fuel Element: Each standard ATR fuel element contains up to 1,200 g U-235, enriched up to 94% U-235. The weight percents of the remaining uranium isotopes are 1.2 wt.% U-234 (max), 0.7 wt.% U-236 (max), and 5.0-7.0 wt.% U-238. The fuel element (ATR Mark VII) fissile material is uranium aluminide (UAl_x). The fuel element weighs not more than 25 lbs, is bagged, and is enclosed in the ATR FHE weighing 15 lbs.

There are four different ATR Mark VII fuel element types designated 7F, 7NB, 7NBH, and YA. The construction of these fuel elements are identical, varying only in the content of the fuel matrix. In the 7F fuel element, all 19 fuel plates are loaded with enriched uranium in an aluminum matrix with the eight outer plates (1 through 4 and 16 through 19) containing boron as

a burnable poison. The fuel element with the greatest reactivity is the 7NB which contains no burnable poison. The 7NBH fuel element is similar to the 7NB fuel element except that it contains one or two borated plates. The YA fuel element is identical to the 7F fuel element except that plate 19 of the YA fuel element is an aluminum alloy plate containing neither uranium fuel nor boron burnable poison. The total U-235 and B-10 content of the YA fuel element is reduced accordingly. A second YA fuel element design (YA-M) has the side plate width reduced by 15 mils.

The ATR fuel elements contain 19 curved fuel plates. A section view of an ATR fuel element is given in Figure 1.2-11. The fuel plates are rolled to shape and swaged into the two fuel element side plates. Fuel plate 1 has the smallest radius, while fuel plate 19 has the largest radius. The fissile material (uranium aluminide) is nominally 0.02-in thick for all 19 plates. Fuel element side plates are fabricated of ASTM B 209, aluminum alloy 6061-T6 or 6061-T651 and are approximately 0.19-in thick. The maximum channel thickness between fuel plates is 0.087 inches.

ATR U-Mo Demonstration Element: The external geometry of the ATR U-Mo demonstration element is essentially identical to the ATR Mark VII YA fuel element and is shown schematically in Figure 1.2-20. The maximum channel thickness between fuel plates is 0.087 inches. The demonstration element contains 18 fueled plates, while plate 19 is an aluminum alloy plate. The demonstration element contains a mixture of UAl_x (HEU) and U-Mo (LEU) fuel plates, with a maximum U-235 mass of 1,240 g. Plates 1 through 4 and 16 through 18 are UAl_x plates identical in construction and composition to a standard HEU ATR fuel element. Boron is included in the UAl_x plates as a burnable poison. Plates 5 through 15 are fueled with an alloy of LEU uranium and molybdenum. The U-Mo fuel meat is nominally 10% molybdenum by weight, and the U-235 is enriched up to 20.0%. For the LEU fuel, the maximum weight percent for U-234 and U-236 are 0.26% and 0.46%, respectively.

The U-Mo fuel meat is nominally 0.013-in thick, and a nominal 0.001-in thick zirconium interlayer is present between the fuel meat and the aluminum cladding (see Figure 1.2-20). The fuel element weighs not more than 32 lbs, is bagged, and is enclosed in the ATR FHE weighing 15 lbs.

1.2.2.2 MIT Fuel Element

Each MIT element contains up to 515 g U-235, enriched up to 94 wt.%. The weight percents of the remaining uranium isotopes are 1.2 wt.% U-234, 0.7 wt.% U-236, and 5.0-7.0 wt.% U-238. Like the ATR fuel element, the MIT fuel element fissile material is uranium aluminide (UAl_x). The fuel element weighs not more than 10 lbs, is bagged, and is enclosed in the MIT FHE weighing 25 lbs.

Each MIT fuel element contains 15 flat fuel plates, as shown in Figure 1.2-12. The fuel plates are fabricated and swaged into the two fuel element side plates. The fuel "meat" is a mixture of uranium metal and aluminum, while the cladding and structural materials are an aluminum alloy. The fissile material (uranium aluminide) is nominally 0.03-in thick and the cladding is nominally 0.025-in thick. Fuel element side plates are fabricated of ASTM B 209, aluminum alloy 6061-T6 and are approximately 0.19-in thick. The maximum channel thickness between fuel plates is 0.090 inches, excluding the thermal grooves. If the 0.012 inch thermal groove is considered, the maximum channel thickness between fuel plates is 0.114 inches.

1.2.2.3 MURR Fuel Element

Each MURR element contains up to 785 g U-235, enriched up to 94 wt.%. The weight percents of the remaining uranium isotopes are 1.2 wt.% U-234, 0.7 wt.% U-236, and 5.0-7.0 wt.% U-238. Like the ATR fuel element, the MURR fuel element fissile material is uranium aluminide (UAl_x). The fuel element weighs not more than 15 lbs, is bagged, and is enclosed in the MURR FHE weighing 30 lbs.

Each MURR fuel element contains 24 curved fuel plates. Fuel plate 1 has the smallest radius, while fuel plate 24 has the largest radius, as shown in Figure 1.2-13. The fuel "meat" is a mixture of uranium metal and aluminum, while the cladding and structural materials are an aluminum alloy. The fuel plates are rolled to shape and swaged into the two fuel element side plates. The fissile material (uranium aluminide) is nominally 0.02-in thick for all 24 plates. Fuel element side plates are fabricated of ASTM B 209, aluminum alloy 6061-T6 or 6061-T651 and are approximately 0.15-in thick. The maximum channel thickness between fuel plates is 0.090 inches.

1.2.2.4 Small Quantity Payload

The small quantity payload consists of a class of research and development plate-type fuels with U-235 as the fissile isotope (i.e., no U-233 or plutonium), with a bounding U-235 loading ≤ 400 g, and U-235 enrichment $\leq 94\%$. Fuel types that fall into the small quantity payload category include RINSC fuel elements, AFIP elements, U-Mo foils, DDEs, MIT loose fuel element plates, and MURR loose fuel element plates.

Individual small quantity payloads are discussed below. Although the fissile mass and enrichment is stated for each payload type, the acceptable limits for any small quantity payload are the bounding quantity of 400 g fissile mass and 94% enrichment. The maximum weight of any small quantity payload, including the SQFHE, is 50 lbs. As stated above, the RINSC fuel element is shipped in the dedicated RINSC FHE.

With the exception of RINSC fuel, which utilizes the RINSC FHE, all small quantity payload items fall within the maximum dimensional bounds of the SQFHE, or approximately 55-in x 3.4-in x 3.4-in. The minimum dimensions for a small quantity payload item are approximately 10-in x 1.5-in x 0.008-in.

1.2.2.4.1 RINSC Fuel Element

Each RINSC element contains up to 283 g U-235, enriched up to 20 wt.%. The weight percents of the remaining uranium isotopes are 0.5 wt.% U-234 (max), 1.0 wt.% U-236 (max), with the balance U-238. The RINSC fuel element fissile material is uranium silicide (U_3Si_2) dispersed in aluminum powder. The fuel element weighs not more than 17 lbs, and is enclosed in the RINSC FHE weighing 28 lbs.

Each RINSC fuel element contains 22 flat fuel plates, as shown in Figure 1.2-14. The fuel plates are fabricated and swaged into the two fuel element side plates. The fuel "meat" is a mixture of uranium silicide and aluminum powder, while the cladding and structural materials are an aluminum alloy. The fissile material (uranium silicide) is nominally 0.02-in thick and the cladding is nominally 0.015-in thick. Fuel element side plates are fabricated of ASTM B 209,

aluminum alloy 6061-T6 and 6061-T651 and are approximately 0.187-in thick. The maximum
channel thickness between fuel plates is 0.096 inches.

1.2.2.4.2 AFIP Fuel Element

Each AFIP element contains up to 365 g U-235, enriched up to approximately 20 wt.%. Each
AFIP element typically contains 4 curved fuel plates, as shown in Figure 1.2-16. The fuel plates
are fabricated and swaged into the two fuel element side plates. The fuel "meat" may be either
dispersion or monolithic. Dispersion fuel meat consists of uranium 7 wt.% molybdenum alloy
(U-7Mo) particles dispersed in an aluminum-silicon matrix. Monolithic fuel meat consists of
uranium 10 wt.% molybdenum alloy (U-10Mo) coated with a thin zirconium interlayer. Both
fuel types are clad in 6061 aluminum. Fuel side plates are fabricated from 6061 aluminum.
Loose plates from an AFIP fuel element are also an allowed content.

1.2.2.4.3 U-Mo Foils

Uranium-Molybdenum (U-Mo) foils are used in the fabrication of test fuels, such as AFIPs and
DDEs. A U-Mo foil contains up to 160 g U-235, enriched up to 94%. The foils are thin and may
contain a zirconium coating, although cladding would not typically be present. The fuel meat
description provided for the AFIP elements also applies to U-Mo foils. More than one U-Mo foil
type may be transported per ATR FFSC.

1.2.2.4.4 Design Demonstration Elements (DDEs)

Each DDE contains up to 365 g U-235, enriched up to 94 wt.%. DDEs are available for the
National Bureau of Standard Reactor (NBSR), the Massachusetts Institute of Technology
Reactor (MITR), and the University of Missouri Reactor (MURR), and are abbreviated as DDE-
NBSR, DDE-MITR, and DDE-MURR. Sketches of the three DDEs are provided in Figures 1.2-
17, -18, and -19. Loose plates from a DDE are also an allowed content.

DDEs may contain either flat or curved fuel plates. Fuel meat consists of U-Mo, so the fuel meat
description provided for the AFIP elements also applies to DDEs.

1.2.2.4.5 MIT and MURR Loose Fuel Element Plates

MIT and MURR loose plates transported as a small quantity payload are limited to 400 grams
U-235. MIT fuel plates have approximately 34.3 g U-235 per plate, and MURR fuel plates have
approximately 19 to 46 g U-235 per fuel plate. The plates may either be flat or rolled to the
geometry required for assembly into the fuel element. Additionally, the plates may be banded or
wire tied in a bundle. A mixture of MIT and MURR fuel plates may be shipped together.

1.2.2.5 ATR Loose Fuel Plates

The maximum weight of the ATR loose plate payload (Figure 1.2-15) is 50 lbs. This weight is
made up of the maximum basket contents weight of 20 lbs and the loose fuel plate basket weight
of 30 lbs.

The loose plate payload is limited to 600 grams U-235. The plates are limited to those used in
ATR fuel elements. The plates may either be flat or rolled to the geometry required for assembly

into the fuel element. For handling convenience, the loose plate basket will be loaded with either flat or rolled plates. Additionally, the plates may be banded or wire tied in a bundle.
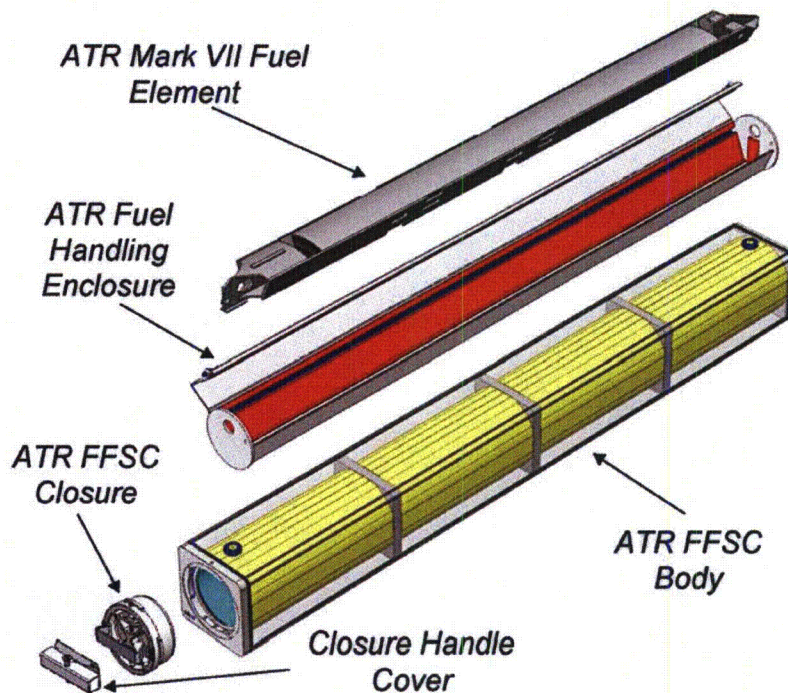
Figure 1.2-1 - Overview of the ATR FFSC (Outer Body Shell Shown Transparent)
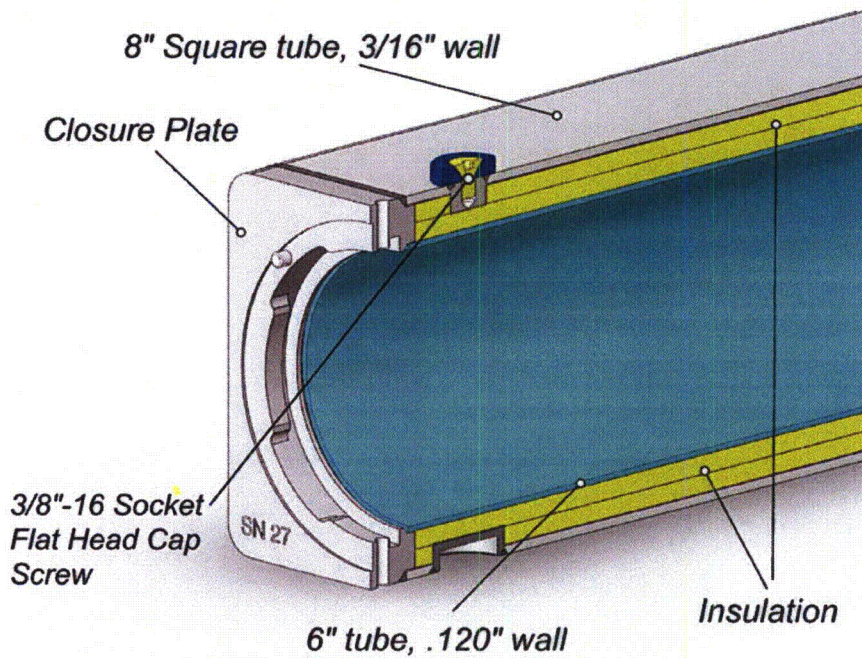
Figure 1.2-2 - Top End Body Sectional View

8" Square tube, 3/16" wall

8" Square plate, 7/8" thick

3/8" thick plate

Insulation

6" tube, .120" wall
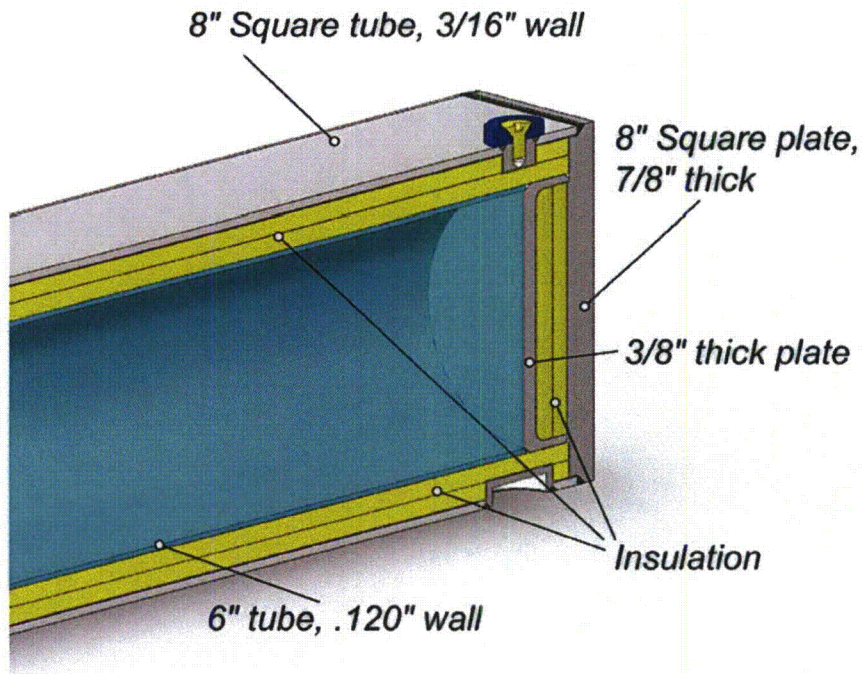
Figure 1.2-3 - Bottom End Body Sectional View

Closure Lug

Locking Pins

Insulation
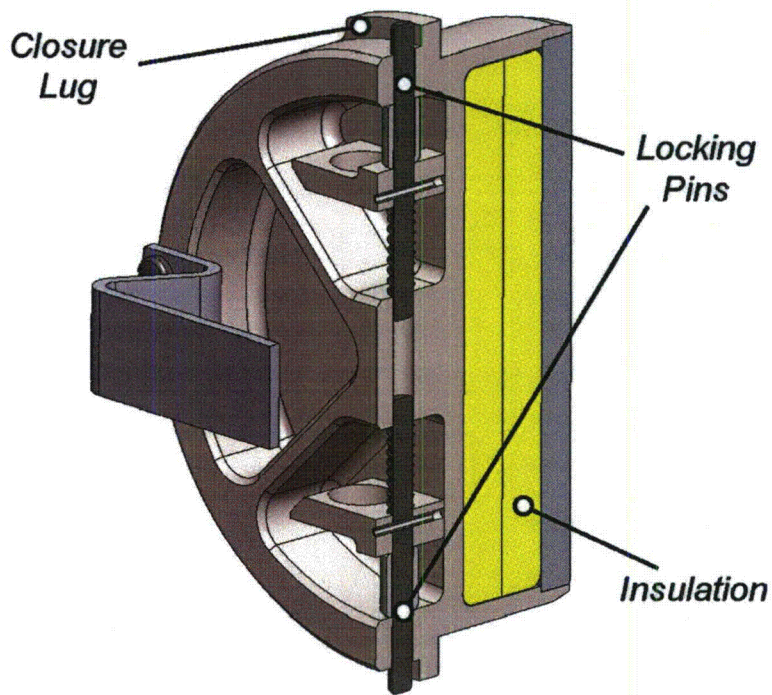
Figure 1.2-4 - Closure Sectional View
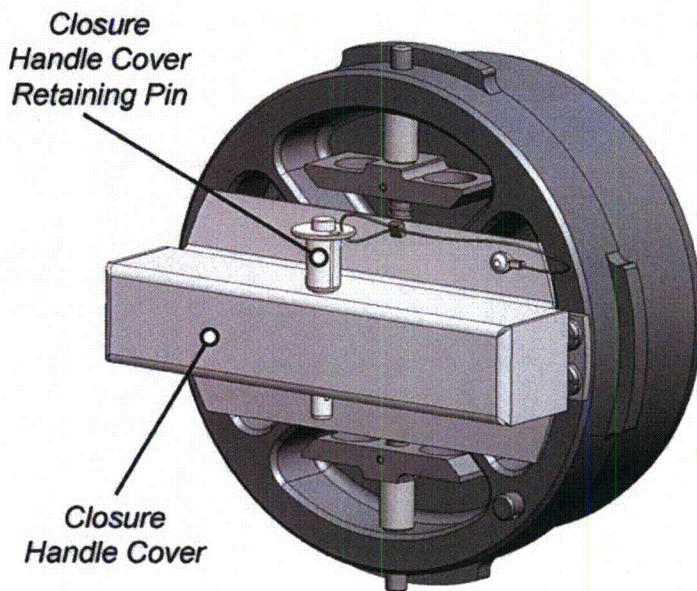
Figure 1.2-5 – Closure Handle Cover
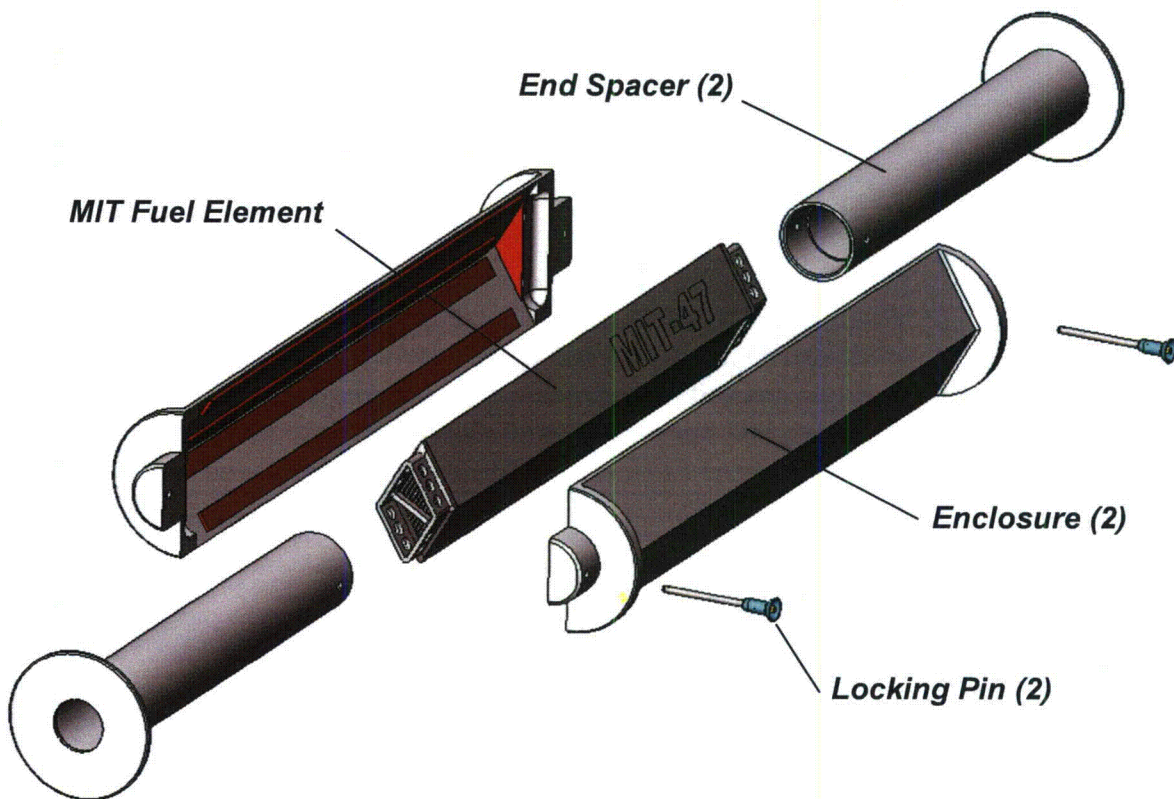
Figure 1.2-6 – MIT Fuel Handling Enclosure
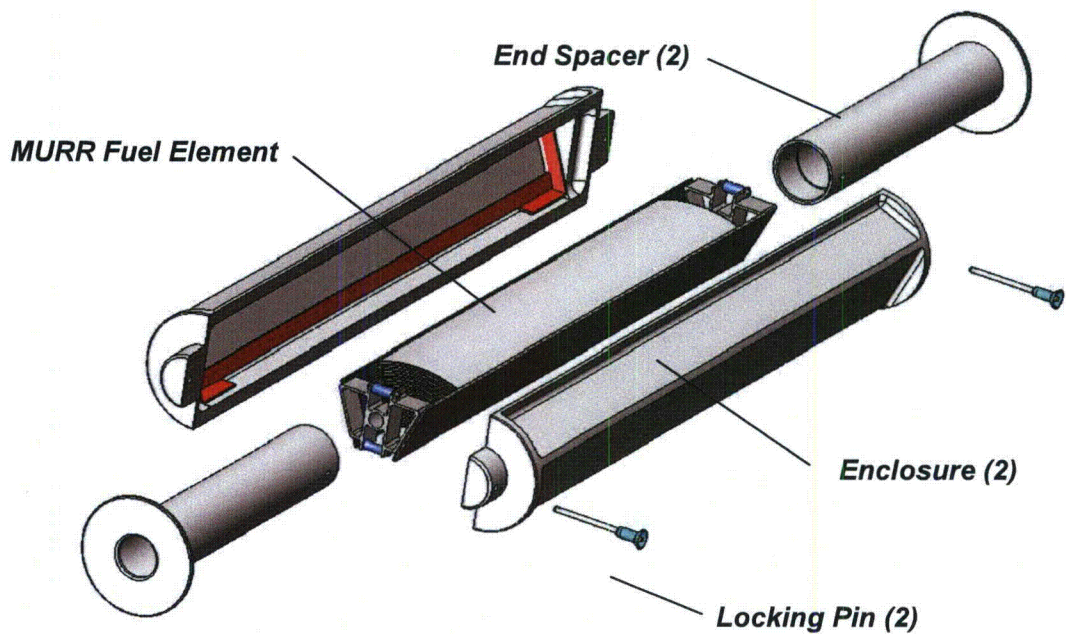
Figure 1.2-7 – MURR Fuel Handling Enclosure
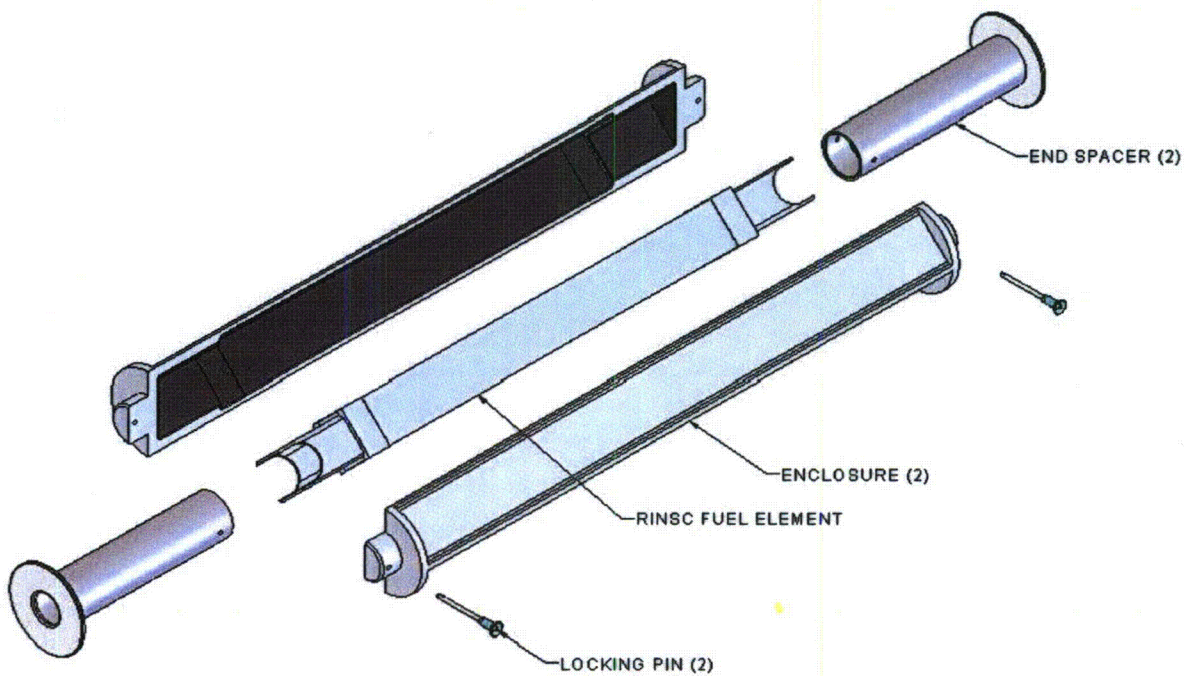
Figure 1.2-8 – RINSC Fuel Handling Enclosure
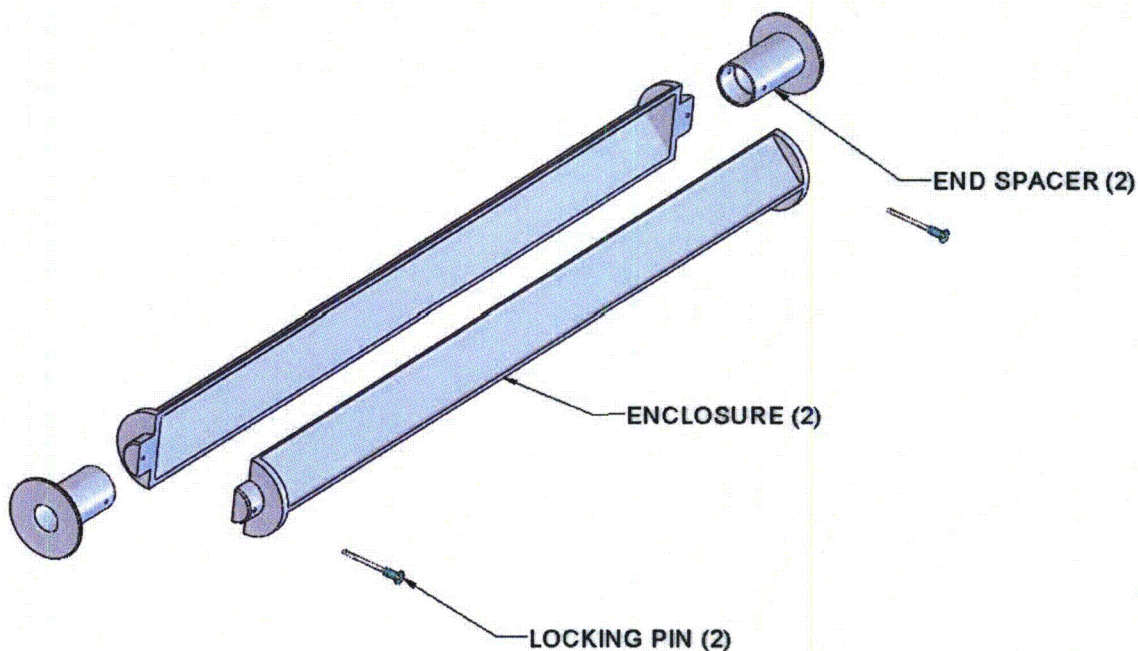
Figure 1.2-9 – Small Quantity Fuel Handling Enclosure
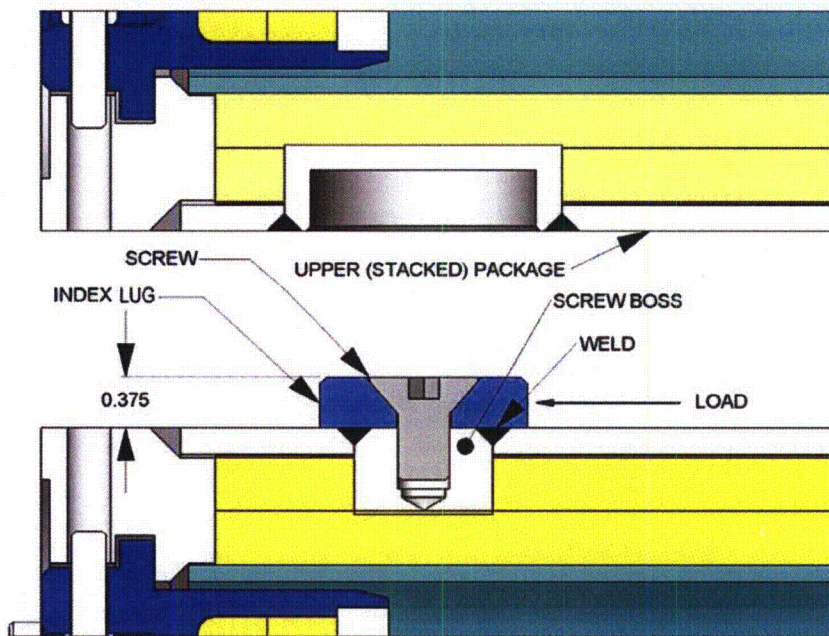
Figure 1.2-10 - Index Lug and Mating Pocket of Stacked Packages
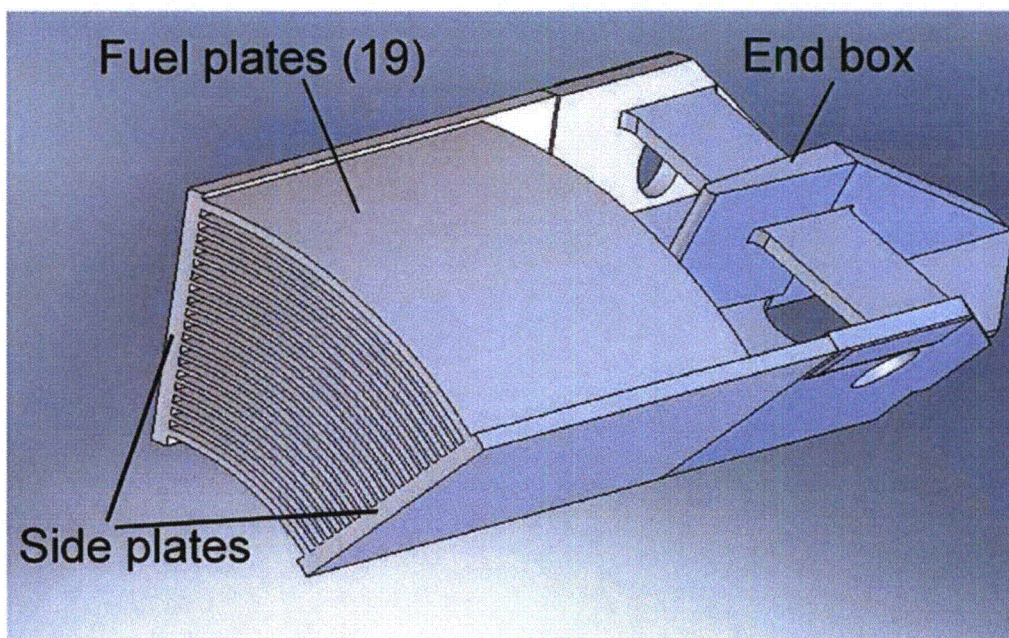
Figure 1.2-11 - ATR Fuel Element – Section View
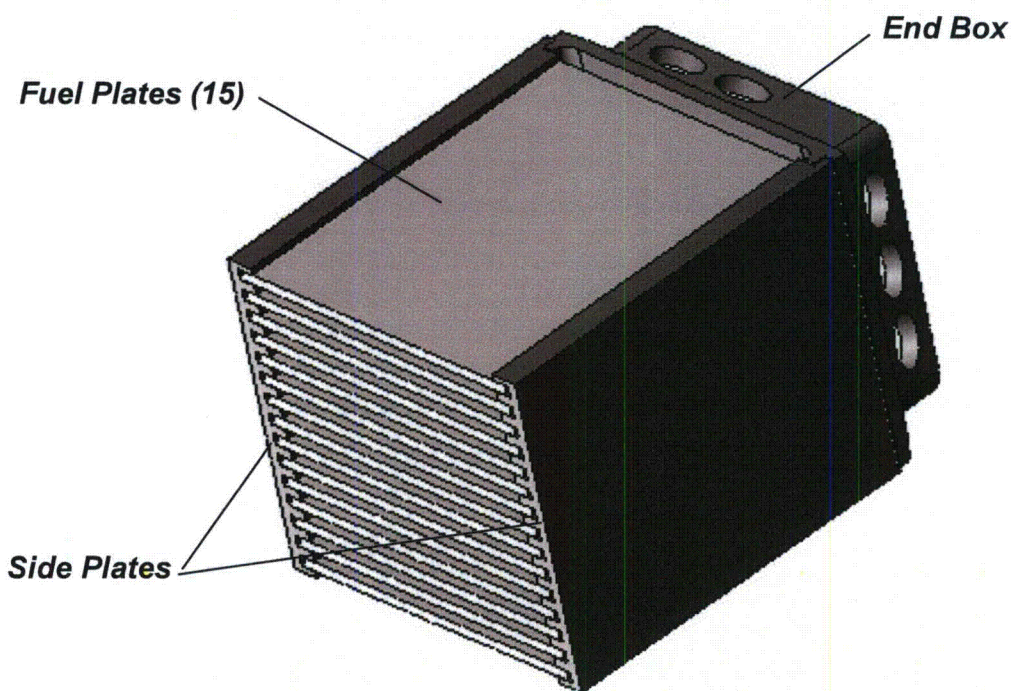
Figure 1.2-12 - MIT Fuel Element – Section View

Fuel Plates (24)

End Box

Side Plates
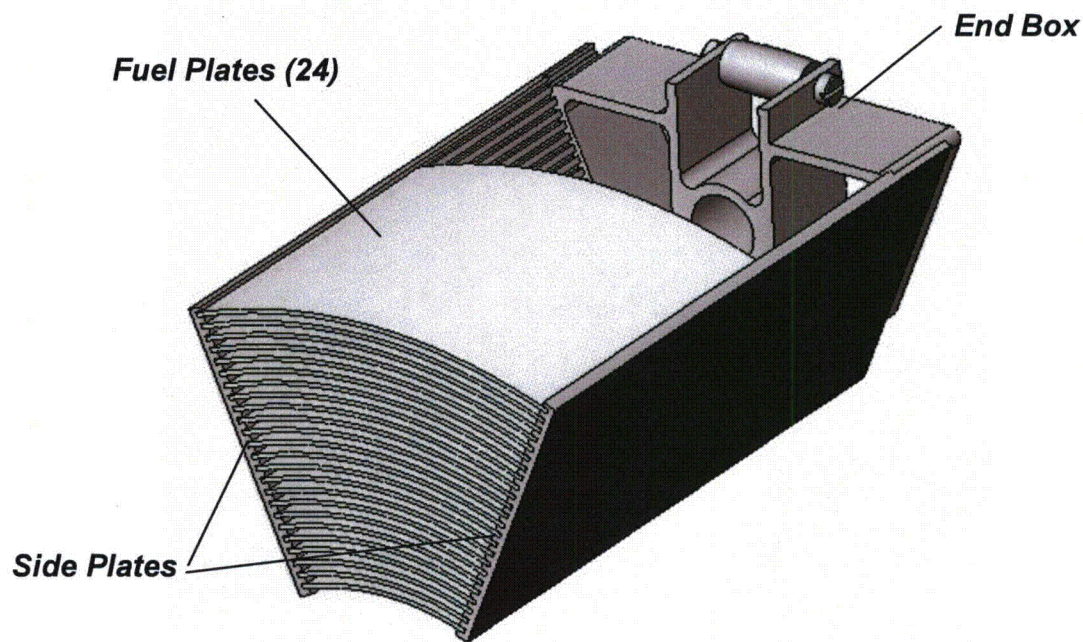
Figure 1.2-13 - MURR Fuel Element – Section View

FUEL PLATES (22)

SIDE PLATES (2)

END BOX (2)

LIFT RODS (2)
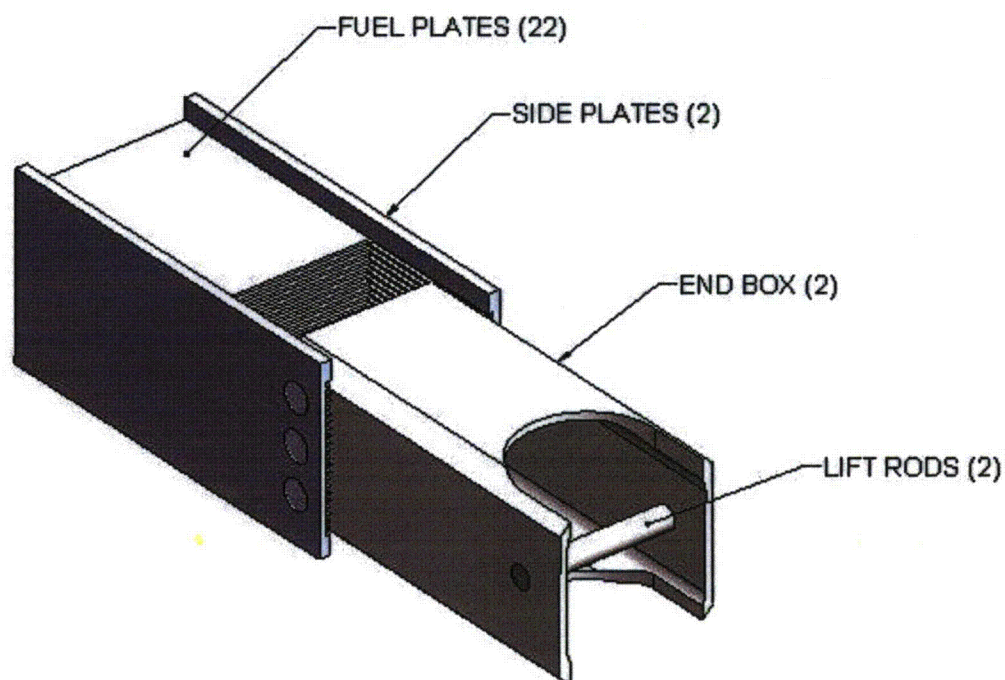
Figure 1.2-14 - RINSC Fuel Element – Section View

Basket Contents (fuel
plates plus dunnage)

Loose Fuel Plate Basket
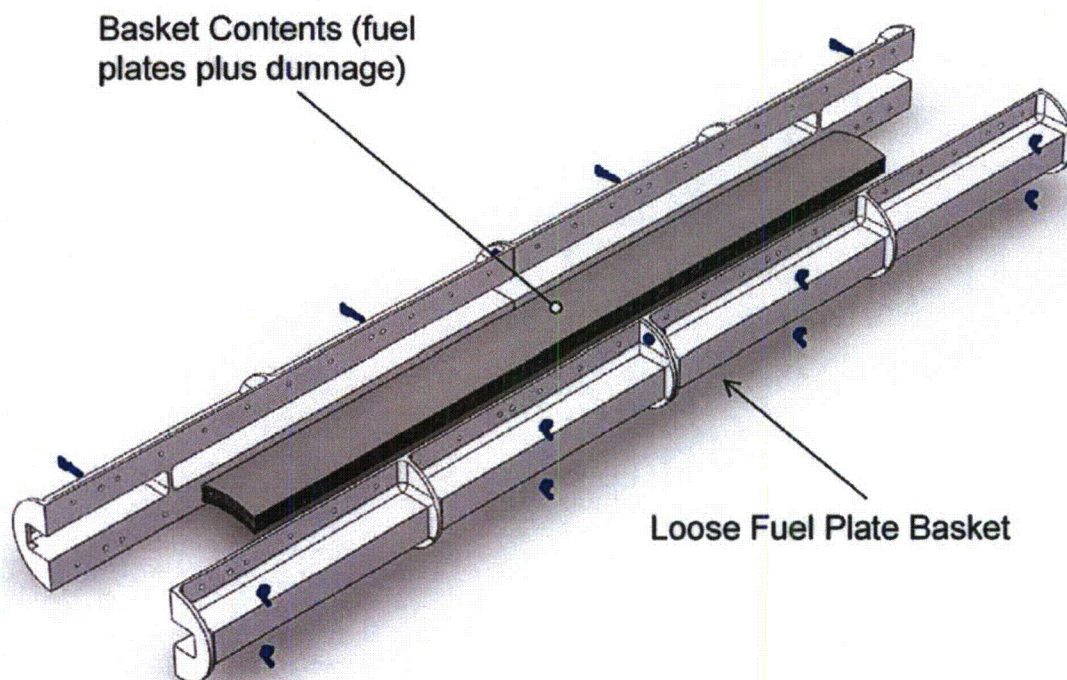
Figure 1.2-15 - Loose Fuel Plate Basket – Exploded View
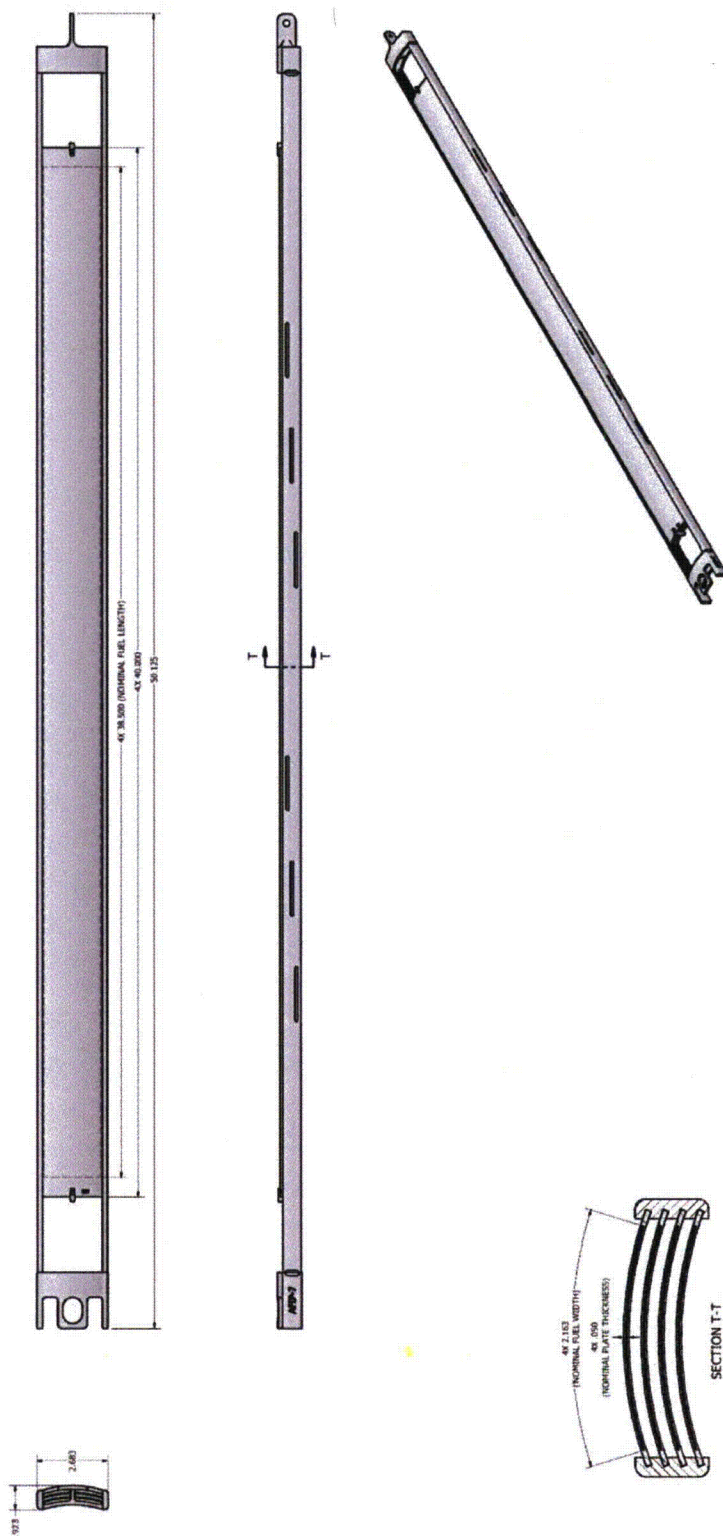
Figure 1.2-16 – AFIP Element
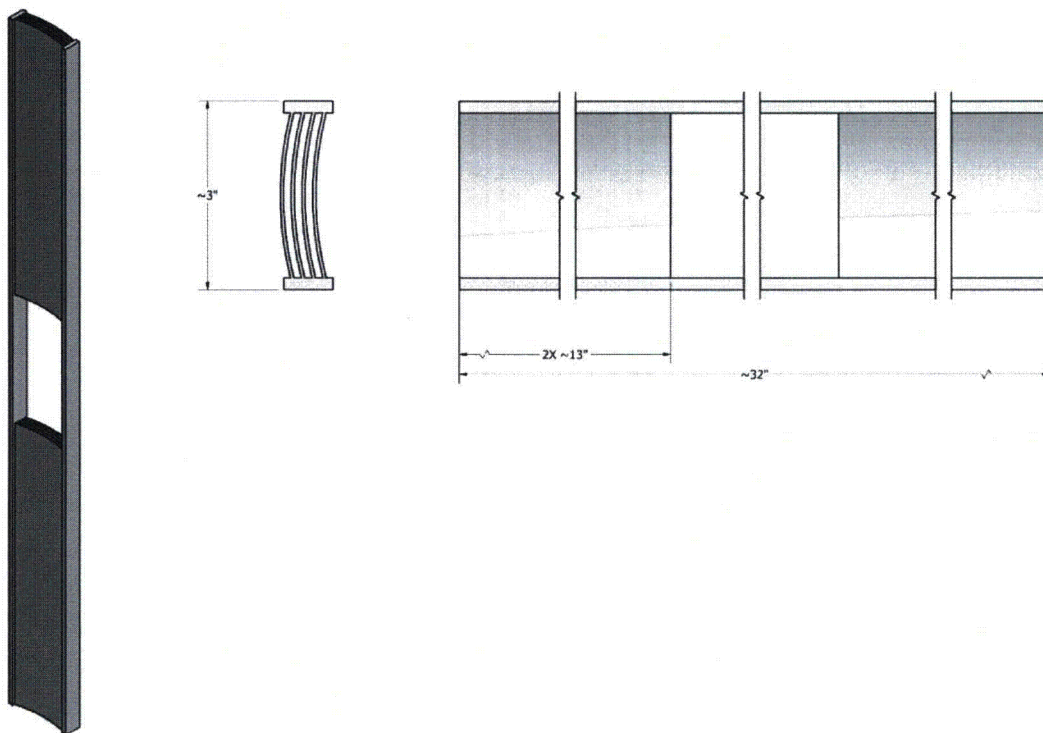
Figure 1.2-17 – DDE-NSBR Element
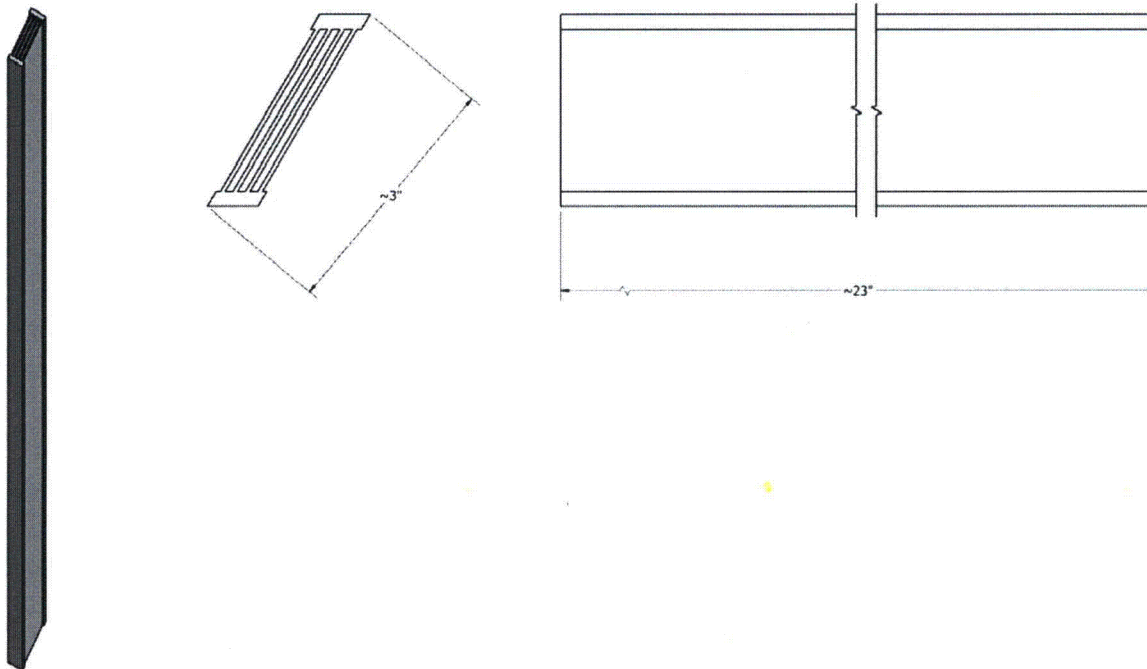
Figure 1.2-18 – DDE-MITR Element
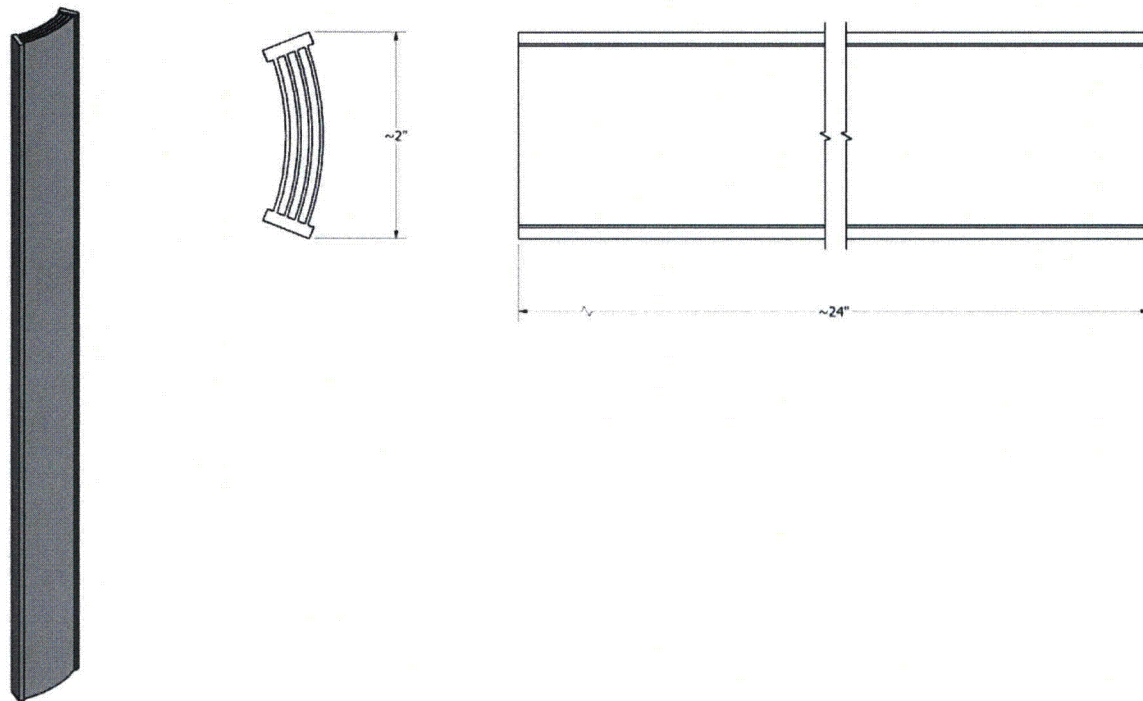
Figure 1.2-19 – DDE-MURR Element

UAl$_x$

U-Mo

UAl$_x$

PLATE 19 is
solid aluminum

(PLATE 1)

(PLATE 15)

(PLATE 14)

(PLATE 13)

(PLATE 12)

(PLATE 11)

(PLATE 5)

(PLATE 10)

(PLATE 6)

(PLATE 9)

(PLATE 7)

(PLATE 8)

Al 6061

Zirconium

U-10Mo

.017

.001

.050

.013
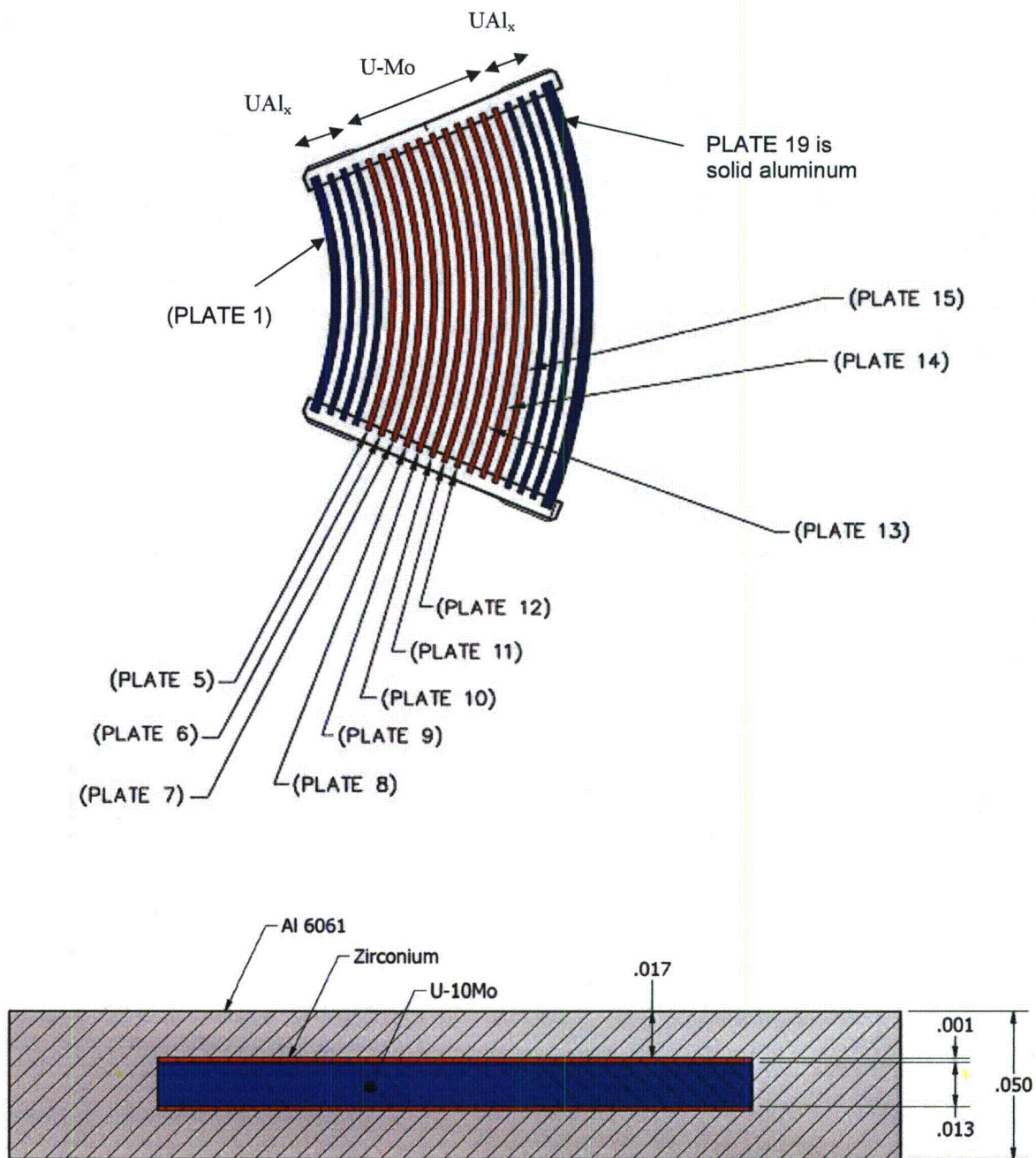
Figure 1.2-20 – ATR U-Mo Demonstration Element

1.2.3 Special Requirements for Plutonium

Because the ATR FFSC does not contain any plutonium, this section does not apply.

1.2.4 Operational Features

There are no operationally complex features in the ATR FFSC. All operational features are readily apparent from an inspection of the drawings provided in Appendix 1.3.2, *Packaging General Arrangement Drawings*. Operation procedures and instructions for loading, unloading, and preparing an empty ATR FFSC for transport are provided in Chapter 7.0, *Operating Procedures*.

1.3 Appendix

1.3.1 Glossary of Terms

AFIP –	ATR Full-size plate In Flux trap Position
ANSI –	American National Standards Institute.
ASME B&PV Code –	American Society of Mechanical Engineers Boiler and Pressure Vessel Code.
ASTM –	American Society for Testing and Materials.
ATR FFSC –	Advanced Test Reactor Fresh Fuel Shipping Container
AWS –	American Welding Society.
DDE –	Design Demonstration Element
HAC –	Hypothetical Accident Conditions.
NCT –	Normal Conditions of Transport.
Closure –	The ATR FFSC package component used to close the package.
Body –	The ATR FFSC package component which houses the payload.
Fuel element	Fuel element and fuel assembly are used interchangeably throughout this document to be the ATR, MIT, MURR, RINSC, AFIP, or DDE fuel element as described in Section 1.2.2, *Contents*.
Index lug –	A thick washer like component secured to the package body at the lift point locations. The index lug provides shear transfer capability between stacked packages.
Pocket –	A recessed feature on the package body that accepts the index lug when packages are stacked.
Fuel Handling Enclosure (FHE)–	Aluminum fabrications used to protect the ATR, MIT, MURR, and RINSC fuel elements from handling damage. The enclosures are faced with neoprene at locations where the fuel element contacts the FHE to minimize fretting of the fuel element at the contact points.
Loose fuel plate basket (LFPB) –	A machined aluminum container in which the unassembled fuel element plates are secured during transport in the ATR FFSC. The loose plate basket is a geometry based criticality control component.

Small Quantity Payload FHE (SQFHE) – see Fuel Handling Enclosure (FHE).

1.3.2 Packaging General Arrangement Drawings

The packaging general arrangement drawings consist of:

- 60501-10, *ATR Fresh Fuel Shipping Container SAR Drawing*, 5 sheets

- 60501-20, *Loose Plate Basket Assembly ATR Fresh Fuel Shipping Container SAR Drawing,* 1 sheet

- 60501-30, *Fuel Handling Enclosure, ATR Fresh Fuel Shipping Container SAR Drawing,* 1 sheet

- 60501-40, *MIT Fuel Handling Enclosure, ATR Fresh Fuel Shipping Container SAR Drawing,* 1 sheet

- 60501-50, *MURR Fuel Handling Enclosure, ATR Fresh Fuel Shipping Container SAR Drawing,* 1 sheet.

- 60501-60, *RINSC Fuel Handling Enclosure, ATR Fresh Fuel Shipping Container SAR Drawing,* 1 sheet.

- 60501-70, *Small Quantity Payload Fuel Handling Enclosure, ATR Fresh Fuel Shipping Container SAR Drawing,* 1 sheet.

2.0 STRUCTURAL EVALUATION

This section presents evaluations demonstrating that the ATR FFSC package meets all applicable structural criteria. The ATR FFSC packaging, consisting of the body and closure, is evaluated and shown to provide adequate protection for each payload; the ATR fuel element, MIT fuel element, MURR fuel element, ATR loose fuel plates, ATR U-Mo demonstration element, or small quantity payloads including the RINSC fuel element, MIT or MURR fuel plates, AFIP elements, U-MO foils, or DDEs. Each fuel element is contained within a corresponding fuel handling enclosure (FHE). The loose fuel plate basket (LFPB) is evaluated to contain only loose fuel plates associated with the ATR fuel element. The small quantity payload loose fuel plates, fuel elements, or foils are contained within a small quantity fuel handling enclosure.

Normal conditions of transport (NCT) and hypothetical accident condition (HAC) evaluations are performed to address 10 CFR §71[1] performance requirements primarily through physical testing. Physical demonstration by testing, including the free drop and puncture events, consists of certification testing utilizing two full-scale certification test units (CTU-1 and CTU-2). CTU-1 included the ATR fuel element payload and CTU-2 included the ATR LFPB and loose plates payload. Certification testing has demonstrated that the key performance objective of criticality control will be met by the ATR FFSC package. Details of the certification test program are provided in Appendix 2.12.1, *Certification Tests on CTU-1*, and Appendix 2.12.2, *Certification Tests on CTU-2*. The evaluation for the MIT and MURR fuel elements is provided in Appendix 2.12.3, *Structural Evaluation for MIT and MURR Fuel*.

2.1 Structural Design

2.1.1 Discussion

The ATR FFSC is a two part packaging consisting of the body and the closure. The body is a single weldment that features square tubing as an outer shell and round tubing for the payload cavity. The closure engages with the body using a bayonet style design. There are four lugs, uniformly spaced on the closure that engages with four slots in the mating body feature. The closure is secured by retracting two spring loaded pins, rotating the closure through approximately 45°, and releasing the spring loaded pins such that the pins engage with mating holes in the body. When the pins are properly engaged with the mating holes the closure is locked.

With the exception of several minor components, all steel used in the ATR FFSC packaging is of a Type 304 stainless steel. Components are joined using full-thickness fillet welds (i.e., fillet welds whose leg size is nominally equal to the lesser thickness of the parts joined) and full and partial penetration groove welds. The fuel containers for the package, the FHEs and the LFPB, are principally of aluminum construction and secured with stainless steel fasteners. The FHEs are a fabrication and the LFPB consists of four machined aluminum components.

A comprehensive discussion of the ATR FFSC packaging design and configuration is provided in Section 1.2, *Package Description*.

---

[1] Title 10, Code of Federal Regulations, Part 71 (10 CFR §71), *Packaging and Transportation of Radioactive Material*, 01-01-06 Edition.

2.1.2 Design Criteria

The ATR FFSC package has been designed to meet the majority of applicable structural requirements of 10 CFR §71 through physical testing. The design objectives for the package are threefold:

1. For NCT, demonstrate that the ATR FFSC package contains the payload without dispersal and that it does not experience a significant reduction in its effectiveness to withstand HAC; and

2. For HAC, demonstrate that the ATR FFSC package contains the payload without dispersal, consistent with conservative bounding assumptions utilized in the criticality analysis.

3. For HAC, demonstrate that the insulation used in the ATR FFSC package remains in place, to protect the payload from excessive heat from the thermal test, within the assumptions utilized in the thermal analysis.

Consequently, the design criteria for NCT are that the ATR FFSC package exhibit only minor damage subsequent to the NCT conditions and tests, including no damage that would materially affect the outcome of the subsequent HAC tests.

For HAC, the design criteria is that the payload will be retained within the packaging subsequent to the HAC test series of free drop, puncture, thermal, and the immersion test of 10 CFR §71.73(c)(5), or subsequent to immersion of an undamaged specimen per 10 CFR §71.73(c)(6).

Material properties are controlled by the acquisition of critical components to ASTM standards, testing, and process control, as described in Section 2.2, *Materials*. Lifting devices that are a structural part of the package are designed with a minimum safety factor of three against yielding. The index lugs located at the top of the package are considered a tiedown devices and are designed to withstand the loading requirements per 10 CFR §71.45(b)(1).

2.1.2.1 Miscellaneous Structural Failure Modes

2.1.2.1.1 Brittle Fracture Assessment

The steel materials utilized in the ATR FFSC package provide adequate fracture toughness. All critical structural components of the packaging are made of Type 304 stainless steel and have a nil ductility transition temperature less than -40°F (-40°C). Therefore, brittle fracture is not a concern for the ATR FFSC packaging.

To confirm the performance of the uranium aluminide (UAl_x) fuel types at reduced temperatures, the ATR fuel element in CTU-1, was subjected to two HAC drops with the payload at approximately -20°F (-29°C). Following all CTU-1 testing, as discussed in Appendix 2.12.1, *Certification Tests on CTU-1*, the package was disassembled and the payload inspected. Upon inspection, the performance of both the payload and packaging, including the reduced temperature tests, was satisfactory. Following all testing, the payload remained within the assumptions presented in Section 6.0, *Criticality Evaluation*.

2.1.2.1.2 Fatigue Assessment

Normal operating cycles do not present a fatigue concern for the ATR FFSC. The packaging does not retain pressure, and consequently fatigue due to pressure cycling cannot occur. Since all structural components of the packaging are made of the same alloy, and since thermal

gradients are small, thermally-induced fatigue is not of concern. Since the packaging is normally handled on a pallet, the lifting features of the packaging are infrequently used, and fatigue of the lifting load path is not of concern.

The only components which are routinely handled are the closure and the fuel handling structures (ATR, MIT, MURR, RINSC fuel handling enclosures, loose plate basket, and small quantity fuel handling enclosure). The closure is designed as a bayonet-type attachment with two spring-loaded locking pins which prevent rotation during transport. Neither the bayonet lugs nor the locking pins experience any significant loading (such as preload or other repeating mechanical loads) in routine usage. If damage to these components were to occur, it will be identified during the inspections discussed in Section 7.1.1, *Preparation for Loading*. Consequently, fatigue of the closure components is not of concern.

The fuel handling structures (fuel handling enclosures and loose plate basket) are simple structures that do not have significant handling loads. These structures are fully exposed to view during loading and unloading, and can be inspected to ensure integrity.

For these reasons, normal operating cycles are not a failure mode of concern for the ATR FFSC packaging. Fatigue associated with normal vibration over the road is discussed in Section 2.6.5, *Vibration*.

2.1.2.1.3 Buckling Assessment

Certification testing has demonstrated that buckling of the ATR FFSC package does not occur as a result of any normal conditions of transport or as a result of the HAC primary test sequence (e.g., the free drop and puncture tests). Buckling of the ATR FFSC body is also shown to not be a concern during the 50 ft immersion test specified under 10 CFR §71.73(c)(6). A discussion of the response to the 50 ft immersion test is provided in Section 2.7.6, *Immersion – All Packages*.

2.1.3 Weights and Centers of Gravity

The maximum gross weight of the ATR FFSC package is 290 lb. The packaging component weights are summarized in Table 2.1-1. The maximum payload weight is 50 lb, for the loose plate payload and small quantity payload, 40 lb for the ATR payload, 35 lb for the MIT payload, 45 lb for the MURR payload, 45 lb for the RINSC payload and 47 lb for the U-Mo demonstration element. The U-Mo demonstration element is the same as ATR element payload except plates 5 through 15 are replaced with reduced enrichment plates of the same size, and plate 19 is solid aluminum. Due to symmetry of design, the center of gravity (CG) of the package is located essentially at the geometric center of the package. Regardless of payload, the center of gravity remains 35 inches from the face of the closure end and 4 inches from the bottom and sides of the package. The packaging components are illustrated in Figure 2.1-1 through Figure 2.1-6.

Table 2.1-1 – ATR FFSC Component Weights

Item	Weight, lb	
	Component	Assembly
ATR FFSC Packaging	- -	240
Body Assembly	230	- -
Closure Assembly	10	- -
Payload – ATR Fuel Assembly	- -	40
ATR Fuel Assembly	25	- -
ATR Fuel Handling Enclosure	15	- -
Payload – MIT Fuel Assembly	- -	35
MIT Fuel Assembly	10	- -
MIT Fuel Handling Enclosure	25	- -
Payload – MURR Fuel Assembly	- -	45
MURR Fuel Assembly	15	- -
MURR Fuel Handling Enclosure	30	- -
Payload – RINSC Fuel Assembly	- -	45
RINSC Fuel Assembly	17	- -
RINSC Fuel Handling Enclosure	28	- -
Payload – Fuel Plates	- -	50
ATR Loose Fuel Plates (including optional dunnage)	20	- -
Loose Fuel Plate Basket	30	- -
Payload – Small Quantities (except RINSC)	- -	50
MIT or MURR Loose Fuel Plates, AFIP Elements, U-Mo Foils, or DDEs	20	- -
Small Quantity Fuel Handling Enclosure	30	- -
Payload – ATR U-Mo Demo Element		47
ATR U-Mo Demo Element	32	--
ATR Fuel Handling Enclosure	15	--
Total LFPB Loaded Package (maximum)	- -	290
Total MURR Loaded Package	- -	285
Total ATR Loaded Package	- -	280
Total MIT Loaded Package	- -	275
Total RINSC Loaded Package	- -	285
Total Small Quantity Loaded Package	- -	290
Total ATR U-Mo Demo Package	- -	287

2.1.4 Identification of Codes and Standards for Package Design

As a Type AF package, the ATR FFSC is designed to meet the performance requirements of 10 CFR 71, Subpart E. Compliance with these requirements is demonstrated via full scale testing of the package under both NCT and HAC, as documented in Section 2.12, *Appendices*. In addition, structural materials which are important to safety are specified using American Society for Testing and Materials (ASTM) standards as shown on the drawings in Appendix 1.3.2, *Packaging General Arrangement Drawings*. Welding procedures and personnel are qualified in accordance with the ASME Code, Section IX. All welds are visually examined on each pass per the requirements of AWS D1.6:1999[2] for stainless steel and AWS D1.2:2003[3] for aluminum. All welds which are important to safety are examined by liquid penetrant test on the final pass using procedures compliant with ASTM E165-02[4].
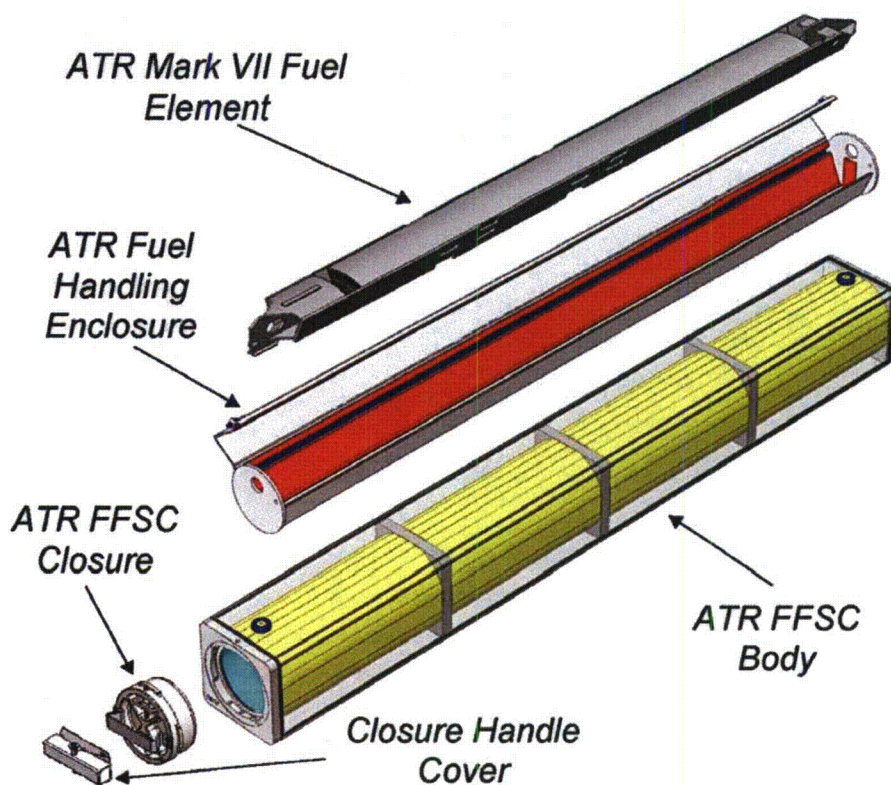
Figure 2.1-1 –Package Components (With ATR Fuel Element)

---

[2] ANSI/AWS D1.6:1999, *Structural Welding Code – Stainless Steel*, American Welding Society (AWS).

[3] ANSI/AWS D1.2:2003, *Structural Welding Code – Aluminum*, American Welding Society (AWS)

[4] American Society for Testing and Materials (ASTM International), ASTM E165-02, *Standard Test Method for Liquid Penetrant Examination*, Feb 2002.

3.0 THERMAL EVALUATION

This chapter identifies and describes the principal thermal design aspects of the ATR FFSC. Further, this chapter presents the evaluations that demonstrate the thermal safety of the ATR FFSC package[1] and compliance with the thermal requirements of 10 CFR 71[2] when transporting a payload consisting of an assembled, unirradiated ATR fuel element, ATR U-Mo demonstration element, MIT fuel element, MURR fuel element, RINSC fuel element, or a payload of loose, unirradiated fuel plates. The loose fuel element plates may be either flat or rolled to the geometry required for assembly into a fuel element. The evaluations in this chapter also bound the thermal safety of the packaging when transporting small quantity payloads that are less than or equal to 400 g U-235, and have enrichment up to 94% U-235. Small quantity payloads are defined in Section 1.2.2.4, *Small Quantity Payloads*.

Specifically, all package components are shown to remain within their respective temperature limits under the normal conditions of transport (NCT). Further, per 10 CFR §71.43(g), the maximum temperature of the accessible package surfaces is demonstrated to be less than 122 °F for the maximum decay heat loading, an ambient temperature of 100 °F, and no insolation. Finally, the ATR FFSC package is shown to retain sufficient thermal protection following the HAC free and puncture drop scenarios to maintain all package component temperatures within their respective short term limits during the regulatory fire event and subsequent package cool-down.

The analysis in the main body of Chapter 3 pertains only to the ATR fuel element, ATR U-Mo demonstration element, and ATR loose plate basket. The analysis for MIT, MURR, RINSC, and small quantity payloads is contained in Section 3.6, *Thermal Evaluation for MIT, MURR, and Small Quantity Payloads*.

3.1 Description of Thermal Design

The ATR FFSC package, illustrated in Figure 1.2-1 through Figure 1.2-5 from Section 1.0, *General Information*, consists of three basic components: 1) a Body assembly, 2) a Closure assembly, and 3) either a Fuel Handling Enclosure (FHE) or a Loose Fuel Plate Basket (LFPB). The FHE is configured to house an assembled ATR fuel element or ATR U-Mo demonstration element, while the LFPB is configured to house loose ATR fuel element plates. The maximum gross weight of the package loaded with an FHE and ATR fuel element or ATR U-Mo demonstration element is approximately 290 pounds. The maximum gross weight of the package loaded with a LFPB containing its maximum payload is approximately 290 pounds.

The ATR FFSC is designed as a Type AF packaging for transportation of an ATR fuel element or a bundle of loose ATR fuel element plates. The packaging is rectangular in shape and is

---

[1] In the remainder of this chapter, the term 'packaging' refers to the assembly of components necessary to ensure compliance with the regulatory requirements, but does not include the payload. The term 'package' includes both the packaging components and the payload of ATR fuel.

[2] Title 10, Code of Federal Regulations, Part 71 (10 CFR 71), *Packaging and Transportation of Radioactive Material*, 01-01-03 Edition.

intended to be transported in racks of multiple packages by highway truck. Since the payload generates essentially no decay heat, the worst case thermal conditions will occur with an individual package fully exposed to ambient conditions. The package performance when configured in a rack of multiple packages will be bounded by that seen for an individual package.

The principal components of the packaging are shown in Figure 1.2-1 and described in more detail below. With the exception of minor components, all steel used in the ATR FFSC packaging is Type 304 stainless steel. Components are joined using full-thickness fillet welds and full and partial penetration groove welds.

3.1.1 Design Features

The primary heat transfer mechanisms within the ATR FFSC are conduction and radiation, while the principal heat transfer from the exterior of the packaging is via convection and radiation to the ambient environment. The Body and Closure assemblies serve as the primary impact and thermal protection for the FHE or the LFPB and their enclosed payloads of an ATR fuel element, ATR U-Mo demonstration element, or loose fuel plates. The FHE and LFPB provide additional thermal shielding of their enclosed payloads during the transient HAC event.

There is no pressure relief system included in the ATR FFSC packaging design. The portions of the packaging that are not directly vented to atmosphere do not contain out-gassing materials. The package insulation is the only non-metallic component located in the enclosed volumes of the package and it is fabricated of a ceramic fiber. The Closure assembly is not equipped with either seals or gaskets so that potential out-gassing of the neoprene material used in ATR fuel tray and the plastic bag material used as a protective sleeve for the fuel element will readily vent without significant pressure build-up in the payload cavity.

The principal thermal design features of each package component are described in the following paragraphs.

3.1.1.1 ATR FFSC Body

The ATR FFSC body is a stainless steel weldment that is approximately 73 inches long and 8 inches square and weighs about 230 lbs (empty). It consists of two nested shells; the outer shell is fabricated of a square stainless steel tube with a 3/16 inch wall thickness, while the inner shell is fabricated from a 6 inch diameter, 0.120 inch wall, stainless steel tube. Three, 1-inch thick stiffening plates (i.e., ribs) are secured to the inner shell by fillet welds at four equally spaced intervals. The ribs are not mechanically attached to the outer shell. Instead, a nominal 0.06 inch air gap exists between the ribs and the outer shell, with a larger nominal gap existing at the corners of the ribs. These design features help to thermally isolate the inner shell from the outer shell during the HAC event.

Further thermal isolation of the inner shell is provided by ceramic fiber thermal insulation which is wrapped around the inner shell between the ribs and by the 28 gauge stainless steel sheet used as a jacket material over the insulation. The insulation is applied in two 0.5-inch thick layers in order to permit over-lapping joints between the layers and prevents direct line-of-sight between the inner shell and the jacket should the insulation shift under normal or accident conditions. The stainless steel jacket maintains the insulation around the inner shell and provides a relatively

low emissivity barrier to radiative heat exchange between the insulation and the outer sleeve. The insulation jacket is pre-formed to the design shape and dimensions prior to installation. As such, the potential for inadvertent compression of the insulation during installation is minimized.

Once assembled, the inner shell, ribs, and the jacketed insulation wrap are slid as a single unit into the outer shell and secured to closure plates at both ends by welding. Thermal insulation is built into the bottom end closure plate of the packaging, while the ATR FFSC closure (see below) provides thermal insulation at the top end closure.

Cross-sectional views showing key elements of the ATR FFSC body are provided in Figure 1.2-2 and Figure 1.2-3. Figure 1.2-2 illustrates a cross sectional view at the top end closure of the package and 1.2-3 presents a similar cross sectional view of the package at the bottom end closure.

3.1.1.2 ATR FFSC Closure

The ATR FFSC closure engages with the body using a bayonet style engagement via four uniformly spaced lugs on the closure that engage with four slots in the mating body feature. The closure incorporates 1 inch of ceramic fiber thermal insulation to provide thermal protection and is designed to permit gas to easily vent through the interface between the closure and the body. The closure weighs approximately 10 pounds and is equipped with a handle to facilitate use with gloved hands.

A cross sectional view of the ATR FFSC closure is illustrated in Figure 1.2-4.

3.1.1.3 Fuel Handling Enclosure (FHE)

The Fuel Handling Enclosure (FHE) is a hinged, aluminum weldment used to protect either an ATR fuel element or ATR U-Mo demonstration element from damage during loading and unloading operations. It is fabricated of thin wall (i.e., 0.09 inch thick) 5052-H32 aluminum sheet and features a hinged lid and neoprene rub strips to minimize fretting of the fuel element side plates where they contact the FHE. The surface of the FHE is neither anodized nor coated, but is left as an 'unfinished' aluminum sheet. Figure 1.2-1 presents an illustration of the FHE. A polyethylene bag is used as a protective sleeve over the ATR fuel and ATR U-Mo demonstration elements.

3.1.1.4 ATR FFSC Loose Fuel Plate Basket (LFPB)

The Loose Fuel Plate Basket (LFPB) serves to maintain the fuel plates within a defined dimensional envelope during transport. The four identical machined segments are machined from a billet of 6061-T651 aluminum and are joined by threaded fasteners (see Figure 1.2-15). A variable number of ATR fuel plates may be housed in the basket, with the maximum payload weight being limited to 20 lbs. or less. The empty weight of the loose fuel plate basket is approximately 30 lbs. Like the FHE, the surface of the LFPB is neither anodized nor coated, but is left with its 'as machined' finish.

3.1.2 Content's Decay Heat

The ATR FFSC is designed as a Type AF packaging for transportation of an unirradiated ATR fuel element, an ATR U-Mo demonstration element, or a bundle of loose, unirradiated ATR fuel | plates. The decay heat associated with unirradiated ATR fuel is negligible. Therefore, no special devices or features are needed or utilized in the ATR FFSC packaging to dissipate the decay heat. Section 1.2.2, *Contents*, provides additional details.

3.1.3 Summary Tables of Temperatures

Table 3.1-1 provides a summary of the package component temperatures under normal and accident conditions. The temperatures for normal conditions are based on an analytical model of the ATR FFSC package for extended operation with an ambient temperature of 100°F and a diurnal cycle for the insolation loading. The temperatures for accident conditions are based on an analytical model of the ATR FFSC package with the worst-case, hypothetical pre-fire damage as predicted based on drop tests using full-scale certification test units (CTUs).

The results for NCT conditions demonstrate that significant thermal margin exists for all package components. This is to be expected since the only significant thermal loads on the package arise from insolation and ambient temperature changes. The payload dissipates essentially zero decay heat. Further, the evaluations for NCT demonstrate that the package skin temperature will be below the maximum temperature of 122°F permitted by 10 CFR §71.43(g) for accessible surface temperature in a nonexclusive use shipment when transported in a 100°F environment with no insolation.

The results for HAC conditions also demonstrate that the design of the ATR FFSC package provides sufficient thermal protection to yield component temperatures that are significantly below the acceptable limits defined for each component. While the neoprene rubber and polyethylene plastic material used to protect the ATR fuel and U-Mo demonstration elements | from damage are expected to reach a sufficient temperature level during the HAC fire event to induce some level of thermal degradation (i.e., melting, charring, the chemical breakdown of the materials into 2 or more substances, etc.), the loss of these components is not critical to the safety of the package. Further, the potential combustion of these materials will be restricted due to the lack of available oxygen to the point that any potential temperature rise will be insignificant. See Sections 3.2.2, *Technical Specifications of Components*, 3.4.3.1, *Maximum HAC Temperatures*, and 3.5.3, *Thermal Decomposition/Combustion of Package Organics*, for more discussion.

3.1.4 Summary Tables of Maximum Pressures

Table 3.1-2 presents a summary of the maximum pressures achieved under NCT and HAC conditions. Since the ATR FFSC package is a vented package, both the maximum normal operating pressure (MNOP) and the maximum pressure developed within the payload compartment under the HAC condition are 0 psig.

Although the volume between the outer and inner shells is sealed, it does not contain organic or other materials that may outgas or thermally degrade. Therefore, the maximum pressure that may develop within the space will be limited to that achieved due to ideal gas expansion. The

maximum pressure rise under NCT will be less than 4 psig, while the pressure rise under HAC conditions will be 39 psig.

Table 3.1-1 – Maximum Temperatures for NCT and HAC Conditions

Location / Component	NCT Hot Conditions	Accident Conditions	Maximum Allowable [1]	
			Normal	Accident
ATR Fuel Element Fuel Plate	147°F	730°F	400°F	1,100°F
ATR Fuel Element Side Plate	148°F	827°F	400°F	1,100°F
Neoprene Rub Strips/Polyethylene Bag	151°F [2]	1,017°F [2]	225°F	N/A
Fuel Handling Enclosure (FHE)	151°F	1,017°F	400°F	1,100°F
Loose Fuel Plate Basket (LFPB)	151°F [2]	746°F	400°F	1,100°F
Inner Shell	157°F	1,422°F	800°F	2,700°F
Ceramic Fiber Insulation, Body				
- Maximum	185°F	1,460°F	2,300°F	2,300°F
- Average	151°F	1,220°F	2,300°F	2,300°F
Ceramic Fiber Insulation, Closure				
- Maximum	145°F	1,418°F	2,300°F	2,300°F
- Average	144°F	1,297°F	2,300°F	2,300°F
Closure	145°F	1,445°F	800°F	2,700°F
Outer Shell	186°F	1,471°F	800°F	2,700°F

Table Notes:

[1] Maximum allowable temperatures are defined in Section 3.2.2, *Technical Specifications of Components*.

[2] Component temperature assumed to be equal to that of the FHE.

Table 3.1-2 – Summary of Maximum Pressures

Condition	Fuel Cavity Pressure	Outer/Inner Shell Cavity Pressure
NCT Hot	0 psi gauge	4 psi gauge
HAC Hot	0 psi gauge	39 psi gauge

3.2 Material Properties and Component Specifications

The ATR FFSC is fabricated primarily of Type 304 stainless steel, 5052-H32 and 6061-T651 aluminum, ceramic fiber insulation, and neoprene rubber. The payload materials include 6061-T6 and/or 6061-0 aluminum, uranium aluminide (UAl_x), and uranium-molybdenum (i.e., U-10Mo in a foil coated with thin zirconium interlayers). A polyethylene plastic bag is used as a protective sleeve over the fuel element.

3.2.1 Material Properties

Table 3.2-1 presents the thermal properties for Type 304 stainless steel and 5052-H32 aluminum from Table TCD of the ASME Boiler and Pressure Vessel Code[3]. Since the HAC analysis requires thermal properties in excess of the maximum temperature point of 400°F provided in Table TCD for 5052-H32 aluminum, the property values for 1100°F (i.e., the approximate melting point for aluminum) are assumed to be the same as those at 400°F. This approach is appropriate for estimating the temperature rise within the fuel basket during the HAC event since the thermal conductivity of aluminum alloys tends to decrease with temperature while the specific heat tends to increase. The density values listed in the table are taken from an on-line database[4]. Properties between the tabulated values are calculated via linear interpolation within the heat transfer code.

Table 3.2-2 presents the thermal properties for the ATR fuel element. For analysis purposes, the material used for the side plates, covers, and fuel cladding are assumed to be 6061-0 aluminum. The thermal properties for the fuel plates are determined as a composite of the cladding and the fuel core materials based on the geometry data for the ATR fuel element[5] and the thermal properties for the ATR fuel element materials[6]. The details of the computed values are presented in Section 3.5.2.4, *Determination of Composite Thermal Properties for ATR Fuel Plates*. For simplicity and given the low sensitivity to temperature, a conservatively high, fixed thermal conductivity value is used for the fuel plates in order to maximize the heat transfer into the fuel components during the HAC event. The specific heat values are computed as a function of temperature to more accurately capture the change in thermal mass for the fuel plates during the HAC event.

The ATR U-Mo demonstration fuel elements are not specifically modeled for this evaluation. Instead, the thermal response of these elements is bounded by the results predicted for other elements. See Section 3.5.2.5, *Thermal Properties for ATR U-Mo Demonstration Element,* for details.

The thermal properties for the non-metallic materials used in the ATR FFSC are presented in Table 3.2-3. The thermal properties for neoprene rubber are based on the *Polymer Data*

---

[3] American Society of Mechanical Engineers (ASME) Boiler and Pressure Vessel Code, Section II, *Materials, Part D – Properties*, Table TCD, Material Group J, 2001 Edition, 2002 and 2003 Addenda, New York

[4] Matweb, Online Material Data Sheets, www.matweb.com.

[5] *ATR Mark VII Fuel Element Assembly*, INEEL Drawing No. DWG-405400, Rev-19.

[6] *Thermophysical And Mechanical Properties Of ATR Core Materials*, Report No. PG-T-91-031, August 1991, EG&G Idaho, Inc.

Handbook[7], while the thermal properties for the ceramic fiber insulation are based on the Unifrax Durablanket® S insulation product[8] with a nominal density of 6 lb/ft^{3}. The thermal properties are for the uncompressed material in both cases. Although the package design requires that the insulation blanket be compressed by up to 20% at the quadrant points, ignoring the compression for the purposes of the thermal modeling and using the thermal properties for the uncompressed material at all locations provides a conservative estimate of the package's performance under the HAC condition. This conclusion arises from the fact that the insulation's thermal conductivity decreases with density for temperatures above approximately 500°F (see Table 3.2-3). For example, the thermal conductivity of 8 pcf insulation at 1000°F and 1400°F is 0.0814 and 0.1340 Btu/hr-ft-°F, respectively, versus the 0.0958 and 0.1614 Btu/hr-ft-°F values for 6 pcf insulation at the same temperatures. While compression will increase conductivity below 500°F, ignoring the effects of compression for NCT conditions has an insignificant effect since the peak package temperatures occur in the vicinity of the ribs and are therefore unaffected by a local increase in the thermal conductivity of the insulation. Further, large thermal margins exist for the NCT conditions.

The thermal properties for air presented in Table 3.2-4 are derived from curve fits[9]. Because the thermal conductivity of air varies significantly with temperature, the computer model calculates the thermal conductivity across air spaces as a function of the mean film temperature. All void spaces within the ATR FFSC package are assumed to be filled with air at atmospheric pressure.

Table 3.2-5 and Table 3.2-6 present the assumed emissivity (ε) for each radiating surface and the solar absorptivity (α) value for the exterior surface. The emissivity of 'as-received' Type 304 stainless steel has been measured[10] as 0.25 to 0.28, while the emissivity of weathered Type 304 stainless steel has been measured[11] from 0.46 to 0.50. For the purpose of this analysis, an emissivity of 0.30 is assumed for the emittance from all interior radiating stainless steel surfaces, while the emissivity for the exterior surfaces of the package is assumed to be 0.45. The solar absorptivity of Type 304 stainless steel is approximately 0.52[12]. Under HAC conditions, the outside of the package is assumed to attain an emissivity of 0.8 in compliance with 10 CFR §71.73(c)(4) and to have a solar absorptivity of 0.9 to account for the possible accumulation of soot.

The 5052-H32 aluminum sheet used to fabricate the FHE will be left with a plain finish while the 6061-T651 billets used to fabricate the Loose Fuel Plate Basket will have a machined surface. The emissivity for either type of finish can be expected to be low (i.e., 0.10 or lower)[12] however, for conservatism, an emissivity of 0.25[12] representative of a heavily oxidized surface is assumed for this evaluation. The 6061-0 aluminum used for the ATR fuel components are assumed to have a

---

[7] *Polymer Data Handbook*, Oxford University Press, Inc., 1999.

[8] Unifrax DuraBlanket S ceramic fiber insulation, Unifrax Corporation, Niagara Falls, NY.

[9] Rohsenow, Hartnett, and Cho, *Handbook of Heat Transfer*, 3rd edition, McGraw-Hill Publishers, 1998.

[10] Frank, R. C., and W. L. Plagemann, *Emissivity Testing of Metal Specimens*. Boeing Analytical Engineering coordination sheet No. 2-3623-2-RF-C86-349, August 21, 1986. Testing accomplished in support of the TRUPACT-II design program.

[11] *"Emissivity Measurements of 304 Stainless Steel"*, Azzazy, M., prepared for Southern California Edison, September 6, 2000, Transnuclear File No. SCE-01.0100.

[12] G. G. Gubareff, J. E. Janssen, and R. H. Torborg, *Thermal Radiation Properties Survey*, 2nd Edition, Honeywell Research Center, 1960.

surface coating of boehmite ($Al_2O_3H_2O$). A 25 μm boehmite film will exhibit a surface emissivity of approximately 0.92[13]. While a fresh fuel element may have a lower surface emissivity, the use of the higher value will provide a conservative estimate of the temperatures achieved during the HAC event.

The ceramic fiber insulation has a surface emissivity of approximately 0.90[12] based on a combination of the material type and surface roughness. The same emissivity is assumed for the neoprene rubber.

3.2.2 Technical Specifications of Components

The materials used in the ATR FFSC that are considered temperature sensitive are the aluminum used for the FHE, the LFPB, the ATR fuel, and the ATR U-Mo demonstration element, the neoprene rubber, and the polyethylene wrap used as a protective sleeve around the ATR fuel element and ATR U-Mo demonstration element. Of these materials, only the aluminum used for the ATR fuel and ATR U-Mo demonstration element is considered critical to the safety of the package. The other materials either have temperature limits above the maximum expected temperatures or are not considered essential to the function of the package.

Type 304 stainless steel has a melting point above 2,700°F[4], but in compliance with the ASME B&PV Code[14], its allowable temperature is limited to 800°F if used for structural purposes. However, the ASME temperature limit generally applies only to conditions where the material's structural properties are relied on for loads postulated to occur in the respective operating mode or load combination (such as the NCT and HAC free drops). Since the package is vented to atmosphere, no critical structural condition exists following the HAC free drop events and, as such, the appropriate upper temperature limit is 800°F for normal conditions and 2,700°F for accident conditions

Aluminum (5052-H32, 6061-0/6061-T6) has a melting point of approximately 1,100°F[4] however for strength purposes the normal operational temperature should be limited to 400°F[3].

The ceramic fiber insulation has a manufacturer's recommended continuous use temperature limit of 2,300°F[8]. There is no lower temperature limit.

The polyethylene plastic wrap used as a protective sleeve around the ATR fuel element and ATR U-Mo demonstration element has a melting temperature of approximately 225 to 250°F[4]. For the purposes of this analysis, the lower limit of 225°F is used. As a thermoplastic, the polyethylene wrap will melt and sag onto the fuel element when exposed to temperatures in excess of 250°F. Further heating could lead to charring (i.e., oxidation in the absence of open combustion) and then thermal decomposition into its volatile components. Thermal decomposition will begin at approximately 750°F. Unpiloted, spontaneous ignition could occur at temperatures of

---

[13] *Heat Transfer in Window Frames with Internal Cavities*, PhD Thesis for Arild Gustavsen, Norwegian University of Science and Technology, Trondheim, Norway, September 2001.

[14] American Society of Mechanical Engineers (ASME) Boiler & Pressure Vessel Code, Section III, *Rules for Construction of Nuclear Facility Components*, Division 1, Subsection NB, *Class 1 Components*, & Subsection NG, *Core Support Structures*, 2001 Edition, 2002 Addendum.

approximately 650°F[15] or higher. The plastic wrap is approximately 7 inches wide (when pressed flat), 67.5 inches long, and weights approximately 3 oz. As demonstrated in Section 3.5.3, *Thermal Decomposition/Combustion of Package Organics*, the available oxygen in the package is sufficient for consumption of less than 1% of the polyethylene. Loss of the plastic wrap is of no consequence to the thermal safety of the ATR FFSC since its effect on conductive and radiative heat transfer is negligible.

The neoprene rub strips used to minimize fretting of the fuel element side plates have a continuous temperature rating of 200 to 250°F and a short term (i.e., 0.5 hour or less) temperature limit of approximately 525°F [16]. For the purposes of this analysis, a limit of 225°F is used for NCT conditions, while a peak temperature of 525°F is assumed for HAC conditions before thermal degradation begins. Since neoprene is a thermoset polymer, it will not melt, but decompose into volatiles as it degrades. The same limitation on oxygen affecting the combustion of polyethylene also affects neoprene. As discussed in Section 3.5.3, *Thermal Decomposition/Combustion of Package Organics*, the thermal damage expected for the neoprene material is expected to be limited to potential de-bonding from the FHE surfaces and a very limited thermal decomposition. Loss of the neoprene rub strips is of no consequence to the thermal safety of the ATR FFSC.

The minimum allowable service temperature for all ATR FFSC components is below -40 °F.

---

[15] Troitzsch, J., *Plastics Flammability Handbook*, 2nd Edition, Oxford University Press, New York, 1990.

[16] Parker O-Ring Handbook, ORD 5700/USA, 2001, www.parker.com.

Table 3.2-1 – Thermal Properties of Package Metallic Materials

Material	Temperature (°F)	Thermal Conductivity (Btu/hr-ft-°F)	Specific Heat (Btu/lb$_m$-°F)	Density (lb$_m$/in^3)
Stainless Steel Type 304	70	8.6	0.114	0.289
	100	8.7	0.115	
	200	9.3	0.119	
	300	9.8	0.123	
	400	10.4	0.126	
	500	10.9	0.128	
	600	11.3	0.130	
	700	11.8	0.132	
	800	12.2	0.133	
	1000	13.2	0.136	
	1200	14.0	0.138	
	1400	14.9	0.141	
	1500	15.3	0.142	
Aluminum Type 5052-H32	70	79.6	0.214	0.097
	100	80.8	0.216	
	150	82.7	0.219	
	200	84.4	0.222	
	250	85.9	0.225	
	300	87.2	0.227	
	350	88.4	0.229	
	400	89.6	0.232	
	1100 [1]	89.6	0.232	

Notes:

[1] Values for 1100°F are assumed equal to values at 400°F.

Table 3.2-2 – Thermal Properties of ATR Fuel Materials

Material	Temperature (°F)	Thermal Conductivity (Btu/hr-ft-°F)	Specific Heat (Btu/lb$_m$-°F)	Density (lb$_m$/in^3)
Aluminum Type 6061-0	32	102.3	-	0.0976
	62	-	0.214	
	80	104.0	-	
	170	107.5	-	
	260	109.2	0.225	
	350	109.8	-	
	440	110.4	0.236	
	530	110.4	-	
	620	109.8	0.247	
	710	108.6	-	
	800	106.9	0.258	
	890	105.2	-	
	980	103.4	0.269	
	1080	101.1	0.275	
ATR Fuel Plate 1[①]	80	60.5	0.177	0.114
	800		0.213	
ATR Fuel Plates 2 and 18[①]	80	78.5	0.189	0.108
	800		0.228	
ATR Fuel Plates 3,4,16 & 17[①]	80	76.2	0.182	0.112
	800		0.220	
ATR Fuel Plates 5 to 15[①]	80	74.6	0.176	0.115
	800		0.212	
ATR Fuel Plate 19[①]	80	54.5	0.173	0.115
	800		0.209	

Notes:

① Values determined based on composite value of aluminum cladding and fuel core material (see Appendix 3.5.2.4). Thermal conductivity value is valid for axial and circumferential heat transfer within fuel plate.

Table 3.2-3 – Thermal Properties of Non-Metallic Materials

Material	Temperature (°F)	Thermal Conductivity (Btu/hr-ft-°F)	Specific Heat (Btu/lb$_m$-°F)	Density (lb$_m$/ft^3)	Comments
Neoprene[1]	---	0.11	0.52	76.8	
Ceramic Fiber Insulation[2]	70	0.0196	0.28	6	
	200	0.0238			
	400	0.0343			
	600	0.0499			
	800	0.0703			
	1000	0.0958			
	1200	0.1262			
	1400	0.1614			
	1600	0.2017			
Ceramic Fiber Insulation[2] [3]	70	0.0300	0.28	8	
	200	0.0313			
	400	0.0369			
	600	0.0463			
	800	0.0620			
	1000	0.0814			
	1200	0.1053			
	1400	0.1340			
	1600	0.1669			

Notes:

[1] Conductivity value represents uncompressed neoprene.

[2] Conductivity values are for uncompressed insulation. Compression of the material will increase the thermal conductivity for temperatures below approximately 500°F where conduction dominates and decrease the thermal conductivity for temperatures above 500°F where heat transfer via radiation dominates.

[3] 8 pcf ceramic fiber insulation is not used in the ATR FFSC Package. Data is provided for comparison purposes to demonstrate the effect of insulation compression on thermal conductivity.

Table 3.2-4 – Thermal Properties of Air

Temperature (°F)	Density lb_m/in^3) [1]	Specific Heat $(Btu/lb_m$-°F)	Dynamic Viscosity $(lb_m$/ft-hr)	Thermal Conductivity (Btu/hr-ft-°F)	Prandtl Number [2]	Coef. Of Thermal Exp. $(°R^{-1})$ [3]
-40		0.240	0.03673	0.0121		
0		0.240	0.03953	0.0131		
50		0.240	0.04288	0.0143		
100		0.241	0.04607	0.0155		
200		0.242	0.05207	0.0178		
300		0.243	0.05764	0.0199		
400	Use Ideal Gas Law w/ Molecular wt = 28.966	0.245	0.06286	0.0220	Compute as $Pr = c_p\mu / k$	Compute as $\beta = 1/(°F+459.67)$
500		0.248	0.06778	0.0240		
600		0.251	0.07242	0.0259		
700		0.253	0.07680	0.0278		
800		0.256	0.08098	0.0297		
900		0.259	0.08500	0.0315		
1000		0.262	0.08887	0.0333		
1200		0.269	0.09620	0.0366		
1400		0.274	0.10306	0.0398		
1500		0.277	0.10633	0.0412		

Table Notes:

1) Density computed from ideal gas law as $\rho = PM/RT$, where R= 1545.35 ft-lbf/lb-mole-R, T= temperature in °R, P= pressure in lbf/ft^2, and M= molecular weight of air. For example, at 100°F and atmospheric pressure of $14.69 lbf/in^2$, $\rho = (14.69*144$ $in^2/ft^2*28.966$ lbm/lb-mole)$/1545.35*(100+459.67) = 0.071$ $lbm/ft^3 = 4.099 \times 10^{-5}$ lbm/in^3.

2) Prandtl number computed as $Pr = c_p\mu / k$, where c_p = specific heat, μ = dynamic viscosity, and k = thermal conductivity. For example, at 100°F, $Pr = 0.241*0.04607/0.0155 = 0.72$.

3) Coefficient of thermal expansion is computed as the inverse of the absolute temperature. For example, at 100°F, $\beta = 1/(100+459.67) = 0.00179$.

Table 3.2-5 – NCT Thermal Radiative Properties

Material	Assumed Conditions	Assumed Emissivity (ε)	Absorptivity (α)
Outer Shell, Exterior Surfaces (Type 304 Stainless Steel)	Weathered	0.45	0.52
Outer Shell, Interior Surface and Inner Shell (Type 304 Stainless Steel)	'As- Received'	0.3	---
Ceramic Fiber Insulation & Neoprene	---	0.90	---
Fuel Handling Enclosure and Loose Fuel Plate Basket (6061-T651 &5052-H32 Aluminum)	Oxidized	0.25	---
ATR Fuel Side Plates and Fuel Cladding (6061-0 Aluminum)	Boehmite film	0.92	---
Ambient Environment	---	1.00	N/A

Table 3.2-6 – HAC Thermal Radiative Properties

Material	Assumed Conditions	Assumed Emissivity (ε)	Absorptivity (α)
Outer Shell, Exterior Surfaces (Type 304 Stainless Steel)	Sooted/Oxidized	0.80	0.90
Outer Shell, Interior Surface and Inner Shell (Type 304 Stainless Steel)	Slightly Oxidized	0.45	---
Ceramic Fiber Insulation & Neoprene	---	0.90	---
Fuel Handling Enclosure and Loose Fuel Plate Basket (6061-T651 &5052-H32 Aluminum)	Oxidized	0.25	---
ATR Fuel Side Plates and Fuel Cladding (6061-0 Aluminum)	Boehmite film	0.92	---
Ambient Environment	---	1.00	N/A

3.3 Thermal Evaluation for Normal Conditions of Transport

This section presents the thermal evaluation of the ATR FFSC for normal conditions of transport (NCT). Under NCT, the package will be transported horizontally. This establishes the orientation of the exterior surfaces of the package for determining the free convection heat transfer coefficients and insolation loading. While the package would normally be transported in tiered stacks of multiple packages, the evaluation for NCT is conservatively based on a single, isolated package since this approach will yield the bounding maximum and minimum temperatures achieved by any of the packages. Further, the surface of the transport trailer is conservatively assumed to prevent heat exchange between the package and the ambient. Thus, the bottom of the ATR FFSC is conservatively treated as an adiabatic surface.

The details of the thermal modeling used to simulate the ATR FFSC package under NCT conditions are provided in Appendix 3.5.2, *Analytical Thermal Model*.

3.3.1 Heat and Cold

3.3.1.1 Maximum Temperatures

The maximum temperature distribution for the ATR FFSC occurs with a diurnal cycle for insolation loading and an ambient air temperature of 100°F, per 10 CFR §71.71(c)(1). The evaluation of this condition is conducted as a transient using the thermal model of an undamaged ATR FFSC described in Appendix 3.5.2.1, *Description of Thermal Model for NCT Conditions*. Figure 3.3-1 and Figure 3.3-2 illustrate the expected heat-up transient for an ATR FFSC loaded with an ATR fuel element. The transient analysis assumes a uniform temperature condition of 70°F for all components prior to loading and exposure to the specified NCT condition at time = 0. The figures demonstrate that the ATR FFSC package will respond rapidly to changes in the level of insolation and will reach it peak temperatures within the first day or two after loading. Table 3.3-1 presents the maximum temperatures reached for various components of the package. As seen from the table, all components are within in their respective temperature limits. Figure 3.3-3 illustrates the predicted temperature distribution within the ATR FFSC package at the time of peak temperature.

The maximum temperature distribution for the ATR FFSC without insolation loads occurs with an ambient air temperature of 100°F. Since the package payload dissipates essentially zero watts of decay heat, the thermal analysis of this condition represents a trivial case and no thermal calculations are performed. Instead, it is assumed that all package components achieve the 100°F temperature under steady-state conditions. The resulting 100°F package skin temperature is below the maximum temperature of 122°F permitted by 10 CFR §71.43(g) for accessible surface temperature in a nonexclusive use shipment.

The ATR FFSC with the ATR U-Mo demonstration element payload is not specifically modeled as part of this evaluation. Instead, its thermal performance is estimated using a qualitative approach based on the thermal characteristics of the other payloads and their associated thermal performance (see Section 3.5.2.5, *Thermal Properties for ATR U-Mo Demonstration Element* for details). Using this approach, it is estimated that the maximum temperatures attained for the transportation of the ATR U-Mo demonstration element are considered bounded by the analysis of the ATR fuel element and no additional analysis is required.

3.3.1.2 Minimum Temperatures

The minimum temperature distribution for the ATR FFSC occurs with a zero decay heat load and an ambient air temperature of -40°F per 10 CFR §71.71(c)(2). The thermal analysis of this condition also represents a trivial case and no thermal calculations are performed. Instead, it is assumed that all package components achieve the -40°F temperature under steady-state conditions. As discussed in Section 3.2.2, *Technical Specifications of Components*, the -40°F temperature is within the allowable operating temperature range for all ATR FFSC package components.

3.3.2 Maximum Normal Operating Pressure

The payload cavity of the ATR FFSC is vented to the atmosphere. As such, the maximum normal operating pressure (MNOP) for the package is 0 psig.

While the volume between the outer and inner shells is sealed, it does not contain organic or other materials that may outgas or thermally degrade. Therefore, the maximum pressure that may develop within the space will be limited to that achieved due to ideal gas expansion. Assuming a temperature of 70°F at the time of assembly and a maximum operating temperature of 190°F (based on the outer shell temperature, see Table 3.3-1, conservatively rounded up), the maximum pressure rise within the sealed volume will be less than 4 psi.

Table 3.3-1 - Maximum Package NCT Temperatures

Location / Component	NCT Hot Conditions	Maximum Allowable [1]
ATR Fuel Element Fuel Plate	147°F	400°F
ATR Fuel Element Side Plate	148°F	400°F
Neoprene Rub Strips/Polyethylene Bag	151°F [2]	225°F
Fuel Handling Enclosure (FHE)	151°F	400°F
Loose Fuel Plate Basket (LFPB)	151°F [2]	400°F
Inner Shell	157°F	800°F
Ceramic Fiber Insulation, Body - Maximum - Average	 185°F 151°F	 2,300°F 2,300°F
Ceramic Fiber Insulation, Closure - Maximum - Average	 145°F 144°F	 2,300°F 2,300°F
Closure	145°F	800°F
Outer Shell	186°F	800°F

Table Notes:

[1] The maximum allowable temperatures under NCT conditions are provided in Section 3.2.2, Technical Specifications of Components.

[2] Component temperature assumed to be equal to that of the FHE.
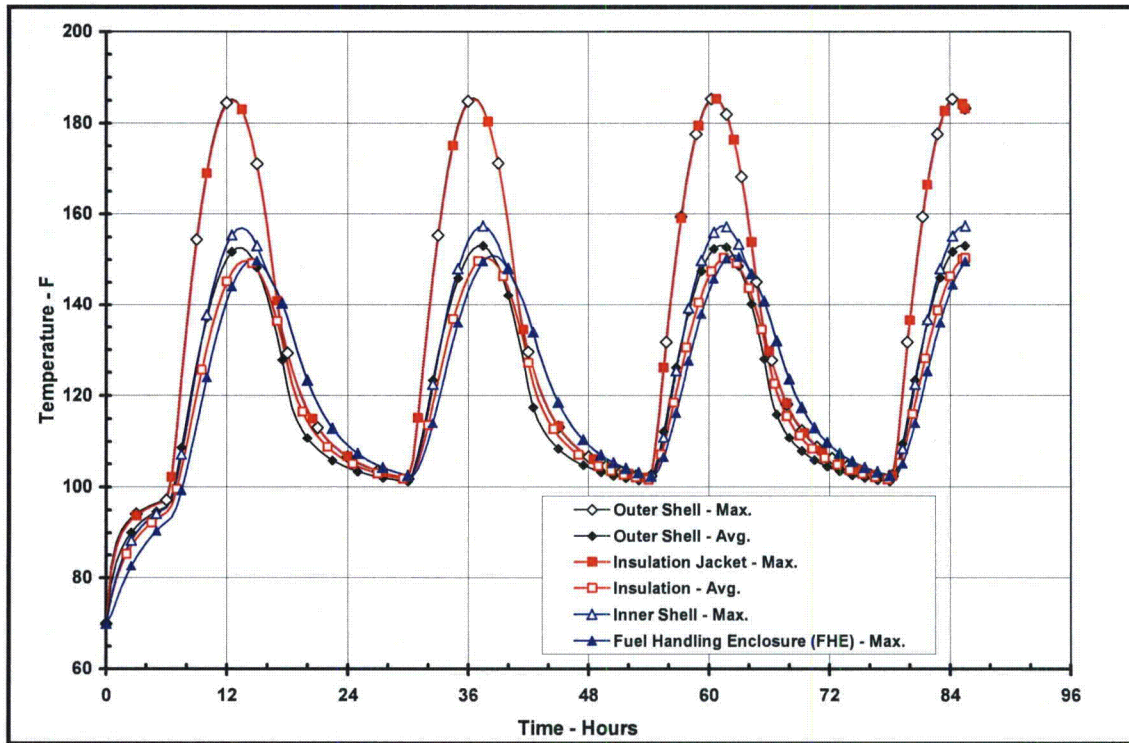
Figure 3.3-1 – ATR FFSC Package Heat-up, NCT Hot Conditions
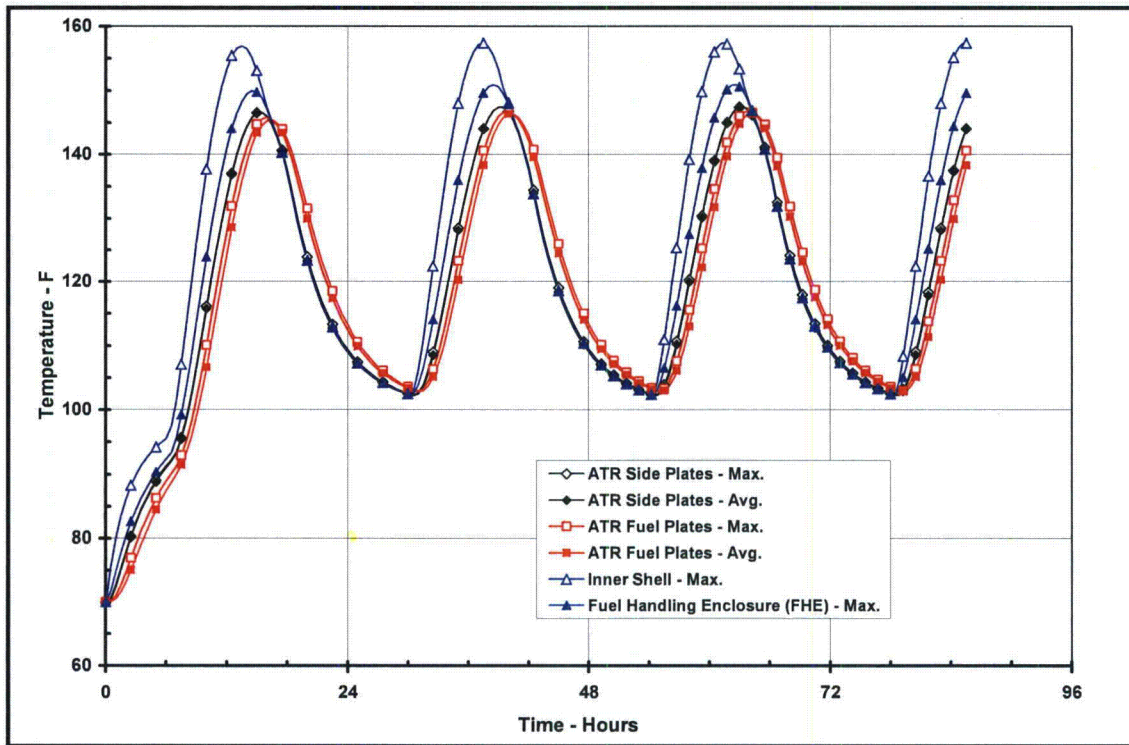
Figure 3.3-2 – ATR Fuel Element Heat-up, NCT Hot Conditions
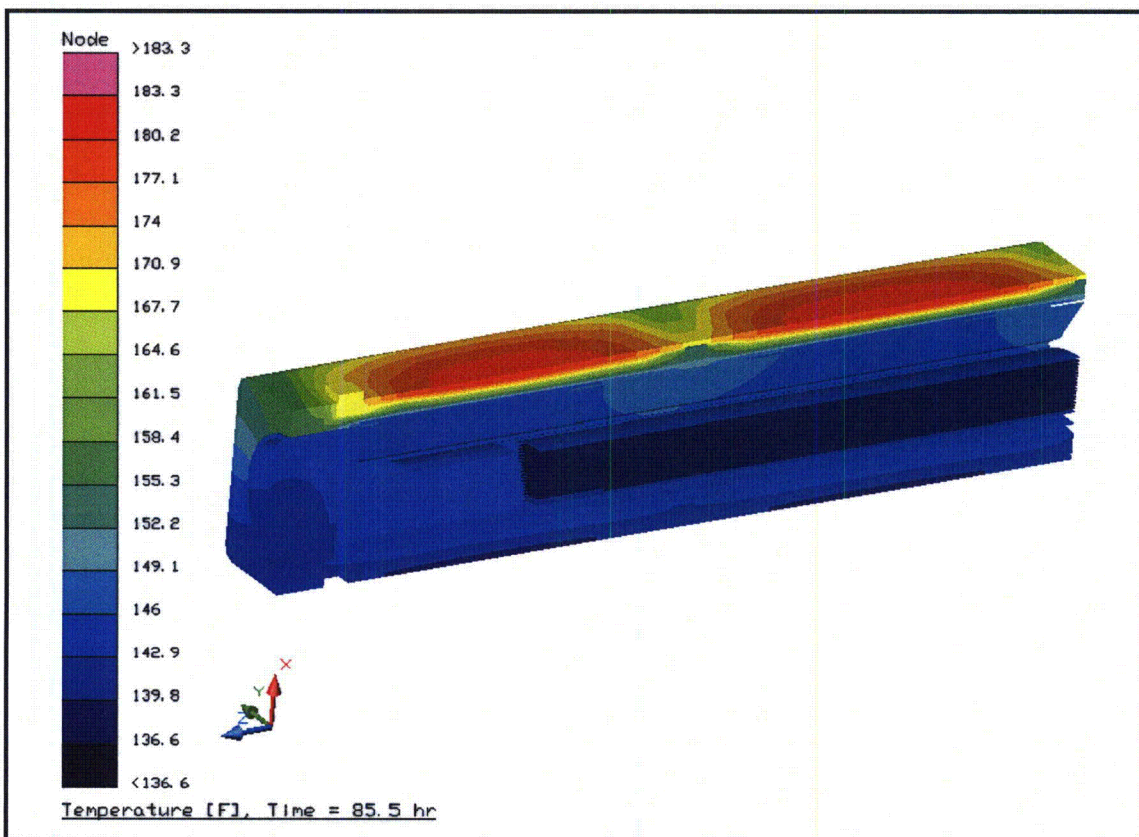
Figure 3.3-3 – Package NCT Temperature Distribution

3.4 Thermal Evaluation for Hypothetical Accident Conditions

This section presents the thermal evaluation of the ATR FFSC package under the hypothetical accident condition (HAC) specified in 10 CFR §71.73(c)(4) based on an analytical thermal model of the ATR FFSC. The analytical model for HAC is a modified version of the quarter symmetry NCT model described in Section 3.5.2.1, *Description of Thermal Model for NCT Conditions*, with the principal model modifications consisting of simulating the expected package damage resulting from the drop events that are assumed to precede the HAC fire and changing the package surface emissivities to reflect the assumed presence of soot and/or surface oxidization.

Physical testing using full scale certified test units (CTUs) is used to establish the expected level of damage sustained by the ATR FFSC package from the 10 CFR 71.73 prescribed free and puncture drops that are assumed to precede the HAC fire event. Appendix 2.12.1, *Certification Tests on CTU-1* and Appendix 2.12.2, *Certification Tests on CTU-2* provide the configuration and initial conditions of the test articles, the test facilities and instrumentation used, and the test results. Section 3.5.2.2, *Description of Thermal Model for HAC Conditions*, provides an overview of the test results, the rationale for selecting the worst-case damage scenario, and the details of the thermal modeling used to simulate the package conditions during the HAC fire event.

3.4.1 Initial Conditions

The initial conditions assumed for the package prior to the HAC event are described below in terms of the modifications made to the NCT thermal model to simulate the assumed package conditions prior to and during the HAC event. These modifications are:

- Simulated the worst-case damage arising from the postulated HAC free and puncture drops as described in Section 3.5.2.2, *Description of Thermal Model for HAC Conditions*,

- Assume an initial, uniform temperature distribution of 100°F based on a zero decay heat package at steady-state conditions with a 100°F ambient with no insolation. This assumption complies with the requirement of 10 CFR §71.73(b)[2] and NUREG-1609[17],

- Increased the emissivity of the external surfaces from 0.45 to 0.8 to account for possible soot accumulation on the surfaces, per 10 CFR §71.73(c)(4),

- Increased the emissivity of the interior surfaces of the outer shell from 0.30 to 0.45 to account for possible oxidization of the surfaces during the HAC event,

Following the free and puncture bar drops, the ATR FFSC package is assumed come to rest in a horizontal position prior to the initiation of the fire event. Since the package geometry is essentially symmetrical about its axial axis, there are no significant thermal differences whether the

---

[17] NUREG-1609, *Standard Review Plan for Transportation Packages for Radioactive Material*, §3.5.5.1, U.S. Regulatory Commission, Office of Nuclear Materials Safety and Standards, March 1999.

package is right-side up, up-side down, or even on its end. The potential for the ATR fuel element payload being re-positioned depending upon the package orientation is not significant to the peak temperatures developed under HAC conditions given the modeling approach used to compute the heat transfer from the inner shell to the ATR fuel element. Therefore, the peak package temperatures predicted under this evaluation are representative of those achieved for any package orientation.

3.4.2 Fire Test Conditions

The fire test conditions analyzed to address the 10 CFR §71.73(c) requirements are as follows:

- The initial ambient conditions are assumed to be 100°F ambient with no insolation,

- At time = 0, a fully engulfing fire environment consisting of a 1,475°F ambient with an emissivity of 1.0 is used to simulate the hydrocarbon fuel/air fire event. The assumption of a flame emissivity of 1.0 bounds the minimum average flame emissivity coefficient of 0.9 specified by 10 CFR §71.73(c)(4),

- The convection heat transfer coefficients between the package and the ambient during the 30-minute fire event are based on an average gas velocity[18] of 10 m/sec. Following the 30-minute fire event the convection coefficients are based on still air,

- The ambient condition of 100°F with insolation is assumed following the 30-minute fire event. Since a diurnal cycle is used for insolation, the evaluation assumes that the 30-minute fire begins at noon so as to maximize the insolation heating during the post-fire cool down period. A solar absorptivity of 0.9 is assumed for the exterior surfaces to account for potential soot accumulation on the package surfaces.

The transient analysis is continued for 11.5 hours after the end of the 30-minute fire to ensure that the peak package temperatures are captured.

3.4.3 Maximum Temperatures and Pressure

3.4.3.1 Maximum HAC Temperatures

The outer shell and the ceramic fiber insulation provide thermal protection to the ATR FFSC package during the HAC fire event. The level of thermal protection can be seen via the thermal response curves presented in Figure 3.4-1 and Figure 3.4-2. As illustrated in the figures, while the exterior of the package quickly rises to nearly the temperature of the fire, the heat flow to the FHE and its enclosed ATR fuel element payload is sufficiently restricted that the maximum temperatures of both the FHE and the ATR fuel element are well below the melting point of aluminum. This result occurs despite the conservative assumption of direct contact between the FHE and the inner shell at 3 locations (e.g., the equivalent of four locations for a full model).

---

[18] Schneider, M.E and Kent, L.A., *Measurements Of Gas Velocities And Temperatures In A Large Open Pool Fire, Heat and Mass Transfer in Fire* - HTD Vol. 73, 1987, ASME, New York, NY.

This level of thermal protections is further illustrated by the perspective views presented in Figure 3.4-3 and Figure 3.4-4 of the temperature distribution in the ATR FFSC package after 30 minutes of exposure to the HAC fire and at the point when the peak ATR fuel element temperature is attained (approximately 22 minutes after the end of the fire). The figures show that the ceramic fiber insulation limits the elevated temperatures resulting from the fire event to regions adjacent to the outer shell. The assumed absence of the ceramic fiber insulation adjacent to the ribs as a result of the pre-fire free drop event can be seen in each figure.

A similar thermal performance is seen for the package when loaded with the Loose Fuel Plate Basket (LFPB). Figure 3.4-5 presents the thermal response curve, while Figure 3.4-6 and Figure 3.4-7 present perspective views of the temperature distribution in the ATR FFSC package after 30 minutes of exposure to the HAC fire and at the point when the peak LFPB temperature is attained (approximately 22 minutes after the end of the fire). A lower maximum temperature is achieved in the LFPB vs. that seen for the FHE because of the higher thermal mass associated with the LFPB. Further, since the LFPB is modeled without its payload of loose fuel plates, these results will bound those seen for a LFPB with a payload.

Table 3.4-1 presents the component temperatures seen prior to the fire, at the end of the 30-minute fire event, and the peak temperature achieved during the entire simulated HAC thermal event. As seen, all temperatures are within their allowable limit. It is expected that the neoprene rub strips and the polyethylene bag used as a protective sleeve for the ATR fuel element will thermally degrade due to the level of temperature achieved. In the case of the polyethylene bag, the bag is expected to melt and sag onto the fuel element when exposed to temperatures in excess of 250°F. Further heating will lead to charring and then thermal decomposition into its volatile components. While spontaneous ignition is unexpected under the unpiloted conditions, the effect would be minimal since, per Section 3.5.3, *Thermal Decomposition/Combustion of Package Organics*, the available oxygen in the package is sufficient for consumption of less than 1% of the polyethylene. As a thermoset polymer, the neoprene is expected to simply decompose into volatiles as it thermally degrades. These components are not critical to the safety of the package and any out-gassing associated with their thermal degradation will not contribute to package pressurization since package is vented.

As with the evaluation for NCT, the thermal performance of the ATR FFSC with the ATR U-Mo demonstration element payload under HAC conditions is not specifically modeled as part of this evaluation. Instead, its thermal performance is estimated using a qualitative approach based on the thermal characteristics of the other payloads and their associated thermal performance (see Section 3.5.2.5, *Thermal Properties for ATR U-Mo Demonstration Element*, for details). Using this approach, it is estimated that the maximum temperatures attained for the transportation of the ATR U-Mo demonstration element are considered bounded by the analysis of the ATR fuel element and no additional analysis is required.

3.4.3.2 Maximum HAC Pressures

The payload cavity of the ATR FFSC is vented to the atmosphere. As such, the maximum pressure achieved under the HAC event will be 0 psig. Section 3.5.3, *Thermal Decomposition/Combustion of Package Organics*, provides the justification for assuming a 0 psig package pressure for the HAC event.

Although the volume between the outer and inner shells is sealed, it does not contain organic or other materials that may outgas or thermally degrade. Assuming a temperature of 70°F at the time of assembly and a maximum temperature of 1,475°F (based on the outer shell temperature, see Table 3.4-1), the maximum pressure rise within the sealed volume due to ideal gas expansion will be less than 39 psig. This level of pressurization will occur for only a few minutes and then quickly reduce as the package cools.

3.4.4 Maximum Thermal Stresses

The temperature difference between the inner and outer shells during the HAC event (see the average inner and outer shell temperatures presented in Figure 3.4-1) will result in differential thermal expansion between the shells. This differential thermal expansion is expected to peak at approximately 6 minutes after the initiation of fire exposure when the average outer shell temperature is 1,344°F and the average inner shell temperature is 196°F. Based on the differential thermal expansion for Type 304 stainless steel[19] the change in length is computed as:

$$DTE = \Delta L_{OuterShell} - \Delta L_{InnerShell} = [\alpha_{OS}(T_{OS} - 70) - \alpha_{IS}(T_{IS} - 70)]L = 0.9 \; inches$$

where:

$\alpha_{OS} = 10.7(10^{-6})$ in/in/°F at 1,300 °F
$\alpha_{IS} = 8.9(10^{-6})$ in/in/°F at 200 °F
$T_{OS} = 1,344$ °F
$T_{IS} = 196$ °F
$L = 73$ inches (conservatively for both shells)

After 6 minutes of exposure to the fire the difference in shell lengths will decrease as the inner shell heats up. The differential expansion will reach 0-inches approximately 6 minutes after the end of the fire event when the inner and outer shells reach thermal equilibrium and then go negative as the outer shell continues to cool faster than the inner shell. The largest negative thermal differential expansion achieved is approximately 0.22-inches.

The result of this variation in differential thermal expansion may take one of three forms:
1) the outer shell buckles outward,
2) the outer shell buckles inward, or
3) the weld attaching the inner shell to either the closure plate or the bottom end plate will fail and permit the outer shell and the affected plate to move freely.

While in reality, a square tube is likely to buckle inward on two of the four faces and outward on the remaining two faces simultaneously, the two buckling modes are treated independently for the purposes of this evaluation. The possibility of the outer shell buckling outwards is the assumption upon which the thermal modeling presented in Section 3.5.2.2, *Description of Thermal Model for HAC Conditions* is based. This mode is seen as likely given the level of metal softening that will occur with the outer shell quickly reaching over 1,200°F and the expected pressurization of the void space between the inner and outer shells. Buckling the outer

---

[19] American Society of Mechanical Engineers (ASME) Boiler and Pressure Vessel Code, Section II, *Materials, Part D – Properties*, 2001 Edition, 2002 and 2003 Addenda, New York ,Table TE-1, Group 3. Coefficient B = 8.9x10⁻⁶ inches/inch/°F at 200°F and 10.7x10⁻⁶ inches/inch/°F at 1,300°F.

shell in this fashion will act to lower the rate of inward heat transfer. As such, ignoring the outer shell's displacement due to differential thermal expansion, as assumed by the HAC thermal modeling, yields conservatively high package temperatures.

The second possibility is that the outer shell buckles inward under the differential thermal expansion. Should this occur, the maximum deflection would be 0.9-inches/2 = 0.45-inches assuming a zero length deflection and only one buckle along the length of the outer shell. In reality, the actual deflection would measure perhaps 0.33-inches after properly accounting for the curvature in the buckled section. Since this level of deflection would still leave 0.5-inches or more of insulation separating the inner shell from the outer shell, no significant impact on the predicted peak HAC temperatures will occur.

The final possibility which the differential thermal expansion may manifest itself is in the failure of the one of the welds attaching the inner shell to the closure and bottom end plates. If this occurs, besides releasing any potential pressure buildup in the void between the inner and outer shells, the outer shell and the associated end plate will extend away from the inner shell at the point of the weld failure. The size of the gap will maximize at about 0.9-inches and then decrease. Since the insulation jacket is cut out to fit around the hardware used to index the packages to one another, the insulation jacket and the underlying insulation will be pulled in the same direction as the outer shell, thus preventing the creation of a gap between the interface of the insulation wrap and the end plate. Even if such a gap would occur, no direct exposure of cavity within the inner shell to the outer shell surfaces will result since the closure plugs at each end of the package are longer than the predicted movement under differential thermal expansion. Instead, the likely and worst case scenario is that the movement of the outer shell, the insulation jacket, and the insulation will create a gap of approximately 0.9-inches at the interface between the first support rib and the insulation. Combining this gap with an insulation shift of up to 1.75-inches at this same locations due to a pre-fire, 30-foot end drop (see Section 3.5.2.2, *Description of Thermal Model for HAC Conditions*) could result in a scenario where there is a 0.9-inch gap between the support rib and the insulation jacket and up to a 0.9 + 1.75 = 2.65-inch gap between the support rib and the end of the insulation wrap. A sensitivity thermal analysis of this geometry showed that the peak inner shell temperature reported in Table 3.4-1 remained bounding, while the maximum temperature of the ATR fuel element increased by less than 25°F. This modest change in temperature occurs because there is little difference in temperature between the outer shell and the stainless steel insulation wrap. Since this level of temperature increase is well within the thermal margins apparent from Table 3.4-1, the potential thermal impact due to the package geometry displacement under differential thermal expansion is seen as being not significant to the safety of the package.

Table 3.4-1 – HAC Temperatures

Location / Component	Pre-fire	End of Fire	Peak	Maximum Allowable [1]
ATR Fuel Element Fuel Plate	100°F	586°F	730°F	1,100°F
ATR Fuel Element Side Plate	100°F	676°F	827°F	1,100°F
Neoprene Rub Strips/ Polyethylene Bag	100°F	1,016°F	1,017°F	N/A
Fuel Handling Enclosure (FHE)	100°F	1,016°F	1,017°F	1,100°F
Loose Fuel Plate Basket (LFPB)	100°F	584°F	746°F	1,100°F
Inner Shell	100°F	1,422°F	1,422°F	2,700°F
Ceramic Fiber Insulation, Body - Maximum - Average	100°F 100°F	1,460°F 1,220°F	1,460°F 1,220°F	2,300°F 2,300°F
Ceramic Fiber Insulation, Closure - Maximum - Average	100°F 100°F	1,418°F 1,297°F	1,418°F 1,297°F	2,300°F 2,300°F
Closure	100°F	1,445°F	1,445°F	2,700°F
Outer Shell	100°F	1,471°F	1,471°F	2,700°F

Table Notes:

[1] The maximum allowable temperatures under HAC conditions are provided in Section 3.2.2, Technical Specifications of Components.
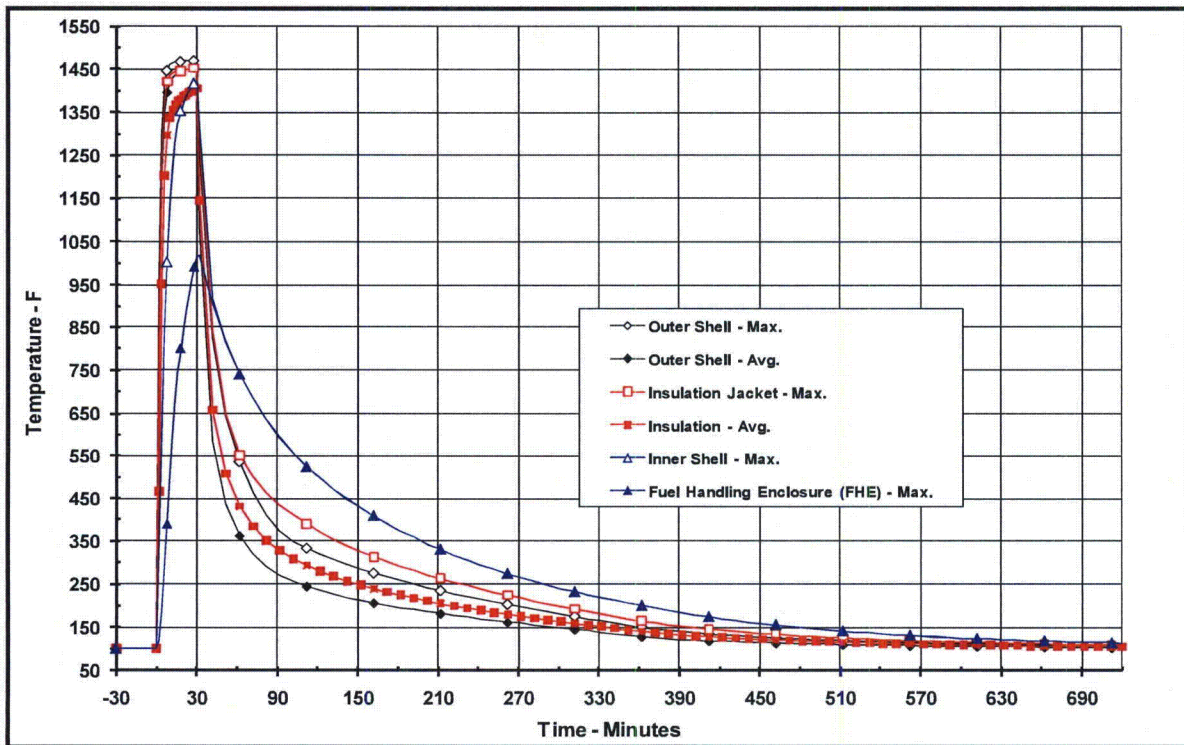
Figure 3.4-1 – ATR FFSC Package Thermal Response to HAC Event
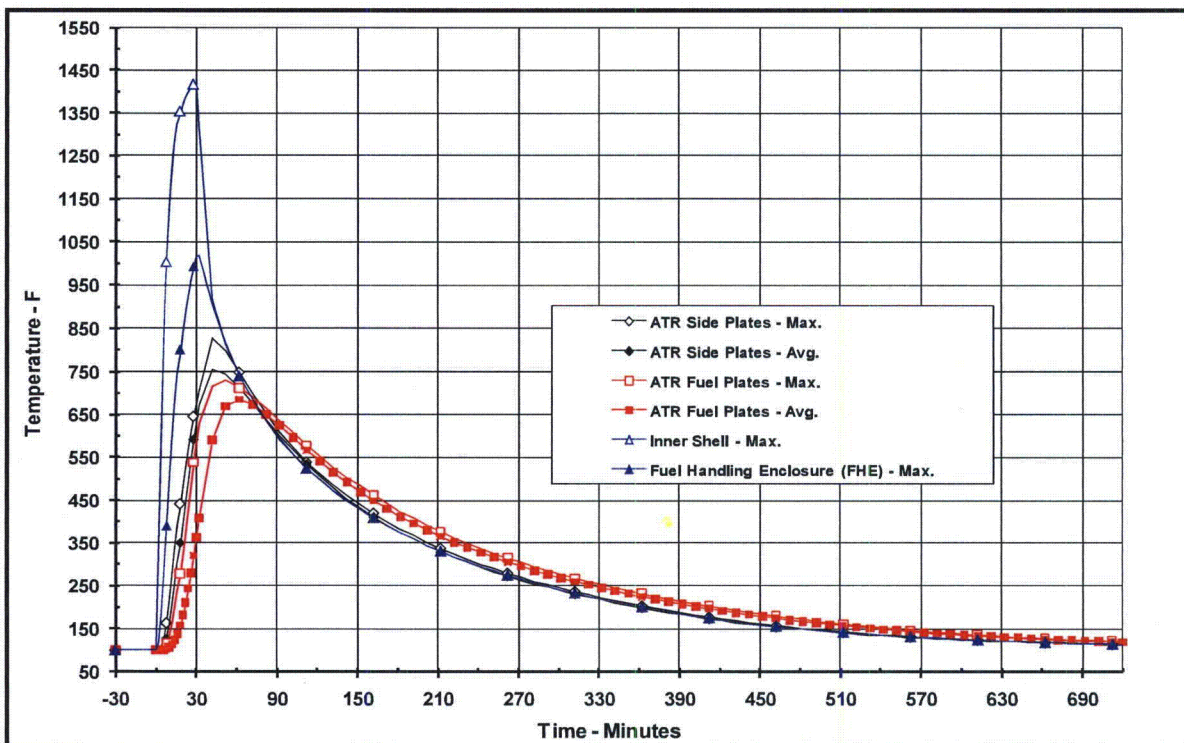
Figure 3.4-2 – ATR Fuel Element Thermal Response to HAC Event
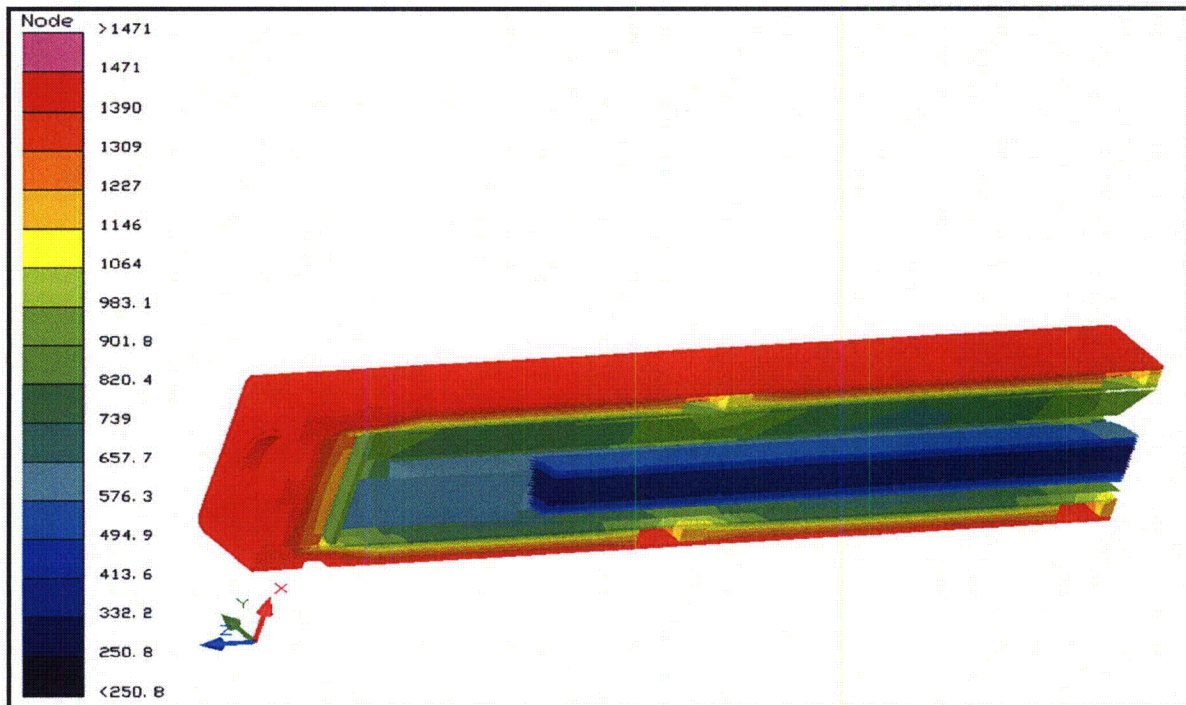
(Note: the positive x-axis is oriented towards the top of the package and the positive z-axis towards the package closure end)

Figure 3.4-3 –Temperature Distribution at End of HAC 30-Minute Fire
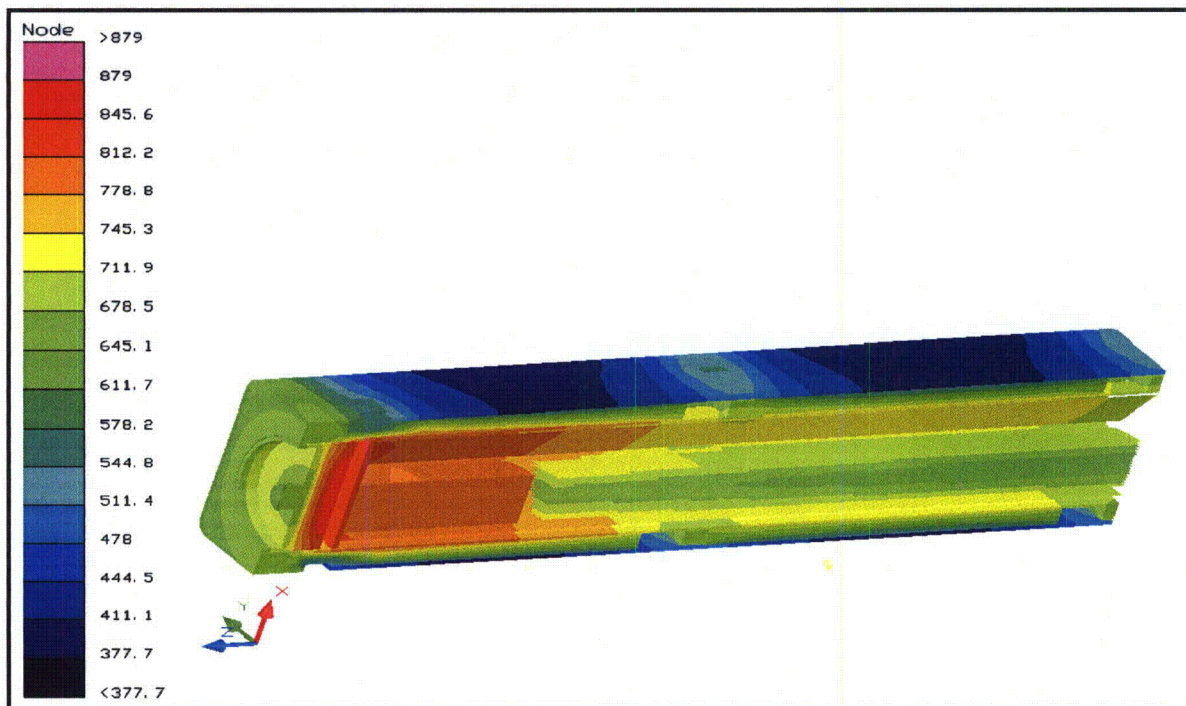
(Note: the positive x-axis is oriented towards the top of the package and the positive z-axis towards the package closure end)

Figure 3.4-4 –Temperature Distribution at Peak ATR Fuel Element Temperature
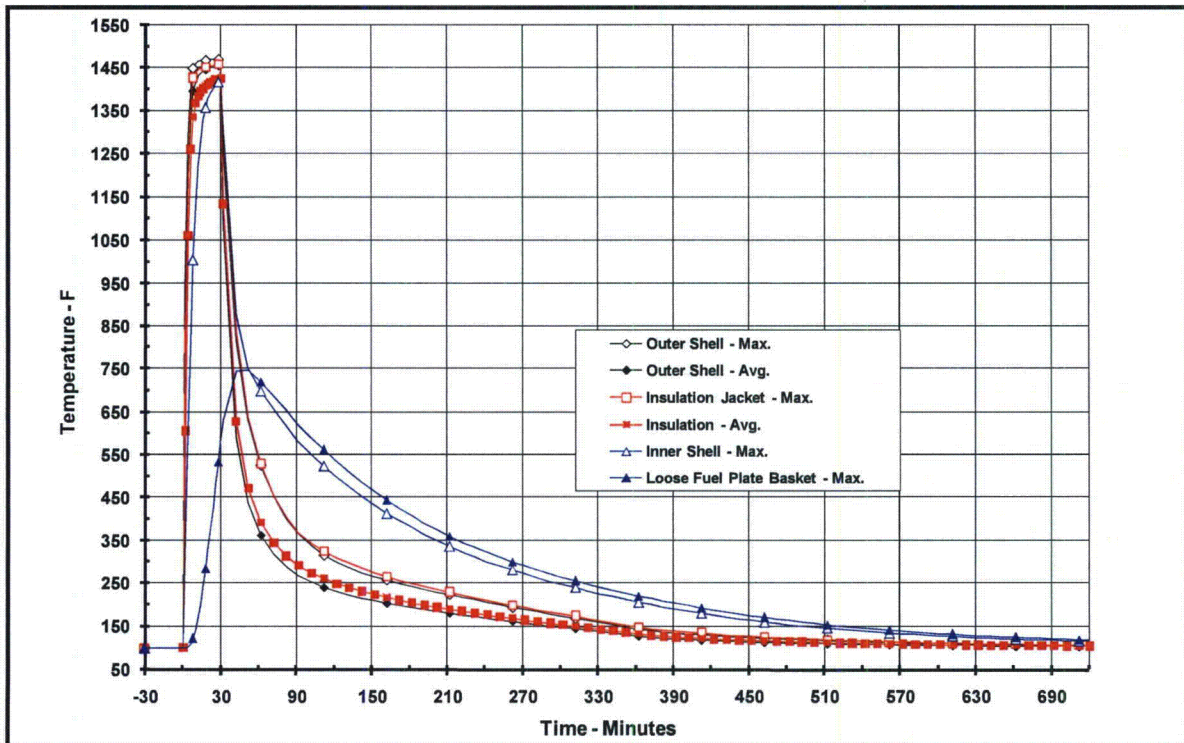
Figure 3.4-5 – ATR FFSC Package with LFPB Thermal Response to HAC Event
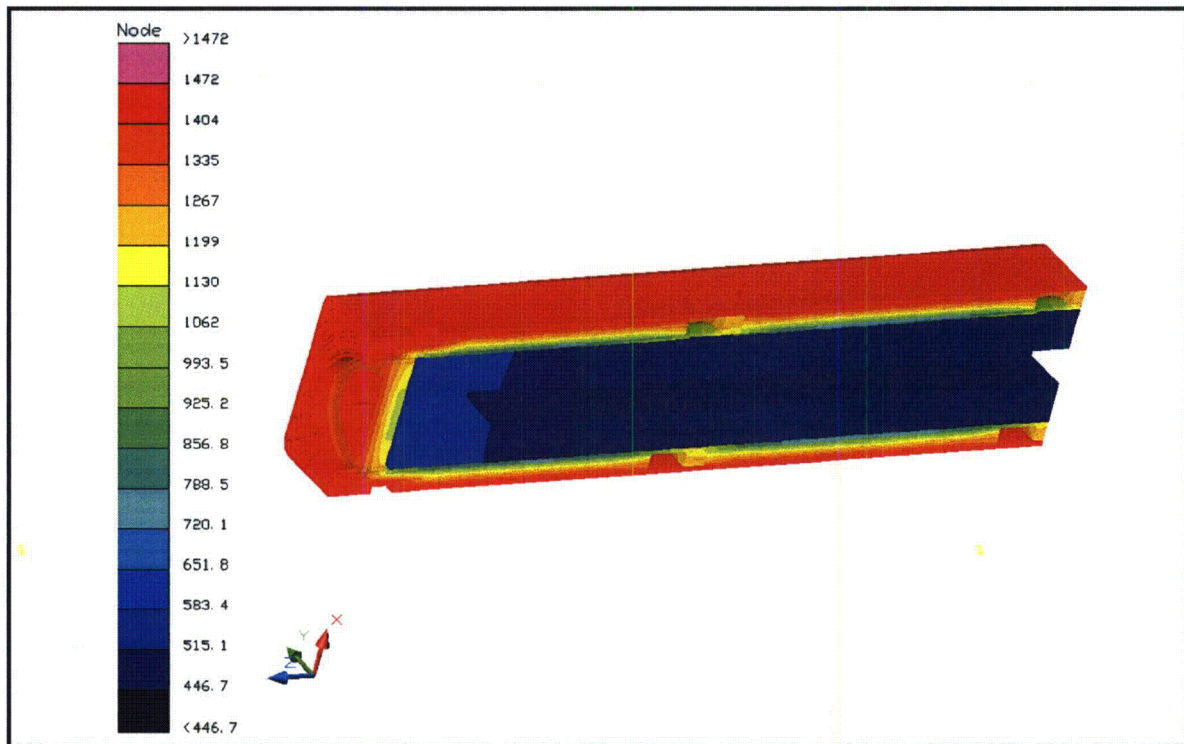
(Note: the positive x-axis is oriented towards the top of the package and the positive z-axis towards the package closure end)

Figure 3.4-6 – FFSC-LFPB Temperature Distribution at End of HAC Fire
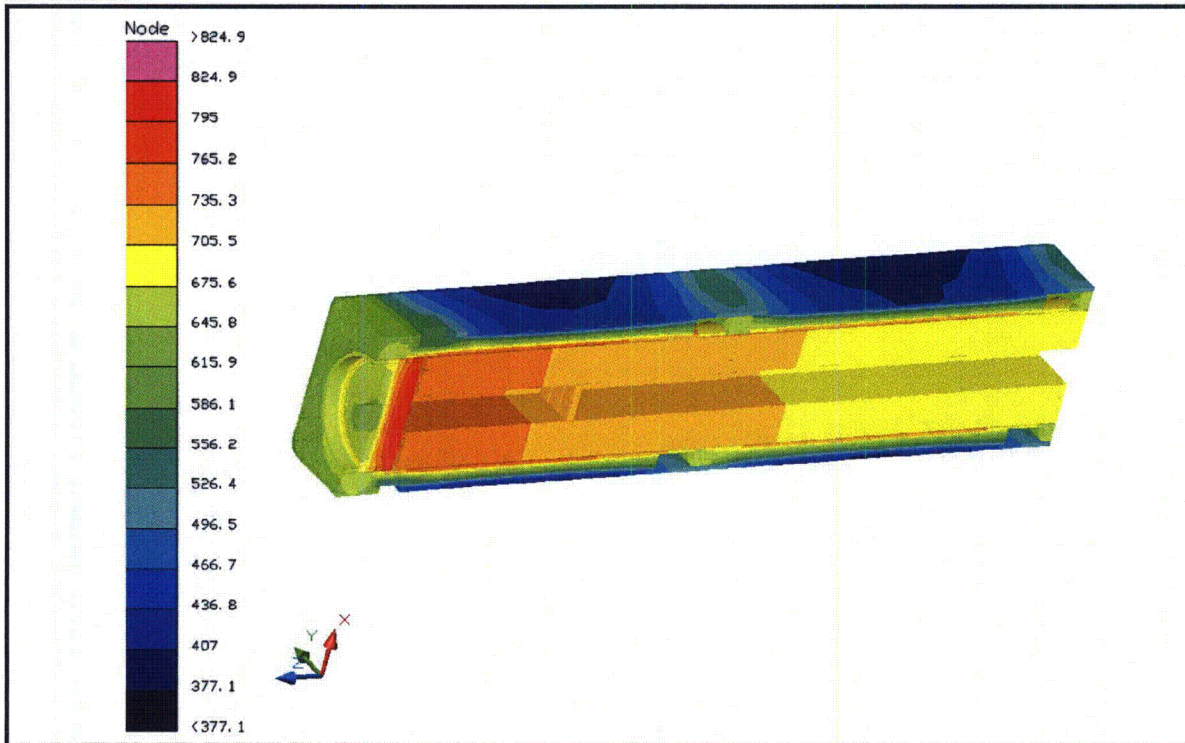
(Note: the positive x-axis is oriented towards the top of the package and the positive z-axis towards the package closure end)

Figure 3.4-7 – FFSC-LFPB Temperature Distribution at Peak LFPB Temperature

3.5 Appendices

3.5.1   Computer Analysis Results

3.5.2   Analytical Thermal Model

3.5.3   Combustion/Decomposition of Package Organics

3.5.1 Computer Analysis Results

Due to the size and number of the output files associated with each analyzed condition, results from the computer analysis are provided on a CD-ROM.

3.5.2 Analytical Thermal Model

The analytical thermal model of the ATR FFSC package was developed for use with the Thermal Desktop[20] and SINDA/FLUINT[21] computer programs. These programs are designed to function together to build, exercise, and post-process a thermal model. The Thermal Desktop® computer program is used to provide graphical input and output display function, as well as computing the radiation exchange conductors for the defined geometry and optical properties. Thermal Desktop® is designed to run as an AutoCAD® application. As such, all of the CAD tools available for generating geometry within AutoCAD® can be used for generating a thermal model. In addition, the use of the AutoCAD® layers tool presents a convenient means of segregating the thermal model into its various elements.

The SINDA/FLUINT computer program is a general purpose code that handles problems defined in finite difference (i.e., lumped parameter) and/or finite element terms and can be used to compute the steady-state and transient behavior of the modeled system. Although the code can be used to solve any physical problem governed by diffusion-type equations, specialized functions used to address the physics of heat transfer and fluid flow make the code primarily a thermal code.

The SINDA/FLUINT and Thermal Desktop® computer programs have been validated for safety basis calculations for nuclear related projects[22,23].

Together, the Thermal Desktop® and SINDA/FLUINT codes provide the capability to simulate steady-state and transient temperatures using temperature dependent material properties and heat transfer via conduction, convection, and radiation. Complex algorithms may be programmed into the solution process for the purposes of computing heat transfer coefficients as a function of the local geometry, gas thermal properties as a function of species content, temperature, and pressure, or, for example, to estimate the effects of buoyancy driven heat transfer as a function of density differences and flow geometry.

3.5.2.1 Description of Thermal Model for NCT Conditions

A 3-dimensional, one-quarter symmetry thermal model of the ATR FFSC is used for the NCT evaluation. The model simulates one-quarter of the package, extending from the closure to the

---

[20] Thermal Desktop®, Versions 4.8 and 5.1, Cullimore & Ring Technologies, Inc., Littleton, CO, 2005/2007.

[21] SINDA/FLUINT, *Systems Improved Numerical Differencing Analyzer and Fluid Integrator*, Versions 4.8 and 5.1, Cullimore & Ring Technologies, Inc., Littleton, CO, 2005/2007.

[22] *Software Validation Test Report for Thermal Desktop® and SINDA/FLUINT*, Versions 4.8 and 5.1, Packaging Technology, Inc., File No. TR-VV-05-001, Rev. 1 and Rev. 2.

[23] *Thermal Desktop® and SINDA/FLUINT Testing and Acceptance Report*, Version 5.1, AREVA Federal Services, LLC, File No. AFS-TR-VV-006, Rev. 0.

axial centerline of the package. Symmetry conditions are assumed about the package's vertical axis and at the axial centerline. This modeling choice captures the full height of the package components and allows the incorporation of the varying insolation loads that will occur at the top and sides of the package. Program features within the Thermal Desktop® computer program automatically compute the various areas, lengths, thermal conductors, and view factors involved in determining the individual elements that make up the thermal model of the complete assembly.

Figure 3.5-1 and Figure 3.5-2 illustrate the 'solid' and 'hidden line' views of the package thermal model. The model simulates one-half of the closure end half of the package (i.e., symmetry is assumed about the package's vertical plane) and extends approximately 36.5 inches in the axial direction (e.g., from closure to the mid-point of the center support rib). As seen from the figure, the modeling captures the various components of the packaging, including the index lug and mating pocket used to align the stacked packages, the recessed exterior surface area of the package closure, the FHE, and the ATR fuel element. Also captured, but not easily seen in the figure due to the scale of the figures, are the nineteen (19) individual fuel plates that comprise the ATR fuel element.

The model is composed of solid and plate type elements representing the various package components. Thermal communication between the various components is via conduction, radiation, and surface-to-surface contact. Since the ATR FFSC Package dissipates essentially no decay heat, the peak temperatures internal to the package are driven by the external heating occurring during NCT and HAC conditions. While the potential for developing convective flows within the air filled cavity between the outer shell and the insulation jacket is small due to the cavity dimensions, if convective heat transfer was to develop it could raise the peak temperatures developed under either NCT or HAC conditions since it would reduce the thermal resistance to heat flowing inward from the outer shell. To address this possibility, the thermal conductivity associated with the air overpack nodes in the lower quadrant of the package are increased by a factor of 2 from that for conduction as a means of simulating the type of enhanced heat transfer that convection would cause. The affected nodes are limited to those in the lower quadrant of the package since, in the assumed horizontal orientation of the package under both NCT and HAC conditions, the buoyancy forces associated with convection will tend to drive the flow in this portion of the package in a circular motion, but would only produce a stratified temperature layer in the upper quadrant.

A total of approximately 8,050 nodes, 2,800 planar elements, and 3,700 solid elements are used to simulate the modeled components. In addition, one boundary node is used to represent the ambient environment for convection purposes and a second boundary node is used to represent the ambient temperature for the purpose of radiation heat transfer.

Figure 3.5-3 and Figure 3.5-4 illustrate the quarter symmetry thermal models of the FHE and the ATR fuel element. The FHE thermal model uses planar elements to represent the 0.09 inch thick sides of the enclosure, while solid elements are used to represent the 0.25 inch thick end cap. Heat transfer between the FHE and the inner shell of the package is modeled as a combination of radiation and conduction across the air-filled void space, as well as via direct contact along 3 edges of the FHE. The contact conductance simulates the physical contact between an impact deformed FHE and the inner shell. Figure 3.5-5 illustrates a cross-section through the combined modeling for the inner shell, the FHE, and the ATR fuel element. The left side of the figure

illustrates the placement of the thermal nodes (indicated by the small circles) used to simulate each of the components, the use of curved elements to represent the 19 fuel plates, and the assumed points of direct contact between the FHE and the inner shell. The right side of the figure includes depiction of the solid elements that are used to simulate the air voids in and around the FHE. The heat transfer between the FHE and the ATR fuel element is computed as conductance through the 0.125 inch thick neoprene rub strips (see Figure 3.5-5) and radiation and conductance through the air voids.

The heat transfer due to direct contact conservatively assumes the FHE has been deformed as a result of the HAC drop event to create 'flat' areas measuring 0.5 inches wide at the lower 2 points of contact, 0.75 inches wide at the top, and extending the entire length of the FHE. Although this type of damage would only occur for the HAC condition (if it occurs at all), it is conservatively assumed for the NCT modeling as well. A conservatively high contact conductance[9] of 1 Btu/min-in^2-°F is assumed.

A detailed model of the ATR fuel element is used to simulate the heat transfer within the fuel element and between the fuel element and the FHE. The detailed thermal model, illustrated in Figure 3.5-4 and Figure 3.5-5, includes a separate representation of each composite fuel plate, the side plates (including the cutouts), and the upper end box casting. Heat transfer between the individual fuel plates is simulated via conduction and radiation across the air space separating the plates. The curvature and separation distance between the plates is based on the information presented in Section 3.5.2.4, *Determination of Composite Thermal Properties for ATR Fuel Plates*. Each quarter segment of the fuel plates is represented by four thermal nodes in the circumferential direction and 16 nodes along its length.

The thermal modeling for the Loose Fuel Plate Basket uses the same model for the ATR FFSC, but replaces the thermal modeling of the FHE and the ATR fuel element with the thermal modeling for the Loose Fuel Plate Basket depicted in Figure 3.5-6. Approximately 500 nodes, 280 planar elements, and 530 solids are used to simulate the basket. Since the payload for the basket may contain a variable number and size of fuel plates, the thermal modeling is based on an empty basket. This approach is conservative since the addition of a payload will serve to increase the thermal mass of the basket and, thus, reduce its temperature rise under the transient conditions associated with the HAC event. Since the unirradiated fuel plates have essentially zero decay heat, there will be no temperature rise between the loose fuel plates and the basket. As such, modeling of the loose fuel plate payload is both unnecessary and conservative for the purposes of this evaluation.

The ATR FFSC with the ATR U-Mo demonstration element payload is not specifically modeled as part of this evaluation. Instead, its thermal performance is estimated using a qualitative approach based on the thermal characteristics of the other payloads and their associated thermal performance as described in Section 3.5.2.5, *Thermal Properties for ATR U-Mo Demonstration Element*.

The heat transfer from the exterior surfaces of the ATR FFSC is modeled as a combination of convection and radiation exchange. Appendix 3.5.2.3, *Convection Coefficient Calculation*, presents the methodology used to compute the convection coefficients from the various surfaces. The radiation exchange is computed using a Monte Carlo, ray tracing technique and includes the affect of reflection and/or transmission, according to the optical properties assigned to each surface (see Section 3.2.1, *Material Properties*).

In addition, heating of the exterior surfaces due to solar insolation is assumed using a diurnal cycle. A sine wave model is used to simulate the variation in the applied insolation on the surfaces of the package over a 24-hour period, except that when the sine function is negative, the insolation level is set to zero. The timing of the sine wave is set to achieve its peak at 12 pm and peak value of the curve is adjusted to ensure that the total energy delivered matched the regulatory values. As such, the total energy delivered in one day by the sine wave solar model is given by:

$$\int_{6\cdot hr}^{18\cdot hr} Q_{peak}\cdot \sin\left(\frac{\pi\cdot t}{12\cdot hr} - \frac{\pi}{2}\right) dt = \left(\frac{24\,hr}{\pi}\right)\cdot Q_{peak}$$

Using the expression above for the peak rate of insolation, the peak rates for top and side insolation may be calculated as follows:

$$Q_{top} = \left(800\frac{cal}{cm^2}\right)\cdot\left(\frac{\pi}{24\,hr}\right) \qquad Q_{top} = 2.68\frac{Btu}{hr\text{-}in^2} = 0.0447\frac{Btu}{min\text{-}in^2}$$

$$Q_{side} = \left(200\frac{cal}{cm^2}\right)\cdot\left(\frac{\pi}{24\,hr}\right) \qquad Q_{sside} = 0.67\frac{Btu}{hr\text{-}in^2} = 0.0112\frac{Btu}{min\text{-}in^2}$$

Conversion factors of 1 cal/cm²-hr = 0.0256 Btu/hr-in² are used in the above calculations. These peak rates are multiplied by the sine function and the solar absorptivity for Type 304 stainless steel (i.e., 0.52) to create the top and side insolation values as a function of time of day.

3.5.2.2 Description of Thermal Model for HAC Conditions

The thermal evaluations for the hypothetical accident condition (HAC) are conducted using an analytical thermal model of the ATR FFSC. The HAC thermal model is a modified version of the quarter symmetry NCT model described in Section 3.5.2.1, *Description of Thermal Model for NCT Conditions,* with the principal model modifications consisting of simulating the expected package damage resulting from the drop events that are assumed to precede the HAC fire and changing the package surface emissivities to reflect the assumed presence of soot and/or surface oxidization.

Physical testing using full scale certified test units (CTUs) is used to establish the expected level of damage sustained by the ATR FFSC package from the 10 CFR 71.73 prescribed free and puncture drops that are assumed to precede the HAC fire event. Appendix 2.12.1, *Certification Tests on CTU-1* and Appendix 2.12.2, *Certification Tests on CTU-2* document the configuration and initial conditions of the test articles, the test facilities, the instrumentation used, and the test results. The drop tests covered a range of hypothetical free drop orientations and puncture bar drops. The results from both sets of CTU drop tests showed the following:

1) The worst case physical damage to the exterior of the package occurs from a CG over corner drop. The resulting damage (depicted in Figure 3.5-7) is thermally insignificant in that there is no breach in the outer shell and the compaction of the underlying insulation is minor and offset by an increase in the gap between the outer shell and the insulation in other areas.

2) The oblique, CG over side puncture bar drop caused a 0.5 inch indentation to the side of the package at the center of the impact region and less near the edges. No tearing of the outer shell occurred.

3) The end drops caused the ceramic fiber insulation to slide axially between each set of ribs, as depicted in Figure 3.5-9. The amount of re-positioning varied from approximately 1 to 1.75 inches and results in the compression of the insulation in the axial direction by 6 to 10%. No compression or shifting of the insulation in the radial direction was noted from the drop tests. While the insulation jacket showed some crimping at the edges, it was essentially undamaged.

Based on the above observations, the NCT was modified for the HAC evaluations via the following steps:

1) A 1.85 inch long segment of insulation was removed between each set of ribs. This degree of insulation re-positioning/compression conservatively bounds the maximum observed distance of 1.75 inches. Heat transfer across the vacated segments of insulation is then computed as radiation and conduction across an air filled space. Figure 3.5-10 illustrates the change made to the NCT thermal model to capture the expected insulation re-positioning. The change in the insulation's thermal conductivity as a result of the compression is conservatively ignored since thermal conductivity decreases with density at temperatures in excess of approximately 500°F (see Table 3.2-3).

2) All other geometric aspects of the NCT thermal model are assumed to be unchanged for the HAC evaluations since the observed damage to the outer shell resulting from the free and puncture drops has a superficial impact to the thermal protection offered by the ATR FFSC to the HAC fire event.

3) The surface emissivities for the various components of the package are revised as presented in Table 3.2-6 vs. that given in Table 3.2-5.

3.5.2.3 Convection Coefficient Calculation

The convective heat transfer coefficient, h_c, has a form of: $h_c = Nu \dfrac{k}{L}$, where k is the thermal conductivity of the gas at the mean film temperature and L is the characteristic length of the vertical or horizontal surface.

Natural convection from each surface is computed based on semi-empirical relationships using the local Rayleigh number and the characteristic length for the surface. The Rayleigh number is defined as:

$$Ra_L = \frac{\rho^2 g_c \beta L^3 \Delta T}{\mu^2} \times Pr$$

where:

g_c = gravitational acceleration, 32.174 ft/s^2

ΔT = temperature difference, °F

μ = dynamic viscosity, lb$_m$/ft-s

L = characteristic length, ft

c_p = specific heat, Btu/lb$_m$-hr-°F

β = coefficient of thermal expansion, °R^{-1}

ρ = density of air at the film temperature, lb$_m$/ft^3

Pr = Prandtl number = $(c_p\,\mu)\,/\,k$

k = thermal conductivity at film temperature

Ra_L = Rayleigh #, based on length 'L'

Note that k, c_p, and μ are each a function of air temperature as taken from Table 3.2-4. Values for ρ are computed using the ideal gas law, β for an ideal gas is simply the inverse of the absolute temperature of the gas, and Pr is computed using the values for k, c_p, and μ from Table 3.2-4. Unit conversion factors are used as required to reconcile the units for the various properties used.

The natural convection from a discrete vertical surface is computed using Equation 6.39 to 6.42 of Rohsenow, et. al.[9], which is applicable over the range $1 <$ Rayleigh number (Ra) $< 10^{12}$:

$$Nu^T = \overline{C}_L Ra^{1/4}$$

$$\overline{C}_L = \frac{0.671}{\left(1 + (0.492/Pr)^{9/16}\right)^{4/9}}$$

$$Nu_L = \frac{2.8}{\ln(1 + 2.8/Nu^T)}$$

$$Nu_t = C_t^V Ra^{1/3}$$

$$C_t^V = \frac{0.13\,Pr^{0.22}}{\left(1 + 0.61\,Pr^{0.81}\right)^{0.42}}$$

$$Nu = \frac{h_c L}{k} = \left[(Nu_L)^6 + (Nu_t)^6\right]^{1/6}$$

Natural convection from horizontal surfaces is computed from Equations 4.39 and 4.40 of Rohsenow, et. al.[9], and Equations 3.34 to 3.36 of Guyer[24], where the characteristic dimension (L) is equal to the plate surface area divided by the plate perimeter. For a heated surface facing upwards or a cooled surface facing downwards and Ra > 1:

$$Nu = \frac{h_c L}{k} = \left[(Nu_L)^{10} + (Nu_t)^{10}\right]^{1/10}$$

$$Nu_L = \frac{1.4}{\ln\left(1 + 1.677/\left(\overline{C}_L Ra^{1/4}\right)\right)}$$

---

[24] Guyer, E.C., *Handbook of Applied Thermal Design*, McGraw-Hill, Inc., 1989.

$$\overline{C_L} = \frac{0.671}{\left[1 + (0.492/Pr)^{9/16}\right]^{4/9}}$$

$$Nu_t = 0.14 Ra^{1/3}$$

For a heated surface facing downwards or a cooled surface facing upwards and $10^3 < Ra < 10^{10}$, the correlation is as follows:

$$Nu = Nu_L = \frac{2.5}{\ln(1 + 2.5/Nu^T)}$$

$$Nu^T = \frac{0.527}{\left(1 + (1.9/Pr)^{9/10}\right)^{2/9}} Ra^{1/5}$$

The forced convection coefficients applied during the HAC fire event are computed using the relationships in Table 6-5 of Kreith[25] for a flat surface, where the characteristic dimension (L) is |
equal to the length along the surface and the free stream flow velocity is V. The heat transfer coefficient is computed based on the local Reynolds number, where the Reynolds number is defined as:

$$Re_L = \frac{V \times \rho \times L}{\mu}$$

For Reynolds number (Re) $< 5 \times 10^5$ and Prandtl number (Pr) > 0.1:

$$Nu = 0.664 \, Re_L^{0.5} \, Pr^{0.33}$$

For Reynolds number (Re) $> 5 \times 10^5$ and Prandtl number (Pr) > 0.5:

$$Nu = 0.036 \, Pr^{0.33} [Re_L^{0.8} - 23,200]$$

Given the turbulent nature of the 30-minute fire event, a characteristic length of 0.25 feet is used for all surfaces to define the probable limited distance for boundary growth.

---

[25] Kreith, Frank, *Principles of Heat Transfer*, 3rd edition, Harper & Row, 1973. |

3.5.2.4 Determination of Composite Thermal Properties for ATR Fuel Plates

The ATR fuel plates are a composite material consisting of a fissile fuel matrix sandwiched within aluminum cladding. For the purposes of this calculation, the fuel composite is treated as a homogenous material with lumped thermal properties as defined below. This modeling approach is justified since the thermal gradient within the fuel element will be very low given that the un-irradiated fuel has essentially no decay heat.
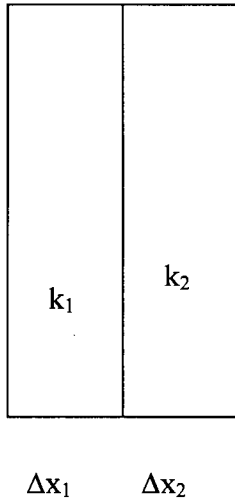
Because of the thinness of the plates, the average conductivity is required only for the axial and circumferential direction. Conductivity through the plates is not required as this analysis assumes a zero temperature gradient in that direction. Mean density and specific heat values are also defined below.

<u>Circumferential and Axial Conductivity</u>

Ignoring the affect of curvature, the heat flow can be written as,

$$q = -\Delta x \Delta z \, \bar{k} \, \frac{\Delta T}{\Delta y} = -\Delta x_1 \Delta z \, k_1 \, \frac{\Delta T}{\Delta y} - \Delta x_2 \Delta z \, k_2 \, \frac{\Delta T}{\Delta y} \quad \text{where}$$

$$\Delta x = \sum_i \Delta x_i$$

From which,

$$\bar{k} = \frac{\Delta x_1 k_1 + \Delta x_2 k_2}{\Delta x}$$

<u>Mean Density</u>

The mean density of the fuel plates is computed from:

$Mass = \Delta x \Delta y \Delta z \, \bar{\rho} = \Delta x_1 \Delta y \Delta z \, \rho_1 + \Delta x_2 \Delta y \Delta z \, \rho_2$, from which we get $\bar{\rho} = \dfrac{\Delta x_1 \rho_1 + \Delta x_2 \rho_2}{\Delta x}$

<u>Mean Specific Heat</u>

In the same manner used to define the mean density, the mean specific heat for the fuel plates is computed as;

$\bar{\rho} \, \bar{c}_p \Delta x \Delta y \Delta z = \rho_1 c_{p_1} \Delta x_1 \Delta y \Delta z + \rho_2 c_{p_2} \Delta x_2 \Delta y \Delta z$ from which we get, $\bar{c}_p = \dfrac{\rho_1 c_{p_1} \Delta x_1 + \rho_2 c_{p_2} \Delta x_2}{\bar{\rho} \, \Delta x}$

The thermal properties for the individual plates making up the ATR fuel element are computed using the above approach and thermophysical and geometric data[6,5] for the ATR fuel element.

Based on these data sources, the radius of the inner plate is 3.015 inches, while the radius of the outer plate is 5.44 inches. The gap between the plates is 0.078 inches. The thickness of the aluminum cladding is 0.015 inches.

While the thermal properties for the aluminum cladding and the fissile fuel matrix material will vary with temperature, for the purposes of this evaluation, fixed material properties are assumed in order to simplify the calculation. To provide conservatism for this modeling approach conservatively low value is assumed for the specific heat for each component, while a conservatively high thermal conductivity value is used. This methodology will result in over-predicting the temperature rise within the composite material during the HAC fire event.

The thermal properties used in this calculation are:
1) Aluminum cladding thermal conductivity = 191 W/m-K, conservatively high value from [6], page 18
2) Fissile fuel matrix (UAl_x) conductivity:
   a. 53 W/m-K, conservatively high based on Table 2.3 from [6], at 300K for fuel plates 1, 2, 18, & 19
   b. 43 W/m-K, conservatively high based on Table 2.3 from [6], at 300K for fuel plates 3, 4, 16, & 17
   c. 36.1 W/m-K, conservatively high based on Table 2.3 from [6], at 300K for fuel plates 5 to 15
3) Aluminum cladding density = 2702 kg/m^3, from [6], page 16
4) Fissile fuel matrix (UAl_x) density:
   a. 3409 kg/m^3, from [6], Table 2.5, for fuel plates 1, 2, 18, & 19
   b. 3671 kg/m^3, from [6], Table 2.5, for fuel plates 3, 4, 16, & 17
   c. 3933 kg/m^3, from [6], Table 2.5, for fuel plates 5 to 15
5) Aluminum cladding specific heat = 896 and 1080 J/kg-K, from [6], Table 3.2, at 300 & 600K, respectively
6) Fissile fuel matrix (UAl_x) specific heat:
   a. 666 & 803 J/kg-K, from [6], Table 2.4, value at 300 & 700K, respectively, for fuel plates 1, 2, 18, & 19
   b. 616 & 743 J/kg-K, from [6], Table 2.4, value at 300 & 700K, respectively, for fuel plates 3, 4, 16, & 17
   c. 573 & 692 J/kg-K, from [6], Table 2.4, value at 300 & 700K, respectively, fuel plates 5 to 15

Table 3.5-1 presents the composite thermal conductivity, specific heat, and density values for each of the nineteen (19) fuel plates making up the ATR fuel element. These composite values are based on the thermal property values given above and the geometry depicted in Figure 3.5-11.

3.5.2.5 Thermal Properties for ATR U-Mo Demonstration Element

The external geometry of the ATR U-Mo demonstration element is essentially identical to the ATR Mark VII YA fuel element. The demonstration element contains 18 fueled plates (plate 19 is a solid aluminum alloy plate). The demonstration element contains a mixture of UAl_x (HEU)

and U-Mo (LEU) fuel plates, with a maximum U-235 mass of 1,240 g. Plates 1 through 4 and 16 through 18 are UAl$_x$ plates identical in construction and composition to a standard HEU ATR fuel element, except boron is included in the UAl$_x$ plates as a burnable poison. Plates 5 through 15 are fueled with an alloy of LEU uranium and molybdenum. The U-Mo fuel meat is nominally 10% molybdenum by weight, and the U-235 is enriched up to 20.0%. For the LEU fuel, the maximum weight percent for U-234 and U-236 are 0.26% and 0.46%, respectively.

The U-Mo fuel meat is nominally 0.013-in thick, and a nominal 0.001-in thick zirconium interlayer is present between the fuel meat and the aluminum alloy cladding. The fuel element weighs 32 lbs or less, is bagged in protective polyethylene sleeve, and is enclosed in the ATR FHE weighing 15 lbs.

The ATR U-Mo demonstration element is not explicitly modeled for this evaluation, but is considered to be bounded by the ATR fuel element. This modeling approach is based data in Creasy[26] and ECAR-841[27], and on the following facts:

1) the thermal characteristics of plates 1 to 4 and 16 to 18 of each element are essentially identical,

2) plates 5 to 15 of the ATR U-Mo demonstration element have lower fuel matrix thermal conductivity, but a slightly higher plate conductivity due to thicker aluminum alloy cladding used. The thermal mass of the plates are essentially the same as plates 5 to 15 of the ATR element (see Table 3.5-2, *Comparison of ATR and ATR U-Mo Demonstration Element Properties*),

3) the solid aluminum alloy plate 19 of the ATR U-Mo demonstration element has a higher thermal mass than the fueled plate 19 of the ATR element. While the thermal conductivity of a solid plate is higher than a fueled plate, the transient response is dominated by the plate's thermal mass, and

4) since the thermal mass dominates the heat transfer relations, the effect of changes in the conductivity are negligible, and the higher combined thermal mass of the ATR U-Mo fuel plates damps the thermal transient response in the model. This will result in a lower peak temperature in the ATR U-Mo demonstration element.

---

[26] Creasy, J.T., M.S. Thesis, Texas A&M University, *Thermal Properties of Uranium-Molybdenum Alloys: Phase Decomposition Effects of Heat Treatments*, December 2011, pp. 14-16.

[27] ECAR-841, *Density of Uranium Molybdenum Alloys*, Idaho National Laboratory, December 17, 2009.

Table 3.5-1 – Composite ATR Fuel Plate Thermal Properties

Plate	Plate Thickness, in	UAlx Thickness, in	Circumferential Conductivity (W/m-K)	Inner radius, in	Outer radius, in	Mean radius, in	Mean density, kg/m^3	Mean specific heat, J/(kg K) @ 300 K	Mean specific heat, J/(kg K) @ 700 K
1	0.08	0.05①	104.8	3.015	3.095	3.055	3143.9	740.1	892.3
2	0.05	0.02	135.8	3.173	3.223	3.198	2984.8	790.9	953.5
3	0.05	0.02	131.8	3.301	3.351	3.326	3089.6	762.9	919.8
4	0.05	0.02	131.8	3.429	3.479	3.454	3089.6	762.9	919.8
5	0.05	0.02	129.0	3.557	3.607	3.582	3194.4	736.9	888.9
6	0.05	0.02	129.0	3.685	3.735	3.710	3194.4	736.9	888.9
7	0.05	0.02	129.0	3.813	3.863	3.838	3194.4	736.9	888.9
8	0.05	0.02	129.0	3.941	3.991	3.966	3194.4	736.9	888.9
9	0.05	0.02	129.0	4.069	4.119	4.094	3194.4	736.9	888.9
10	0.05	0.02	129.0	4.197	4.247	4.222	3194.4	736.9	888.9
11	0.05	0.02	129.0	4.325	4.375	4.350	3194.4	736.9	888.9
12	0.05	0.02	129.0	4.453	4.503	4.478	3194.4	736.9	888.9
13	0.05	0.02	129.0	4.581	4.631	4.606	3194.4	736.9	888.9
14	0.05	0.02	129.0	4.709	4.759	4.734	3194.4	736.9	888.9
15	0.05	0.02	129.0	4.837	4.887	4.862	3194.4	736.9	888.9
16	0.05	0.02	131.8	4.965	5.015	4.990	3089.6	762.9	919.8
17	0.05	0.02	131.8	5.093	5.143	5.118	3089.6	762.9	919.8
18	0.05	0.02	135.8	5.221	5.271	5.246	2984.8	790.9	953.5
19	0.1	0.07①	94.4	5.349	5.449	5.399	3196.9	724.3	873.2

① An average UAlx thickness of 0.020 inches exists for Plates 1 an 19 vs. the 0.05 and 0.07 inches assumed by this analysis based on the assumption of a constant cladding thickness. However, for the purposes of developing composite fuel plate properties for this evaluation, the UAlx thicknesses identified in the table yield conservative bounding thermal property values.

Table 3.5-2 – Comparison of ATR and ATR U-Mo Demonstration Element Properties

Property for Plates 5 to 15	UAl$_x$-Al Fuel Matrix	U-Mo Fuel Matrix
Density (kg/m^3)	3933	17,200
Specific Heat (J/kg-K) @ 600 K	660	155
Thermal Conductivity (W/m-K)	36.1 to 34.8 (273<T<800 K)	11.7 to 26.9 (298 K<T< 773 K)
Heat Capacity (J/m^3-K) – calculated from values above	2.60 x 10^6	2.67 x 10^6
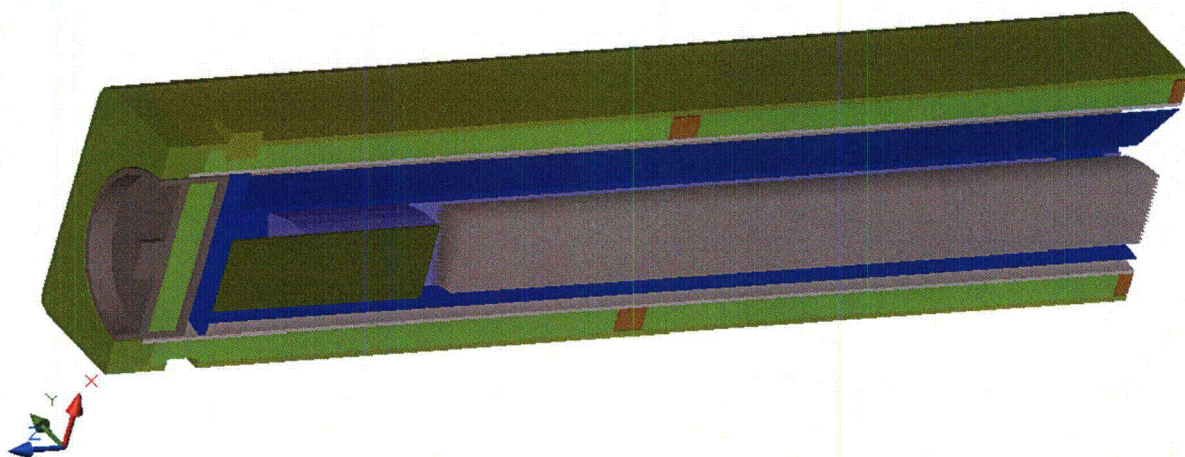
(Note: the positive x-axis is oriented towards the top of the package and the positive z-axis towards the package closure end)
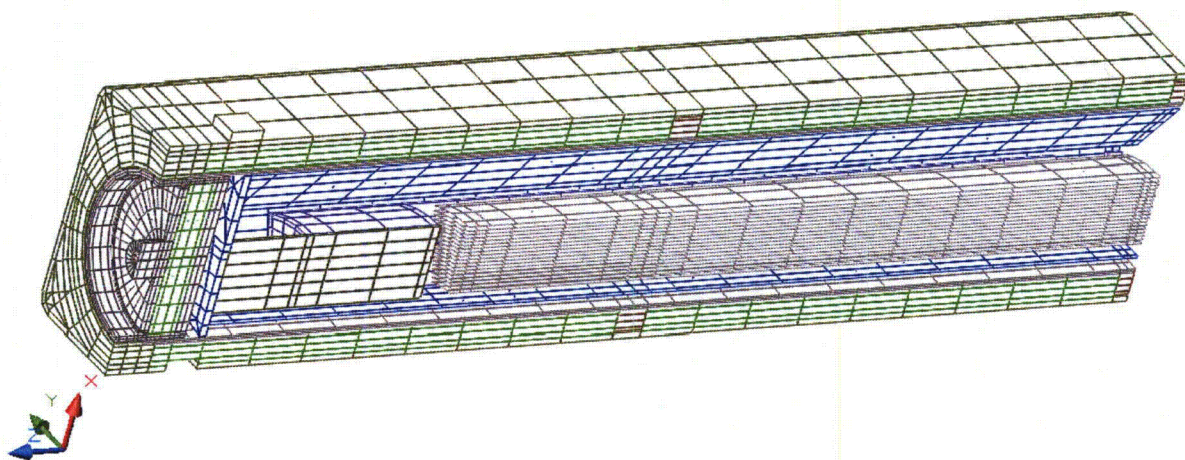
(Note: the positive x-axis is oriented towards the top of the package and the positive z-axis towards the package closure end)

Figure 3.5-1 – 'Solid' and & 'Hidden Line' Views of Package Quarter
Symmetry Thermal Model
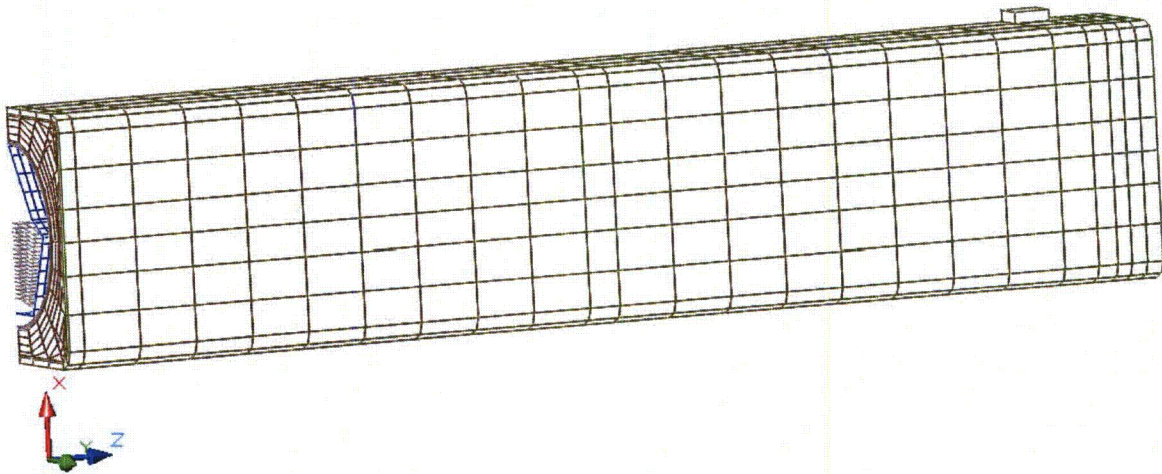
(Note: the positive x-axis is oriented towards the top of the package and the positive z-axis towards the package closure end)

Figure 3.5-2 – Reverse, 'Hidden Line' View of Package Quarter Symmetry Thermal Model
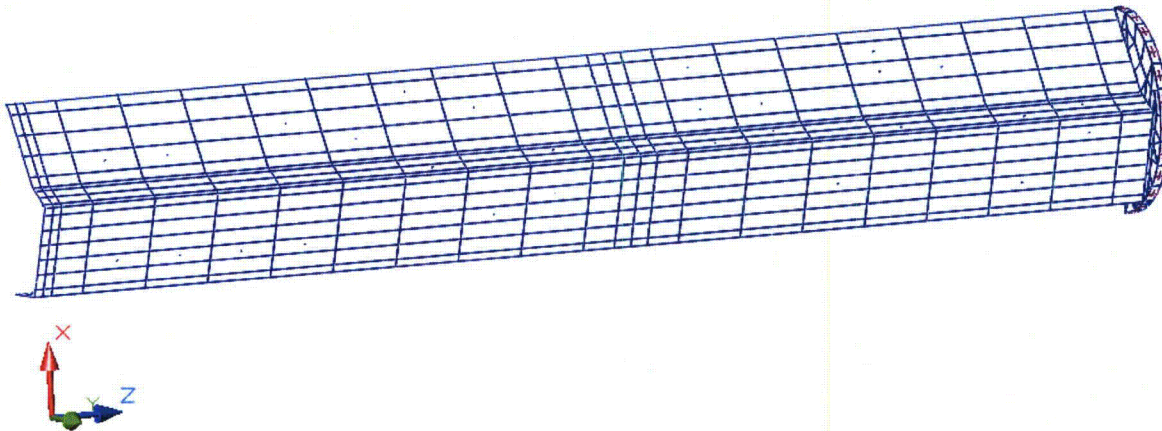
(Note: the positive x-axis is oriented towards the top of the package and the positive z-axis towards the package closure end)

Figure 3.5-3 – Reverse, 'Hidden Line' View of FHE Quarter Symmetry Thermal Model
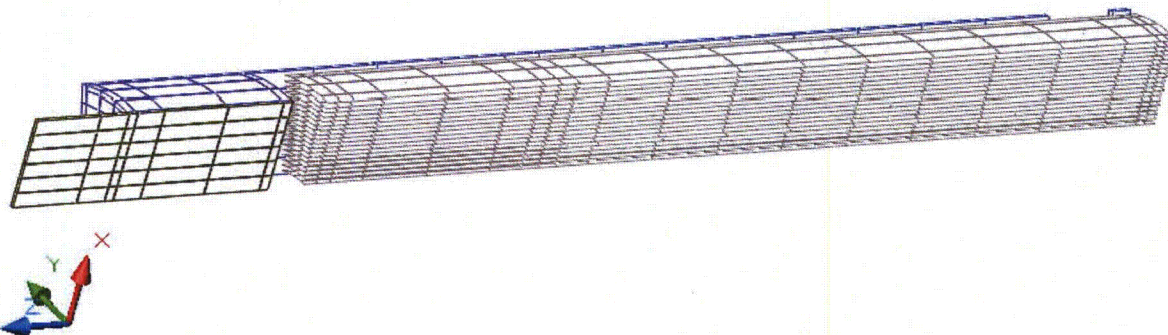
ATR Fuel Element Modeling, View Along Centerline of Element
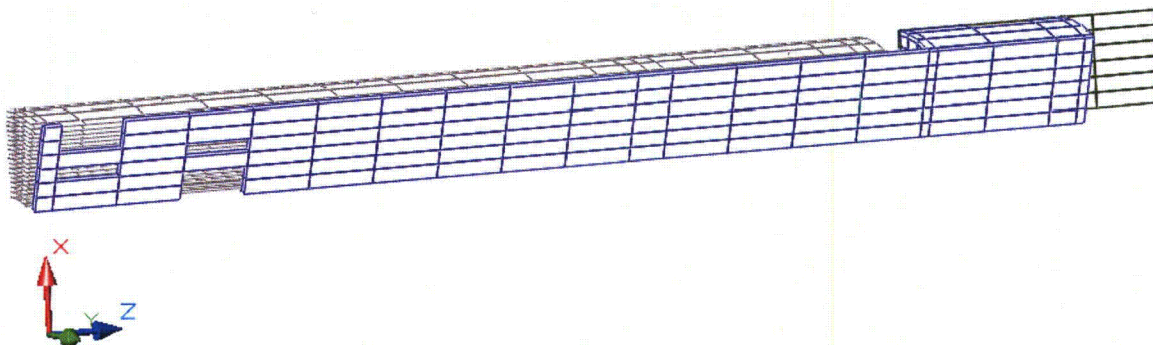
ATR Fuel Element Modeling, View Along Outside of Element

(Note: the positive x-axis is oriented towards the top of the package and the positive z-axis towards the package closure end)

Figure 3.5-4 – Centerline and Side Views of ATR Fuel Element Thermal Model

Modeling Showing Direct Contact   Modeling with 'Solid' Elements for Air
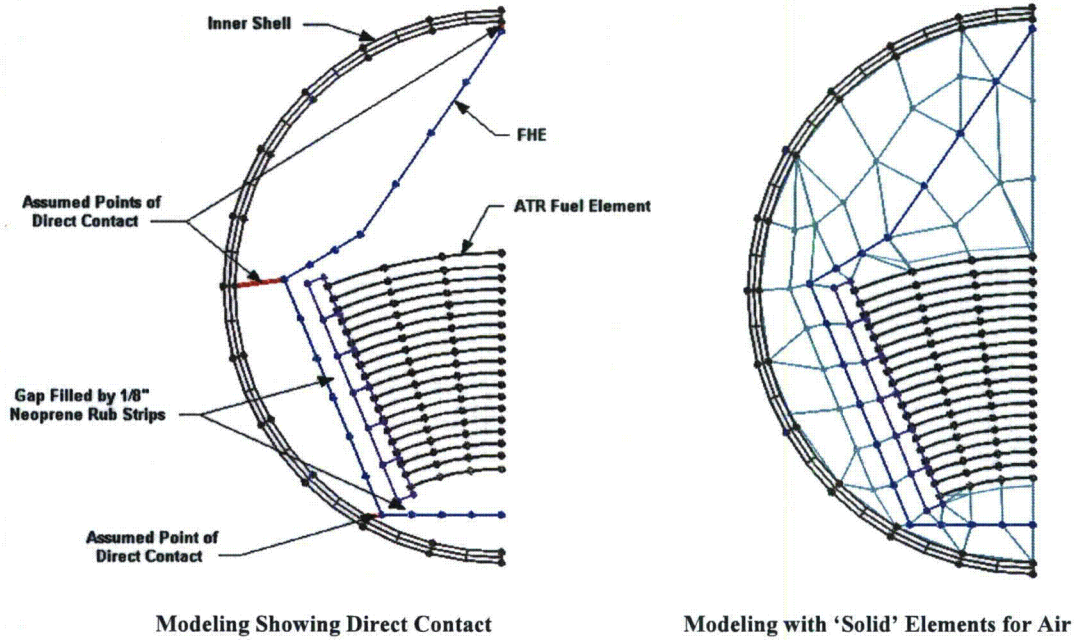
Figure 3.5-5 – Thermal Model of ATR Fuel Element and FHE within Inner Shell
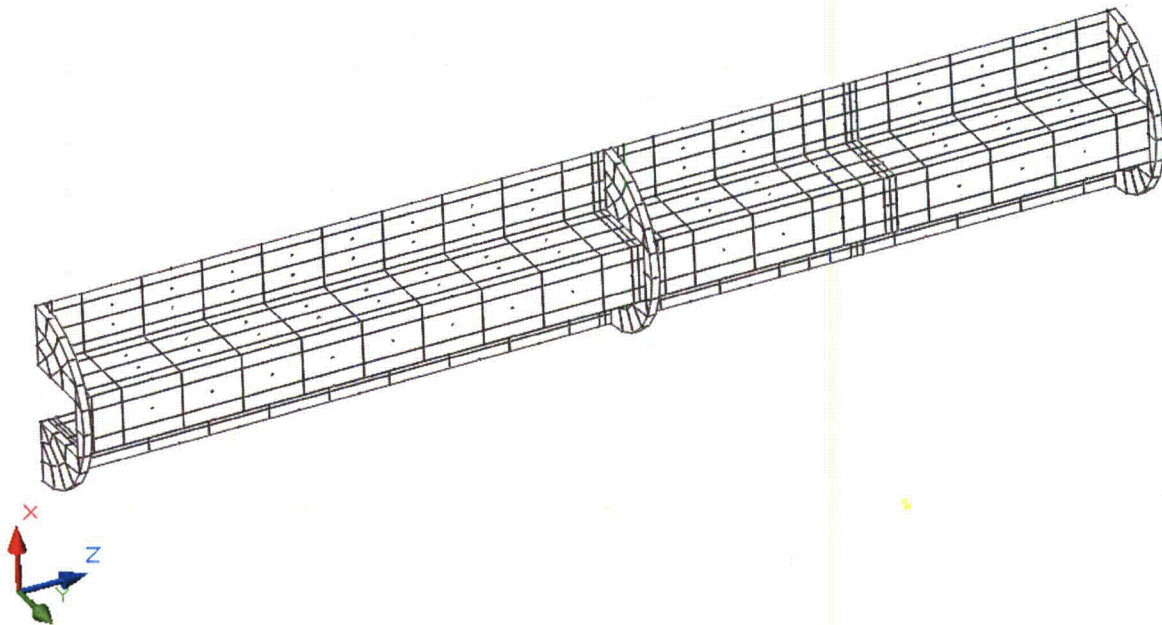
(Note: the positive x-axis is oriented towards the top of the package and the positive z-axis towards the package closure end)

Figure 3.5-6 – Thermal Model of Loose Fuel Plate Basket (LFPB)
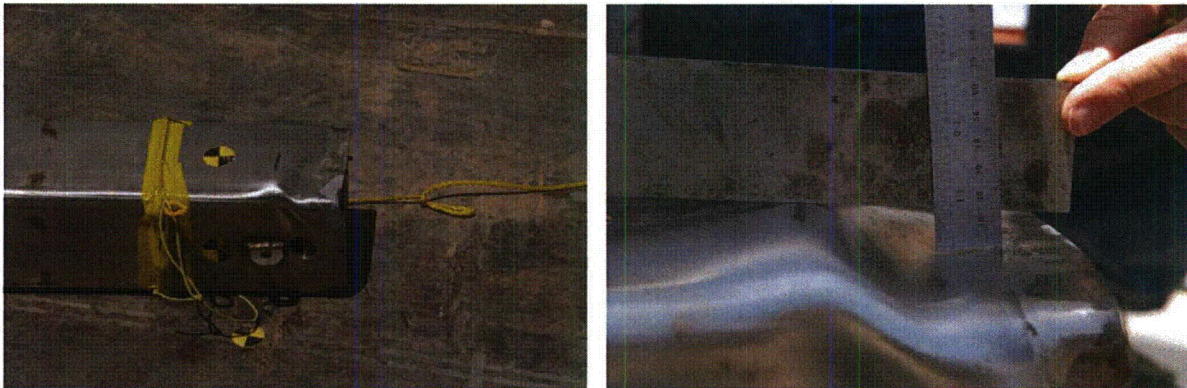
Figure 3.5-7 – Worst Case Package Damage Arising from Corner Drop
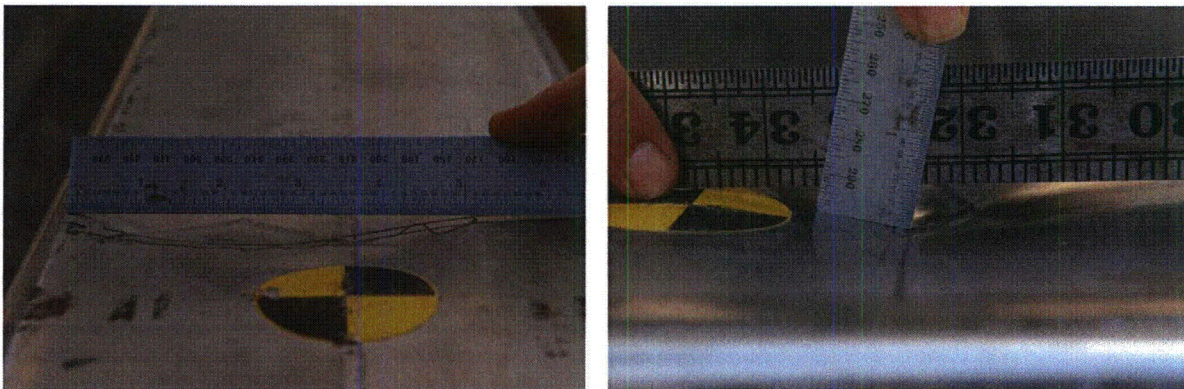
Figure 3.5-8 – Worst Case Package Damage Arising from Oblique Puncture Drop

Figure 3.5-9 – Insulation Re-positioning Arising from End Drop
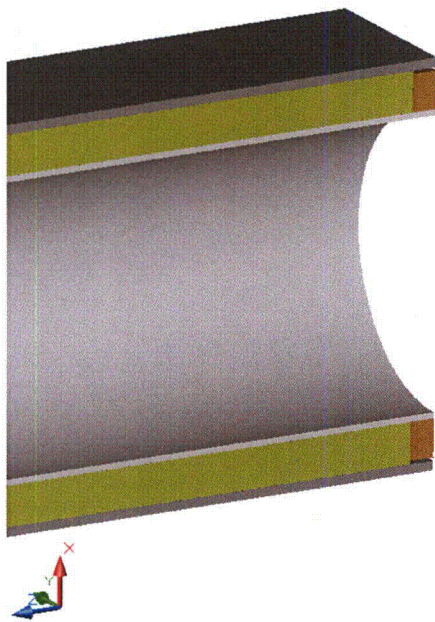
Insulation Modeling for NCT Conditions
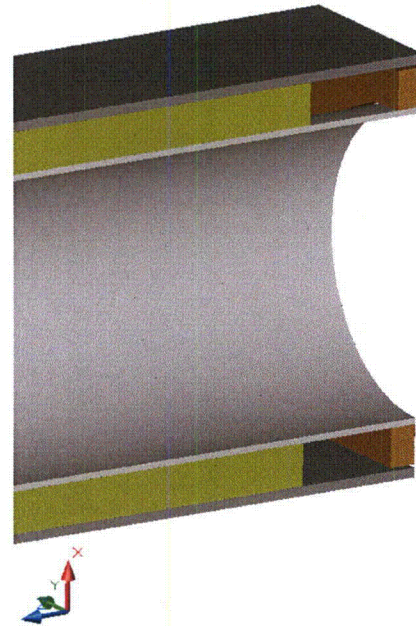
Insulation Modeling for HAC Conditions

Figure 3.5-10 – Thermal Modeling of Insulation Re-positioning for HAC Conditions
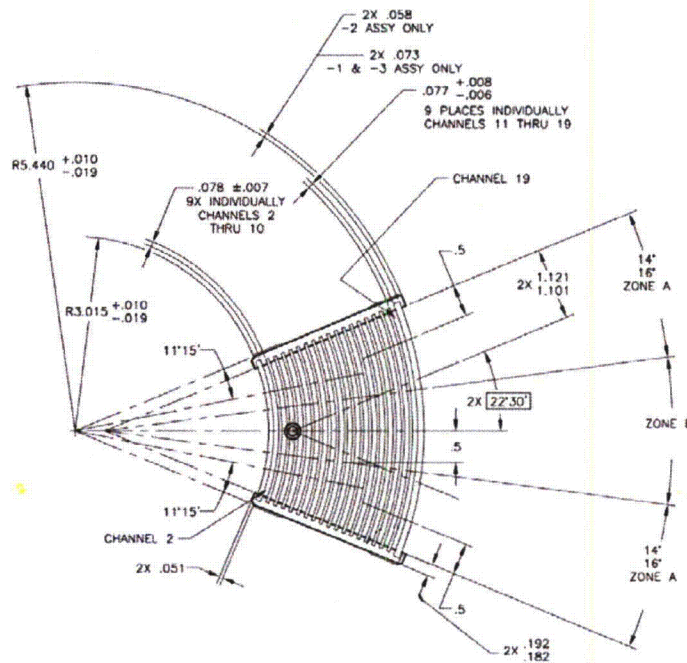
Figure 3.5-11 – ATR Fuel Element Cross Section

3.5.3 Thermal Decomposition/Combustion of Package Organics

The organic material in the ATR FFSC subject to thermal decomposition and/or combustion is limited to polyethylene, neoprene, and the adhesive used to attach the neoprene. The fuel elements and, optionally, the loose fuel plates are enclosed in polyethylene bags prior to their placement in the FHEs and loose plate basket. The bags serve no safety function beyond providing investment protection of the payload material. Similarly, neoprene (polychloroprene) rub strips are attached via adhesive to the FHEs to provide investment protection against fretting on the elements and loose plates. As such, the loss of the organic material under either NCT or HAC conditions has no safety implication beyond the potential for gas and heat generation. The following sections provide a bounding assessment on the potential safety impact associated with the loss of organic material within the ATR FFSC package.

3.5.3.1 Organic Material Within Package

The amount of organic material in the package varies with the payload configuration. While the bounding amount of polyethylene is constant at 100 g, the amount of neoprene varies with payload configuration. The sections below identify the quantity and important thermal properties associated with the organic materials present in the ATR FFSC package.

Polyethylene
Properties of polyethylene related to its thermal decomposition/combustion are as follows:
  a) chemical formulation[7]: $-[CH_2- CH_2]_n-$,
  b) heat of combustion (ΔH_c)[28]: 46,500 kJ/kg,
  c) oxygen index[29,30]: 17.4%,
  d) melting temperature[30]: 109-135°C
  e) temperature for 1% decomposition[30]: 275°C
  f) autoignition temperature[31]: 330 to 410°C

Oxygen index (OI) is the minimum oxygen concentration required to support self-sustaining combustion of the polymer. Since piloted conditions do not exist within the ATR FFSC payload cavity, self-sustaining combustion of the polyethylene can't occur when the oxygen concentration drops below 17.4%. Low oxygen concentrations will not only prevent self-sustaining combustion, but will raise the autoignition temperature. Combustion of polyethylene in air is governed by the following equation:

$$C_2H_4 + 3(O_2 + 3.76N_2) \rightarrow 2CO_2 + 2H_2O + 11.28N_2$$
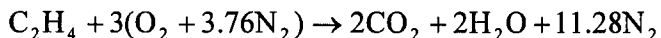
The above equation demonstrates that complete combustion of a mole of polyethylene requires 3 moles of oxygen and, since oxygen constitutes approximately 21% of air, 14.28 moles of air. The total quantity of gas generated is 15.28 moles, or an increase of 7% over the original gas

[28] NUREG-1805, Fire Dynamics Tools, Nuclear Regulatory Commission, Washington, D.C.

[29] office.wendallhull.com/matdb/

[30] *SFPE Handbook of Fire Protection Engineering*, 3rd Edition, Section 1, Chapter 7, Table 1.7-4, NFPA, 2003.

[31] *MSDS for Polyethylene*, #1488, prepared by International Programme on Chemical Safety, 2004.

quantity existing before combustion. Per SAR section 1.2.2, the amount of polyethylene in the package is limited to 100 g or less. Based on a molecular weight of approximately 28 g/g-mole of polyethylene, the 3.57 g-moles of polyethylene represented by the 100 g would require 3.57 x 14.28 = 50.98 g-moles of air for complete combustion.

Neoprene

Properties of neoprene (polychloroprene) related to its thermal decomposition/combustion are as follows:

   a) chemical formulation[7]: -$[CH_2-Cl-C=CH-CH_2]_n$-,
   b) heat of combustion (ΔH_c)[28]: 10,300 kJ/kg,
   c) oxygen index[29,32]: 32-35% at one atmosphere,
   d) melting temperature: N/A - thermoset material
   e) temperature for initial decomposition[30]: 342°C
   f) autoignition temperature[32]: >380°C in a 21% oxygen concentration environment.

As a thermoset plastic, uncontrolled heating of neoprene will result in reaching the decomposition temperature before the melting point is obtained. The high oxygen index demonstrates why neoprene can't support combustion without an external ignition source. The typical adhesives[33] used to bond the rub strips to the FHEs consist of principally of solvents that outgas during the curing process. The non-volatile components consist of polymers, including polychloroprene, and cure and vulcanization agents. As a result, the cured adhesive layer exhibits properties[33] similar to neoprene.

Combustion of neoprene in air is governed by the following equation:

$$C_4H_5Cl + 5.25(O_2 + 3.76N_2) \rightarrow 4CO_2 + 2.5H_2O + Cl + 19.74N_2$$
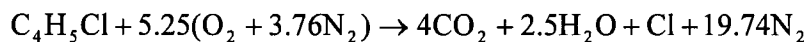
From the above equation, complete combustion of a mole of neoprene is seen to require 5.25 moles of oxygen and, since oxygen constitutes approximately 21% of air, 24.99 moles of air. The total quantity of gas generated is 27.24 moles, or an increase of 9% over the original gas quantity existing before combustion.

Based on the surface area of rub strips depicted on each SAR drawing, a thickness of 0.125 in, and an adhesive layer thickness of 2 mils, the total quantity of neoprene and neoprene like material used in each FHE is summarized in Table 3.5-3. With a molecular weight of approximately 88.5 g/g-mole of neoprene, the 4.62 g-moles of neoprene represented by the minimum 409 g of neoprene contained within the 60501-40 FHE assembly would require 4.62 x 24.99 = 115.5 g-moles of air for complete combustion.

The same limitation on package oxygen that prevents significant combustion of polyethylene will also prevent combustion of the neoprene. Further, given the higher oxygen index and autoignition temperature for neoprene versus polyethylene, there is a low probability any neoprene material will be involved in combustion. Instead, it is expected that the only damage to be incurred by the neoprene will be a de-bonding from the FHE surfaces and a small amount of

---

[32] *Safe Use of Oxygen and Oxygen Systems*, ASTM, 2nd Edition.

[33] Product and MSDS sheets for 3M™ Spray 80 Neoprene Contact Adhesive or 3M™ Scotch-Weld Neoprene Contact Adhesive 1357.

thermal decomposition. Since thermal decomposition is an endothermic process, the loss of the material will act to lower the temperatures predicted within the FHE.

3.5.3.2 Air Quantity Within Package

Since the ATR FFSC payload cavity is not sealed, the quantity of gas filling the cavity volume will vary with time as a function of the cavity's bulk gas temperature, the thermal decomposition of the enclosed organic material, and diffusion of gas through the package closure gaps. The following sections address these various mechanisms affecting the air/oxygen content within the package.

Potential Combustion Due to Resident Air Quantity

The ATR FFSC payload cavity has a length of 67.88 in and a diameter of 5.76 in. The gross cavity volume is 1768.8 in^3. The ATR fuel element and the ATR FHE have volumes of approximately 155 and 223 in^3, based on weights of 25 and 15 lbs, respectively, and mean densities of 0.112 and 0.097 lbs/ in^3, respectively. The net cavity space is therefore approximately 1,391 in^3 (22.8 liters). Table 3.5-4 summarizes the net cavity volume existing for all payload configurations. As seen from the table, only the MIT FHE (SAR drawing 60501-40) loaded with a MIT fuel element results in a larger net cavity volume than the ATR FHE (SAR drawing 60501-30) loaded with an ATR fuel element. Given the substantially higher HAC temperature predicted for the ATR FHE (see Section 3.4, *Thermal Evaluation for Hypothetical Accident Conditions*) versus that for the MIT FHE (see Section 3.6, *Thermal Evaluation for MIT, MURR, and Small Quantity Payloads*) and the larger quantity of neoprene used (see Table 3.5-3), the ATR FHE is the appropriate payload configuration for assessing the thermal safety related to the organic material in the package.

At 100°F, approximately 0.9 g-moles of air are required to fill a 1,391 in^3 (22.8 liters) cavity space to a pressure of 14.7 psia, while at 626°F (330°C, i.e., the lower autoignition temperature for polyethylene), the quantity of air required to fill the cavity space drops to approximately 0.5 g-mole. As such, the resident air quantity in the payload cavity is sufficient to support combustion of less than 1% of the polyethylene (i.e., 0.5 g-mole/50.98 g-mole air per 100 g polyethylene). The potential heat release from this quantity of polyethylene is: 1% x 100 g x 46,500 kJ/kg = 46,500 J = 44 Btu. Based on a combined ATR payload weight of 40 lbs and a specific heat of approximately 0.2 Btu/lb$_m$-°F[34], the net increase in the mean payload temperature would be less than 6°F even if this heat release occurred instantaneously. The use of the combined payload weight for this calculation is appropriate since the combustion occurs in the vapor space and not on a surface. Further, combustion of the limiting 1% of the polyethylene can neither occur instantaneously nor in only one concentrated area since the availability of the oxygen within the cavity will be rate limited by the diffusion process from reaching the potential site(s) of polyethylene combustion. In fact, oxygen diffusion will also prevent the entire resident oxygen quantity from being consumed. As such, the estimated 6°F rise in payload temperature is highly conservative.

---

[34] Approximate specific heat of ATR fuel plates per Table 3.2-2

Given the lower heat of combustion of neoprene versus that for polyethylene and the greater air quantity needed for complete combustion, the potential temperature rise from the combustion of polyethylene bounds that for neoprene by a factor of over 3.

Potential Combustion Due to Air Induced Via Pressure Forces

Once the residual air existing in the payload cavity prior to the start of the HAC event is consumed, further combustion will require additional air to enter the cavity via pressure and diffusion forces. The pressure forces will arise due to the balance between ideal gas expansion/contraction and gas generation within the package versus the pressure resistance associated with gas flow through the gaps around the package closure. Heatup of the package during the 30-minute fire event will result in elevated cavity pressure and a continuous outflow of gas from the cavity. This gas flow will switch to an inflow condition once the peak bulk gas temperature is reached and the package begins to cool down.

While an accurate estimate of the gas flow due to pressure forces requires a detailed modeling of the flow paths and resistance factors, a bounding estimate on the rate of gas flow into the package due to pressure differential can be made by assuming zero vent resistance and zero internal gas generation. These assumptions assure that the minimum gas quantity is achieved at the point where packaging cooling begins, thus maximizing the potential for the reverse gas flow necessary to restore atmospheric pressure within the package.

Assuming that the bulk average gas temperature within the package is represented by the mean of the average temperatures over the length of the package's inner shell and the FHE, the cavity gas quantity within the package can be estimated as a function of time during the HAC transient. Figure 3.5-12 presents the predicted package gas quantity for the HAC transient depicted in Figure 3.4-1 for the ATR fuel element. As seen, the package gas quantity rapidly drops during the 30-minute fire event as the cavity gas expands under HAC heating. Shortly after the cessation of the fire event, the package begins to cool and the gas flow switches to an inflow. However, due to the rate of package cooldown, greater than 10 hours are required to restore the approximately 0.5 g-moles of gas expelled during package heatup. The calculated reverse gas flow peaks at 0.0025 g-moles per minute. The potential polyethylene combustion supported by this flow rate is 0.0025 g-moles per minute x 100 g polyethylene per 50.98 g-mole air x 46,500 kJ/kg = 228.1 J/min = 0.22 Btu/min. Clearly this flow rate is too low to permit any significant rate of combustion, especially when considering the facts that the reverse gas flowrate decreases rapidly from this peak rate and that accounting for flow resistance through the vent geometry will reduce this potential heat gain even more.

When the above discussion is added to the fact that the oxygen concentration at the start of the inflow condition will be well below the oxygen index of 17.5% required to support combustion, the fact that oxygen diffusion within the package will extend the time for the entering air to reach the site of elevated polyethylene temperatures, and as seen in Figure 3.5-12, that the package temperatures will fall below the lower autoignition temperature for polyethylene after 90 minutes, it is reasonable to conclude that the contribution to package heatup from airflow due to pressure differential is essentially zero.

Potential Combustion Due to Air Induced Via Diffusion

Beside pressure differential, the other force available to drive oxygen inflow to the package cavity is diffusion. Assuming that the oxygen inside the package cavity is consumed as fast as it enters, the rate of oxygen diffusion can be determined via Fick's first law or:

$$J = -\rho \times D \times \frac{\partial w}{\partial y}$$

where: J = mass flux of oxygen per area, g/cm^2
D = diffusion coefficient of oxygen in nitrogen, cm^2/sec
ρ = density of air, g/cm^3
$\frac{\partial w}{\partial y}$ = change in mass fraction of oxygen over diffusion path

While diffusion of oxygen in nitrogen is used to reflect that fact that the environment within the payload cavity is assumed to be oxygen depleted, in reality there is little difference between diffusion in air or nitrogen. The diffusion coefficient is a function of temperature and pressure. Diffusion increases with increasing temperature since the molecules move rapidly and decreases with increasing pressure since higher fluid density increases the number of molecules per unit volume, increasing the number of collisions, thus slowing the speed of transport. The diffusion coefficient for oxygen in air at 1 atm and 25°C is 0.206 cm^2/sec[35]. Since the fluid pressure is assumed to remain near atmospheric throughout the HAC event, there is no need to adjust the diffusion coefficient for pressure effects. However, the temperature of the fluid both within and exterior to the package will increase significantly during the HAC transient, thus necessitating an adjustment[36] in the diffusion coefficient via:

$$D_{O-N} = 0.0018583 \sqrt{T^3 \times \left(\frac{1}{M_O} + \frac{1}{M_N}\right)} \times \frac{1}{P \times \sigma_{O-N}^2 \times \Omega_{D,O-N}}$$

where: D = diffusion coefficient of oxygen in air, cm^2/sec
T = temperature, K
M = molecular mass of oxygen and nitrogen
P = pressure, atm
$\Omega_{D,O-N}$ = collision integral for molecular diffusion of oxygen in nitrogen
σ_{O-N} = collision diameter, Angstroms

From Table E.1 and the equations provided in Transport Phenomena[36], M_O = 31.999, M_N = 28.013, σ_O = 3.433, σ_N = 3.667, ε_O/κ = 113, and ε_N/κ = 99.8. σ_{O-N} = 0.5x(3.433 + 3.667) = 3.55. ε_{O-N}/κ = (113 x 99.8)$^{0.5}$ = 106.2. Assuming the maximum flame temperature of 1475°F (1075K), the dimensionless temperature is $\kappa T/\varepsilon_{O-N}$ = 1075/106.2 = 10.1. From Table E.2[36], $\Omega_{D,O-N}$ = 0.741. Thus, D_{O-N} at a pressure of 1 atm and 1475°F is 1.815 cm^2/sec.

---

[35] *CRC Handbook of Engineering Tables*, Dorf, R. editor, CRC Press LLC, 2004.

[36] *Transport Phenomena*, 2nd Ed., Eqn 17.3-12 and Appendix E, Bird, R., Stewart, W, and Lightfoot, E., John Wiley & Sons, Inc., 2002.

The bayonet type closure plug for the ATR FFSC package results in a labyrinth like leakage path (see Figure 3.5-13). To conservatively bound the available leakage area for air exchange via diffusion, the closure plug geometry can be simplified as simply the barrel portion (i.e., flow path over segment A-B, Figure 3.5-13). Per the Table 3.5-5, the maximum diffusion area represented by this flow path is 1.71 in^2 (11 cm^2). Based on the derived diffusion coefficient, an air density of 0.000325 g/cm^3 at 1475°F (1075K), and a total diffusion path length of 2.5 in (6.4 cm, i.e., the total length of the closure plug), the maximum diffusion rate during the 30-minute fire event is calculated as:

$$J \times \text{Area} = -0.000325 \text{ g/cm}^3 \times 1.815 \text{ cm}^2/\text{sec} \times \frac{0.21 - 0}{6.4} \times 11 \text{ cm}^2$$

$$J \times \text{Area} = 0.00021 \text{ g/sec} = 0.0004 \text{ g-mole/min}$$

Following the fire event, the ambient temperature will drop to 100°F and the ambient density will rise to 0.001128 g/cm^3. The diffusion coefficient for oxygen in air at 1 atm and 25°C is 0.206 cm^2/sec[35], or approximately 11% of the diffusion coefficient determined for the fire conditions. The net effect of the higher density and lower diffusion coefficient is a diffusion rate of 0.00008 g/sec, or 38% of the rate determined at fire conditions.

Based on the 0.22 Btu/min temperature rise determined in the previous section for the 0.0026 g-mole/min oxygen flow associated with the pressure differential, the 0.0004 g-mole/min oxygen diffusion rate would generate a maximum 0.03 Btu/min temperature rise, dropping to less than 0.013 Btu/min following the end of the fire event. Since accounting for the diffusion resistance within the payload cavity will reduce the potential heat generation rate even more, a reasonable conclusion is that the contribution to package heatup from oxygen diffusion can be ignored.

3.5.3.3 Pressure Loss Across Closure Leakage Path

The ATR FFSC package is not sealed, but uses a bayonet type closure plug that results in a labyrinth like leakage path, see Figure 3.5-13. The size of the various pathways illustrated in the figure are listed in Table 3.5-5. The maximum pressure rise within the package is associated with the minimum flow area and the maximum gas generation and thermal expansion, with the total pressure loss estimated from a summation of the individual pressure losses associated with each portion of the flow path. Normalizing the individual pressure losses to the flow velocity in the A-B channel allows direct addition of the individual loss coefficients and eases the calculation of the pressure loss based on a single flow velocity. The normalizing to flow velocity involves multiplying the calculated loss coefficient by the square of the area ratio.

The entrance loss at the beveled portion of the closure plug can be estimated using a conical inlet with adjoining wall (i.e, Diagram 3-7[37]). Based on a 15° bevel angle on closure plug and L/D$_h$ > 0.6, the total loss coefficient at the entrance is:

$$\xi_1 = \frac{\Delta P}{0.5\rho v^2} = 0.13$$

---

[37] *Handbook of Hydraulic Resistance*, 3rd Ed., Idelchik, I.E., Begell House Publishers, 1996.

where v is the flow velocity upstream of the inlet area. This value is conservatively increased to $\xi_1 = 0.50$ for a blunt, flush inlet (Diagram 3-1[37]). Since the loss coefficient is based on the flow velocity after entering the gap, no adjustment for flow area in A-B is necessary:

$$K_1 = \xi_1 = 0.5$$

The pressure loss associated with flow in the A-B channel is a function of wall friction losses. Given the short path length and smooth wall surfaces, the associated pressure loss will be insignificant and can be ignored.

Flow between B-B' can be approximated as a 90-degree turn with sharp corners (Diagram 6-6[37]). Here the rectangular side length ratio (a_o/b_o) is equal to (5.64 x pi)/((5.76-5.64)/2) = 295.3 and the ratio of cross section areas (b_1/b_o) is equal to 0.006/0.06 = 0.1 (based on the minimum gap width after the turn). With these values, the loss factor extrapolated from Diagram 6-6 is $\xi_2 = 3.1$. Given uncertainties in the extrapolation, the computed value is doubled to 6.2 for conservatism[38]. Since the loss coefficient is based on the flow velocity in the gap approaching the turn, no adjustment for flow area in A-B is necessary:

$$K_2 = \xi_2 = 6.2$$

Flow between B'-E can also be approximated as a 90-degree sharp corner turn (Diagram 6-6[37]). Again, the rectangular side length ratio (a_o/b_o) is equal to (5.967 x pi)/(0.006 min gap) = 3124 and the ratio of cross section areas (b_1/b_o) is equal to 0.235/0.006 = 39. With these values, the loss factor can be conservatively estimated from Diagram 6-6 as $\xi_3 = 0.55$. Converting to the loss coefficient based on the gap area for flow path A-B yields:

$$K_3 = \xi_3 \left(\frac{0.45}{0.11}\right)^2 = 9.20$$

Flow between E-F can also be approximated as a sudden expansion with a discharge to ambient. A loss factor of 1 is used to account for these losses. Converting to the loss coefficient based on the gap area for flow path A-B yields:

$$K_4 = \xi_4 \left(\frac{0.45}{1.77}\right)^2 = 0.06$$

The parallel flow path to B'-E consisting of B'-C, C-D, and D-E can be conservatively ignored as its inclusion will serve to lower the estimated total pressure loss. Therefore, a bounding estimate of the total loss factor associated with the minimum expected flow path areas is calculated as $K_1 + K_2 + K_3 + K_4 = 0.5 + 6.2 + 9.2 + 0.06 = 16$.

The pressure loss for flow through the closure plug leakage path can be computed as a function of velocity and density via $\Delta P = 16 \times 0.5 \frac{\rho v^2}{g_c}$. Since mass flow is also a function of velocity and

---

[38] This flow loss is a reasonable upper bound given a worst case assumption that the flow comes to a complete stop before the turn and then needs to re-accelerate into the smaller gap. When adjusted for velocity differences, the flow loss under this worst case scenario would be approximately $(0.45 \text{ in}^2/0.11 \text{ in}^2)^2 \times 0.5 = 8.4$, where 0.5 is the loss factor associated with a blunt inlet fitting.

density, $\overset{\bullet}{m} = \rho \times v \times \text{Area}$, the pressure loss relationship can be re-formulated as a function of mass flow via:

$$\Delta P = 16 \times 0.5 \frac{\rho \left[\overset{\bullet}{m}/(\rho \times \text{Area}) \right]^2}{g_c}$$

where Area is the flow area in the path A-B (0.45 in^2 minimum) and the density is for the bulk gas temperature. From the data used to develop Figure 3.5-12, the maximum gas flow required to maintain atmospheric pressure within the ATR FFSC cavity due to only ideal gas expansion occurs during package heatup. The peak flowrate of 0.035 g-mole/min occurs approximately 8 minutes after the start of the 30-minute HAC fire and when the bulk gas temperature within the payload cavity has reached 230°F (110°C). Based on a molecular weight of 28.96 g/g-mole for air, the associated mass flow and density are 1.01 g/min (0.00004 lb$_m$/sec) and the gas density is 0.00091 g/cm^3 (0.057 lb$_m$/ft^3. Substituting these values into the above equation yields a $\Delta P = 0.1$ psi for the conservative assumption of minimum flow areas within all vent gaps. The pressure loss at nominal gap dimensions will be even lower.

This maximum pressure rise due to thermal expansion of the cavity gas is too low to create an issue. Thermal decomposition of polyethylene and neoprene will generate additional gases that would need to be vented. While only a small fraction of the material is expected to be thermally decomposed due to a combination of the temperature levels achieved and the time above the thermal decomposition temperature level, a bounding maximum pressure rise can be estimated assuming the entire inventory of both polyethylene and neoprene decomposes over a 60 minute period. The potential gas quantity associated with the total decomposition of the 100 g of polyethylene is 100 g/(28 g/g-mole) x 2 g-moles H$_2$ per g-mole polyethylene = 7.14 g-moles H$_2$. Similarly, the 1,926 g of neoprene associated with the SAR 60501-70 FHE assembly will generate 1926 g/(88.5 g/g-mole) x (2 g-moles H$_2$ + 1 g-moles HCl) per g-mole neoprene = 65.3 g-moles H$_2$ and HCl. The combined gas generation rate is therefore (7.14 + 65.3 g-mole)/60 minutes, or 1.21 g-moles/minute.

Based on the pressure loss associated with the 1.01 g/min flow rate due to gas expansion, the combined pressure loss of thermal decomposition and gas expansion would be:

$$\Delta P = 0.1 \, \text{psi} \times \left(\frac{1.01 + 1.21 \, \text{g - moles}}{1.01 \, \text{g - moles}} \right)^2 = 0.5 \, \text{psi}$$

This bounding pressure rise is also insignificant, especially given the conservative assumption of minimum flow areas within all vent gaps. As such, the assumption of a 0 psig pressure throughout the HAC event is valid for the purposes of determining the safety basis of the design.

Based on the level of and type of damage noted in Appendix 2.12.1, *Certification Tests on CTU-1* and Appendix 2.12.2, *Certification Tests on CTU-2*, no change to the net vent areas based on the assumed minimum gaps is expected. Thus the above conclusions remain valid for the damaged package configuration as well.

Table 3.5-3 – Neoprene Quantity Per Assembly

SAR Drawing	Neoprene Surface Area, in^2	Neoprene Volume, in^3	Neoprene Adhesive Volume, in^3	Neoprene Quantity, g[1]
60501-10	N/A	N/A	N/A	N/A
60501-20	N/A	N/A	N/A	N/A
60501-30	475	59	1.0	1210 g
60501-40	162	20	0.3	409 g
60501-50	266	33	0.5	676 g
60501-60	547	68	1.1	1393 g
60501-70	748	94	1.5	1926 g

Notes: [1] Based on density of 1.23 g/cm^3 (76.8 lb/ft^3 per Table 3.2-3)

Table 3.5-4 – Net Cavity Volume vs. Payload Assembly

SAR Drawing	Gross Cavity Volume, in^3	FHE Volume, in^3	Payload Volume, in^3	Net Cavity Volume, in^3	Comments
60501-20	1768.8	307.4[1]	168.1[2]	1293.3	ATR Loose Plate FHE
60501-30	"	154.6[3]	223.2[4]	1390.9	ATR FHE - Design basis selection due to combination of net cavity size and peak HAC temperature for FHE
60501-40	"	256.1[5]	88.5[6]	1424.1	MIT FHE
60501-50	"	307.4[7]	126.1[8]	1335.4	MURR FHE
60501-60	"	286.9[9]	142.9[9]	1339.0	RINSC FHE
60501-70	"	307.4[1]	168.1[2]	1293.3	Small Quantity FHE

Notes: [1] Based on 30 lb weight and density of 0.0976 in^3 per Tables 2.1-1 and 3.2-2
[2] Based on 20 lb weight and density of 0.112 in^3 per Tables 2.1-1 and 3.2-2
[3] Based on 15 lb weight and density of 0.097 in^3 per Tables 2.1-1 and 3.2-1
[4] Based on 25 lb weight and density of 0.112 in^3 per Tables 2.1-1 and 3.2-2
[5] Based on 25 lb weight and density of 0.0976 in^3 per Tables 2.1-1 and 3.2-2
[6] Based on 10 lb weight and density of 0.113 in^3 per Tables 2.1-1 and 3.6-4
[7] Based on 30 lb weight and density of 0.0976 in^3 per Tables 2.1-1 and 3.2-2
[8] Based on 15 lb weight and density of 0.119 in^3 per Tables 2.1-1 and 3.6-4
[9] Based on 28 lb weight and density of 0.0976 in^3 per Tables 2.1-1 and 3.2-2
[10] Based on 17 lb weight and density of 0.119 in^3 per Tables 2.1-1 and 3.6-4

Table 3.5-5 – Closure Leakage Path Areas

Flow Path	Inner/Outer Diameter, in	Gap Width/Length, in	Flow Path Area, in^2
A to B	5.64 ± 0.01 5.76 ± 0.06①	1.69	Max: 1.71 Min: 0.45
B to B'	5.70 (mean)	0.006 to 0.03②	Max: 0.54 Min: 0.11
B' to C	5.967 (min)	0.006 to 0.03②	Max: 0.56 Min: 0.11
C to D	6.38 ± 0.02 6.44 ± 0.01	0.281	Max: 0.91 Min: 0.30
D to E	6.21 (mean)	0.006 to 0.03②	Max: 0.59 Min: 0.12
B' to E	5.967 ± 0.01 6.44 ± 0.01	0.281	Max: 1.92③ Min: 1.77③
E to F	5.967 ± 0.01 6.44 ± 0.01	0.56	Max: 1.92③ Min: 1.77③

Notes: ① Tolerance from ASTM A269

② Based on bayonet tab of width of 0.25 in. centered in slot width of 0.281 in., and tolerances of +0.01 on both parts.

③ Based on 40% of gross area accounting for area of bayonet tabs and ignoring additional smaller gaps
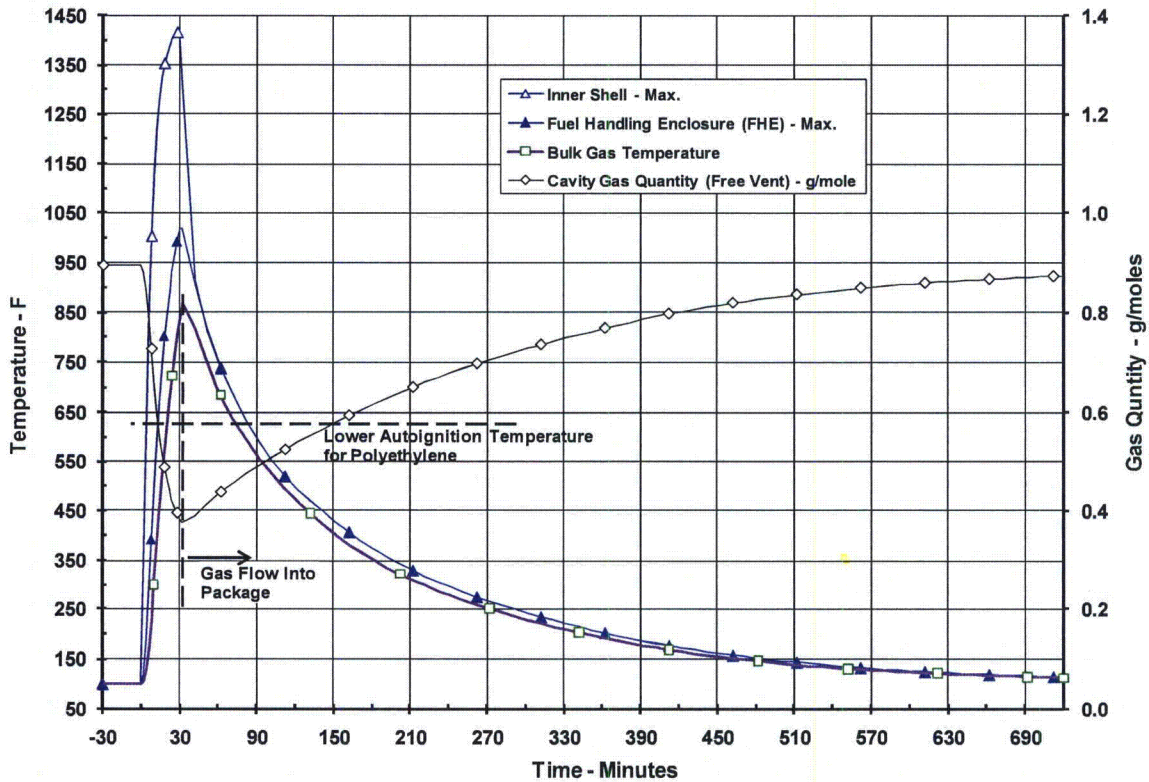
Figure 3.5-12 – Free Vent Gas Flow During HAC Transient
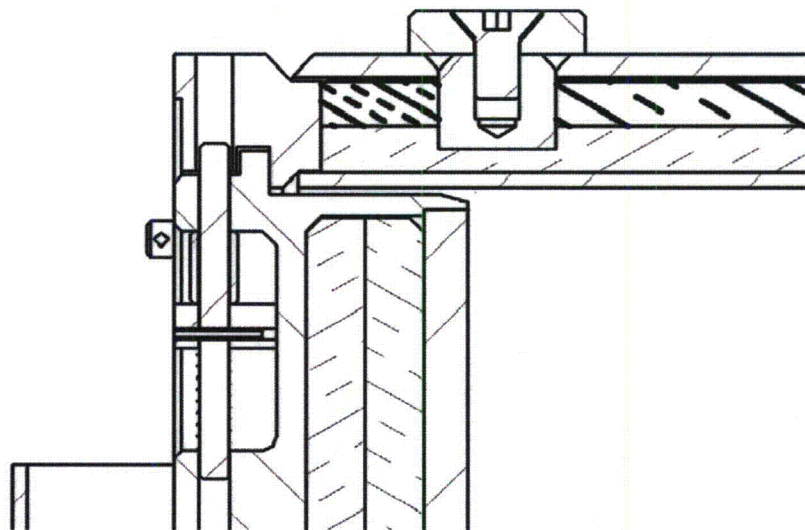
a) Package Closure
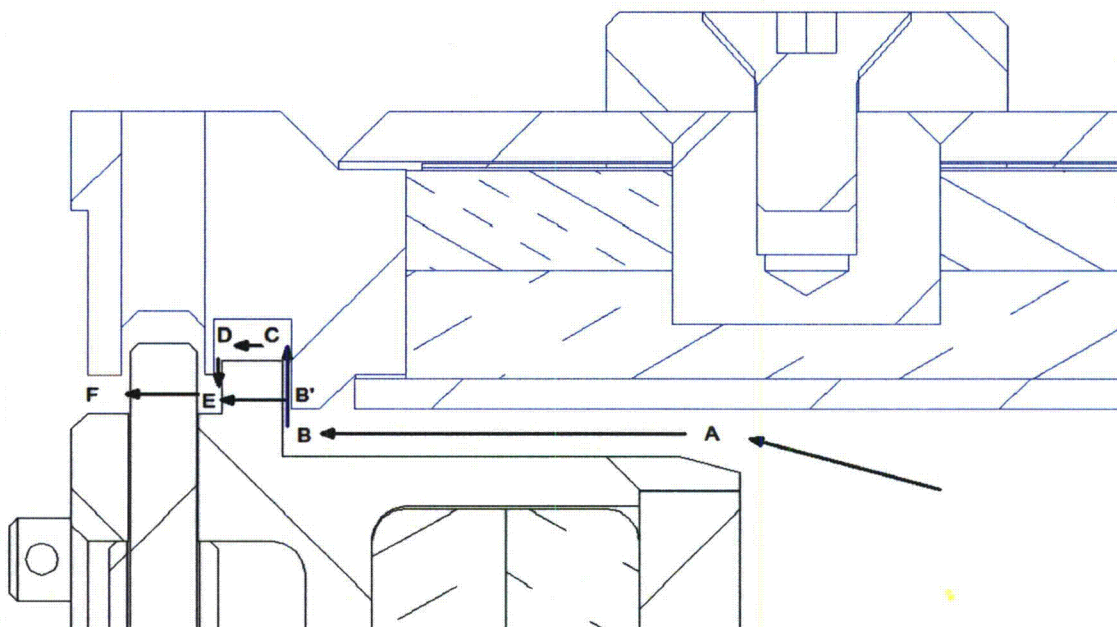
b) Enlarged Flow Paths at Package Closure

Figure 3.5-13 – Free Vent Gas Flow Path

3.6 Thermal Evaluation for MIT, MURR, and Small Quantity Payloads

This section identifies and describes the principal thermal design aspects of the ATR FFSC for the transport of one assembled MIT fuel element, one assembled MURR fuel element, or small quantity payloads as described in Section 1.2.2.4, *Small Quantity Payload*. The evaluation presented herein demonstrates that the thermal performance of the ATR FFSC when transporting these payloads is bounded by the temperatures reported for the transport of the ATR fuel element payload. Specifically, the evaluations presented herein demonstrate the thermal safety of the ATR FFSC package[1] complies with the thermal requirements of 10 CFR 71[2] when transporting a payload consisting of either an assembled, unirradiated MIT fuel element, MURR fuel element, RINSC fuel element, AFIP fuel element, DDE, loose, unirradiated MIT or MURR fuel element plates, U-Mo foils, or other small quantity payloads as described in Section 1.2.2.4, *Small Quantity Payload*.

All package components are shown to remain within their respective temperature limits under the normal conditions of transport (NCT). Further, per 10 CFR §71.43(g), the maximum temperature of the accessible package surfaces is demonstrated to be less than 122 °F for the maximum decay heat loading, an ambient temperature of 100 °F, and no insolation. Finally, the ATR FFSC package is shown to retain sufficient thermal protection following the HAC free and puncture drop scenarios to maintain all package component temperatures within their respective short term limits during the regulatory fire event and subsequent package cool-down.

3.6.1 Description of Thermal Design

The ATR FFSC package, as described and illustrated in Chapter 1.0, *General Information*, consists of three basic components: 1) a Body assembly, 2) a Closure assembly, and 3) either a Fuel Handling Enclosure (FHE) or a Loose Fuel Plate Basket (LFPB). The FHE is configured to house an assembled MIT or MURR fuel element, while the LFPB is configured to house loose ATR fuel element plates. The maximum gross weight of the package loaded with a MIT FHE and MIT fuel element is approximately 275 lbs. When loaded with either a MURR FHE and a MURR fuel element or a small quantity FHE and a small quantity payload, the maximum gross weight is approximately 290 lbs. The maximum gross weight of the package loaded with a LFPB containing its maximum payload of loose ATR fuel plates is approximately 290 lbs.

The ATR FFSC is designed as a Type AF packaging. The packaging is rectangular in shape and is intended to be transported in racks of multiple packages by highway truck. Since the payload generates essentially no decay heat, the worst case thermal conditions will occur with an individual package fully exposed to ambient conditions. The package performance when configured in a rack of multiple packages will be bounded by that seen for an individual package.

The thermal design aspects of the principal components of the packaging are described in more detail in Section 3.1, *Description of Thermal Design*. The paragraphs below present the thermal design features of the MIT, MURR, and small quantity payloads and their associated FHEs.

3.6.2   Design Features

3.6.2.1 MIT FHE

The MIT FHE is a machined, two-piece aluminum enclosure used to protect the MIT fuel element from damage during loading and unloading operations. The FHE consists of two identical machined segments fabricated from 3-inch 6061 aluminum plate stock. The FHE features neoprene rub strips to minimize fretting of the fuel element side plates where they contact the FHE. The FHE is neither anodized nor coated, but is left as unfinished aluminum. Spacer weldments on either end of the enclosure halves are used to position and support the MIT FHE within the ATR FFSC cavity. The spacers are also fabricated of 6061 aluminum. Figure 1.2-6 presents an exploded view of the MIT FHE and its spacers. Figure 1.2-12 presents a section view of a MIT fuel element. A polyethylene bag is used as a protective sleeve over the MIT fuel element. The design weight of the MIT FHE is 25 lbs.

3.6.2.2 MURR FHE

The MURR FHE is also a machined, two-piece aluminum enclosure used to protect the MURR fuel element from damage during loading and unloading operations. Like the MIT FHE, the two identical machined segments of the MURR FHE are fabricated from 3-inch 6061 aluminum plate stock and features neoprene rub strips to minimize fretting of the fuel element side plates. The FHE is neither anodized nor coated, but is left as unfinished aluminum. Spacer weldments on either end of the enclosure halves are used to position and support the FHE within the ATR FFSC cavity. The spacers are also fabricated of 6061 aluminum. Figure 1.2-7 presents an exploded view of the MURR FHE and its spacers. Figure 1.2-13 presents a section view of a MURR fuel element. A polyethylene bag is used as a protective sleeve over the MURR fuel element. The design weight of the MURR FHE is 30 lbs.

3.6.2.3 Small Quantity Payloads FHE

The small quantity payloads are transported in two FHEs: the RINSC fuel elements are transported in a dedicated FHE, and all other small quantity payloads are transported in the SQFHE.

3.6.2.3.1 RINSC FHE

Like the MIT and MURR FHEs, the RINSC FHE is fabricated as a machined, two-piece aluminum enclosure from 6061 aluminum plate stock. Neoprene rub strips are again used to minimize fretting of the fuel element side plates. The FHE is neither anodized nor coated, but is left as unfinished aluminum. Spacer weldments on either end of the enclosure halves are used to position and support the FHE within the ATR FFSC cavity. The spacers are also fabricated of 6061 aluminum. Figure 1.2-8 presents an exploded view of the RINSC FHE and its spacers. Figure 1.2-14 presents a section view of a RINSC fuel element. A polyethylene bag is used as a protective sleeve over the RINSC fuel element. The design weight of the RINSC FHE is 28 lbs.

3.6.2.3.2 SQFHE

The small quantity payload FHE (SQFHE) is like the MIT, MURR, and RINSC FHEs is fabricated as a machined, two-piece aluminum enclosure from 6061 aluminum plate stock. Neoprene rub strips may be used to minimize fretting of the fuel element side plates. The FHE is neither anodized nor coated, but is left as unfinished aluminum. Spacer weldments on either end of the enclosure halves are used to position and support the FHE within the ATR FFSC cavity. The spacers are also fabricated of 6061 aluminum. Figure 1.2-9 presents an exploded view of the SQFHE and its spacers. Figures 1.2-16 through 1.2-19 present views of potential small quantity payloads. A polyethylene bag may be used as a protective sleeve over the small quantity payloads. The design weight of the SQFHE is 30 lbs.

3.6.3   Content's Decay Heat

The ATR FFSC is designed as a Type AF packaging for transportation of an unirradiated fuel elements or a bundle of loose, unirradiated fuel plates. The decay heat associated with un-irradiated fuel is negligible. Therefore, no special devices or features are needed or utilized in the ATR FFSC packaging to dissipate the decay heat. Section 1.2.2, *Contents*, provides additional details regarding the potential contents of the ATR FFSC.

3.6.4   Summary Tables of Temperatures

Table 3.6-1 provides a summary of the maximum package component temperatures achieved under NCT and HAC conditions for either the MIT or MURR fuel element payloads. These temperatures are either bounded by or similar to those reported in Table 3.1-1 for the transport of the ATR fuel element payload. Those values unbounded by the values found in Table 3.6-1 remain well below the maximum allowable temperatures. Based on the results for the MURR fuel element, the maximum temperatures achieved under NCT and HAC conditions for the small quantity payloads (including the RINSC fuel element) are shown by qualitative analysis below to also be bounded by the results presented in Table 3.1-1.

The MIT and MURR payload temperatures for NCT are based on an analytical model of the ATR FFSC package under extended operation with an ambient temperature of 100°F and a diurnal cycle for the insolation loading. The temperatures for HAC are based on an analytical model of the ATR FFSC package with the worst-case, hypothetical pre-fire damage as predicted based on drop tests using full-scale certification test units (CTUs). The ATR FFSC with the small quantity payloads was not specifically modeled as part of this evaluation. Instead, its thermal performance is estimated using a qualitative approach based on the thermal characteristics of the other payloads and their associated thermal performance.

The MIT and MURR payload results for NCT demonstrate that significant thermal margin exists for all package components. This is expected since the only significant thermal loads on the package arise from insolation and ambient temperature changes. The payload dissipates essentially zero decay heat. Further, the evaluations for NCT demonstrate that the package skin temperature will be below the maximum temperature of 122°F permitted by 10 CFR §71.43(g) for accessible surface temperature in an nonexclusive use shipment when transported in a 100°F environment with no insolation. Given the significant thermal margin existing for the other

payloads and the similar materials of fabrication, the small quantity payloads are also predicted to exhibit large thermal margins.

The MIT and MURR payload results for HAC conditions demonstrate that the design of the ATR FFSC package provides sufficient thermal protection to yield component temperatures that are significantly below the acceptable limits defined for each component. While the neoprene rubber and polyethylene plastic material used to protect the fuel element from damage are expected to reach a sufficient temperature level during the HAC fire event to induce thermal decomposition, the loss of these components is not critical to the safety of the package. As demonstrated in Section 3.5.3, *Thermal Decomposition/Combustion of Package Organics*, the available oxygen in the package, plus that which may enter the package under pressure differential and gas diffusion forces, is insufficient to result in any significant heat generation due to combustion. Given the similar materials of fabrication and equivalent thermal mass as the MURR payload, the small quantity payloads are also predicted to exhibit large thermal margins under HAC conditions.

3.6.5   Summary Tables of Maximum Pressures

Table 3.6-2 presents a summary of the maximum pressures achieved under NCT and HAC conditions. Since the ATR FFSC package is a vented package, both the maximum normal operating pressure (MNOP) and the maximum pressure developed within the payload compartment under the HAC condition are 0 psig. Section 3.5.3, *Thermal Decomposition/Combustion of Package Organics*, provides the justification for assuming a 0 psig package pressure for the HAC event.

Although the volume between the outer and inner shells is sealed, it does not contain organic or other materials that may outgas or thermally decompose. Therefore, the maximum pressure that may develop within the space will be limited to that achieved due to ideal gas expansion. The maximum pressure rise under NCT will be less than 4 psig, while the pressure rise under HAC conditions will be 39 psig.

Table 3.6-1 – Maximum Temperatures for NCT and HAC Conditions

Location / Component	NCT Hot Conditions	Accident Conditions	Maximum Allowable [1]	
			Normal	Accident
Fuel Element Fuel Plate	143°F	640°F	400°F	1,100°F
Fuel Element Side Plate	143°F	644°F	400°F	1,100°F
Neoprene Rub Strips/Polyethylene Bag	143°F [2]	710°F	225°F	N/A
Fuel Handling Enclosure (FHE)	143°F	710°F	400°F	1,100°F
Inner Shell	157°F	1,417°F	800°F	2,700°F
Ceramic Fiber Insulation, Body - Maximum - Average	184°F 149°F	1,462°F 1,253°F	2,300°F 2,300°F	2,300°F 2,300°F
Ceramic Fiber Insulation, Closure - Maximum - Average	145°F 143°F	1,402°F 1,236°F	2,300°F 2,300°F	2,300°F 2,300°F
Closure	145°F	1,439°F	800°F	2,700°F
Outer Shell	184°F	1,475°F	800°F	2,700°F

Table Notes:

[1] Maximum allowable temperatures are defined in Section 3.2.2, *Technical Specifications of Components*.

[2] Component temperature assumed to be equal to that of the FHE.

Table 3.6-2 – Summary of Maximum Pressures

Condition	Fuel Cavity Pressure	Outer/Inner Shell Cavity Pressure
NCT Hot	0 psi gauge	4 psi gauge
HAC Hot	0 psi gauge	39 psi gauge

3.6.6 Material Properties and Component Specifications

The ATR FFSC is fabricated primarily of Type 304 stainless steel, 5052-H32 and 6061-T651 aluminum, ceramic fiber insulation, and neoprene rubber. The payload materials include 6061-T6 and/or 6061-0 aluminum, uranium aluminide (UAl_x), uranium silicide (U_3Si_2), and uranium molybdenum (U-7Mo in an aluminum-silicon matrix or U-10Mo in a foil coated with thin zirconium interlayers). A polyethylene plastic bag is used as a protective sleeve over the fuel element.

3.6.6.1 Material Properties

The material specifications for the ATR FFSC package are defined in Section 3.2.1, *Material Properties*. Table 3.6-3 presents the thermal properties for 6061 aluminum used for the MIT and MURR FHEs, as taken from Table TCD of the ASME Boiler and Pressure Vessel Code[3]. Although the design permits a variety of aluminum tempers to be used, a single data set is provided since the material temper has little to no effect on its thermal properties. Further, because the HAC analysis requires thermal properties in excess of the maximum temperature point of 400°F provided in Table TCD, the property values at 1100°F (i.e., the approximate melting point for aluminum) are assumed to be the same as those at 400°F. This approach is appropriate for estimating the temperature rise within the fuel basket during the HAC event since the thermal conductivity of aluminum alloys tends to decrease with temperature while the specific heat tends to increase. The density values listed in the table are taken from an on-line database[4]. Properties between the tabulated values are calculated via linear interpolation within the heat transfer code.

Table 3.6-4 presents the thermal properties for the MIT and MURR fuel elements. For analysis purposes, the material used for the side plates and end fittings are assumed to be 6061-0 aluminum. The thermal properties for the fuel plates are determined as a composite of the cladding and the fuel core materials based on the geometry data for the MIT and MURR fuel element[39,40] and the thermal properties for the ATR fuel element materials[6]. This approach is the same as used for the ATR fuel element. The details of the computed values are presented in Appendix 3.6.9.2.3, *Determination of Composite Thermal Properties for MIT and MURR Fuel Plates*. For simplicity, the thermal properties are assumed to be constant with temperature based on the use of conservatively high thermal conductivity and conservatively low specific heat values. This approach maximizes the heat transfer into the fuel components during the HAC event, while under-estimating the ability of the components to store the heat.

The RINSC fuel elements are fabricated with a nominally 0.020-in thick mixture of uranium silicide (U_3Si_2) and aluminum powder as the fuel "meat" and a nominally 0.015-in thick aluminum alloy cladding. The twenty-two (22) flat fuel plates have a 2.8-in width, an overall length of 25-in, and an active fuel region of 22.5 to 24.0-in. These fuel plate meat and cladding

---

[39] *Massachusetts Institute of Technology, Test Research Training Reactor 3 Fuel Plate*, EG&G, Idaho, Inc., Drawing No. 410368, Rev. A.

[40] *University of Missouri at Columbia, Test Research Training Reactor 4 MURR Fuel Plate*, EG&G, Idaho, Inc., Drawing No. 409406, Rev. E.

thicknesses match those of the interior plates for the ATR fuel element and are similar to those for the MURR fuel plates. The side plates are fabricated of ASTM B 209, aluminum alloy 6061-T6 and 6061-T651 and are approximately 0.188-in thick. This is similar to the side plate thicknesses of the ATR, MITR, and MURR fuel elements.

The thermal conductivity of the RINSC fuel plates are similar to data obtained in the measurements of the thermal conductivities for the uranium aluminide (UAl$_x$) based fuels[41]. Similarly, the thermal mass of the fuel plates are comparable despite the higher density of uranium silicide versus uranium aluminide since the ratio of the specific heats of the two materials is nearly the inverse of the density ratio.

The additional small quantity payloads, including AFIP elements, U-Mo foils, DDEs, MIT and MURR loose fuel plates, and other fresh fuels with total U-235 loading ≤ 400 g and U-235 enrichment ≤ 94% are fabricated as described in Section 1.2.2.4, *Small Quantity Payload*. Small quantity payloads may be shipped with aluminum dunnage.

The thermal properties for air and for the non-metallic materials used in the ATR FFSC are presented in Section 3.2.1, *Material Properties*, as is the assumed emissivity (ε) for each radiating surface and the solar absorptivity (α) value for the exterior surface. The 6061-0 aluminum used for the MIT and MURR fuel components are assumed to have a surface coating of boehmite (Al$_2$O$_3$H$_2$O). A 25 μm boehmite film will exhibit a surface emissivity of approximately 0.92[13]. While a fresh fuel element may have a lower surface emissivity, the use of the higher value will provide a conservative estimate of the temperatures achieved during the HAC event.

3.6.6.2 Technical Specifications of Components

The materials used in the ATR FFSC that are considered temperature sensitive include the aluminum used for the FHEs, the LFPB, and the fuel elements, the neoprene rubber, and the polyethylene wrap used as a protective sleeve around the fuel elements. Of these materials, only the aluminum used for the fuel elements is considered critical to the safety of the package. The other materials either have temperature limits above the maximum expected temperatures or are not considered essential to the function of the package.

Section 3.2.2, *Technical Specifications of Components*, presents the basis for the temperature limits of the various components. These temperature limits are applicable to this safety evaluation as well.

---

[41] IAEA-TECDOC-643, *Research Reactor Core Conversion Guidebook*, Volume 4: Fuels (Appendices I-K), International Atomic Energy Agency, Vienna, Austria.

Table 3.6-3 – Thermal Properties of Package Metallic Materials

Material	Temperature (°F)	Thermal Conductivity (Btu/hr-ft-°F)	Specific Heat (Btu/lb$_m$-°F)	Density (lb$_m$/in^3)
Aluminum Type 6061-T651 / T6511	70	96.1	0.214	0.098
	100	96.9	0.216	
	150	98.0	0.220	
	200	99.0	0.222	
	250	99.8	0.224	
	300	100.6	0.227	
	350	101.3	0.230	
	400	101.9	0.231	
	1100 [1]	101.9	0.231	

Notes:

[1] Values for 1100°F are assumed equal to values at 400°F.

Table 3.6-4 – Thermal Properties of MIT and MURR Fuel Materials

Material	Temperature (°F)	Thermal Conductivity (Btu/hr-ft-°F)	Specific Heat (Btu/lb$_m$-°F)	Density (lb$_m$/in^3)
Aluminum Type 6061-0	32	102.3	-	0.0976
	62	-	0.214	
	80	104.0	-	
	170	107.5	-	
	260	109.2	0.225	
	350	109.8	-	
	440	110.4	0.236	
	530	110.4	-	
	620	109.8	0.247	
	710	108.6	-	
	800	106.9	0.258	
	890	105.2	-	
	980	103.4	0.269	
	1080	101.1	0.275	
MURR Fuel Plate[1]	80	57.9	0.165	0.121
	800		0.200	
MIT Fuel Plate[1]	80	72.6	0.176	0.115
	800		0.212	

Notes:

[1] Values determined based on composite value of aluminum cladding and fuel core material (see Appendix 3.5.2.4). Thermal conductivity value is valid for axial and circumferential heat transfer within fuel plate.

3.6.7   Thermal Evaluation for Normal Conditions of Transport

The ATR FFSC with the MIT or MURR fuel element payloads is transported horizontally under normal conditions of transport (NCT). This establishes the orientation of the exterior surfaces of the package for determining the free convection heat transfer coefficients and insolation loading. While the package would normally be transported in tiered stacks of multiple packages, the evaluation for NCT is conservatively based on a single, isolated package since this approach will yield the bounding maximum and minimum temperatures achieved by any of the packages. Further, since the surface of the transport trailer is conservatively assumed to prevent heat exchange between the package and the ambient, the bottom of the ATR FFSC is treated as an adiabatic surface.

The details of the thermal modeling used to simulate the ATR FFSC package under NCT conditions are provided in Appendix 3.5.2, *Analytical Thermal Model*, while details of the thermal modeling of the MIT and MURR FHEs and fuel elements are provided in Appendix 3.6.9.2.1, *Description of MIT and MURR Payload Thermal Models for NCT Conditions*. The ATR FFSC with small quantity payloads was not specifically modeled as part of this evaluation. Instead, its thermal performance is estimated using a qualitative approach based on the thermal characteristics of the other payloads and their associated thermal performance. See below for the details of this qualitative basis.

3.6.7.1 Heat and Cold

3.6.7.1.1 Maximum Temperatures

The maximum temperature distribution for the ATR FFSC occurs with a diurnal cycle for insolation loading and an ambient air temperature of 100°F, per 10 CFR §71.71(c)(1). The evaluation of this condition is conducted as a transient using the thermal model of an undamaged ATR FFSC described in Appendix 3.6.9.2.1, *Description of MIT and MURR Payload Thermal Models for NCT Conditions*. Figure 3.6-1 illustrates the expected heat-up transient for an ATR FFSC loaded with a MIT fuel element. The transient analysis assumes a uniform temperature condition of 70°F for all components prior to loading and exposure to the specified NCT condition at time = 0.

The figures demonstrate that the ATR FFSC package will respond rapidly to changes in the level of insolation and will reach it peak temperatures within the first day or two after loading. The higher thermal mass of the MIT FHE on a unit length basis versus that of the ATR FHE is reflected in the delayed response of the MIT FHE to changes in the inner shell temperature, whereas the ATR FHE was seen in Figure 3.3-1 to respond more rapidly. A similar temperature response curve is seen for the MURR FHE.

Table 3.6-5 presents the maximum temperatures reached for various components of the package. As seen from the table, all components are within in their respective temperature limits. Figure 3.6-2 illustrates the predicted temperature distribution within the ATR FFSC package with a MIT fuel element payload at the end of the evaluated transient heat up period and near the time of peak temperature. Figure 3.6-3 presents the temperature distribution within the ATR FFSC package with a MURR fuel element payload.

The maximum temperature distribution for the ATR FFSC without insolation loads occurs with an ambient air temperature of 100°F. Since the package payload dissipates essentially zero watts of decay heat, the thermal analysis of this condition represents a trivial case and no thermal calculations are performed. Instead, it is assumed that all package components achieve the 100°F temperature under steady-state conditions. The resulting 100°F package skin temperature is below the maximum temperature of 122°F permitted by 10 CFR §71.43(g) for accessible surface temperature in a nonexclusive use shipment.

The ATR FFSC with the small quantity payload was not specifically modeled as part of this evaluation. Instead, its thermal performance is estimated using a qualitative approach based on the thermal characteristics of the other payloads and their associated thermal performance. Using this approach, it is estimated that the maximum temperatures attained for the transportation of the small quantity payload within the ATR FFSC will be bounded by that presented for the MURR payload. This conclusion is based on the facts that the combined weight of the small quantity payload and MURR FHE's with their enclosed fuel elements, plates, or foils are similar (see Section 1.2.2.3, *MURR Fuel Element*, and Section 1.2.2.4, *Small Quantity Payload*), the FHE's are both fabricated of 6061 aluminum, and the fuel elements have similar thermal properties (see Section 3.6.6.1). This conclusion is further supported by the fact that Table 3.6-5 demonstrates that the MIT and MURR fuel elements produce essentially the same peak NCT temperatures despite their design differences. As such, the limited design differences between the MURR and small quantity payloads will not yield a significant difference in their NCT thermal response.

The ATR FFSC with the RINSC fuel element payload is not specifically modeled as part of this evaluation. Instead, its thermal performance is estimated using a qualitive approach based on the thermal characteristics of the other payloads and their associated thermal performance. (See Section 3.6.9.2.4, *Determination of Thermal Properties for RINSC Element* for details). Using this approach, it is estimated that the maximum temperatures attained for the transportation of the RINSC fuel element is considered bounded by the analysis of the MURR payload and no additional analysis is required.

3.6.7.1.2 Minimum Temperatures

The minimum temperature distribution for the ATR FFSC occurs with a zero decay heat load and an ambient air temperature of -40°F per 10 CFR §71.71(c)(2). The thermal analysis of this condition also represents a trivial case and no thermal calculations are performed. Instead, it is assumed that all package components achieve the -40°F temperature under steady-state conditions. As discussed in Section 3.2.2, *Technical Specifications of Components*, the -40°F temperature is within the allowable operating temperature range for all ATR FFSC package components.

3.6.7.2 Maximum Normal Operating Pressure

The payload cavity of the ATR FFSC is vented to the atmosphere. As such, the maximum normal operating pressure (MNOP) for the package is 0 psig.

While the volume between the outer and inner shells is sealed, it does not contain organic or other materials that may outgas or thermally decompose. Therefore, the maximum pressure that may develop within the space will be limited to that achieved due to ideal gas expansion. Assuming a temperature of 70°F at the time of assembly and a maximum operating temperature of

190°F (based on the outer shell temperature, see Table 3.6-5, conservatively rounded up), the maximum pressure rise within the sealed volume will be less than 4 psi.

Table 3.6-5 – Maximum Package NCT Temperatures

Location / Component	MIT Fuel Payload	MURR Fuel Payload	Maximum Allowable [1]
Fuel Element Fuel Plate	143°F	142°F	400°F
Fuel Element Side Plate	143°F	142°F	400°F
Neoprene Rub Strips/Polyethylene Bag	143°F [2]	142°F [2]	225°F
Fuel Handling Enclosure (FHE)	143°F	142°F	400°F
Inner Shell	157°F	157°F	800°F
Ceramic Fiber Insulation, Body			
- Maximum	184°F	184°F	2,300°F
- Average	149°F	148°F	2,300°F
Ceramic Fiber Insulation, Closure			
- Maximum	145°F	145°F	2,300°F
- Average	143°F	143°F	2,300°F
Closure	145°F	145°F	800°F
Outer Shell	184°F	184°F	800°F

Table Notes:

[1] The maximum allowable temperatures under NCT conditions are provided in Section 3.2.2, *Technical Specifications of Components*.

[2] Component temperature assumed to be equal to that of the FHE.
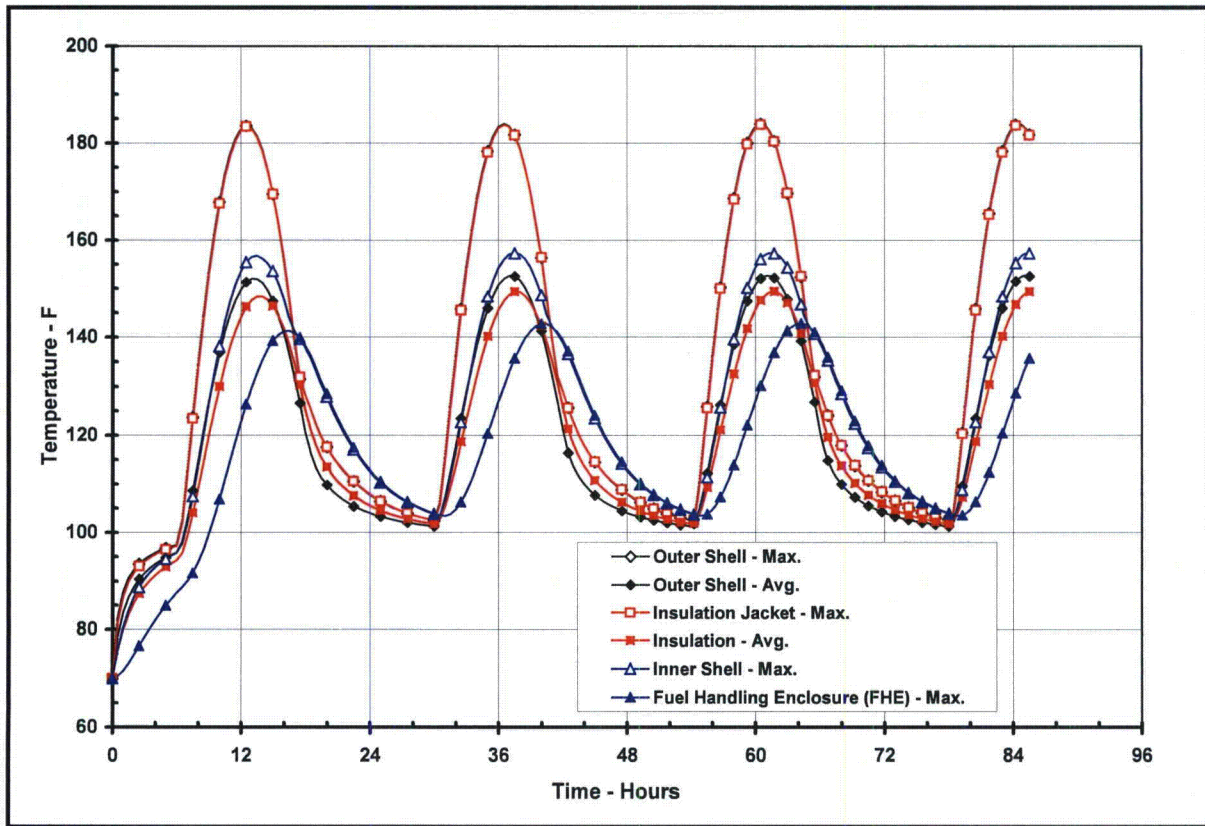
Figure 3.6-1 – ATR FFSC Package Heat-up with MIT Payload, NCT Hot Conditions
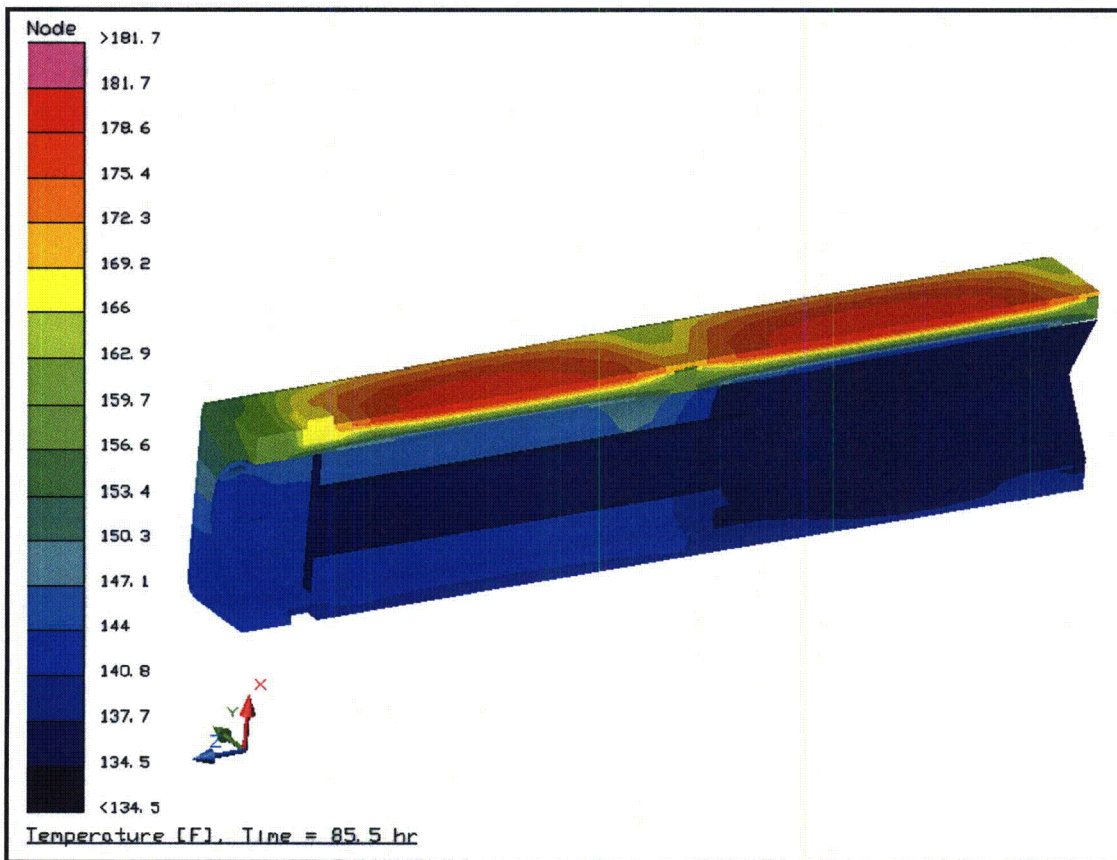
Figure 3.6-2 – Package NCT Temperature Distribution for MIT Payload
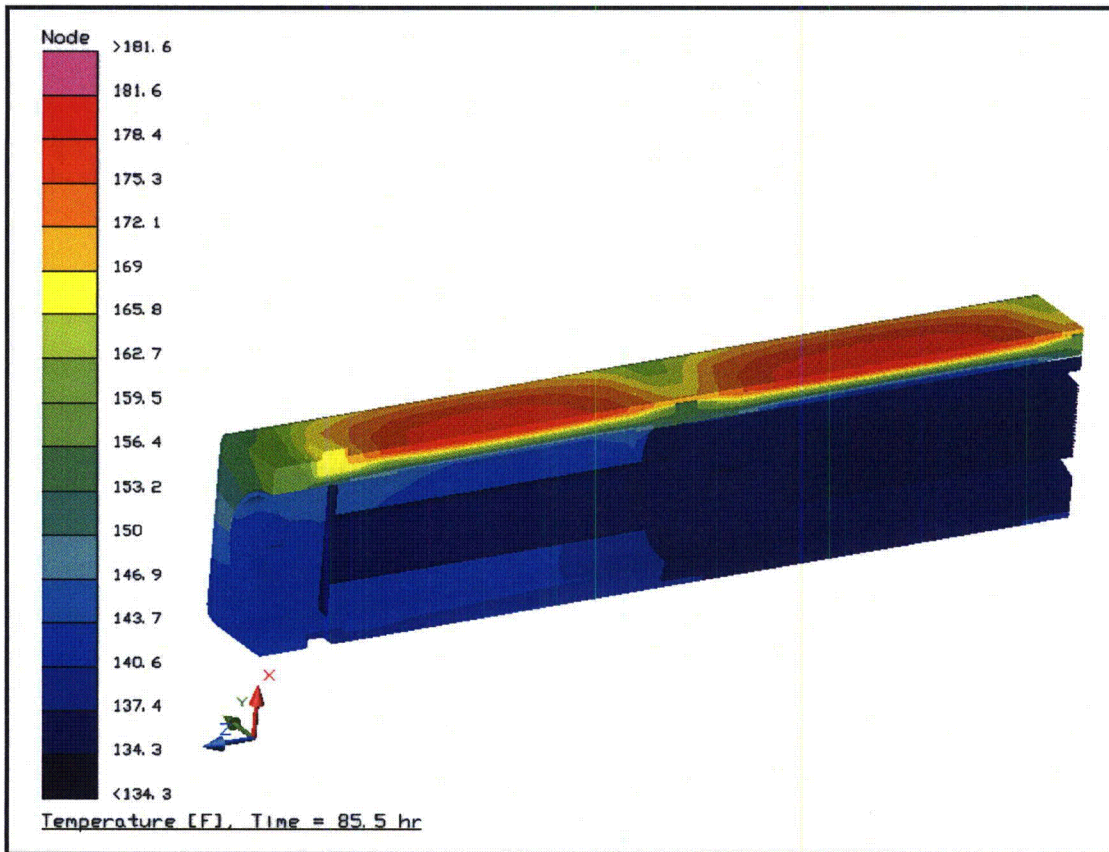
Figure 3.6-3 – Package NCT Temperature Distribution for MURR Payload

3.6.8   Thermal Evaluation for Hypothetical Accident Conditions

This section presents the thermal evaluation of the ATR FFSC package under the hypothetical accident condition (HAC) specified in 10 CFR §71.73(c)(4)[2] based on an analytical thermal model. The analytical model of the ATR FFSC for HAC is a modified version of the quarter symmetry NCT model described in Appendix 3.5.2.1, *Description of Thermal Model for NCT Conditions*, with the principal model modifications consisting of simulating the expected package damage resulting from the drop events that are assumed to precede the HAC fire and changing the package surface emissivities to reflect the assumed presence of soot and/or surface oxidization. The analytical model of the MIT and MURR fuel elements are the same as those described in Appendix 3.6.9.2.1, *Description of MIT and MURR Payload Thermal Models for NCT Conditions*. The evaluations of the ATR FFSC with a small quantity payload and RINSC under HAC conditions are accomplished using a qualitative approach in the same manner as accomplished for NCT conditions (see Section 3.6.7.1.1, *Maximum Temperatures*).

Physical testing using full scale certified test units (CTUs) is used to establish the expected level of damage sustained by the ATR FFSC package from the 10 CFR 71.73 prescribed free and puncture drops that are assumed to precede the HAC fire event. Appendix 3.5.2.2, *Description of Thermal Model for HAC Conditions*, provides an overview of the test results, the rationale for selecting the worst-case damage scenario, and the details of the thermal modeling used to simulate the package conditions during the HAC fire event.

3.6.8.1 Initial Conditions

The initial conditions assumed for the package prior to the HAC event are described below in terms of the modifications made to the NCT thermal model to simulate the assumed package conditions prior to and during the HAC event. These modifications are:

- Simulated the worst-case damage arising from the postulated HAC free and puncture drops as described in Appendix 3.5.2.2, *Description of Thermal Model for HAC Conditions*,

- Assume an initial, uniform temperature distribution of 100°F based on a zero decay heat package at steady-state conditions with a 100°F ambient with no insolation. This assumption complies with the requirement of 10 CFR §71.73(b)[2] and NUREG-1609[17],

- Increased the emissivity of the external surfaces from 0.45 to 0.8 to account for possible soot accumulation on the surfaces, per 10 CFR §71.73(c)(4),

- Increased the emissivity of the interior surfaces of the outer shell from 0.30 to 0.45 to account for possible oxidization of the surfaces during the HAC event,

Following the free and puncture bar drops, the ATR FFSC package is assumed come to rest in a horizontal position prior to the initiation of the fire event. Given that the package geometry is essentially symmetrical about its axial axis, there are no significant thermal differences whether the package is right-side up, up-side down, or on its side. The MIT, MURR, RINSC, and small quantity payloads are not expected to be re-positioned as a result of the pre-fire drop and puncture bar events based on the limited damage seen for the ATR FHE as a result of the drop tests

conducted on the ATR FFSC presented in Section 2.12.1, *Certification Tests on CTU-1*, and given the greater robustness of the MIT, MURR, RINSC, and small quantity payload FHEs. However, even if the end spacers are conservatively assumed to buckle as a result of the HAC drop event, no significant temperature increase will occur since direct contact between the FHE and the closure plug will be prevented and because the average radial heat transfer through the sides of the package does not change significantly as a function of axial position. Therefore, the peak package temperatures predicted under this evaluation based on no payload re-positioning or reconfiguration are representative of those achieved for any package orientation and/or credible re-positioning of the enclosed payloads.

3.6.8.2 Fire Test Conditions

The fire test conditions analyzed to address the 10 CFR §71.73(c) requirements are as follows:

- The initial ambient conditions are assumed to be 100°F ambient with no insolation,

- At time = 0, a fully engulfing fire environment consisting of a 1,475°F ambient with an emissivity of 1.0 is used to simulate the hydrocarbon fuel/air fire event. The assumption of a flame emissivity of 1.0 bounds the minimum average flame emissivity coefficient of 0.9 specified by 10 CFR §71.73(c)(4),

- The convection heat transfer coefficients between the package and the ambient during the 30-minute fire event are based on an average gas velocity[18] of 10 m/sec. Following the 30-minute fire event the convection coefficients are based on still air,

- The ambient condition of 100°F with insolation is assumed following the 30-minute fire event. Since a diurnal cycle is used for insolation, the evaluation assumes that the 30-minute fire begins at noon so as to maximize the insolation heating during the post-fire cool down period. A solar absorptivity of 0.9 is assumed for the exterior surfaces to account for potential soot accumulation on the package surfaces.

The transient analysis is continued for 11.5 hours after the end of the 30-minute fire to ensure that the peak package temperatures are captured.

3.6.8.3 Maximum Temperatures and Pressure

3.6.8.3.1 Maximum HAC Temperatures

The thermal performance of the ATR FFSC package loaded with a MIT fuel element payload is summarized in Table 3.6-6, while Table 3.6-7 presents a summation of the results with a MURR fuel element payload. With the exception of the neoprene rub strips and the polyethylene bag used as a protective sleeve around the fuel elements, all other components of the package are seen to remain well below their allowable short term temperature limits. As with the ATR payload, the thermal decomposition of the neoprene strips and polyethylene bag will not impact the safety of the package and any associated out-gassing will not contribute to package pressurization since the package is vented. As demonstrated in Section 3.5.3, *Thermal*

Decomposition/Combustion of Package Organics, the available oxygen in the package is sufficient for consumption of less than 1% of the polyethylene and the quantity of air that enters the cavity under pressure differential and gas diffusion forces is insignificant. The discussion in Section 3.5.3 also provides validation of a 0 psig package pressure for the HAC event.

The outer shell and the ceramic fiber insulation provide thermal protection to the ATR FFSC package during the HAC fire event. The level of thermal protection can be seen via the thermal response curves presented in Figure 3.6-4 and Figure 3.6-5 for the ATR FFSC package loaded with a MIT and MURR fuel element payload, respectively. As seen from the figures, while the exterior of the package quickly rises to nearly the temperature of the fire, the heat flow to the FHE and its enclosed fuel element payloads is sufficiently restricted to limit the maximum temperatures of both the FHE and the fuel element to well below the melting point of aluminum. The higher thermal mass of the MIT and MURR FHEs in comparison with that of the ATR FHE is reflected in their correspondingly slower heat up and longer cool down during the fire transient when compared to that see in Figure 3.4-1 for the ATR FHE. The higher temperature reached by the MURR FHE versus that seen for the MIT FHE is due to the conservative assumption of direct contact between the FHE and the inner shell along two line locations for the MURR FHE versus one line location for the MIT FHE. Similarly, the difference in the shape of the FHE temperature response curve seen for the MIT FHE between 30 minutes and 60 minutes versus that seen for the MURR FHE for the same time period is related to the fact that the top end of the shorter MIT FHE lies below one of the package's support ribs while the top of the MURR FHE is adjacent to it (see Figures 3.6-6 and 3.6-7).

Although the peak temperature achieved by the MURR FHE is about 20°F hotter than that achieved by the MIT FHE, the peak temperatures reached by the MIT and MURR fuel elements are approximately the same. This results from a combination of the higher thermal mass and greater separation distance between the end of the fuel element and the start fuel plates associated with the MURR fuel element versus that for the MIT fuel element.

The results demonstrate that thermal performance is similar to that achieved with the transport of a LFPB payload (see Section 3.4.3, *Maximum Temperature and Pressure*) due to the fact that these FHE have a thermal mass similar to that of the LFPB. The result of the higher thermal mass is that the MIT and MURR FHEs have a peak temperature that is approximately 300°F cooler than that seen for the ATR FHE and the enclosed fuel elements reach peak temperatures that are 90 to 180°F cooler than that seen for the ATR fuel element. The thermal performance of the ATR FFSC packaging with either the MIT or MURR payload is similar to that seen for the ATR payload.

As with the evaluation for NCT, the thermal performance of the ATR FFSC with the small quantity payload and RINSC under HAC conditions was not specifically modeled as part of this evaluation. Instead, based on the similarity between the MURR and small quantity payloads, the thermal performance is qualitatively estimated to be bounded by that presented for the MURR payload. Since the combined weight of the small quantity payload and MURR FHE's with their enclosed fuel elements, plates, or foils are similar (see Section 1.2.2.3, *MURR Fuel Element*, and Section 1.2.2.4, *Small Quantity Payload*) and the thermal mass of the two payloads are similar, the transient response of the small quantity payload can be expected to be similar to that presented for the MURR payload. This conclusion is further supported by the fact that Table 3.6-6 and Table 3.6-7 show that similar transient results occur for the MIT and MURR fuel

element payloads despite their design differences. As such, the limited design differences between the MURR and small quantity payloads will not yield a significant difference in their HAC thermal response. Additionally, the SQFHE thermal response without its small quantity payload is expected to be similar with the conservative ATR LFPB thermal response. The empty SQFHE and LFPB are constructed of similar materials and have the same thermal mass of 30 lbs. The LFPB thermal evaluation is conservatively performed without its loose fuel plate payload, see Sections 3.4.3.1 and 3.5.2.1 for discussion of the LFPB thermal evaluation. Therefore, use of the SQFHE for any payload amount up to the maximum loaded SQFHE weight of 50 lbs is bounded by the thermal response of the LFPB evaluation. The addition of any small quantity payload mass to the SQFHE will increase the thermal mass and thereby increase the conservatism of the thermal response with respect to the empty LFPB thermal evaluation results.

3.6.8.3.2 Maximum HAC Pressures

The payload cavity of the ATR FFSC is vented to the atmosphere. As such, the maximum pressure achieved under the HAC event will be 0 psig. Section 3.5.3, *Thermal Decomposition/Combustion of Package Organics*, provides the justification for assuming a 0 psig package pressure for the HAC event.

Although the volume between the outer and inner shells is sealed, it does not contain organic or other materials that may outgas or thermally decompose. Assuming a temperature of 70°F at the time of assembly and a maximum temperature of 1,475°F (based on the outer shell temperature, see Table 3.6-6), the maximum pressure rise within the sealed volume due to ideal gas expansion will be less than 39 psig. This level of pressurization will occur for only a few minutes and then quickly reduce as the package cools.

3.6.8.4 Maximum Thermal Stresses

The ATR FFSC package is fabricated principally of sheet metal and relatively thin structural steel shapes. As such, the thermal stresses developed within each component during the HAC fire event will be low and not significant to the safety of the package.

The temperature difference that exists between the inner and outer shells during the HAC event (see the average inner and outer shell temperatures presented in Figure 3.6-4) will result in differential thermal expansion between the shells. The thermal impact related to the potential package geometry displacement due to this differential thermal expansion was evaluated in Section 3.4.4, *Maximum Thermal Stresses*, and found not to be significant to the safety of the package.

Table 3.6-6 – HAC Temperatures with MIT Payload

Location / Component	Pre-fire	End of Fire	Peak	Maximum Allowable [1]
MIT Fuel Element Fuel Plate	100°F	345°F	640°F	1,100°F
MIT Fuel Element Side Plate	100°F	346°F	643°F	1,100°F
Neoprene Rub Strips/Polyethylene Bag	100°F	599°F	690°F	N/A
Fuel Handling Enclosure (FHE)	100°F	599°F	690°F	1,100°F
Inner Shell	100°F	1,417°F	1,417°F	2,700°F
Ceramic Fiber Insulation, Body - Maximum - Average	100°F 100°F	1,462°F 1,253°F	1,462°F 1,253°F	2,300°F 2,300°F
Ceramic Fiber Insulation, Closure - Maximum - Average	100°F 100°F	1,401°F 1,233°F	1,401°F 1,233°F	2,300°F 2,300°F
Closure	100°F	1,439°F	1,439°F	2,700°F
Outer Shell	100°F	1,475°F	1,475°F	2,700°F

Table Notes:

[1] The maximum allowable temperatures under HAC conditions are provided in Section 3.2.2, *Technical Specifications of Components*.

Table 3.6-7 – HAC Temperatures with MURR Payload

Location / Component	Pre-fire	End of Fire	Peak	Maximum Allowable [1]
MURR Fuel Element Fuel Plate	100°F	371°F	636°F	1,100°F
MURR Fuel Element Side Plate	100°F	380°F	644°F	1,100°F
Neoprene Rub Strips/Polyethylene Bag	100°F	648°F	710°F	N/A
Fuel Handling Enclosure (FHE)	100°F	648°F	710°F	1,100°F
Inner Shell	100°F	1,417°F	1,417°F	2,700°F

Ceramic Fiber Insulation, Body
  - Maximum
  - Average
	100°F
	100°F
		1,462°F
		1,222°F
			1,462°F
			1,222°F
				2,300°F
				2,300°F

Ceramic Fiber Insulation, Closure
  - Maximum
  - Average
	100°F
	100°F
		1,402°F
		1,236°F
			1,402°F
			1,236°F
				2,300°F
				2,300°F

Closure	100°F	1,439°F	1,439°F	2,700°F
Outer Shell	100°F	1,475°F	1,475°F	2,700°F

Table Notes:

[1] The maximum allowable temperatures under HAC conditions are provided in Section 3.2.2, *Technical Specifications of Components*.

Figure 3.6-4 – ATR FFSC Package Thermal Response to HAC Event with MIT Payload
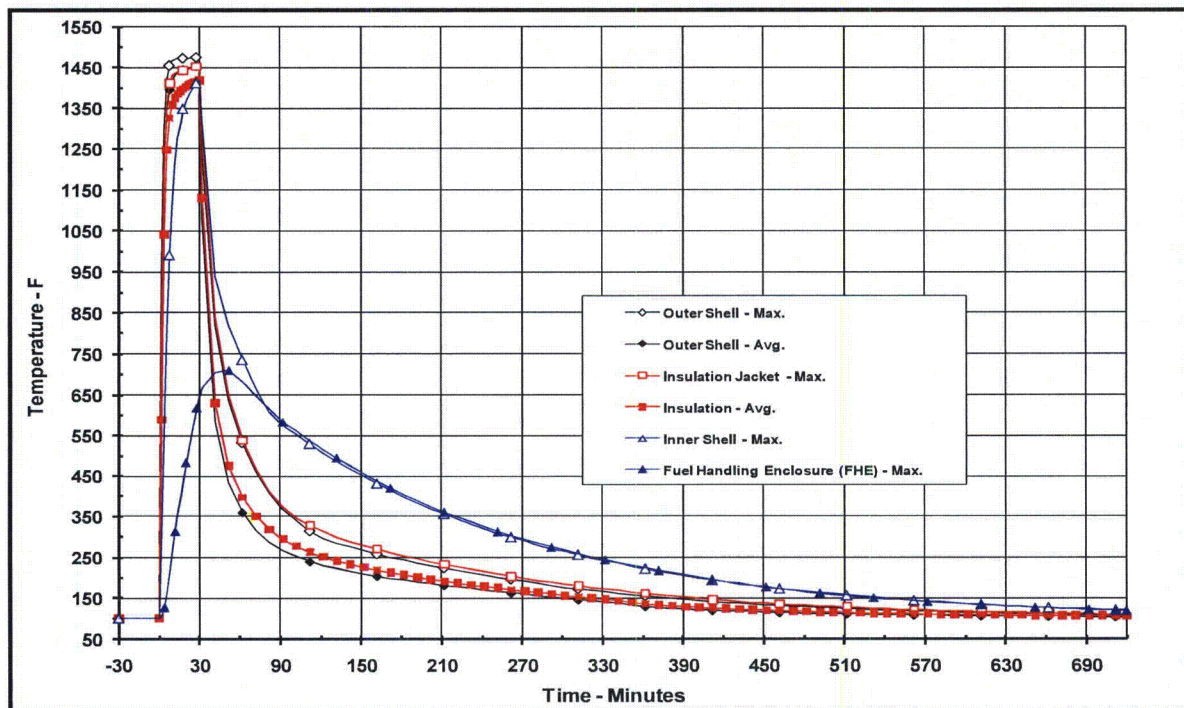
Figure 3.6-5 – ATR FFSC Package Thermal Response to HAC Event with MURR Payload
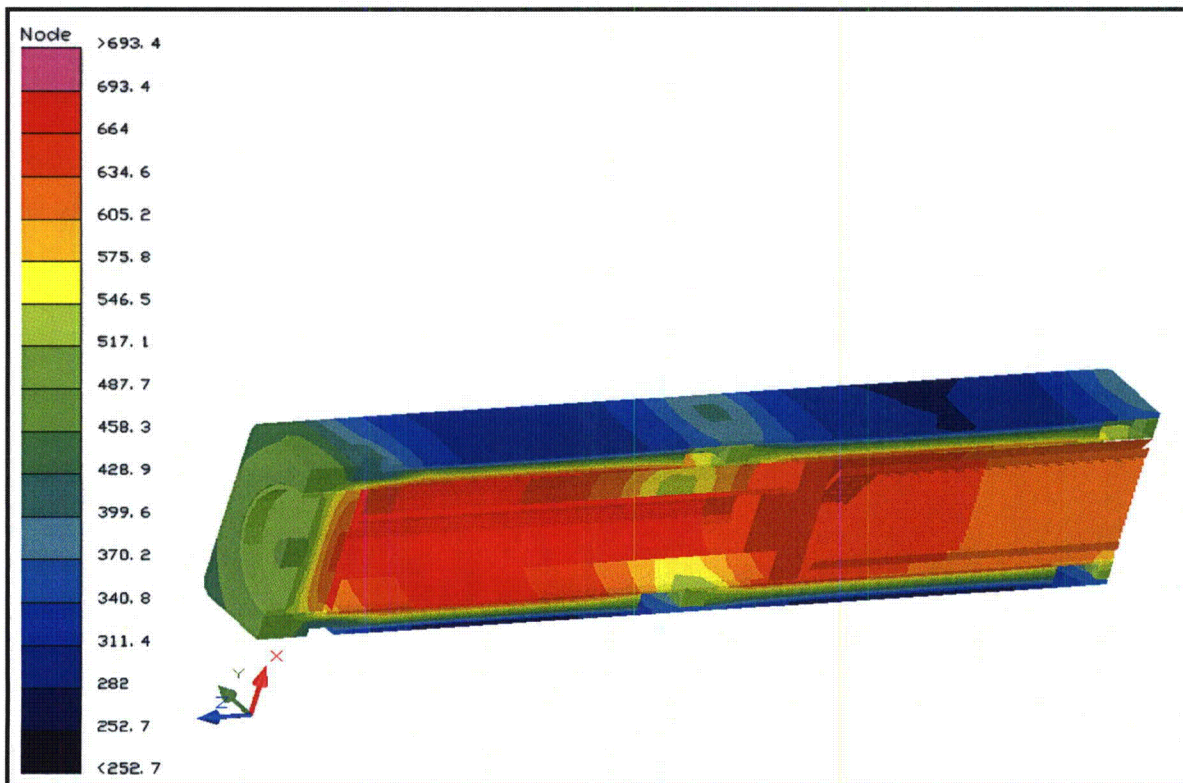
(Note: the positive x-axis is oriented towards the top of the package and the positive z-axis towards the package closure end)

Figure 3.6-6 –Temperature Distribution at Time of Peak MIT Fuel Element Temperature
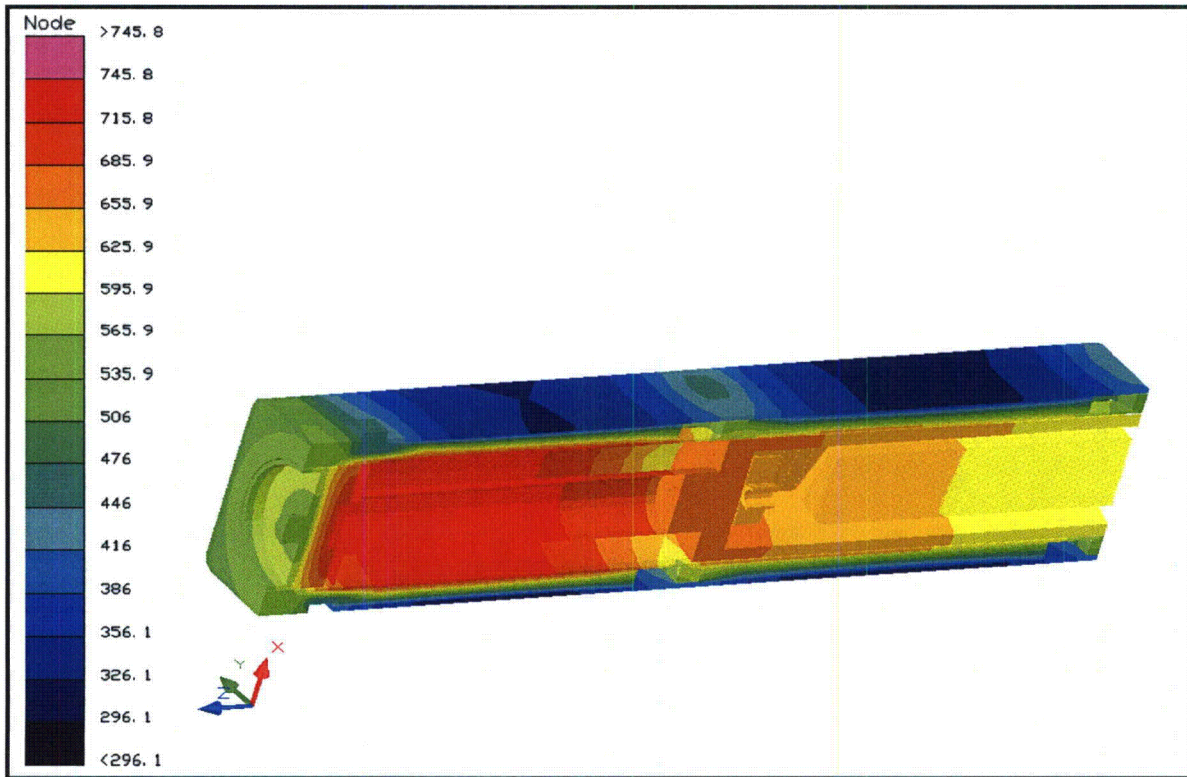
(Note: the positive x-axis is oriented towards the top of the package and the positive z-axis towards the package closure end)

Figure 3.6-7 –Temperature Distribution at Time of Peak MURR Fuel Element Temperature

3.6.9 Appendices

3.6.9.1 Computer Analysis Results

3.6.9.2 Analytical Thermal Model

3.6.9.1 Computer Analysis Results

Due to the size and number of the output files associated with each analyzed condition, results from the computer analysis are provided on a CD-ROM.

3.6.9.2 Analytical Thermal Model

The analytical thermal model of the ATR FFSC package and the MIT and MURR fuel element payloads were developed for use with the Thermal Desktop[®20] and SINDA/FLUINT[21] computer programs. These programs are designed to function together to build, exercise, and post-process a thermal model. Appendix 3.5.2, *Analytical Thermal Model*, provides an overview of the capability and functionality of these programs. The SINDA/FLUINT and Thermal Desktop[®] computer programs have been validated for safety basis calculations for nuclear related projects[22]. The ATR FFSC with the small quantity payload was not specifically modeled as part of this evaluation. Instead, its thermal performance is estimated using a qualitative approach based on the thermal characteristics of the other payloads and their associated thermal performance.

3.6.9.2.1 Description of MIT and MURR Payload Thermal Models for NCT Conditions

A 3-dimensional, one-quarter symmetry thermal model of the ATR FFSC is used for the NCT evaluation. The model simulates one-quarter of the package, extending from the closure to the axial centerline of the package. Symmetry conditions are assumed about the package's vertical axis and at the axial centerline. This modeling choice captures the full height of the package components and allows the incorporation of the varying insolation loads that will occur at the top and sides of the package. Program features within the Thermal Desktop[®] computer program automatically compute the various areas, lengths, thermal conductors, and view factors involved in determining the individual elements that make up the thermal model of the complete assembly. Details of the thermal modeling of the ATR FFSC packaging are provided in Appendix 3.5.2.1, *Description of Thermal Model for NCT Conditions*.

A detailed model of the MIT and MURR fuel elements are used to simulate the heat transfer within the fuel elements and between the fuel element and their associated FHEs and spacer weldments. The detailed thermal models, illustrated in Figure 3.6-8 to Figure 3.6-13, include a separate representation of each composite fuel plate, the side plates, and the end fittings. Heat transfer between the individual fuel plates is simulated via conduction and radiation across the air space separating the plates. The curvature and separation distance between the plates is based on the information presented in Appendix 3.6.9.2.3, *Determination of Composite Thermal Properties for MIT and MURR* Fuel Plates.

The thermal modeling for the MIT fuel element and FHE is similar to that described for the ATR fuel element payload. Figure 3.6-8 illustrates the quarter symmetry thermal model of the MIT FHE and one of the two spacer weldments. The FHE thermal model uses planar elements to represent the 0.19 inch thick sides of the enclosure and the 0.25 inch thick elements of the spacer weldment. Solid elements are used to represent the ends of the FHE. Heat transfer between the FHE and the inner shell of the package is modeled as a combination of radiation and conduction across the air-filled void space, as well as via direct contact along 1 edge of the FHE. The contact conductance simulates a conservative idealized physical contact (i.e., a flat, smooth interface and that the FHE is oriented within the package such that the edge is aligned with the vertical axis of the package) between the FHE and the inner shell. Due to the robustness of the MIT FHE, no change to the direct contact between the FHE and the inner shell conservatively assumed for the NCT condition is expected as a result of the HAC drop event.

Figure 3.6-9 illustrates a cross-section through the combined modeling for the inner shell, the FHE, and the MIT fuel element. The left side of the figure illustrates the placement of the thermal nodes (indicated by the small circles) used to simulate each of the components, the use of planar elements to represent the 15 fuel plates, and the assumed points of direct contact between the FHE and the inner shell. The right side of the figure includes depiction of the solid elements that are used to simulate the air voids around the FHE. The heat transfer between the FHE and the MIT fuel element is computed as conductance through the 0.125 inch thick neoprene rub strips and radiation and conductance through the air voids.

Figure 3.6-10 illustrates a side and end view of the thermal model of the MIT fuel element as it would be for a complete fuel element. Approximately 1,140 nodes, 350 planar elements, and 445 solids are used to represent the quarter symmetry thermal model of the MIT fuel element, FHE, and the spacer weldment.

The thermal modeling for the MURR fuel element and FHE is similar to that described above for the MIT fuel element payload. Figure 3.6-11 illustrates the quarter symmetry thermal model of the MURR FHE and one of the two spacer weldments. The FHE thermal model uses planar elements to represent the 0.19 inch thick sides of the enclosure and the 0.25 inch thick elements of the spacer weldment. Solid elements are used to represent the ends of the FHE. Heat transfer between the FHE and the inner shell of the package is modeled as a combination of radiation and conduction across the air-filled void space, as well as via direct contact along 2 edges of the FHE. The contact conductance simulates a conservative idealized physical contact (i.e., a flat, smooth interface and an alignment that places 2 edges of the FHE in contact) between the FHE and the inner shell. Due to the robustness of the MURR FHE, no change to the direct contact between the FHE and the inner shell conservatively assumed for the NCT condition is expected as a result of the HAC drop event.

Figure 3.6-12 illustrates a cross-section through the combined modeling for the inner shell, the FHE, and the MURR fuel element. The left side of the figure illustrates the placement of the thermal nodes (indicated by the small circles) used to simulate each of the components, the use of curved, planar elements to represent the 24 fuel plates, and the assumed points of direct contact between the FHE and the inner shell. The right side of the figure includes depiction of the solid elements that are used to simulate the air voids around the FHE. The heat transfer between the FHE and the MURR fuel element is computed as conductance through the 0.125 inch thick neoprene rub strips and radiation and conductance through the air voids.

Figure 3.6-13 illustrates a side and end view of the quarter symmetry thermal modeling used for the MURR fuel element. Approximately 1,400 nodes, 700 planar elements, and 340 solids are used to represent the quarter symmetry thermal model of the MURR fuel element, FHE, and the spacer weldment.

The heat transfer from the exterior surfaces of the ATR FFSC is modeled in the same manner as that used for the evaluation of the ATR fuel element payload and assumes a combination of convection and radiation exchange. Appendix 3.5.2.3, *Convection Coefficient Calculation*, presents the methodology used to compute the convection coefficients from the various surfaces. The radiation exchange is computed using a Monte Carlo, ray tracing technique and includes the affect of reflection and/or transmission, according to the optical properties assigned to each surface (see Section 3.2.1, *Material Properties*).

In addition, heating of the exterior surfaces due to solar insolation is assumed using a diurnal cycle. The methodology used to simulate and apply the insolation loading is described in Appendix 3.5.2.1, *Description of Thermal Model for NCT Conditions*.

3.6.9.2.2 Description of Thermal Model for HAC Conditions

The thermal evaluations for the hypothetical accident condition (HAC) are conducted in the same manner and using the same methodology as that described in Appendix 3.6.9.2.1, *Description of MIT and MURR Payload Thermal Models for NCT Conditions*. No change to the geometry or position of the MIT and MURR fuel element payloads are expected as a result of the drop and puncture bar events that are assumed to precede the HAC fire event.

3.6.9.2.3 Determination of Composite Thermal Properties for MIT and MURR Fuel Plates

The MIT and MURR fuel plates are a composite material consisting of a fissile fuel matrix sandwiched within aluminum cladding. For the purposes of this calculation, the fuel composite is treated as a homogenous material with lumped thermal properties. The methodology used to compute the composite thermal properties for each fuel element is the same as that described in Appendix 3.5.2.4, *Determination of Composite Thermal Properties for ATR Fuel Plates*.

Each MIT element contains up to 515 g U-235, enriched up to 94 wt.%, which equates to a density of approximately 1.5 g U/cc in the fuel matrix. The thermal properties for the individual plates making up the MIT fuel element are computed using the approach used with the ATR Fuel Plates and the geometric data[39,42] for the MIT fuel element. Each of the fifteen (15) fuel plates contained in the MIT fuel element has a thickness of 0.08 inches and a width of 2.526 inches. The nominal gap between the plates is 0.078 inches. Since the aluminum cladding contains 110 grooves on each side of the plate, the effective thickness of the cladding is reduced from 0.025 inches to 0.02 inches. Table 3.6-8 presents the composite thermal conductivity, specific heat, and density values for the fuel plates. These composite values are based on the described geometry of the fuel plates and the same thermophysical data[6] used for the ATR fuel plates.

The thermal properties for the MIT element used are:

1) Aluminum cladding thermal conductivity = 191 W/m-K, conservatively high value from [6], page 18
2) Fissile fuel matrix (UAl$_x$) conductivity = 38.5 W/m-K, conservatively high based on Table 2.3 from [6] at 300K for 1.5 g U/cc
3) Aluminum cladding density = 2702 kg/m^3, from [6], page 16
4) Fissile fuel matrix (UAl$_x$) density = 3846 kg/m^3, from [6], Table 2.5 for 1.5 g U/cc
5) Aluminum cladding specific heat = 896 & 1080 J/kg-K, from [6], Table 3.2 at 300 & 700K, respectively
6) Fissile fuel matrix (UAl$_x$) specific heat = 587 & 709 J/kg-K, from [6], Table 2.4, value at 300 & 700K, respectively, for 1.5 g U/cc

---

[42] *Massachusetts Institute of Technology, Test Research Training Reactor 3 Welded Fuel Element Assembly*, EG&G Idaho, Inc. Drawing No. DWG-419486, Rev. A.

Each MURR element contains up to 785 g U-235, enriched up to 94 wt.%, which equates to a density of approximately 1.44 g U/cc in the fuel matrix. The thermal properties for the individual plates making up the MURR fuel element are also computed using the approach used with the ATR Fuel Plates and the geometric data[40,43] for the MURR fuel element. Due to the curved geometry of the twenty-four (24) fuel plates contained in the MURR fuel element, each plate has a different geometry. The inner plate has an inner radius of 2.77 inches and an arc length of 1.993 inches, while the outer plate has an inner radius of 5.76 inches and an arc length of 4.342 inches. The nominal gap between the plates is 0.08 inches. The thickness of the aluminum cladding is 0.01 inches. Table 3.6-9 presents the composite thermal conductivity, specific heat, and density values for the twenty four (24) fuel plates making up the MURR fuel element. These composite values are based on the described geometry of the fuel plates and the same thermophysical data[6] used for the ATR fuel plates.

The thermal properties for the MURR fuel element used in this calculation are:

1) Aluminum cladding thermal conductivity = 191 W/m-K, conservatively high value from [6], page 18

2) Fissile fuel matrix (UAl$_x$) conductivity = 39.8 W/m-K, conservatively high based on Table 2.3 from [6], at 300K for 1.44 g U/cc

3) Aluminum cladding density = 2702 kg/m^3, from [6], page 16

4) Fissile fuel matrix (UAl$_x$) density = 3793 kg/m^3, from [6], Table 2.5 for 1.44 g U/cc

5) Aluminum cladding specific heat = 896 & 1080 J/kg-K, from [6], Table 3.2, at 300 & 700K, respectively

6) Fissile fuel matrix (UAl$_x$) specific heat = 596 & 719 J/kg-K, from [6], Table2.4, value at 300 & 700K, respectively, for 1.44 g U/cc

3.6.9.2.4 Determination of Thermal Properties for RINSC Element

The RINSC fuel elements are fabricated with a nominally 0.020-in thick mixture of uranium silicide (U$_3$Si$_2$) and aluminum powder as the fuel "meat" and a nominally 0.015-in thick aluminum alloy cladding. The twenty-two (22) flat fuel plates have a 2.8-in width, an overall length of 25-in, and an active fuel region of 22.5 to 24.0-in. The fuel plate meat and cladding thicknesses match those of the interior plates for the ATR fuel element and are similar to those for the MURR fuel plates. The side plates are fabricated of ASTM B 209, aluminum alloy 6061-T6 and 6061-T651 and are approximately 0.188-in thick. This is similar to the side plate thicknesses of the ATR, MITR, and MURR fuel elements.

The thermal conductivity of the RINSC fuel plates[41] are similar to data obtained in the measurements of the thermal conductivities for the uranium aluminide (UAl$_x$) based fuels[6]. Similarly, the thermal mass of the fuel plates are comparable despite the higher density of uranium silicide versus uranium aluminide since the ratio of the specific heats of the two materials is nearly the inverse of the density ratio.

---

[43] *University of Missouri at Columbia, MURR UAlx Fuel Element Assembly,* EG&G Idaho, Inc. Drawing No. DWG-409407, Rev. N.

The ATR FFSC with the RINSC fuel element payload is not specifically modeled as part of this evaluation. Instead, its thermal performance is estimated using a qualitative approach based on the maximum temperatures attained for the transportation of the MURR fuel element within the ATR FFSC. This conclusion is based on the facts that the combined weight of the RINSC and MURR FHE's with their enclosed fuel elements are the same, the FHE's are both fabricated of 6061 aluminum, and the fuel elements have similar thermal properties (see above). This conclusion is further supported by the fact that the MIT and MURR fuel elements produce essentially the same peak temperatures despite their design differences. As such, the limited design differences between the MURR and RINSC payloads will not yield a significant difference in their thermal response.

Table 3.6-8 – Composite MIT Fuel Plate Thermal Properties

Plate	Plate Thickness, in	UAlx Thickness, in	Axial and Circumferential Conductivity (W/m-K)	Plate Width, in	Mean density, kg/m^3	Mean specific heat, J/(kg K) @ 300 K	Mean specific heat, J/(kg K) @ 700 K
1 to 15	0.08*	0.03	125.6	2.314	3192.3	736.5	888.4

* - mean plate thickness estimated at 0.07 inches after allowance for ribbing

Table 3.6-9 – Composite MURR Fuel Plate Thermal Properties

Plate	Plate Thickness, in	UAlx Thickness, in	Axial and Circumferential Conductivity (W/m-K)	Inner radius, in	Outer radius, in	Plate Arc Length, in	Mean density, kg/m^3	Mean specific heat, J/(kg K) @ 300K	Mean specific heat, J/(kg K) @ 700 K
1	0.05	0.03	100.3	2.77	2.82	1.993	3288.8	692.6	835.2
2	0.05	0.03	100.3	2.9	2.95	2.095	3288.8	692.6	835.2
3	0.05	0.03	100.3	3.03	3.08	2.197	3288.8	692.6	835.2
4	0.05	0.03	100.3	3.16	3.21	2.300	3288.8	692.6	835.2
5	0.05	0.03	100.3	3.29	3.34	2.402	3288.8	692.6	835.2
6	0.05	0.03	100.3	3.42	3.47	2.504	3288.8	692.6	835.2
7	0.05	0.03	100.3	3.55	3.6	2.606	3288.8	692.6	835.2
8	0.05	0.03	100.3	3.68	3.73	2.708	3288.8	692.6	835.2
9	0.05	0.03	100.3	3.81	3.86	2.810	3288.8	692.6	835.2
10	0.05	0.03	100.3	3.94	3.99	2.912	3288.8	692.6	835.2
11	0.05	0.03	100.3	4.07	4.12	3.014	3288.8	692.6	835.2
12	0.05	0.03	100.3	4.2	4.25	3.116	3288.8	692.6	835.2
13	0.05	0.03	100.3	4.33	4.38	3.218	3288.8	692.6	835.2
14	0.05	0.03	100.3	4.46	4.51	3.321	3288.8	692.6	835.2
15	0.05	0.03	100.3	4.59	4.64	3.423	3288.8	692.6	835.2
16	0.05	0.03	100.3	4.72	4.77	3.525	3288.8	692.6	835.2
17	0.05	0.03	100.3	4.85	4.9	3.627	3288.8	692.6	835.2
18	0.05	0.03	100.3	4.98	5.03	3.729	3288.8	692.6	835.2
19	0.05	0.03	100.3	5.11	5.16	3.831	3288.8	692.6	835.2
20	0.05	0.03	100.3	5.24	5.29	3.933	3288.8	692.6	835.2
21	0.05	0.03	100.3	5.37	5.42	4.035	3288.8	692.6	835.2
22	0.05	0.03	100.3	5.5	5.55	4.137	3288.8	692.6	835.2
23	0.05	0.03	100.3	5.63	5.68	4.239	3288.8	692.6	835.2
24	0.05	0.03	100.3	5.76	5.81	4.342	3288.8	692.6	835.2
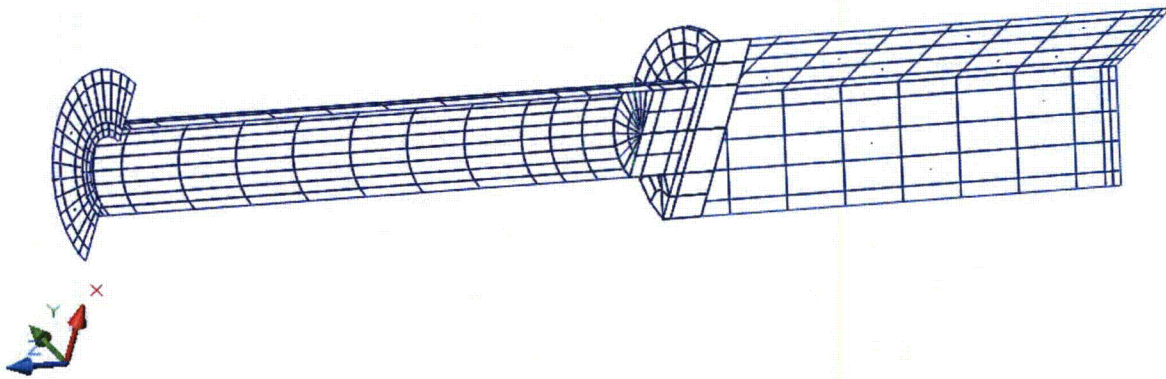
(Note: the positive x-axis is oriented towards the top of the package and the positive z-axis towards the package closure end)

Figure 3.6-8 – 'Hidden Line' View of MIT FHE and Spacer Quarter Symmetry Thermal Model
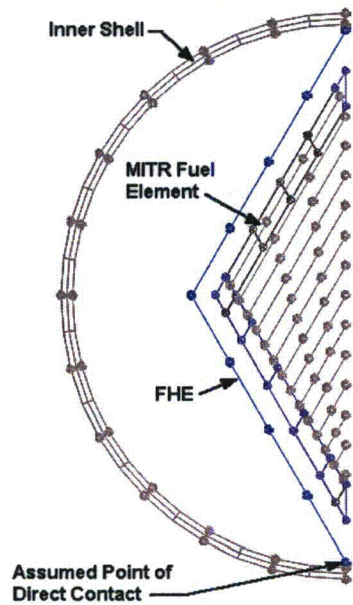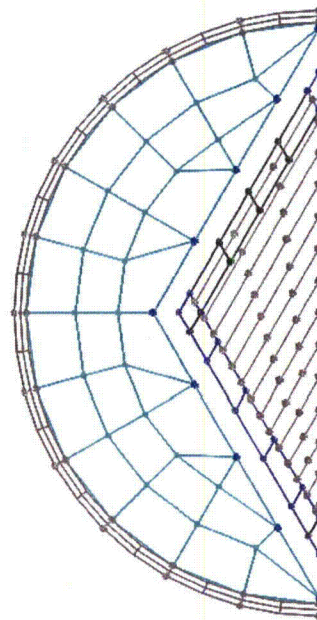
Modeling Showing Direct Contact   Modeling with 'Solid' Elements for Air

Figure 3.6-9 – Thermal Model of MIT Fuel Element and FHE within Inner Shell
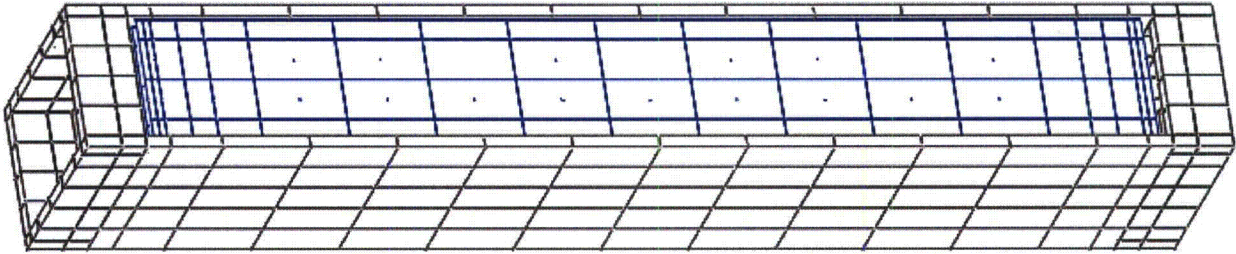
MIT Fuel Element Model, Side View of Full Element
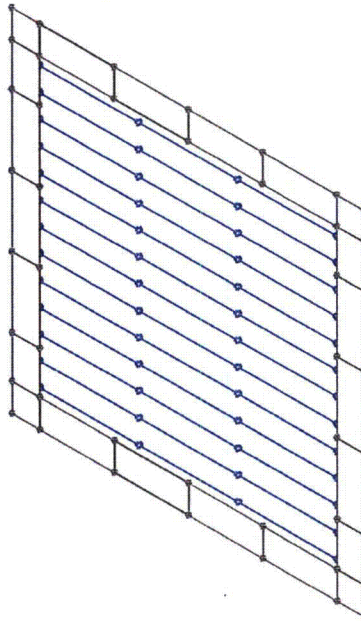
MIT Fuel Element Model, End View of Full Element

Figure 3.6-10 – Side and End Views of MIT Fuel Element Thermal Model
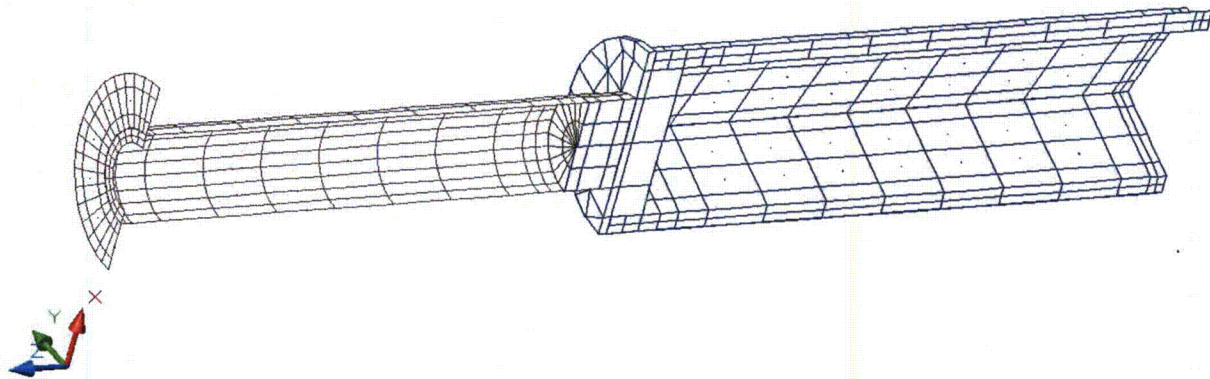
(Note: the positive x-axis is oriented towards the top of the package and the positive z-axis towards the package closure end)

Figure 3.6-11 – 'Hidden Line' View of MURR FHE and Spacer Quarter Symmetry Thermal Model
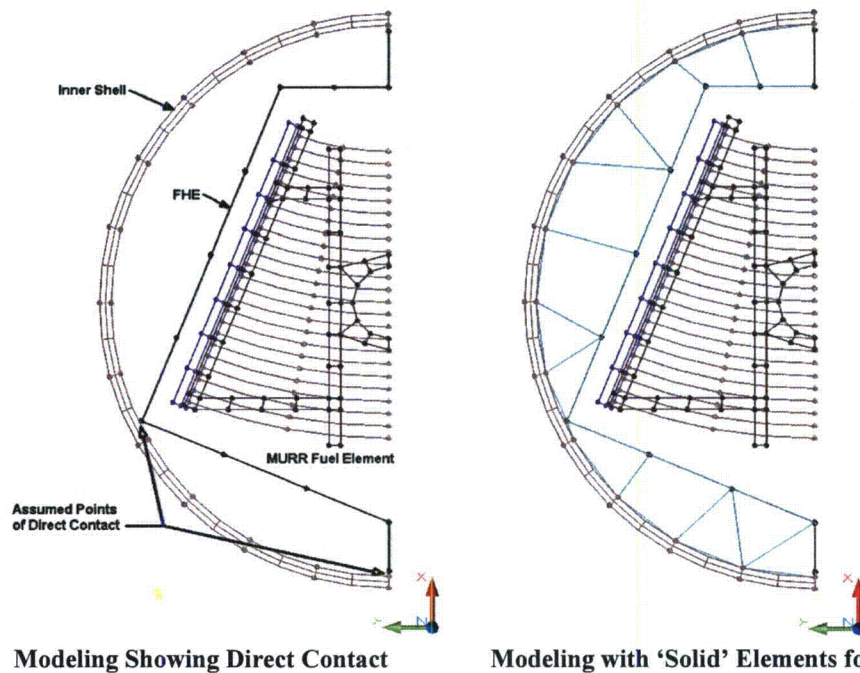
Modeling Showing Direct Contact   Modeling with 'Solid' Elements for Air

Figure 3.6-12 – Thermal Model of MURR Fuel Element and FHE within Inner Shell
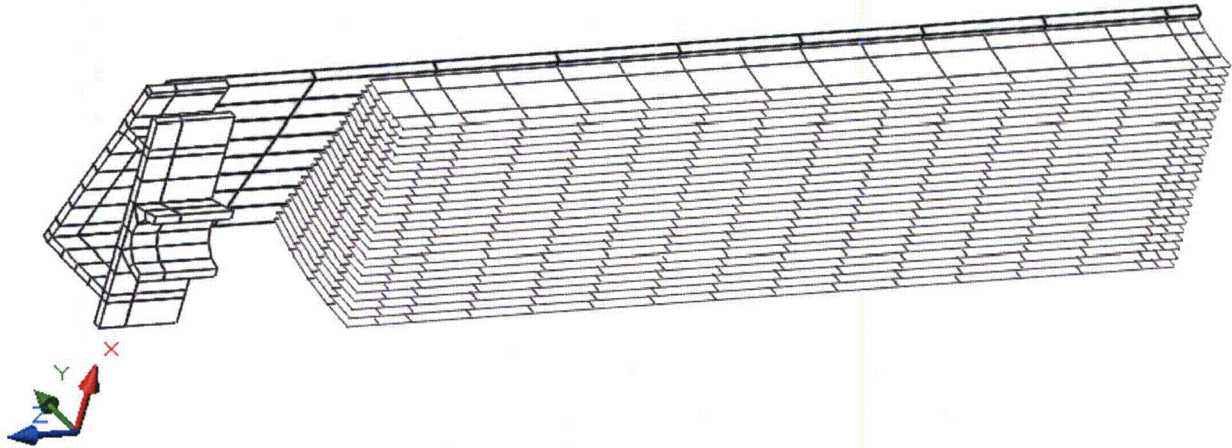
MURR Fuel Element Model, Side View of Quarter Symmetry Model
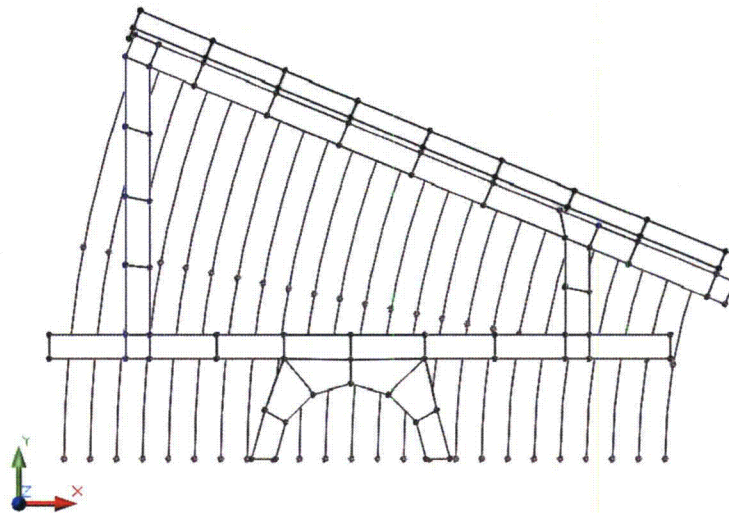
MURR Fuel Element Model, End View of Quarter Symmetry Model

Figure 3.6-13 – Side and End Views of MURR Fuel Element Thermal Model

4.0 CONTAINMENT

4.1 Description of the Containment System

The containment function of the ATR FFSC is to confine the fuel elements or loose plates within the packaging during Normal Conditions of Transport (NCT) and Hypothetical Accident Conditions (HAC).

The package body is a stainless steel weldment that consists of two nested shells. The outer shell is an 8-in square stainless steel tube with a 3/16-in thick wall, and the inner shell is a 6-in diameter stainless steel tube with a 0.120-in thick wall. Components are joined using full-thickness fillet welds (i.e., fillet welds whose leg size is nominally equal to the lesser thickness of the parts joined) and full and partial penetration groove welds. The end of the body is welded closed with 0.88-in plate.

The lid end of the package is closed with a simple closure device. The closure engages with the body using a bayonet style design. There are four lugs, uniformly spaced on the closure, that engage with four slots in the mating body fixture. The closure is secured by two retracting spring loaded pins, rotating the closure through 45°, and releasing the spring loaded pins such that the pins engage with the mating holes on the body. When the pins are properly engaged with the mating holes the closure is locked and cannot be removed unintentionally.

The containment boundary is defined as the boundary of the cavity formed by the closure and inner stainless steel tube. For criticality control purposes, the fuel element must remain within this boundary during NCT and HAC. No seals or gaskets are utilized within the package.

To prevent unauthorized operation, a small post on the closure is drilled to receive a tamper indicating device (TID) wire. An identical post is located on the body and is also drilled for the TID wire. For ease in operation, there are two TID posts on the body. There are only two possible angular orientations for the closure installation and the duplicate TID post on the body enables TID installation in both positions.

4.1.1 Type A Fissile Packages

The ATR FFSC is classified as a Type A Fissile package. The Type A Fissile package is constructed and prepared for shipment so that there is no loss or dispersal of the radioactive contents, and no significant increase in external surface radiation levels, and no substantial reduction in the effectiveness of the packaging during normal conditions of transport. The fissile material is contained within the containment boundary. Chapter 6.0, *Criticality Evaluation*, demonstrates that the package remains subcritical under normal and hypothetical accident conditions.

The ATR FFSC contains four radioactive isotopes: U-234, U-235, U-236, and U-238. The A_2 value for U-235 and U-238 is unlimited, while the minimum A_2 value for U-234 and U-236 is 0.16 Ci for slow lung absorption. To compute the mixture A_2 for the HEU payloads, the maximum value of 1200 g U-235 is assumed, with a low weight fraction of 90% to maximize the mass of uranium. Therefore, the total mass of uranium is 1200/0.9 = 1333 g U. The maximum weight percents of U-234 (1.2%) and U-236 (0.7%) are assumed to maximize the mass of these isotopes. The balance is treated as U-238. For this conservative isotopic mix, the mixture A_2 is

0.164 Ci. The package activity for this mixture is 0.103 Ci (mostly due to U-234); therefore, the package contains approximately $0.6A_2$.

For the U-Mo demonstration element, the maximum value of 1240 g U-235 is utilized. Plates 1 through 4 and 16 through 18 are HEU with U-234 and U-236 compositions as defined in the previous paragraph. Plates 5 through 15 are LEU with a U-235 weight fraction of 20%. For these plates, the maximum weight percents of U-234 (0.26%) and U-236 (0.46%) are utilized to maximize the mass of these isotopes. Although the A_2 value for uranium enriched to 20% or less is unlimited, the mixture A_2 is conservatively computed using the total mass of U-234 and U-236 in the element. The mixture A_2 and package activity are essentially identical to the standard ATR element, and the package contains approximately $0.6A_2$ when transporting the U-Mo demonstration element.

4.1.2 Type B Packages

The content of the ATR FFSC package is high-enriched uranium with approximately $0.6A_2$ for release purposes. As a fissile package the ATR FFSC must meet the release rates for Type B packages when required by the total amount of radioactive material. However, because the A_2 value of the contents is less than 1 A_2, the package is classified as Type A and there are no release limits except as necessary for criticality control.

4.2 Containment under Normal Conditions of Transport

The ATR, MIT, MURR, or small quantity payloads, or the loose fuel plates are confined within the packaging under NCT. This is verified by full-scale testing, as discussed in Section 2.6, *Normal Conditions of Transport*. The test units survived the NCT drop tests with minimal damage to the packaging and no damage to the fuel elements. The maximum internal pressure in the package does not exceed atmospheric pressure because the closure is not sealed with a gasket or other sealing material. Because the ATR FFSC is a Type A Fissile package, leakage rate testing is not required.

4.3 Containment under Hypothetical Accident Conditions

The radioactive material contents of the ATR FFSC package must meet the containment requirements of 10 CFR §71.55(e) such that the package would be subcritical under the HAC.

The test program demonstrates that the package contains the fuel elements or loose fuel plates under the HAC events sufficient to maintain criticality control. The full-scale HAC drop tests summarized in Section 2.7, *Hypothetical Accident Conditions*, confirm the HAC performance of the package. The closure remained intact throughout all the drop sequences, and the fuel element remained confined within the inner stainless steel tube. The non-fissile end boxes on the fuel element shattered as expected but the fueled portion of the element remained intact and retained its geometry. There was no dispersal of fissile material. The criticality evaluation presented in Section 6.0, *Criticality Evaluation*, evaluates the contents in the most reactive credible configuration and with water moderation as required.

Because the ATR FFSC package is a Type A Fissile package and the contents are less than 1 A_2, the performance requirements of 10 CFR §71.51 do not apply.

4.4 Leakage Rate Tests for Type B Packages

The ATR FFSC is a Type A Fissile package; therefore, this section does not apply.

6.0 CRITICALITY EVALUATION

The following analyses demonstrate that the ATR FFSC complies with the requirements of 10 CFR §71.55[1] and §71.59. Based on a 5x5 array of damaged packages, the Criticality Safety Index (CSI), per 10 CFR §71.59, is 4.0.

The analysis in the main body of Chapter 6 pertains only to the ATR fuel element and ATR loose plate basket. The analysis for MIT and MURR fuel is contained in Section 6.10, *Criticality Analysis for MIT and MURR Fuel*. The analysis for the small quantity payloads is contained in Section 6.11, *Criticality Analysis for Small Quantity Payloads*. The analysis for the ATR U-Mo demonstration element is contained in Section 6.12, *Criticality Analysis for the U-Mo Demonstration Element*.

6.1 Description of Criticality Design

6.1.1 Design Features Important for Criticality

A comprehensive description of the ATR FFSC is provided in Section 1.2, *Packaging Description*, and in the drawings in Appendix 1.3.2, *Packaging General Arrangement Drawings*. This section summarizes those design features important for criticality.

No poisons are utilized in the package. For the fuel element payload, the separation provided by the packaging (outer tube minimum flat-to-flat dimension of 7.9-in, inner tube maximum inner diameter of 5.814-in), along with the limit on the number of packages per shipment, is sufficient to maintain criticality safety. For the loose plate payload, in addition to the design features noted above, moderation of the loose plates is controlled by the loose plate basket, which confines the fuel plates to a rectangular area.

6.1.2 Summary Table of Criticality Evaluation

The upper subcritical limit (USL) for ensuring that the ATR FFSC (single package or package array) is acceptably subcritical, as determined in Section 6.8, *Benchmark Evaluations*, is:

$$USL = 0.9209$$

The package is considered to be acceptably subcritical if the computed k_{safe} (k_s), which is defined as $k_{effective}$ (k_{eff}) plus twice the statistical uncertainty (σ), is less than or equal to the USL, or:

$$k_s = k_{eff} + 2\sigma \leq USL$$

The USL is determined on the basis of a benchmark analysis and incorporates the combined effects of code computational bias, the uncertainty in the bias based on both benchmark-model and computational uncertainties, and an administrative margin. The results of the benchmark analysis indicate that the USL is adequate to ensure subcriticality of the package.

The packaging design is shown to meet the requirements of 10 CFR 71.55(b) when the package is limited to either one 1200 g U-235 ATR fuel element, or 600 g U-235 in the form of ATR

---

[1] Title 10, Code of Federal Regulations, Part 71 (10 CFR 71), *Packaging and Transportation of Radioactive Material*.

loose fuel plates. Moderation by water in the most reactive credible extent is utilized in both the NCT and HAC analyses. In the single package NCT models, full-density water fills the accessible cavity, while in the single package HAC models, full-density water fills all cavities. In the fuel element models, the most reactive credible configuration is utilized by maximizing the gap between the fuel plates. Maximizing this gap maximizes the moderation and hence the reactivity because the system is under moderated. In the loose plate model, no credit is taken for the dunnage plates and the optimal pitch and fuel arrangement is utilized. In all single package models, 12-in of water reflection is utilized.

In the NCT and HAC array cases, partial moderation is considered to maximize array interaction effects. A 9x9x1 array is utilized for the NCT array, while a 5x5x1 array is utilized in the HAC array. In all array models, 12-in of water reflection is utilized.

The maximum results of the ATR fuel element criticality calculations are summarized in Table 6.1-1. The maximum calculated k_s is 0.8362, which occurs for the optimally moderated NCT array case. The NCT array is more reactive than the HAC array because the NCT array is larger, and moderation is allowed in both conditions. In this case, the fuel element is moderated with full-density water, the inner tube is moderated with 0.3 g/cm^3 water, and void is modeled between the insulation and outer tube.

The maximum results of the loose plate basket criticality calculations are summarized in Table 6.1-2. The maximum calculated k_s is 0.7747, which occurs for the optimally moderated NCT array case. The NCT array is more reactive than the HAC array because the NCT array is larger, and moderation is allowed in both conditions. In this case, the loose fuel plate basket is moderated with full-density water, the inner tube is moderated with 0.5 g/cm^3 water, and void is modeled between the insulation and outer tube.

It may be noted when comparing Table 6.1-1 and Table 6.1-2 the fuel element payload is more reactive than the loose plate basket payload.

Table 6.1-1 – Summary of Criticality Evaluation (Fuel Element Payload)

Normal Conditions of Transport (NCT)	
Case	k_s
Single Unit Maximum	0.4224
9x9 Array Maximum	0.8362
Hypothetical Accident Conditions (HAC)	
Case	k_s
Single Unit Maximum	0.4524
5x5 Array Maximum	0.7453
USL = 0.9209	

6.12 Appendix D: Criticality Analysis for the U-Mo Demonstration Element

The Advanced Test Reactor (ATR) Fresh Fuel Shipping Container (FFSC) is used to transport a single high-enriched uranium ATR fuel element. A demonstration element has been developed using low-enriched uranium (LEU) for several of the fuel plates. To achieve the necessary fissile mass in the LEU fuel plates, the fuel matrix for these plates is being changed from UAl_x to U-Mo, which allows a much higher uranium density. Several full-sized U-Mo demonstration elements are to be tested in the ATR. Therefore, a criticality analysis is performed for the U-Mo demonstration element to allow shipment in the ATR FFSC. The following analyses demonstrate that the ATR FFSC complies with the requirements of 10 CFR §71.55 and §71.59. Based on the analysis, the Criticality Safety Index (CSI), per 10 CFR §71.59, is 4.0.

6.12.1 Description of Criticality Design

6.12.1.1 Design Features

No special design features are required to maintain criticality safety. No poisons are utilized in the package. The separation provided by the packaging (outer flat-to-flat dimension of 7.9-in), along with the limit on the number of packages per shipment, is sufficient to maintain criticality safety.

6.12.1.2 Summary Table of Criticality Evaluation

The upper subcritical limit (USL) for ensuring that the ATR FFSC (single package or package array) is acceptably subcritical, as determined in Section 6.12.8, *Benchmark Evaluations*, is:

$$USL = 0.9209$$

The package is considered to be acceptably subcritical if the computed k_{safe} (k_s), which is defined as $k_{effective}$ (k_{eff}) plus twice the statistical uncertainty (σ), is less than or equal to the USL, or:

$$k_s = k_{eff} + 2\sigma \leq USL$$

The USL is determined on the basis of a benchmark analysis and incorporates the combined effects of code computational bias, the uncertainty in the bias based on both benchmark-model and computational uncertainties, and an administrative margin. The results of the benchmark analysis indicate that the USL is adequate to ensure subcriticality of the package.

The packaging design is shown to meet the requirements of 10 CFR 71.55(b). Moderation by water in the most reactive credible extent is utilized in both the normal conditions of transport (NCT) and hypothetical accident conditions of transport (HAC) analyses. In the single package NCT models, full-density water fills the accessible cavity, while in the single package HAC models, full-density water fills all cavities. In the fuel element models, the most reactive credible configuration is utilized by maximizing the gap between the fuel plates. Maximizing this gap maximizes the moderation and hence the reactivity because the system is undermoderated. In all single package models, 12-in of water reflection is utilized.

In the NCT and HAC array cases, partial moderation is considered to maximize array interaction effects. A 9x9x1 array is utilized for the NCT array, while a 5x5x1 array is utilized in the HAC array. In all array models, 12-in of water reflection is utilized.

The maximum results of the criticality calculations are summarized in Table 6.12-1. The maximum calculated k_s is 0.7879, which occurs for the optimally moderated NCT array case. The NCT array is more reactive than the HAC array because the NCT array is larger, and moderation is allowed in both conditions. In this case, the fuel element is moderated with full-density water, the inner tube is moderated with 0.3 g/cm^3 water, and void is modeled between the insulation and outer tube.

Table 6.12-1 – Summary of Criticality Evaluation, U-Mo Demonstration Element

Normal Conditions of Transport (NCT)	
Case	k_s
Single Unit Maximum	0.4055
9x9 Array Maximum	0.7879
Hypothetical Accident Conditions (HAC)	
Case	k_s
Single Unit Maximum	0.4344
5x5 Array Maximum	0.7054
USL = 0.9209	

6.12.1.3 Criticality Safety Index

A 5x5 array (2N = 25, or N = 12.5) is utilized for the HAC array calculations, while a 9x9 array (5N = 81, or N = 16.2) is utilized for the NCT array calculations. Therefore, the criticality safety index is computed with the smaller value of N, or 50/N = 50/12.5 = 4.0. With a CSI = 4.0, a maximum of twenty-five (25) packages are allowed per exclusive use shipment.

6.12.2 Fissile Material Contents

The package can accommodate one ATR U-Mo demonstration element. A schematic of the demonstration element is provided in Figure 6.12-1. The demonstration element contains 19 plates. Plates 1-4 and 16-18 are standard UAl_x, plates 5-15 are U-Mo, and plate 19 is solid aluminum (no fuel). Each element contains 1215.73 ± 21.15 g U-235.

For the UAl_x plates, the U-235 is enriched up to 94%, with 1.2 wt.% U-234 (max), and 0.7 wt.% U-236 (max). For the U-Mo plates, the U-235 is enriched up to 19.95%, with 0.26 wt.% U-234 (max), and 0.46 wt.% U-236 (max).

The external geometry of the demonstration element is essentially identical to the external geometry of a standard ATR element shown on Figure 6.2-1. The width (or arc length) of the U-Mo fuel meat is also the same as a standard UAl_x element. However, the U-Mo fuel meat

thickness is 0.013-in, and a 0.001-in zirconium interlayer is present between the fuel meat and the cladding. The cladding material is aluminum 6061 for all fuel plates.

The standard ATR fuel element models are modified to be consistent with the U-Mo demonstration element. It was determined in Section 6.4.1.2.1, *Fuel Element Payload Parametric Evaluation*, that reactivity for an ATR element is maximized when the arc length of the fuel meat is maximized, so the maximum fuel meat arc lengths for a standard ATR element are used without modification.

It is necessary to determine the number densities of the fuel meat. To determine the number densities of the fuel meat, it is first necessary to compute the volume of the fuel meat. The volume of the fuel meat for each plate is the arc length of the meat multiplied by the fuel length (48-in) and meat thickness (0.02-in for UAl_x, and 0.013-in for U-Mo). The fuel meat volumes are provided in Table 6.12-2.

The mass of U-235 varies for each fuel plate. The nominal U-235 loading for each plate is provided in Table 6.12-3. The tolerance on the U-235 mass in each plate is $\pm 2\%$. A bounding U-235 mass for each plate is developed by applying the maximum tolerance to each plate, as indicated in Table 6.12-3. The total as-modeled U-235 mass for the demonstration element is then 1240.0 g. This conservatively exceeds the maximum value of $1215.73 + 21.15 = 1236.88$ g U-235.

From the fuel meat volumes and U-235 mass per plate, the fuel number densities for each plate are computed and are provided in Table 6.12-4. The UAl_x fuel meat composition is based on a conservative enrichment of 94%, and the U-Mo fuel meat composition is based on a conservative enrichment of 20.0%. The U-234 and U-236 weight percents utilized in the calculations are representative values based on half of the maximum values for each fuel meat type.

The number densities for the UAl_x fuel meat are computed using the same methodology as described in Section 6.2, *Fissile Material Contents*. The number densities for the U-Mo fuel meat are computed by first determining the U-235 gram density for each plate. Using a conservative enrichment of 20.0%, the total uranium density is computed as $\rho_{U235}/0.2$. Because the U-Mo alloy is 10 wt.% molybdenum, the total U-Mo density is computed as $\rho_U/0.9$. The number densities of all constituents are then computed based upon the computed gram densities for each plate.

The demonstration element is modeled explicitly in MCNP, including the 0.001-in thick zirconium interlayers. The MCNP representation of the demonstration element is shown in Figure 6.12-2.

Table 6.12-2 – Fuel Volume Computation (maximum arc length)

Plate	Fuel Meat	Fuel Meat Arc Length (cm)	Fuel Meat Thickness (cm)	Fuel Length (cm)	Fuel Meat Volume (cm³)
1	UAl$_x$	4.2247	0.0508	121.92	26.1660
2	UAl$_x$	5.0209	0.0508	121.92	31.0974
3	UAl$_x$	5.2764	0.0508	121.92	32.6796
4	UAl$_x$	5.5319	0.0508	121.92	34.2618
5	U-Mo	5.7873	0.0330	121.92	23.2985
6	U-Mo	6.0427	0.0330	121.92	24.3269
7	U-Mo	6.2982	0.0330	121.92	25.3551
8	U-Mo	6.5536	0.0330	121.92	26.3834
9	U-Mo	6.8090	0.0330	121.92	27.4116
10	U-Mo	7.0644	0.0330	121.92	28.4399
11	U-Mo	7.3198	0.0330	121.92	29.4681
12	U-Mo	7.5752	0.0330	121.92	30.4962
13	U-Mo	7.8306	0.0330	121.92	31.5244
14	U-Mo	8.0860	0.0330	121.92	32.5525
15	U-Mo	8.3414	0.0330	121.92	33.5807
16	UAl$_x$	8.5968	0.0508	121.92	53.2443
17	UAl$_x$	8.8521	0.0508	121.92	54.8260
18	UAl$_x$	9.0058	0.0508	121.92	55.7776
19	Plate 19 is solid aluminum				

Table 6.12-3 – U-235 Mass per Plate

Plate	Nominal U-235 Mass Per Plate (g)	Maximum U-235 Mass Per Plate (g)
1	24.3	24.79
2	29.1	29.68
3	38.7	39.47
4	40.4	41.21
5	66.35	67.68
6	69.45	70.84
7	72.52	73.97
8	75.62	77.13
9	78.69	80.26
10	81.78	83.42
11	84.85	86.55
12	87.95	89.71
13	91.02	92.84
14	94.12	96.00
15	97.18	99.12
16	64.0	65.28
17	65.9	67.22
18	53.8	54.88
19	0	0
Total	1215.73	1240.0

Table 6.12-4 – Fuel Number Densities

Plate	U-234	U-235	U-236	U-238	Al	Mo	Total
				(atom/b-cm)			
1	1.5558E-05	2.4269E-03	8.9982E-06	1.2874E-04	5.2567E-02	-	5.5147E-02
2	1.5676E-05	2.4455E-03	9.0668E-06	1.2972E-04	5.2536E-02	-	5.5136E-02
3	1.9838E-05	3.0947E-03	1.1474E-05	1.6416E-04	5.1458E-02	-	5.4749E-02
4	1.9753E-05	3.0815E-03	1.1425E-05	1.6346E-04	5.1480E-02	-	5.4757E-02
5	4.8582E-05	7.4422E-03	8.5223E-05	2.9261E-02	-	1.0129E-02	4.6966E-02
6	4.8702E-05	7.4607E-03	8.5434E-05	2.9333E-02	-	1.0154E-02	4.7082E-02
7	4.8793E-05	7.4745E-03	8.5592E-05	2.9388E-02	-	1.0173E-02	4.7170E-02
8	4.8895E-05	7.4903E-03	8.5773E-05	2.9450E-02	-	1.0195E-02	4.7269E-02
9	4.8972E-05	7.5020E-03	8.5907E-05	2.9496E-02	-	1.0211E-02	4.7343E-02
10	4.9055E-05	7.5147E-03	8.6052E-05	2.9546E-02	-	1.0228E-02	4.7423E-02
11	4.9120E-05	7.5248E-03	8.6167E-05	2.9585E-02	-	1.0242E-02	4.7487E-02
12	4.9199E-05	7.5367E-03	8.6304E-05	2.9632E-02	-	1.0258E-02	4.7562E-02
13	4.9255E-05	7.5454E-03	8.6404E-05	2.9666E-02	-	1.0270E-02	4.7617E-02
14	4.9324E-05	7.5559E-03	8.6525E-05	2.9708E-02	-	1.0284E-02	4.7684E-02
15	4.9368E-05	7.5627E-03	8.6602E-05	2.9734E-02	-	1.0293E-02	4.7726E-02
16	2.0136E-05	3.1412E-03	1.1646E-05	1.6663E-04	5.1381E-02	-	5.4721E-02
17	2.0136E-05	3.1412E-03	1.1646E-05	1.6662E-04	5.1381E-02	-	5.4721E-02
18	1.6158E-05	2.5207E-03	9.3456E-06	1.3371E-04	5.2411E-02	-	5.5091E-02
19	Plate 19 is solid aluminum						
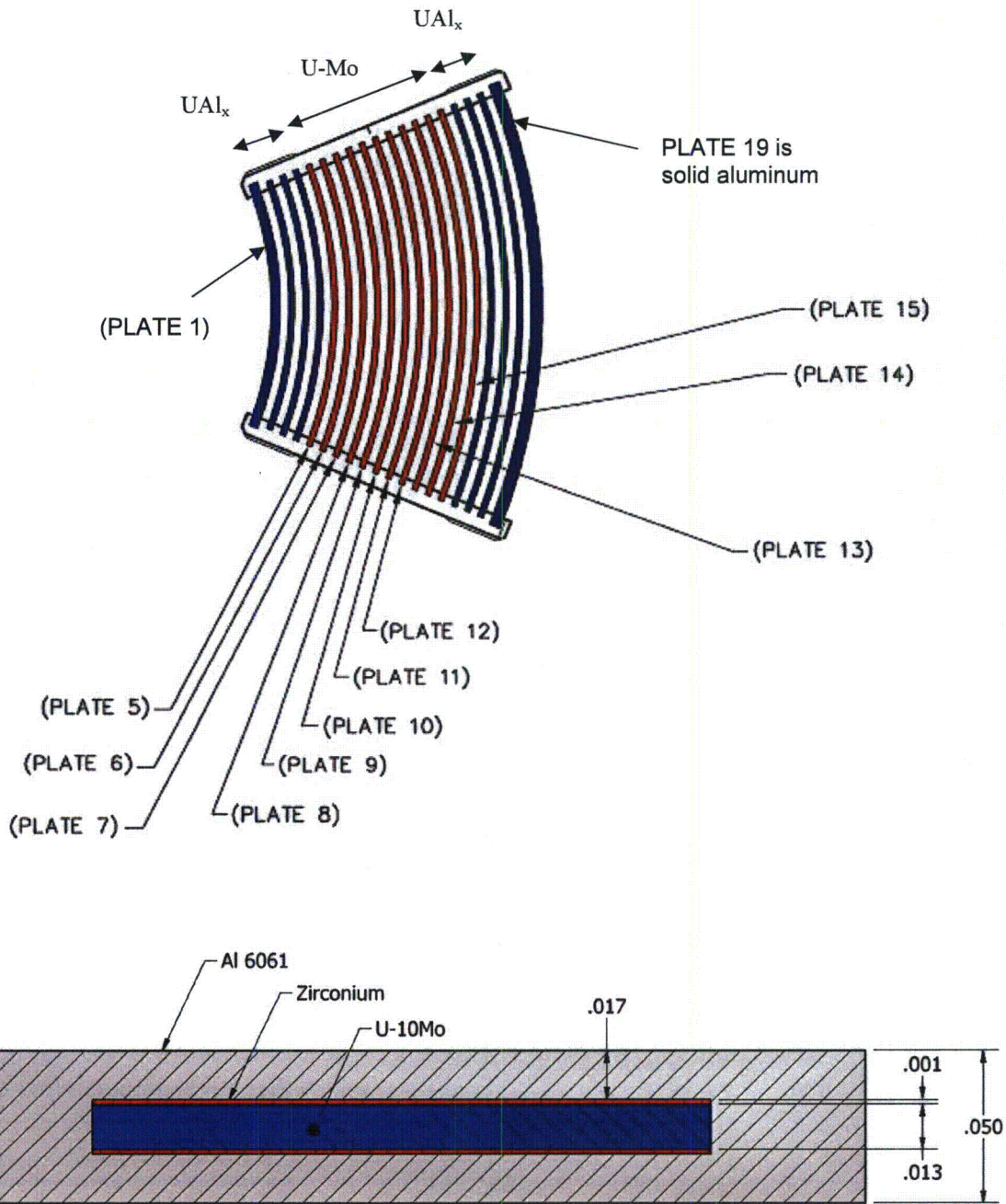
U-Mo Plate (plates 5-15)

Figure 6.12-1 – U-Mo Demonstration Element

Plate 19

Plate 1

Zr

U-Mo

Al

Close-up of U-Mo Plate
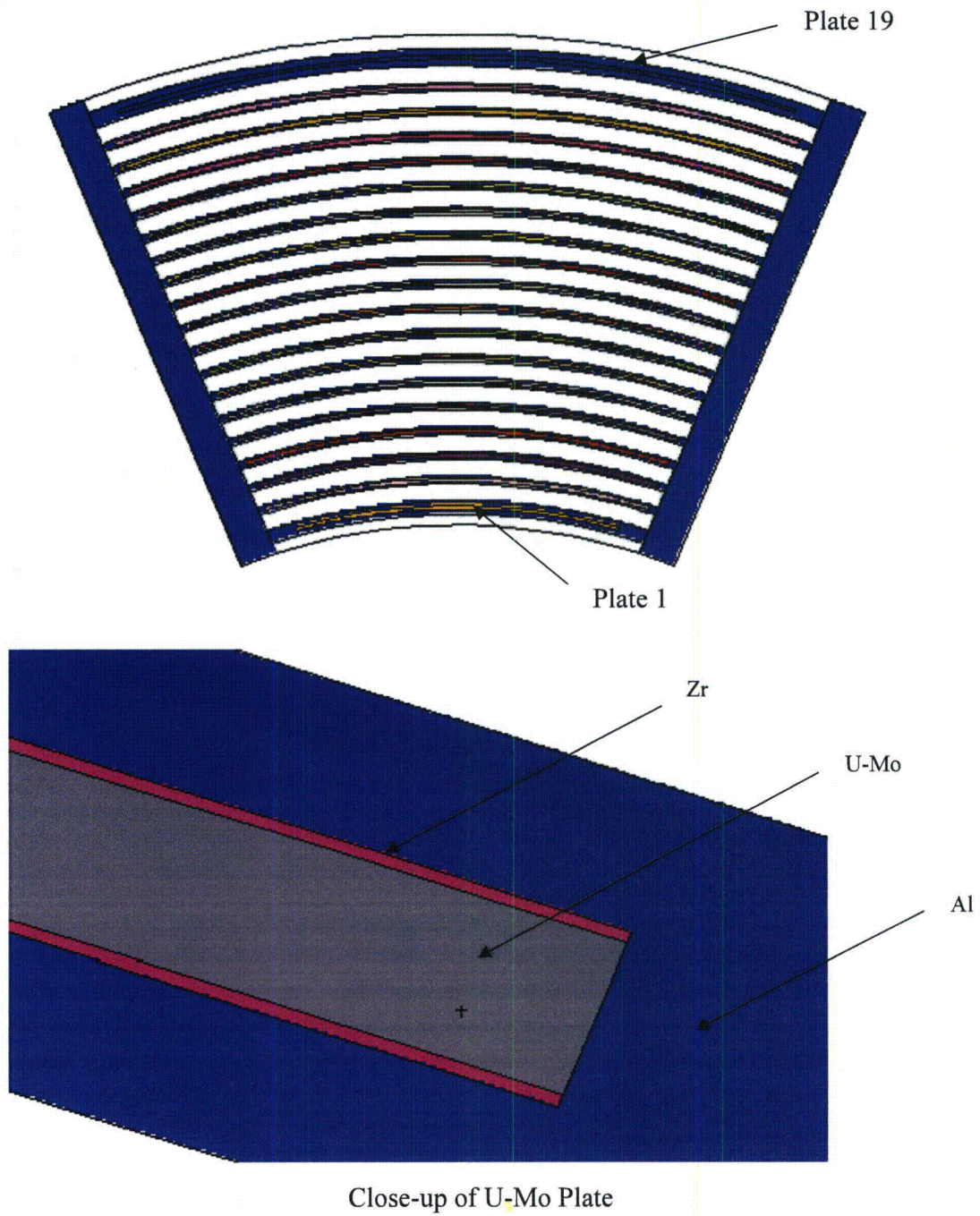
Figure 6.12-2 – U-Mo Demonstration Element MCNP Model

6.12.3 General Considerations

6.12.3.1 Model Configuration

The model configuration is relatively simple. Most packaging details are conservatively ignored, particularly at the ends. Because the package is long and narrow, array configurations will stack only in the lateral directions (e.g., 5x5x1). Therefore, the end details, for both the package and the fuel element, are conservatively ignored external to the active fuel region, and these end regions are simply modeled as full-density water.

Tolerances on the packaging are selected to result in the most reactive condition, as described in Section 6.3.1, *Model Configuration*. The standard ATR models are utilized with no change to the packaging descriptions.

The package consists of two primary structural components, a circular inner tube and a square outer tube. The modeled tube OD is 6.03-in, the modeled wall thickness is 0.108-in, and the modeled tube ID is 5.814-in. The outer tube is modeled with a wall thickness of 0.169-in and outer dimension of 7.9-in.

In the NCT single package models, the inner tube, insulation, and outer tube are modeled explicitly, as shown in Figure 6.12-3 and Figure 6.12-4. Although negligible water ingress is expected during NCT, the inner cavity of the package is assumed to be flooded with water because the package lid does not contain a seal. However, the region between the insulation and the outer tube will remain dry because water cannot enter this region. The Fuel Handling Enclosure (FHE) is conservatively ignored. Modeling the FHE would decrease water reflection in the single package model. However, the neoprene along the sides of the FHE is modeled explicitly using a thickness of 1/8-in. Because neoprene will reduce the reactivity due to parasitic absorption in chlorine, chlorine is removed from the neoprene, and the density is reduced accordingly. In the model, the fuel element is conservatively positioned at the radial center of the inner tube to maximize neutron reflection. The package is reflected with 12-in of full-density water.

The HAC single package model is essentially the same as the NCT single package model. Damage in the drop tests was shown to be negligible and concentrated at the ends of the package. As the ends of the package are not modeled, this end damage does not affect the modeling. The various side drops resulted in only minor localized damage to the outer tube, and no observable bulk deformation of the package. Therefore, the minor damage observed will not impact the reactivity. The insulation is replaced with full-density water, and the region between the insulation and outer tube is also filled with full-density water (see Figure 6.12-5). The treatment of the FHE is the same as the NCT single package model.

In the NCT array models, a 9x9x1 array is utilized. Although the FHE would survive NCT events with no damage, the FHE is conservatively ignored and the fuel elements are pushed toward the center of the array. Because the fuel elements are transported in a thin (~0.01-in) plastic bag, this plastic bag is assumed to act as a boundary for partial moderation effects. The plastic bag is not modeled explicitly, because it is too thin to have an appreciable effect on the reactivity. Therefore, it is postulated that the fuel element channels may fill with full-density water, while the region between the fuel element and inner tube fills with variable density water. The partial moderation effects that could be achieved by modeling the FHE explicitly are

essentially addressed by the partial moderation analysis using the plastic bag. Also, modeling the FHE explicitly would result in the fuel elements being significantly pushed apart, which is a less reactive condition. Axial movement of the fuel elements is not considered because axial movement would increase the effective active height of the system and reduce the reactivity due to increased leakage.

In the HAC array models, a 5x5x1 array is utilized. The HAC array models are essentially the same as the NCT array models, except additional cases are developed to determine the reactivity effect of allowing variable density water in the region between the inner and outer tubes. The FHE is conservatively ignored for the reasons stated in the previous paragraph. Because the NCT and HAC models are very similar and the NCT models utilize a larger array, the NCT array models are more reactive than the HAC array models.

The detailed moderation assumptions for these cases are discussed more fully in Section 6.12.5, *Evaluation of Package Arrays under Normal Conditions of Transport*, and Section 6.12.6, *Package Arrays under Hypothetical Accident Conditions*.

6.12.3.2 Material Properties

The fuel meat compositions are provided in Table 6.12-4. For the U-Mo plates, the zirconium interlayer is modeled as pure zirconium with a density of 6.506 g/cm^3. All aluminum alloy structural materials are modeled as pure aluminum with a density of 2.7 g/cm^3. The material properties of the packaging materials are provided in Section 6.3.2, *Material Properties*.

6.12.3.3 Computer Codes and Cross-Section Libraries

MCNP5 v1.30 is used for the criticality analysis. All cross sections utilized are at room temperature (293.6 K). The uranium isotopes utilize preliminary ENDF/B-VII cross section data that are considered by Los Alamos National Laboratory to be more accurate than ENDF/B-VI cross sections. ENDF/B-V cross sections are utilized for chromium, nickel, and iron because natural composition ENDF/B-VI cross sections are not available for these elements. The remaining isotopes utilize ENDF/B-VI cross sections. Titles of the cross sections utilized in the models have been extracted from the MCNP output (when available) and provided in Table 6.12-5. The $S(\alpha,\beta)$ card LWTR.60T is used to simulate hydrogen bound to water.

All cases are run with 2500 neutrons per generation for 250 generations, skipping the first 50. The 1-sigma uncertainty is approximately 0.001 for all cases.

6.12.3.4 Demonstration of Maximum Reactivity

The reactivities of the NCT and HAC single package cases are small, with $k_s < 0.5$.

The NCT and HAC array cases are similar. For the NCT array, a 9x9x1 array is utilized, while in the HAC array, a smaller 5x5x1 array is utilized. Because negligible damage was observed in the drop tests, the package dimensions are the same between the NCT and HAC models. Dimensions of both the fuel element and packaging are selected to maximize reactivity, and close-water reflection is utilized. In both NCT and HAC array cases, flooding with partial moderation is allowed in the central cavity, and the fuel elements are pushed toward the center of the array. The FHE is not modeled explicitly because the FHE would increase the fuel element

spacing and decrease the reactivity. Any partial moderation effects of the FHE are essentially addressed by the partial moderation analysis for the fuel element itself.

In the NCT array models, insulation is modeled between the inner and outer tubes. In the HAC array models for the standard ATR fuel element, it was determined in Section 6.6, *Package Arrays under Hypothetical Accident Conditions*, that it is conservative to model the insulation rather than treating this region as void or water. Therefore, in the demonstration element HAC models, insulation is modeled in all cases. In both sets of models, chlorine-free neoprene is modeled adjacent to the fuel element side plates, although the effect on the reactivity is small. No models in which the neoprene is allowed to decompose and homogeneously mix with the water are developed, as this scenario is already bounded by the variable water density search.

The NCT array is more reactive than the HAC array, primarily because the NCT array is significantly larger. The most reactive case (Case MO13) results in a k_s = 0.78785, which is below the USL of 0.9209. Note that the demonstration element is less reactive than a standard ATR fuel element.

Table 6.12-5 – Cross Section Libraries Utilized

Isotope/Element	Cross Section Label (from MCNP output)
1001.62c	1-h-1 at 293.6K from endf-vi.8 njoy99.50
6000.66c	6-c-0 at 293.6K from endf-vi.6 njoy99.50
8016.62c	8-o-16 at 293.6K from endf-vi.8 njoy99.50
13027.62c	13-al-27 at 293.6K from endf-vi.8 njoy99.50
14000.60c	14-si-nat from endf/b-vi
15031.66c	15-p-31 at 293.6K from endf-vi.6 njoy99.50
17000.66c	17-cl-0 at 293.6K from endf-vi.0 njoy99.50
24000.50c	njoy
25055.62c	25-mn-55 at 293.6K from endf/b-vi.8 njoy99.50
26000.55c	njoy
28000.50c	njoy
40000.66c	40-zr-0 at 293.6K from endf-vi.1 njoy99.50
42000.66c	42-mo-0 at 293.6K from endf-vi.0 njoy99.50
92234.69c	92-u-234 at 293.6K from t16 u234la4 njoy99.50
92235.69c	92-u-235 at 293.6K from t16 u235la9d njoy99.50
92236.69c	92-u-236 at 293.6K from t16 u236la2d njoy99.50
92238.69c	92-u-238 at 293.6K from t16 u238la8h njoy99.50

1-in insulation

12-in water reflector

1/8-in neopren

6.03-in

7.9-in
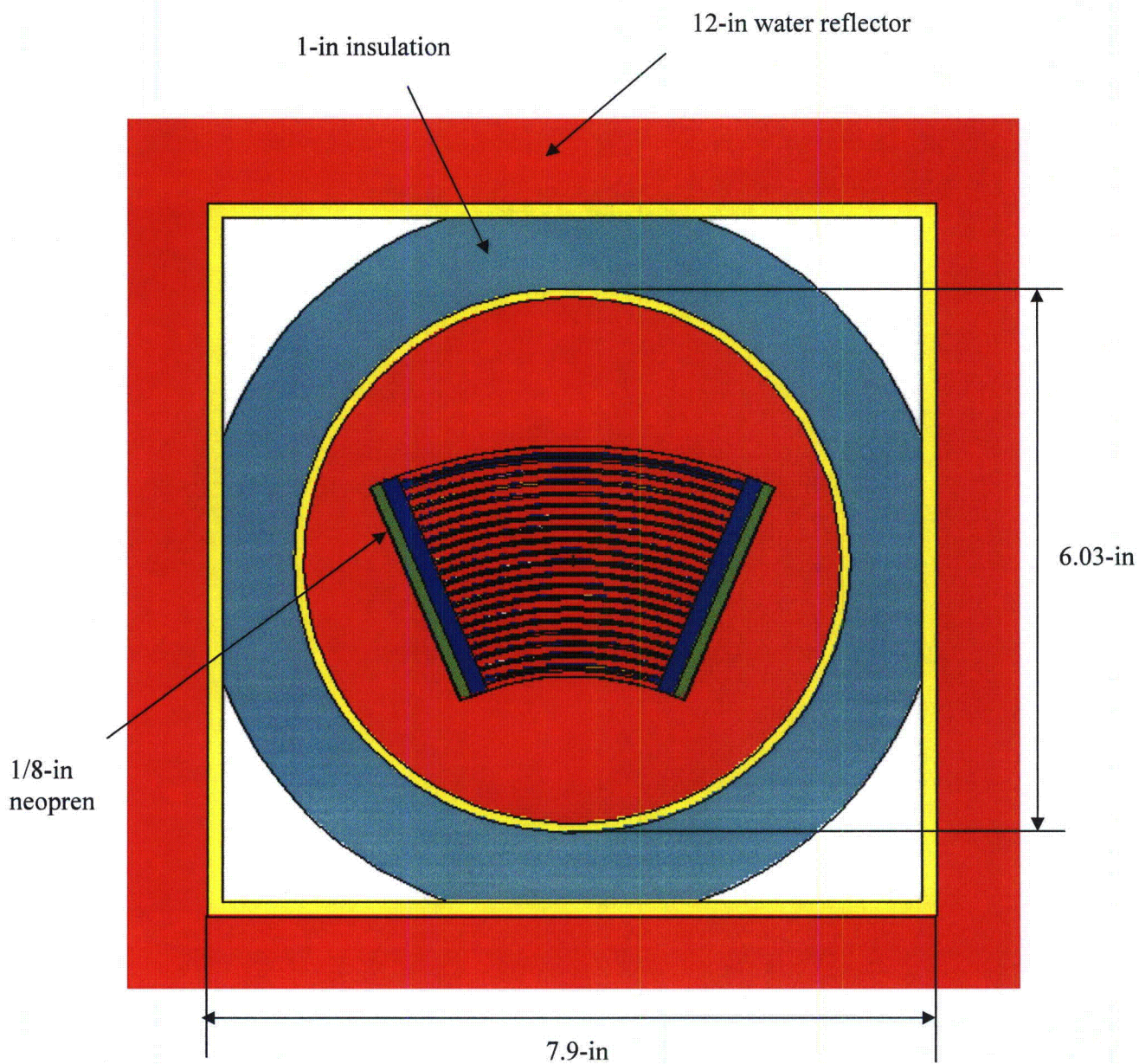
Figure 6.12-3 – NCT Single Package Model (planar view)

48-in
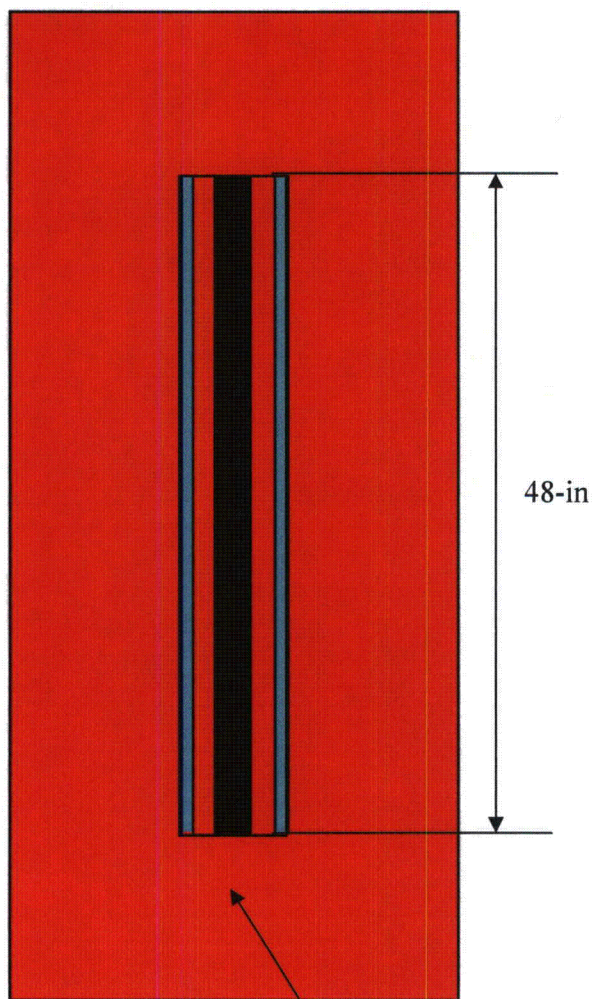
Note that the ends of both the
fuel element and package are
conservatively treated simply as
a water reflector.

Figure 6.12-4 – NCT Single Package Model (axial view)

Insulation and void replaced
with water.
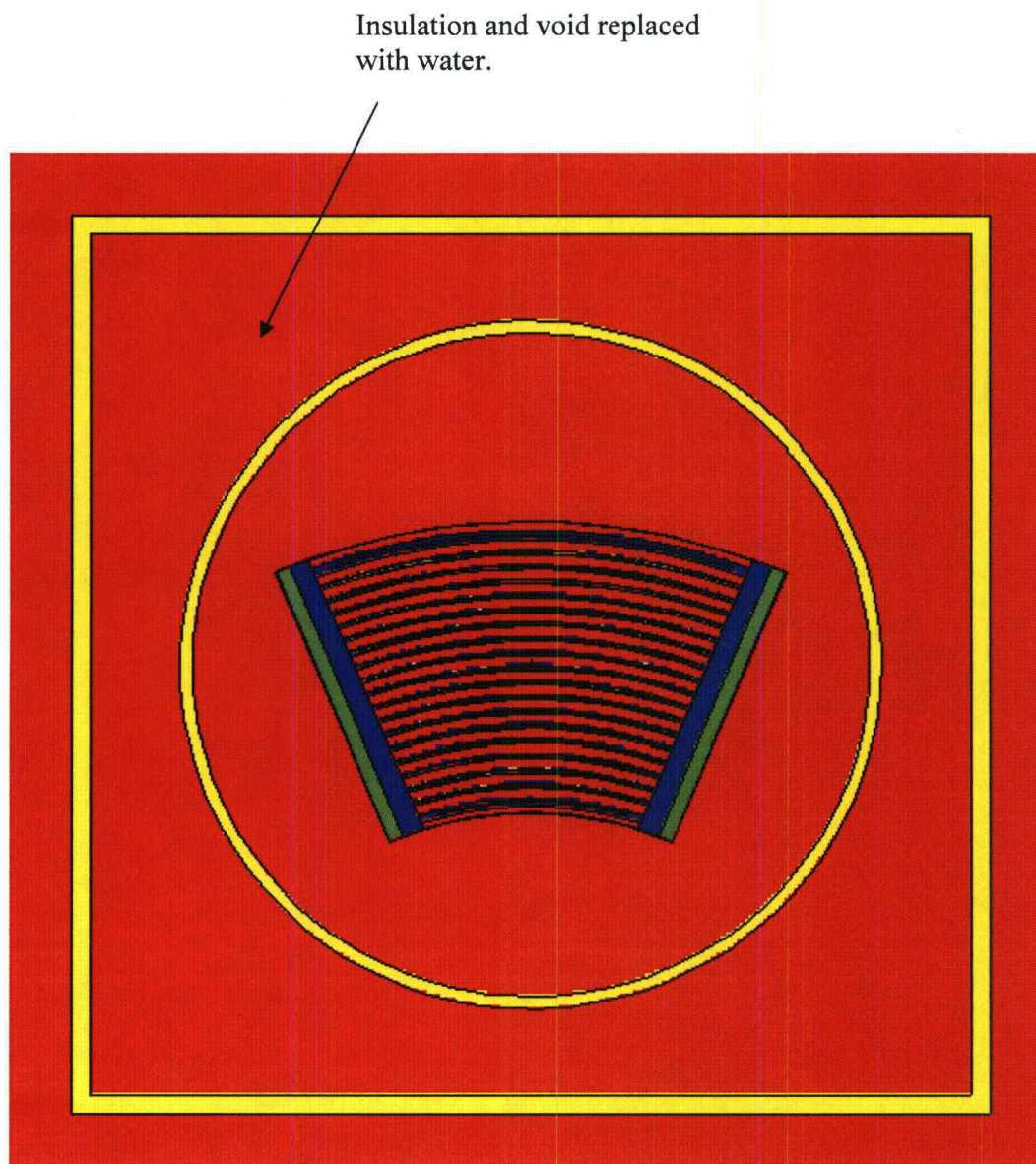
Figure 6.12-5 – HAC Single Package Model (planar view)

6.12.4 Single Package Evaluation

6.12.4.1 Single Package Configuration

6.12.4.1.1   NCT Single Package Configuration

The geometry of the NCT single package configuration is discussed in Section 6.12.3.1, *Model Configuration*. A detailed parametric analysis of standard ATR fuel was performed in Section 6.4.1.2.1, *Fuel Element Payload Parametric Evaluation*. It was determined that reactivity for ATR-type fuel is maximized by maximizing the arc length of the fuel meat and maximizing the channel spacing between fuel plates. These conclusions are applicable to the U-Mo demonstration element because the fuel element geometry is the same and the fissile loading per plate is very similar to the standard ATR fuel element. Therefore, the demonstration elements are modeled with the maximum fuel meat arc lengths and a bounding channel spacing of 0.089-in. A channel spacing of 0.089-in is the maximum local channel spacing (0.087-in) with an additional margin of 0.002-in. This channel spacing is achieved by artificially reducing the cladding thickness.

Only the most reactive NCT single package configuration for a standard ATR fuel element is repeated with the U-Mo demonstration element. Results are provided in Table 6.12-6, Case MO1. This case features an inner tube flooded with full-density water. Neoprene is modeled, but chlorine is conservatively removed from the neoprene because chlorine acts as a poison. The package is reflected with 12-in of water. For this case, $k_s = 0.40552$, which is below the USL of 0.9209.

6.12.4.1.2   HAC Single Package Configuration

The packaging and fuel geometry of the HAC single package configuration is discussed in Section 6.12.3.1, *Model Configuration*. The HAC single package geometry is the same as the NCT single package geometry, except the insulation and region between the inner and outer tubes is replaced with water.

Only the most reactive HAC single package configuration for a standard ATR fuel element is repeated with the U-Mo demonstration element because the fuel element geometry is the same and the fissile loading per plate is very similar to the standard ATR fuel element. Results are provided in Table 6.12-6, Case MO2. This case features an inner tube flooded with full-density water. Neoprene is modeled, but chlorine is conservatively removed from the neoprene because chlorine acts as a poison. The package is reflected with 12-in of water. For this case, $k_s = 0.43443$, which is below the USL of 0.9209.

Note that the most reactive HAC single package case for a standard HEU ATR fuel element has $k_s = 0.45237$ (see Table 6.4-5). Therefore, the U-Mo demonstration element is less reactive than a standard HEU ATR fuel element.

6.12.4.2 Single Package Results

Following are the tabulated results for the single package cases.

Table 6.12-6 – Single Package Results

Case ID	Filename	k_{eff}	σ	k_s $(k+2\sigma)$
NCT				
MO1	NS_MO	0.40358	0.00097	0.40552
HAC				
MO2	HS_MO	0.43257	0.00093	0.43443

6.12.5 Evaluation of Package Arrays under Normal Conditions of Transport

6.12.5.1 NCT Array Configuration

The NCT array model is a 9x9x1 array of the NCT single package model, see Figure 6.12-6. Although an 8x8x1 array is of sufficient size to justify a CSI = 4.0, the larger 9x9x1 array is utilized simply for modeling convenience. The entire array is reflected with 12-in of full-density water.

The fuel elements are pushed to the center of the array and rotated to minimize the distance between the fuel elements. This geometry is not feasible for NCT, because the FHE would force the fuel elements to remain in the center of the package, although the FHE does allow rotation. Therefore, it is conservative to ignore the FHE to minimize the separation distance. In addition, a small notch is added to the neoprene so that the fuel element may be translated to the maximum extent without interfering with the inner tube geometry. This notch is not present in the single package models.

It was determined in the analysis for the standard ATR fuel element that the most reactive NCT array configuration has full-density water between fuel plates, variable density water inside the inner tube, and a channel spacing of 0.089-in. Therefore, only this configuration is investigated for the demonstration element because the fuel element geometry is the same and the fissile loading per plate is very similar to the standard ATR fuel element.

The results are provided in Table 6.12-7. Reactivity is at a maximum for Case MO13, which has 0.3 g/cm^3 water inside the inner tube, and k_s = 0.78785. The maximum result is far below the USL of 0.9209.

Case MO13 is the most reactive demonstration element case. Note that is it significantly less reactive than the equivalent standard ATR NCT array case, which has k_s = 0.83616 (see Table 6.5-1). To determine if the molybdenum in the fuel could potentially be acting as a poison, an additional case (Case MO21) is run "for information only" with no molybdenum in the fuel matrix. For Case MO21, k_s = 0.79228, which is a negligible increase from Case MO13 compared to the USL of 0.9209. Therefore, it is concluded that molybdenum has little effect on

the system reactivity. It is inferred that reactivity differences between the demonstration element and a standard ATR element are largely related to increased parasitic absorption in U-238.

6.12.5.2 NCT Array Results

The results for the NCT array cases are provided in the following table.

Table 6.12-7 – NCT Array Results

Case ID	Filename	Water Density Between Tubes (g/cm³)	Water Density Inside Inner Tube (g/cm³)	Water Density Between Plates (g/cm³)	k_{eff}	σ	k_s (k+2σ)
MO10	NA_MO_P000	0	0	1.0	0.73196	0.00116	0.73428
MO11	NA_MO_P010	0	0.1	1.0	0.76638	0.00107	0.76852
MO12	NA_MO_P020	0	0.2	1.0	0.77779	0.00126	0.78031
MO13	**NA_MO_P030**	**0**	**0.3**	**1.0**	**0.78557**	**0.00114**	**0.78785**
MO14	NA_MO_P040	0	0.4	1.0	0.78312	0.00110	0.78532
MO15	NA_MO_P050	0	0.5	1.0	0.77669	0.00111	0.77891
MO16	NA_MO_P060	0	0.6	1.0	0.76518	0.00114	0.76746
MO17	NA_MO_P070	0	0.7	1.0	0.75554	0.00102	0.75758
MO18	NA_MO_P080	0	0.8	1.0	0.74778	0.00113	0.75004
MO19	NA_MO_P090	0	0.9	1.0	0.73366	0.00112	0.73590
MO20	NA_MO_P100	0	1.0	1.0	0.72399	0.00114	0.72627
Case MO13 without Molybdenum in Fuel - For Information Only							
MO21	NA_NOMO_P030	0	0.3	1.0	0.78990	0.00119	0.79228
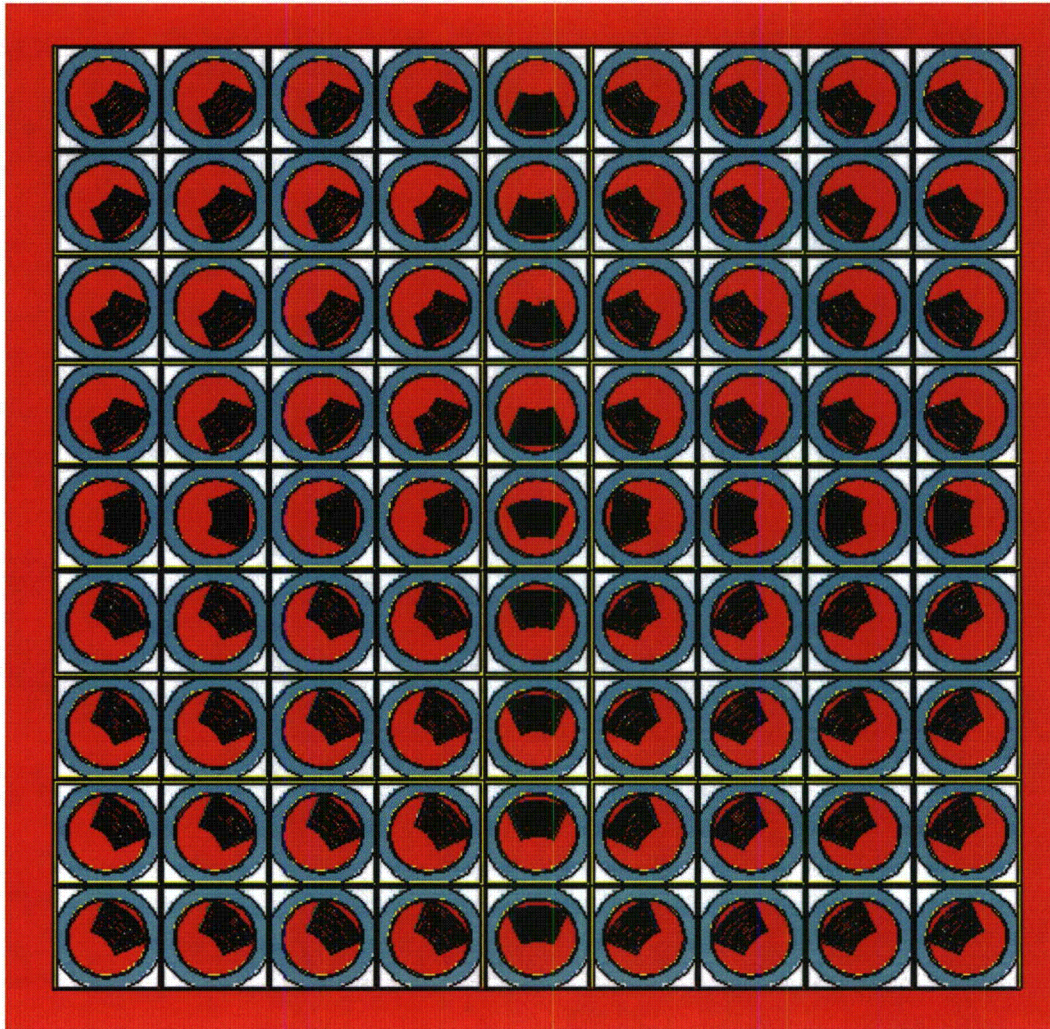
Figure 6.12-6 – NCT Array Geometry

6.12.6 Package Arrays under Hypothetical Accident Conditions

6.12.6.1 HAC Array Configuration

The HAC array model is a 5x5x1 array of the HAC single package model. It was determined in the analysis for the standard ATR element that the most reactive HAC array configuration features full-density water between the fuel plates, a channel spacing of 0.089-in, variable density water inside the inner tube, insulation modeled with void present between the insulation and outer tube, and neoprene modeled without chlorine. Therefore, only this configuration is investigated for the demonstration element because the fuel element geometry is the same and the fissile loading per plate is very similar to the standard ATR fuel element. This configuration is shown in Figure 6.12-7.

The results are provided in Table 6.12-8. Case MO36 is the most reactive, with a water density of 0.6 g/cm^3 inside the inner tube and k_s = 0.70543. This result is below the USL of 0.9209. Note that this result is lower than the maximum NCT array case because the HAC and NCT array models are quite similar, except the NCT array uses a much larger 9x9x1 configuration.

6.12.6.2 HAC Array Results

Following are the tabulated results for the HAC array cases.

Table 6.12-8 – HAC Array Results

Case ID	Filename	Water Density Between Tubes (g/cm^3)	Water Density Inside Inner Tube (g/cm^3)	Water Density Between Plates (g/cm^3)	k_{eff}	σ	k_s $(k+2\sigma)$
MO30	HA_MO_P000	0	0	1.0	0.58525	0.00099	0.58723
MO31	HA_MO_P010	0	0.1	1.0	0.62456	0.00105	0.62666
MO32	HA_MO_P020	0	0.2	1.0	0.65775	0.00116	0.66007
MO33	HA_MO_P030	0	0.3	1.0	0.67626	0.00119	0.67864
MO34	HA_MO_P040	0	0.4	1.0	0.69053	0.00115	0.69283
MO35	HA_MO_P050	0	0.5	1.0	0.69590	0.00117	0.69824
MO36	**HA_MO_P060**	**0**	**0.6**	**1.0**	**0.70311**	**0.00116**	**0.70543**
MO37	HA_MO_P070	0	0.7	1.0	0.70183	0.00113	0.70409
MO38	HA_MO_P080	0	0.8	1.0	0.70024	0.00121	0.70266
MO39	HA_MO_P090	0	0.9	1.0	0.69510	0.00121	0.69752
MO40	HA_MO_P100	0	1.0	1.0	0.69183	0.00109	0.69401
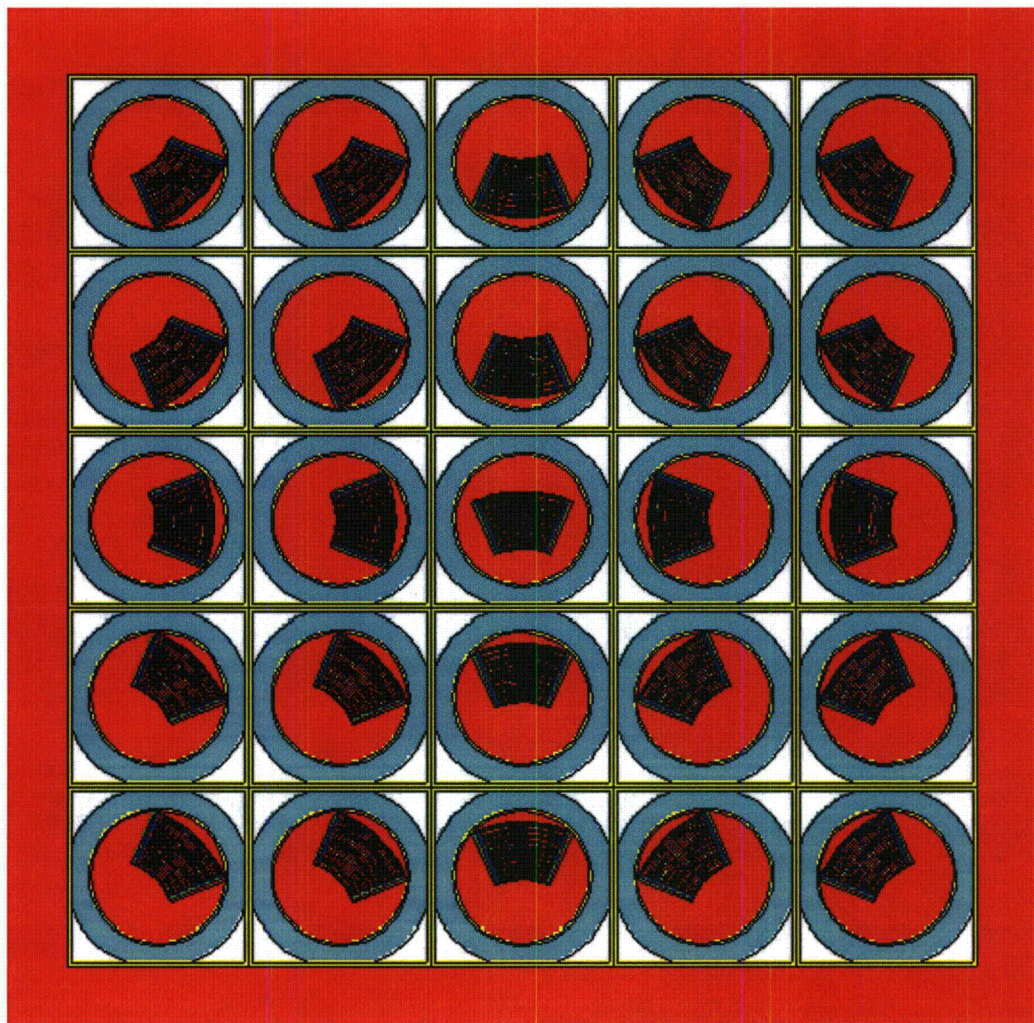
Figure 6.12-7 – HAC Array Geometry

6.12.7 Fissile Material Packages for Air Transport

This section is not applicable.

6.12.8 Benchmark Evaluations

The Monte Carlo computer program MCNP5 v1.30[15] is utilized for this analysis. MCNP has been used extensively in criticality evaluations for several decades and is considered a standard in the industry.

The ORNL USLSTATS code[16] is used to establish a USL for the analysis. USLSTATS provides a simple means of evaluating and combining the statistical error of the calculation, code biases, and benchmark uncertainties. The USLSTATS calculation uses the combined uncertainties and data to provide a linear trend and an overall uncertainty. Computed multiplication factors, k_{eff}, for the package are deemed to be adequately subcritical if the computed value of k_s is less than or equal to the USL as follows:

$$k_s = k_{eff} + 2\sigma \leq USL$$

The USL includes the combined effects of code bias, uncertainty in the benchmark experiments, uncertainty in the computational evaluation of the benchmark experiments, and an administrative margin. This methodology has accepted precedence in establishing criticality safety limits for transportation packages complying with 10 CFR 71.

6.12.8.1 Applicability of Benchmark Experiments

The critical experiment benchmarks are selected from the *International Handbook of Evaluated Criticality Safety Benchmark Experiments*[17] based upon their similarity to the ATR Fresh Fuel Shipping Container and contents. The important selection parameters are HEU and LEU uranium plate-type fuels with a thermal spectrum. Thirty-five benchmarks are available for HEU plate fuel, while only one is available for LEU plate fuel. Therefore, the plate-type benchmarks are supplemented with 54 LEU rod benchmarks, for a total of 90 benchmarks. The titles for all utilized experiments are listed in Table 6.12-9.

Ideally, benchmarks would be limited to those with a fuel matrix of HEU UAl_x and LEU U-Mo, aluminum cladding, and no absorbers, consistent with the ATR demonstration element criticality models. However, no experiment set is available that meets all of these criteria since U-Mo fuel is in a research and development stage, and benchmarks for U-Mo fuel designs are not available. Therefore, the selected experiments are subdivided into two general subsets, plate-type

---

[15] MCNP5, "*MCNP – A General Monte Carlo N-Particle Transport Code, Version 5; Volume II: User's Guide*," LA-CP-03-0245, Los Alamos National Laboratory, April, 2003.

[16] USLSTATS, "*USLSTATS: A Utility To Calculate Upper Subcritical Limits For Criticality Safety Applications,*" Version 1.4.2, Oak Ridge National Laboratory, April 23, 2003.

[17] OECD Nuclear Energy Agency, *International Handbook of Evaluated Criticality Safety Benchmark Experiments*, NEA/NSC/DOC(95)03, September, 2010.

benchmarks and LEU rod benchmarks. Trending is performed for both subsets of benchmarks and the entire benchmark set. The USL selected is the minimum of all sets.

The primary difference between the U-Mo demonstration element and a standard ATR element is the presence of molybdenum rather than aluminum in the fuel matrix. It is demonstrated in Section 6.12.5, *Evaluation of Package Arrays under Normal Conditions of Transport*, that deletion of molybdenum from the MCNP model has very little effect on the reactivity. Therefore, because molybdenum has little effect on the reactivity and margins to the USL are very large, the lack of U-Mo benchmarks has little effect on the USL and is acceptable.

LEU-COMP-THERM-009 uses various separator plates. Only cases 1-8 (steel separators) and 24-27 (aluminum and/or zircaloy separators) are utilized, and the rest are considered not applicable. LEU-COMP-THERM-010 uses various reflector plates. Only cases 9-19 (steel reflectors) are utilized, and the rest are considered not applicable.

Note that IEU-COMP-THERM-014 consists of a single LEU plate-type benchmark with U_3Si_2-Al fuel meat and is the experiment that is closest to meeting all of the desired criteria.

6.12.8.2 Bias Determination

The USL is calculated by application of the USLSTATS computer program. USLSTATS receives as input the k_{eff} as calculated by MCNP, the total 1-σ uncertainty (combined benchmark and MCNP uncertainties), and a trending parameter. Six trending parameters have been selected: (1) Energy of the Average neutron Lethargy causing Fission (EALF), (2) U-235 number density, (3) channel spacing, (4) ratio of the number of hydrogen atoms in a unit cell to the number of U-235 atoms in a unit cell (H/U-235), (5) plate pitch, and (6) U-235 enrichment. The channel spacing and plate pitch parameters are applied only to the plate-type benchmarks.

The uncertainty value, σ_{total}, assigned to each case is a combination of the benchmark uncertainty for each experiment, σ_{bench}, and the Monte Carlo uncertainty associated with the particular computational evaluation of the case, σ_{MCNP}, or:

$$\sigma_{total} = (\sigma_{bench}^2 + \sigma_{MCNP}^2)^{\frac{1}{2}}$$

These values are input into the USLSTATS program in addition to the following parameters, which are the values recommended by the USLSTATS user's manual:

- P, proportion of population falling above lower tolerance level = 0.995 (note that this parameter is required input but is not utilized in the calculation of USL Method 1)

- 1-γ, confidence on fit = 0.95

- α, confidence on proportion P = 0.95 (note that this parameter is required input but is not utilized in the calculation of USL Method 1)

- Δk_m, administrative margin used to ensure subcriticality = 0.05.

These data are followed by triplets of trending parameter value, computed k_{eff}, and uncertainty for each case. A confidence band analysis is performed on the data for each trending parameter using USL Method 1. The USL generated for each of the trending parameters utilized is provided in Table 6.12-10. All benchmark data used as input to USLSTATS are reported in

Table 6.12-11. The results for each trending parameter are discussed in the following paragraphs.

Energy of the Average neutron Lethargy causing Fission (EALF)

The EALF is used as the first trending parameter for the benchmark cases. The EALF comparison provides a means to observe neutron spectral dependencies or trends. The range of applicability for the benchmarks is $5.222E-08$ MeV $\leq$ EALF $\leq 3.217E-07$ MeV. The ATR demonstration element cases fall within the range of applicability. This parameter is trended on all benchmarks and the subset of plate and rod-type benchmarks. A minimum USL based on EALF of 0.9254 occurs for the plate-type benchmarks.

U-235 Number Density

The U-235 number density is used as the second trending parameter for the benchmark cases. The range of applicability for the benchmarks is $4.879E-04$ atom/b-cm $\leq$ U-235 $\leq 3.926E-03$ atom/b-cm. The U-235 number densities for UAl_x plates 1 through 4 and 16 through 18 fall within the range of applicability, while the number densities for U-Mo plates 5 through 15 exceed the range of applicability (maximum value $= 7.563E-03$ atom/b-cm). However, the average U-235 number density for the fuel element is $4.843E-03$ atom/b-cm.

This parameter is trended on all benchmarks and the subset of plate and rod-type benchmarks. A minimum USL based on U-235 number density of 0.9239 occurs for the plate-type benchmarks. If this USL is extrapolated based on the average value, the estimated USL is 0.9219. Note that it is not expected that the U-235 number density trend is a truly physical trend because MCNP performs no special cross-section processing.

Channel Spacing

The channel spacing is used as the third trending parameter for the benchmark cases. The range of applicability for the benchmarks is $6.457E-02$ in $\leq$ channel spacing ≤ 0.107 in. The ATR demonstration element channel spacing of 0.089-in falls within the range of applicability. Trending is performed only over the plate-type benchmarks, and the minimum USL over the range of applicability is 0.9228.

H/U-235 Atom Ratio

The H/U-235 atom ratio is used as the fourth trending parameter for the benchmark cases. The H/U-235 atom ratio is defined here as the ratio of hydrogen atoms to U-235 atoms in a unit cell. The range of applicability for the benchmarks is $65.100 \leq$ H/U235 ≤ 399.0. This parameter for the demonstration element is computed by the following equation:

$$N_H * C/(N_{U235} * M)$$

where,

N_H is the hydrogen number density ($6.687E-02$ atom/b-cm)

C is the channel spacing (0.089-in)

N_{U235} is the U-235 number density (variable)

M is the fuel meat width (0.02-in for UAl_x and 0.013-in for U-Mo)

The benchmark cases are a mixture of plate and rod-type benchmarks. The H/U-235 ratios for the plate-type benchmarks are computed as shown above, while the H/U-235 ratios for the rod-type benchmarks are computed using the area of a fuel pellet in place of "M" and water area inside a unit cell in place of "C."

If this parameter is computed for all 18 fueled plates, the ratio ranges from 60.5 to 122.6 for the demonstration element fuel plates. This parameter is trended on all benchmarks and the subset of plate and rod-type benchmarks. The minimum USL for this parameter over the range of applicability is 0.9251. This range is only slightly outside the range of applicability at the lower end (60.5 vs. 65.1) and is considered acceptable.

Plate Pitch

The fuel plate pitch is used as the fifth trending parameter for the benchmark cases. The range of applicability for the benchmarks is 0.12457-in $\leq P \leq$ 0.165-in. The fuel plate pitch is fixed at 0.128-in for all models (excluding the pitch for plate 1, which is slightly bigger because this plate is thicker). This pitch falls within the range of the benchmark experiments. Trending is performed only over the plate-type benchmarks, and the minimum USL over the range of applicability is 0.9225.

Enrichment

The U-235 enrichment is used as the sixth trending parameter for the benchmark cases. The range of applicability for the benchmarks is 2.35% $\leq E \leq$ 93.2%. The U-Mo demonstration element is comprised of U-Mo plates with an enrichment of 20%, and UAl_x plates with an enrichment of 94%. The enrichment of the U-Mo plates is within the range of applicability, and the enrichment of the UAl_x plates is only slightly outside the range of applicability and is considered acceptable. This parameter is trended on all benchmarks and the subset of plate and rod-type benchmarks. A minimum USL based on enrichment of 0.9224 occurs for the plate-type benchmarks.

Recommended USL

Based on the trending over six parameters, a minimum USL of 0.9224 occurs for the enrichment parameter. However, the benchmarking analysis documented in Section 6.8, *Benchmark Evaluations*, for the standard HEU element resulted in a USL of 0.9209. Both for consistency and added conservatism, a USL of 0.9209 is selected for this analysis.

Table 6.12-9 – Benchmark Experiments Utilized

Series	Title
Plate-Type Benchmarks	
HEU-COMP-THERM-022	SPERT III Stainless-Steel-Clad Plate-Type Fuel in Water
HEU-MET-THERM-006	SPERT-D Aluminum-Clad Plate-Type Fuel in Water, Dilute Uranyl Nitrate, or Borated Uranyl Nitrate
HEU-MET-THERM-022	Advanced Test Reactor: Serpentine Arrangement of Highly Enriched Water-Moderated Uranium-Aluminide Fuel Plates Reflected by Beryllium
IEU-COMP-THERM-014	RA-6 Reactor: Water Reflected, Water Moderated $U(19.77)_3Si_2$-Al Fuel Plates
Rod-Type Benchmarks	
LEU-COMP-THERM-001	Water-Moderated $U(2.35)O_2$ Fuel Rods in 2.032-cm Square-Pitched Arrays
LEU-COMP-THERM-002	Water-Moderated $U(4.31)O_2$ Fuel Rods in 2.54-cm Square-Pitched Arrays
LEU-COMP-THERM-006	Critical Arrays of Low-Enriched UO_2 Fuel Rods with Water-to-Fuel Volume Ratios Ranging From 1.5 to 3.0
LEU-COMP-THERM-009	Water-Moderated Rectangular Clusters of $U(4.31)O_2$ Fuel Rods (2.54-cm Pitch) Separated by Steel, Boral, Copper, Cadmium, Aluminum, or Zircaloy-4 Plates (Cases 1-8 and 24-27 only)
LEU-COMP-THERM-010	Water-Moderated $U(4.31)O_2$ Fuel Rods Reflected by Two Lead, Uranium, or Steel Walls (Cases 9-19 only)

Table 6.12-10 – USL Results

Trending Parameter (X)	Minimum USL Over Range of Applicability	Range of Applicability
All Benchmarks (90)		
EALF (MeV)	0.9323	5.22170E-08 <= X <= 3.21670E-07
U-235 Number Density (atom/b-cm)	0.9285	4.87850E-04 <= X <= 3.92600E-03
H/U-235	0.9325	65.100 <= X <= 399.00
Enrichment (%)	0.9321	2.35 <= X <= 93.2
Plate-Type Benchmarks (36)		
EALF (MeV)	0.9254	5.22170E-08 <= X <= 1.58510E-07
U-235 Number Density (atom/b-cm)	0.9239	1.84900E-03 <= X <= 3.92600E-03
Channel spacing (in)	0.9228	6.45700E-02 <= X <= 0.10669
H/U-235	0.9251	65.100 <= X <= 147.00
Plate Pitch (in)	0.9225	0.12457 <= X <= 0.16535
Enrichment (%)	0.9224	19.77 <= X <= 93.2
Rod-Type Benchmarks (54)		
EALF (MeV)	0.9400	9.65510E-08 <= X <= 3.21670E-07
U-235 Number Density (atom/b-cm)	0.9403	4.87850E-04 <= X <= 1.01020E-03
H/U-235	0.9396	105.50 <= X <= 399.00
Enrichment (%)	0.9404	2.35 <= X <= 4.31

Table 6.12-11 – Benchmark Experiment Data

No	Case	k	σ_{mcnp}	σ_{bench}	σ_{total}	EALF (MeV)	U-235 (atom/b-cm)	Channel Spacing (in)	H/U-235	Plate Pitch (in)	Enrichment (%)
1	hct022_c01	0.98862	0.00059	0.0081	0.0081	9.542E-08	3.3155E-03	0.06457	65.1	0.12457	93.2
2	hct022_c02	0.98860	0.00055	0.0081	0.0081	9.677E-08	3.3155E-03	0.06457	65.1	0.12457	93.2
3	hct022_c03	0.98924	0.00061	0.0081	0.0081	9.861E-08	3.3155E-03	0.06457	65.1	0.12457	93.2
4	hct022_c04	0.98919	0.00062	0.0081	0.0081	9.920E-08	3.3155E-03	0.06457	65.1	0.12457	93.2
5	hct022_c05	0.98706	0.00062	0.0081	0.0081	9.543E-08	3.3155E-03	0.06457	65.1	0.12457	93.2
6	hct022_c06	0.99001	0.00061	0.0081	0.0081	9.857E-08	3.3155E-03	0.06457	65.1	0.12457	93.2
7	hct022_c07	0.98892	0.00063	0.0081	0.0081	9.872E-08	3.3155E-03	0.06457	65.1	0.12457	93.2
8	hct022_c08	0.98824	0.00063	0.0081	0.0081	9.964E-08	3.3155E-03	0.06457	65.1	0.12457	93.2
9	hct022_c09	0.98797	0.00061	0.0081	0.0081	9.634E-08	3.3155E-03	0.06457	65.1	0.12457	93.2
10	hct022_c10	0.98867	0.00061	0.0081	0.0081	9.925E-08	3.3155E-03	0.06457	65.1	0.12457	93.2
11	hct022_c11	0.98967	0.00060	0.0081	0.0081	9.997E-08	3.3155E-03	0.06457	65.1	0.12457	93.2
12	hmt006_c01	0.99240	0.00082	0.0044	0.0045	8.481E-08	1.8490E-03	0.06457	116.5	0.12457	93.17
13	hmt006_c02	0.99333	0.00088	0.0040	0.0041	7.043E-08	1.8490E-03	0.06457	116.5	0.12457	93.17
14	hmt006_c03	0.99705	0.00077	0.0040	0.0041	6.317E-08	1.8490E-03	0.06457	116.5	0.12457	93.17
15	hmt006_c04	0.99113	0.00078	0.0040	0.0041	6.202E-08	1.8490E-03	0.06457	116.5	0.12457	93.17
16	hmt006_c05	0.99230	0.00079	0.0040	0.0041	5.852E-08	1.8490E-03	0.06457	116.5	0.12457	93.17
17	hmt006_c06	0.99010	0.00071	0.0040	0.0041	5.615E-08	1.8490E-03	0.06457	116.5	0.12457	93.17
18	hmt006_c07	0.98783	0.00073	0.0040	0.0041	5.432E-08	1.8490E-03	0.06457	116.5	0.12457	93.17
19	hmt006_c08	0.98246	0.00071	0.0040	0.0041	5.256E-08	1.8490E-03	0.06457	116.5	0.12457	93.17
20	hmt006_c09	0.98657	0.00072	0.0040	0.0041	5.222E-08	1.8490E-03	0.06457	116.5	0.12457	93.17
21	hmt006_c10	0.99885	0.00085	0.0040	0.0041	8.220E-08	1.8490E-03	0.06457	116.5	0.12457	93.17
22	hmt006_c11	0.98965	0.00081	0.0040	0.0041	6.236E-08	1.8490E-03	0.06457	116.5	0.12457	93.17
23	hmt006_c12	0.99425	0.00071	0.0040	0.0041	5.428E-08	1.8490E-03	0.06457	116.5	0.12457	93.17
24	hmt006_c13	1.01283	0.00086	0.0040	0.0041	8.231E-08	1.8490E-03	0.06457	116.5	0.12457	93.17
25	hmt006_c14	0.98495	0.00071	0.0061	0.0061	5.715E-08	1.8490E-03	0.06457	116.5	0.12457	93.17

(continued)

Table 6.12-11 – Benchmark Experiment Data

No	Case	k	σ_{mcnp}	σ_{bench}	σ_{total}	EALF (MeV)	U-235 (atom/b-cm)	Channel Spacing (in)	H/U-235	Plate Pitch (in)	Enrichment (%)
26	hmt006_c15	0.98155	0.00073	0.0040	0.0041	5.638E-08	1.8490E-03	0.06457	116.5	0.12457	93.17
27	hmt006_c16	0.99241	0.00078	0.0040	0.0041	6.330E-08	1.8490E-03	0.06457	116.5	0.12457	93.17
28	hmt006_c17	0.98946	0.00082	0.0040	0.0041	7.384E-08	1.8490E-03	0.06457	116.5	0.12457	93.17
29	hmt006_c18	0.99252	0.00088	0.0040	0.0041	8.009E-08	1.8490E-03	0.06457	116.5	0.12457	93.17
30	hmt006_c19	0.99442	0.00070	0.0040	0.0041	5.222E-08	1.8490E-03	0.06457	113.9	0.12457	93.17
31	hmt006_c20	0.99319	0.00082	0.0040	0.0041	6.461E-08	1.8490E-03	0.06457	113.7	0.12457	93.17
32	hmt006_c21	0.99604	0.00076	0.0040	0.0041	6.923E-08	1.8490E-03	0.06457	113.7	0.12457	93.17
33	hmt006_c22	0.99552	0.00079	0.0040	0.0041	7.408E-08	1.8490E-03	0.06457	113.6	0.12457	93.17
34	hmt006_c23	1.00066	0.00078	0.0040	0.0041	7.637E-08	1.8490E-03	0.06457	113.5	0.12457	93.17
35	hmt022_c01	0.99179	0.00013	0.0035	0.0035	1.585E-07	3.9260E-03	0.078	66.0	0.12800	93.0
36	ict014	0.99647	0.00059	0.0014	0.0015	8.821E-08	2.4170E-03	0.10669	147.0	0.16535	19.77
37	lct001_c01	0.99562	0.00076	0.0030	0.0031	1.007E-07	4.8785E-04	na	399.0	na	2.35
38	lct001_c02	0.99637	0.00079	0.0030	0.0031	9.962E-08	4.8785E-04	na	399.0	na	2.35
39	lct001_c03	0.99385	0.00071	0.0030	0.0031	9.883E-08	4.8785E-04	na	399.0	na	2.35
40	lct001_c04	0.99543	0.00075	0.0030	0.0031	9.956E-08	4.8785E-04	na	399.0	na	2.35
41	lct001_c05	0.99271	0.00075	0.0030	0.0031	9.795E-08	4.8785E-04	na	399.0	na	2.35
42	lct001_c06	0.99376	0.00079	0.0030	0.0031	9.917E-08	4.8785E-04	na	399.0	na	2.35
43	lct001_c07	0.99561	0.00074	0.0031	0.0032	9.655E-08	4.8785E-04	na	399.0	na	2.35
44	lct001_c08	0.99224	0.00072	0.0030	0.0031	9.843E-08	4.8785E-04	na	399.0	na	2.35
45	lct002_c01	0.99550	0.00072	0.0020	0.0021	1.181E-07	1.0102E-03	na	271.0	na	4.31
46	lct002_c02	0.99611	0.00073	0.0020	0.0021	1.175E-07	1.0102E-03	na	271.0	na	4.31
47	lct002_c03	0.99499	0.00071	0.0020	0.0021	1.172E-07	1.0102E-03	na	271.0	na	4.31
48	lct002_c04	0.99486	0.00072	0.0018	0.0019	1.171E-07	1.0102E-03	na	271.0	na	4.31
49	lct002_c05	0.99254	0.00078	0.0019	0.0021	1.145E-07	1.0102E-03	na	271.0	na	4.31
50	lct006_c01	0.99488	0.00077	0.0020	0.0021	2.482E-07	6.0830E-04	na	164.7	na	2.596

(continued)

Table 6.12-11 – Benchmark Experiment Data

No	Case	k	σ_{mcnp}	σ_{bench}	σ_{total}	EALF (MeV)	U-235 (atom/b-cm)	Channel Spacing (in)	H/U-235	Plate Pitch (in)	Enrichment (%)
51	lct006_c02	0.99547	0.00074	0.0020	0.0021	2.550E-07	6.0830E-04	na	164.7	na	2.596
52	lct006_c03	0.99481	0.00083	0.0020	0.0022	2.626E-07	6.0830E-04	na	164.7	na	2.596
53	lct006_c04	0.99708	0.00069	0.0020	0.0021	1.903E-07	6.0830E-04	na	201.1	na	2.596
54	lct006_c05	0.99634	0.00076	0.0020	0.0021	1.958E-07	6.0830E-04	na	201.1	na	2.596
55	lct006_c06	0.99599	0.00066	0.0020	0.0021	2.012E-07	6.0830E-04	na	201.1	na	2.596
56	lct006_c07	0.99464	0.00070	0.0020	0.0021	2.061E-07	6.0830E-04	na	201.1	na	2.596
57	lct006_c08	0.99551	0.00077	0.0020	0.0021	2.109E-07	6.0830E-04	na	201.1	na	2.596
58	lct006_c09	0.99613	0.00075	0.0020	0.0021	1.419E-07	6.0830E-04	na	272.3	na	2.596
59	lct006_c10	0.99722	0.00069	0.0020	0.0021	1.446E-07	6.0830E-04	na	272.3	na	2.596
60	lct006_c11	0.99622	0.00068	0.0020	0.0021	1.489E-07	6.0830E-04	na	272.3	na	2.596
61	lct006_c12	0.99640	0.00068	0.0020	0.0021	1.523E-07	6.0830E-04	na	272.3	na	2.596
62	lct006_c13	0.99655	0.00074	0.0020	0.0021	1.557E-07	6.0830E-04	na	272.3	na	2.596
63	lct006_c14	0.99497	0.00070	0.0020	0.0021	1.196E-07	6.0830E-04	na	329.1	na	2.596
64	lct006_c15	0.99717	0.00068	0.0020	0.0021	1.222E-07	6.0830E-04	na	329.1	na	2.596
65	lct006_c16	0.99617	0.00069	0.0020	0.0021	1.250E-07	6.0830E-04	na	329.1	na	2.596
66	lct006_c17	0.99542	0.00070	0.0020	0.0021	1.289E-07	6.0830E-04	na	329.1	na	2.596
67	lct006_c18	0.99593	0.00071	0.0020	0.0021	1.310E-07	6.0830E-04	na	329.1	na	2.596
68	lct009_c01	0.99386	0.00075	0.0021	0.0022	1.175E-07	1.0102E-03	na	256.2	na	4.31
69	lct009_c02	0.99508	0.00073	0.0021	0.0022	1.170E-07	1.0102E-03	na	256.2	na	4.31
70	lct009_c03	0.99365	0.00077	0.0021	0.0022	1.172E-07	1.0102E-03	na	256.2	na	4.31
71	lct009_c04	0.99535	0.00069	0.0021	0.0022	1.168E-07	1.0102E-03	na	256.2	na	4.31
72	lct009_c05	0.99609	0.00063	0.0021	0.0022	1.187E-07	1.0102E-03	na	256.2	na	4.31
73	lct009_c06	0.99539	0.00074	0.0021	0.0022	1.169E-07	1.0102E-03	na	256.2	na	4.31
74	lct009_c07	0.99676	0.00073	0.0021	0.0022	1.187E-07	1.0102E-03	na	256.2	na	4.31
75	lct009_c08	0.99309	0.00074	0.0021	0.0022	1.172E-07	1.0102E-03	na	256.2	na	4.31

(continued)

Table 6.12-11 – Benchmark Experiment Data (concluded)

No	Case	k	σ_{mcnp}	σ_{bench}	σ_{total}	EALF (MeV)	U-235 (atom/b-cm)	Channel Spacing (in)	H/U-235	Plate Pitch (in)	Enrichment (%)
76	lct009_c24	0.99520	0.00070	0.0021	0.0022	1.168E-07	1.0102E-03	na	256.2	na	4.31
77	lct009_c25	0.99492	0.00067	0.0021	0.0022	1.167E-07	1.0102E-03	na	256.2	na	4.31
78	lct009_c26	0.99480	0.00077	0.0021	0.0022	1.166E-07	1.0102E-03	na	256.2	na	4.31
79	lct009_c27	0.99491	0.00085	0.0021	0.0023	1.164E-07	1.0102E-03	na	256.2	na	4.31
80	lct010_c09	0.99797	0.00077	0.0021	0.0022	1.267E-07	1.0102E-03	na	256.3	na	4.31
81	lct010_c10	0.99775	0.00078	0.0021	0.0022	1.232E-07	1.0102E-03	na	256.3	na	4.31
82	lct010_c11	1.00076	0.00069	0.0021	0.0022	1.197E-07	1.0102E-03	na	256.3	na	4.31
83	lct010_c12	0.99679	0.00078	0.0021	0.0022	1.165E-07	1.0102E-03	na	256.3	na	4.31
84	lct010_c13	0.99366	0.00070	0.0021	0.0022	1.155E-07	1.0102E-03	na	256.3	na	4.31
85	lct010_c14	0.99729	0.00075	0.0028	0.0029	3.217E-07	1.0102E-03	na	105.5	na	4.31
86	lct010_c15	0.99775	0.00079	0.0028	0.0029	3.072E-07	1.0102E-03	na	105.5	na	4.31
87	lct010_c16	0.99823	0.00077	0.0028	0.0029	2.997E-07	1.0102E-03	na	105.5	na	4.31
88	lct010_c17	0.99923	0.00076	0.0028	0.0029	2.938E-07	1.0102E-03	na	105.5	na	4.31
89	lct010_c18	0.99796	0.00082	0.0028	0.0029	2.868E-07	1.0102E-03	na	105.5	na	4.31
90	lct010_c19	0.99726	0.00084	0.0028	0.0029	2.807E-07	1.0102E-03	na	105.5	na	4.31

6.12.9 Sample Input File

A sample input file (NA_MO_P030) is provided for the most reactive case (Case MO13).

```
ATR
999        0        -320:321:-322:323:-324:325                imp:n=0
900        0        310 -311 312 -313 24 -25      fill=3       imp:n=1
901        2 -1.0 (311:-310:313:-312:-24:25) 320 -321 322 -323 324 -325  imp:n=1
c
c       Universe 1: ATR Fuel Element (infinitely long)
c
2          3 -2.7        -6 8 9 -10                  u=1 imp:n=1 $ left Al piece
4          3 -2.7        -5 7 9 -10                  u=1 imp:n=1 $ right Al piece
6          10 5.5147E-02 52 -53 -14 -13              u=1 imp:n=1 $ plate 1
8          3 -2.7        51 -54   -7 -8      #6      u=1 imp:n=1
10         2 -1.00       54 -55   -7 -8              u=1 imp:n=1
c
12         11 5.5136E-02 56 -57 -16 -15              u=1 imp:n=1 $ plate 2
14         3 -2.7        55 -58   -7 -8      #12     u=1 imp:n=1
16         2 -1.00       58 -59   -7 -8              u=1 imp:n=1
c
18         12 5.4749E-02 60 -61 -16 -15              u=1 imp:n=1 $ plate 3
20         3 -2.7        59 -62   -7 -8      #18     u=1 imp:n=1
22         2 -1.00       62 -63   -7 -8              u=1 imp:n=1
c
24         13 5.4757E-02 64 -65 -16 -15              u=1 imp:n=1 $ plate 4
26         3 -2.7        63 -66   -7 -8      #24     u=1 imp:n=1
28         2 -1.00       66 -67   -7 -8              u=1 imp:n=1
c
30         14 4.6966E-02  68 -69 -16 -15             u=1 imp:n=1 $ plate 5 U-Mo
31         7 -6.506      400 -68 -16 -15             u=1 imp:n=1 $ zirc
32         7 -6.506      -401 69 -16 -15             u=1 imp:n=1 $ zirc
33         3 -2.7        67 -70   -7 -8  #30 #31 #32 u=1 imp:n=1
34         2 -1.00       70 -71   -7 -8              u=1 imp:n=1
c
35         15 4.7082E-02 72 -73 -16 -15              u=1 imp:n=1 $ plate 6 U-Mo
36         7 -6.506      402 -72 -16 -15             u=1 imp:n=1 $ zirc
37         7 -6.506      -403  73 -16 -15\           u=1 imp:n=1 $ zirc
38         3 -2.7        71 -74   -7 -8  #35 #36 #37 u=1 imp:n=1
39         2 -1.00       74 -75   -7 -8              u=1 imp:n=1
c
40         16 4.7170E-02 76 -77 -16 -15              u=1 imp:n=1 $ plate 7 U-Mo
41         7 -6.506      404 -76 -16 -15             u=1 imp:n=1 $ zirc
42         7 -6.506      -405  77 -16 -15            u=1 imp:n=1 $ zirc
43         3 -2.7        75 -78   -7 -8  #40 #41 #42 u=1 imp:n=1
44         2 -1.00       78 -79   -7 -8              u=1 imp:n=1
c
45         17 4.7269E-02 80 -81 -16 -15              u=1 imp:n=1 $ plate 8 U-Mo
46         7 -6.506      406 -80 -16 -15             u=1 imp:n=1 $ zirc
47         7 -6.506      -407  81 -16 -15            u=1 imp:n=1 $ zirc
48         3 -2.7        79 -82   -7 -8  #45 #46 #47 u=1 imp:n=1
49         2 -1.00       82 -83   -7 -8              u=1 imp:n=1
c
50         18 4.7343E-02 84 -85 -16 -15              u=1 imp:n=1 $ plate 9 U-Mo
51         7 -6.506      408 -84 -16 -15             u=1 imp:n=1 $ zirc
52         7 -6.506      -409  85 -16 -15            u=1 imp:n=1 $ zirc
53         3 -2.7        83 -86   -7 -8  #50 #51 #52 u=1 imp:n=1
54         2 -1.00       86 -87   -7 -8              u=1 imp:n=1
c
55         19 4.7423E-02 88 -89 -16 -15              u=1 imp:n=1 $ plate 10 U-Mo
56         7 -6.506      410 -88 -16 -15             u=1 imp:n=1 $ zirc
57         7 -6.506      -411  89 -16 -15            u=1 imp:n=1 $ zirc
58         3 -2.7        87 -90   -7 -8  #55 #56 #57 u=1 imp:n=1
59         2 -1.00       90 -91   -7 -8              u=1 imp:n=1
c
60         20 4.7487E-02 92 -93 -16 -15              u=1 imp:n=1 $ plate 11 U-Mo
```

```
61      7 -6.506        412 -92 -16 -15                         u=1 imp:n=1 $ zirc
62      7 -6.506        -413  93 -16 -15                        u=1 imp:n=1 $ zirc
63      3 -2.7           91 -94   -7 -8         #60 #61 #62      u=1 imp:n=1
64      2 -1.00          94 -95   -7 -8                         u=1 imp:n=1
c
65      21 4.7562E-02    96 -97 -16 -15                         u=1 imp:n=1 $ plate 12 U-Mo
66      7 -6.506        414 -96 -16 -15                         u=1 imp:n=1 $ zirc
67      7 -6.506        -415  97 -16 -15                        u=1 imp:n=1 $ zirc
68      3 -2.7           95 -98   -7 -8         #65 #66 #67      u=1 imp:n=1
69      2 -1.00          98 -99   -7 -8                         u=1 imp:n=1
c
70      22 4.7617E-02   100 -101 -16 -15                        u=1 imp:n=1 $ plate 13 U-Mo
71      7 -6.506        416 -100 -16 -15                        u=1 imp:n=1 $ zirc
72      7 -6.506        -417  101 -16 -15                       u=1 imp:n=1 $ zirc
73      3 -2.7           99 -102   -7 -8        #70 #71 #72      u=1 imp:n=1
74      2 -1.00         102 -103   -7 -8                        u=1 imp:n=1
c
75      23 4.7684E-02   104 -105 -16 -15                        u=1 imp:n=1 $ plate 14 U-Mo
76      7 -6.506        418 -104 -16 -15                        u=1 imp:n=1 $ zirc
77      7 -6.506        -419  105 -16 -15                       u=1 imp:n=1 $ zirc
78      3 -2.7          103 -106   -7 -8        #75 #76 #77      u=1 imp:n=1
79      2 -1.00         106 -107   -7 -8                        u=1 imp:n=1
c
80      24 4.7726E-02   108 -109 -16 -15                        u=1 imp:n=1 $ plate 15 U-Mo
81      7 -6.506        420 -108 -16 -15                        u=1 imp:n=1 $ zirc
82      7 -6.506        -421  109 -16 -15                       u=1 imp:n=1 $ zirc
83      3 -2.7          107 -110   -7 -8        #80 #81 #82      u=1 imp:n=1
84      2 -1.00         110 -111   -7 -8                        u=1 imp:n=1
c
96      25 5.4721E-02   112 -113 -16 -15            u=1 imp:n=1 $ plate 16
98      3 -2.7          111 -114   -7 -8       #96  u=1 imp:n=1
100     2 -1.00         114 -115   -7 -8            u=1 imp:n=1
c
102     26 5.4721E-02   116 -117 -16 -15            u=1 imp:n=1 $ plate 17
104     3 -2.7          115 -118   -7 -8       #102 u=1 imp:n=1
106     2 -1.00         118 -119   -7 -8            u=1 imp:n=1
c
108     27 5.5091E-02   120 -121 -18 -17            u=1 imp:n=1 $ plate 18
110     3 -2.7          119 -122   -7 -8       #108 u=1 imp:n=1
112     2 -1.00         122 -123   -7 -8            u=1 imp:n=1
c
114     3 -2.7          124 -125 -14 -13            u=1 imp:n=1 $ plate 19 (dummy)
116     3 -2.7          123 -126   -7 -8       #114 u=1 imp:n=1
120     2 -1.00         126 -10 -8 -7                u=1 imp:n=1 $ above 19
121     2 -1.00           9 -51 -8 -7                u=1 imp:n=1 $ below 1
122     5 -0.737          5 -11 9 -10               u=1 imp:n=1 $ right neoprene
123     5 -0.737        -12 6 9 -10                 u=1 imp:n=1 $ left neoprene
125     2 -1.0          12:11:-9:10                 u=1 imp:n=1
c
c       Universe 20: ATR with pipe (center)
c
200     0      -27 -26 22 -23:26 -20 22 -28:27 -21 22 -28   trcl=1
               fill=1   u=20 imp:n=1
201     2 -0.3      #200 -200                   u=20 imp:n=1 $ between ATR/pipe
202     4 -7.94      200 -201                   u=20 imp:n=1 $ pipe
203     6 -0.096     201 -203 250 -251 252 -253 u=20 imp:n=1 $ insulation
204     0            203 250 -251 252 -253      u=20 imp:n=1 $ insulation to tube
205     4 -7.94      -250:251:-252:253          u=20 imp:n=1 $ tube to inf
c
c       Universe 21: ATR with pipe (down)
c
210     0      -27 -26 22 -23:26 -20 22 -28:27 -21 22 -28   trcl=2
               fill=1   u=21 imp:n=1
211     2 -0.3      #210 -200                   u=21 imp:n=1 $ between ATR/pipe
212     4 -7.94      200 -201                   u=21 imp:n=1 $ pipe
213     6 -0.096     201 -203 250 -251 252 -253 u=21 imp:n=1 $ insulation
214     0            203 250 -251 252 -253      u=21 imp:n=1 $ insulation to tube
```

```
215      4 -7.94      -250:251:-252:253        u=21 imp:n=1 $ tube to inf
c
c        Universe 22: ATR with pipe (up)
c
220      0  -27 -26 22 -23:26 -20 22 -28:27 -21 22 -28  trcl=3
              fill=1  u=22 imp:n=1
221      2 -0.3      #220 -200                 u=22 imp:n=1 $ between ATR/pipe
222      4 -7.94      200 -201                 u=22 imp:n=1 $ pipe
223      6 -0.096    201 -203 250 -251 252 -253 u=22 imp:n=1 $ insulation
224      0           203 250 -251 252 -253      u=22 imp:n=1 $ insulation to tube
225      4 -7.94      -250:251:-252:253         u=22 imp:n=1 $ tube to inf
c
c        Universe 23: ATR with pipe (right)
c
230      0  -27 -26 22 -23:26 -20 22 -28:27 -21 22 -28  trcl=4
              fill=1  u=23 imp:n=1
231      2 -0.3      #230 -200                 u=23 imp:n=1 $ between ATR/pipe
232      4 -7.94      200 -201                 u=23 imp:n=1 $ pipe
233      6 -0.096    201 -203 250 -251 252 -253 u=23 imp:n=1 $ insulation
234      0           203 250 -251 252 -253      u=23 imp:n=1 $ insulation to tube
235      4 -7.94      -250:251:-252:253         u=23 imp:n=1 $ tube to inf
c
c        Universe 24: ATR with pipe (left)
c
240      0  -27 -26 22 -23:26 -20 22 -28:27 -21 22 -28  trcl=5
              fill=1  u=24 imp:n=1
241      2 -0.3      #240 -200                 u=24 imp:n=1 $ between ATR/pipe
242      4 -7.94      200 -201                 u=24 imp:n=1 $ pipe
243      6 -0.096    201 -203 250 -251 252 -253 u=24 imp:n=1 $ insulation
244      0           203 250 -251 252 -253      u=24 imp:n=1 $ insulation to tube
245      4 -7.94      -250:251:-252:253         u=24 imp:n=1 $ tube to inf
c
c        Universe 25: ATR with pipe (up right)
c
250      0  -27 -26 22 -23:26 -20 22 -28:27 -21 22 -28  trcl=6
              fill=1  u=25 imp:n=1
251      2 -0.3      #250 -200                 u=25 imp:n=1 $ between ATR/pipe
252      4 -7.94      200 -201                 u=25 imp:n=1 $ pipe
253      6 -0.096    201 -203 250 -251 252 -253 u=25 imp:n=1 $ insulation
254      0           203 250 -251 252 -253      u=25 imp:n=1 $ insulation to tube
255      4 -7.94      -250:251:-252:253         u=25 imp:n=1 $ tube to inf
c
c        Universe 26: ATR with pipe (up left)
c
260      0  -27 -26 22 -23:26 -20 22 -28:27 -21 22 -28  trcl=7
              fill=1  u=26 imp:n=1
261      2 -0.3      #260 -200                 u=26 imp:n=1 $ between ATR/pipe
262      4 -7.94      200 -201                 u=26 imp:n=1 $ pipe
263      6 -0.096    201 -203 250 -251 252 -253 u=26 imp:n=1 $ insulation
264      0           203 250 -251 252 -253      u=26 imp:n=1 $ insulation to tube
265      4 -7.94      -250:251:-252:253         u=26 imp:n=1 $ tube to inf
c
c        Universe 27: ATR with pipe (down right)
c
270      0  -27 -26 22 -23:26 -20 22 -28:27 -21 22 -28  trcl=8
              fill=1  u=27 imp:n=1
271      2 -0.3      #270 -200                 u=27 imp:n=1 $ between ATR/pipe
272      4 -7.94      200 -201                 u=27 imp:n=1 $ pipe
273      6 -0.096    201 -203 250 -251 252 -253 u=27 imp:n=1 $ insulation
274      0           203 250 -251 252 -253      u=27 imp:n=1 $ insulation to tube
275      4 -7.94      -250:251:-252:253         u=27 imp:n=1 $ tube to inf
c
c        Universe 28: ATR with pipe (down left)
c
280      0  -27 -26 22 -23:26 -20 22 -28:27 -21 22 -28  trcl=9
              fill=1  u=28 imp:n=1
281      2 -0.3      #280 -200                 u=28 imp:n=1 $ between ATR/pipe
```

```
282    4 -7.94      200 -201                          u=28 imp:n=1 $ pipe
283    6 -0.096     201 -203 250 -251 252 -253        u=28 imp:n=1 $ insulation
284    0            203 250 -251 252 -253             u=28 imp:n=1 $ insulation to tube
285    4 -7.94      -250:251:-252:253                 u=28 imp:n=1 $ tube to inf
c
c      Universe 3: Array of Packages
c
300    0       -300 301 -302 303 imp:n=1 u=3 lat=1 fill=-4:4 -4:4 0:0
               25 25 25 25 22 26 26 26 26
               25 25 25 25 22 26 26 26 26
               25 25 25 25 22 26 26 26 26
               25 25 25 25 22 26 26 26 26
               23 23 23 23 20 24 24 24 24
               27 27 27 27 21 28 28 28 28
               27 27 27 27 21 28 28 28 28
               27 27 27 27 21 28 28 28 28
               27 27 27 27 21 28 28 28 28

5      p  2.4142136 -1 0 -0.2665911 $ right Al outer
6      p -2.4142136 -1 0 -0.2665911 $ left Al outer
7      p  2.4142136 -1 0 -1.474587  $ right Al inner
8      p -2.4142136 -1 0 -1.474587  $ left Al inner
9      cz 7.52856                   $ Al boundary
10     cz 14.015466                 $ Al boundary
11     p  2.4142136 -1 0  0.563076  $ right neoprene
12     p -2.4142136 -1 0  0.563076  $ left neoprene
c
13     p  2.4142136 -1 0 -2.4370013 $ plate 1 & 19 meat
14     p -2.4142136 -1 0 -2.4370013 $ plate 1 & 19 meat
15     p  2.4142136 -1 0 -1.7732672 $ plate 2-17 meat
16     p -2.4142136 -1 0 -1.7732672 $ plate 2-17 meat
17     p  2.4142136 -1 0 -1.9060140 $ plate 18 meat
18     p -2.4142136 -1 0 -1.9060140 $ plate 18 meat
c
20     p  2.4142136 -1 0   0.6      $ right u0 boundary
21     p -2.4142136 -1 0   0.6      $ left u0 boundary
22     cz 7.51                      $ u0 boundary
23     cz 14.02                     $ u0 boundary
24     pz -60.96                    $ bottom of fuel
25     pz  60.96                    $ top of fuel (48")
26     p  2.4142136 -1 0  0.0       $ neoprene notch
27     p -2.4142136 -1 0  0.0       $ neoprene notch
28     cz 13.9                      $ neoprene notch
c
51     cz 7.67207   $ fuel plate 1 (0.089)
52     cz 7.7343
53     cz 7.7851
54     cz 7.84733
c
55     cz 8.07339   $ fuel plate 2
56     cz 8.09752
57     cz 8.14832
58     cz 8.17245
c
59     cz 8.39851   $ fuel plate 3
60     cz 8.42264
61     cz 8.47344
62     cz 8.49757
c
63     cz 8.72363   $ fuel plate 4
64     cz 8.74776
65     cz 8.79856
66     cz 8.82269
c
67     cz 9.04875   $ fuel plate 5
400    cz 9.07923
68     cz 9.08177
```

```
69        cz 9.11479
401       cz 9.11733
70        cz 9.14781
c
71        cz 9.37387   $ fuel plate 6
402       cz 9.40435
72        cz 9.40689
73        cz 9.43991
403       cz 9.44245
74        cz 9.47293
c
75        cz 9.69899   $ fuel plate 7
404       cz 9.72947
76        cz 9.73201
77        cz 9.76503
405       cz 9.76757
78        cz 9.79805
c
79        cz 10.02411  $ fuel plate 8
406       cz 10.05459
80        cz 10.05713
81        cz 10.09015
407       cz 10.09269
82        cz 10.12317
c
83        cz 10.34923  $ fuel plate 9
408       cz 10.37971
84        cz 10.38225
85        cz 10.41527
409       cz 10.41781
86        cz 10.44829
c
87        cz 10.67435  $ fuel plate 10
410       cz 10.70483
88        cz 10.70737
89        cz 10.74039
411       cz 10.74293
90       {cz 10.77341
c
91        cz 10.99947  $ fuel plate 11
412       cz 11.02995
92        cz 11.03249
93        cz 11.06551
413       cz 11.06805
94        cz 11.09853
c
95        cz 11.32459  $ fuel plate 12
414       cz 11.35507
96        cz 11.35761
97        cz 11.39063
415       cz 11.39317
98        cz 11.42365
c
99        cz 11.64971  $ fuel plate 13
416       cz 11.68019
100       cz 11.68273
101       cz 11.71575
417       cz 11.71829
102       cz 11.74877
c
103       cz 11.97483  $ fuel plate 14
418       cz 12.00531
104       cz 12.00785
105       cz 12.04087
419       cz 12.04341
106       cz 12.07389
c
```

```
107        cz 12.29995  $ fuel plate 15
420        cz 12.33043
108        cz 12.33297
109        cz 12.36599
421        cz 12.36853
110        cz 12.39901
c
111        cz 12.62507  $ fuel plate 16
112        cz 12.6492
113        cz 12.7
114        cz 12.72413
c
115        cz 12.95019  $ fuel plate 17
116        cz 12.97432
117        cz 13.02512
118        cz 13.04925
c
119        cz 13.27531  $ fuel plate 18
120        cz 13.29944
121        cz 13.35024
122        cz 13.37437
c
123        cz 13.60043  $ fuel plate 19 (0.089)
124        cz 13.68806
125        cz 13.73886
126        cz 13.82649
c
200        cz 7.3838 $ IR pipe
201        cz 7.6581 $ OR pipe
202        cz 38.1   $ 12" water
203        cz 10.1981 $ 1" insulation
c
250        px  -9.6032 $ square tube
251        px   9.6032
252        py  -9.6032
253        py   9.6032
c
300        px  10.033 $ lattice surfaces/sq. tube
301        px -10.033
302        py  10.033
303        py -10.033
310        px -90.297 $ 9x9 bounds
311        px  90.297
312        py -90.297
313        py  90.297
320        px -120.777 $ outer bounds
321        px  120.777
322        py -120.777
323        py  120.777
324        pz -91.44
325        pz  91.44

m2         1001.62c  2           $ water
           8016.62c  1
mt2        lwtr.60t
m3         13027.62c 1           $ Al
m4         6000.66c    -0.08     $ SS-304
           14000.60c   -1.0
           15031.66c   -0.045
           24000.50c   -19.0
           25055.62c   -2.0
           26000.55c   -68.375
           28000.50c   -9.5
m5         1001.62c  -0.056920   $ neoprene
           6000.66c  -0.542646
c          17000.66c -0.400434
m6         13027.62c  -26.5      $ insulation material
```

```
              14000.60c  -23.4
              8016.62c   -50.2
m7            40000.66c 1            $ zirc
m10           92234.69c 1.5558E-05 $ fuel plate 1
              92235.69c 2.4269E-03
              92236.69c 8.9982E-06
              92238.69c 1.2874E-04
              13027.62c 5.2567E-02
c             total     5.5147E-02
m11           92234.69c 1.5676E-05 $ fuel plate 2
              92235.69c 2.4455E-03
              92236.69c 9.0668E-06
              92238.69c 1.2972E-04
              13027.62c 5.2536E-02
c             total     5.5136E-02
m12           92234.69c 1.9838E-05 $ fuel plate 3
              92235.69c 3.0947E-03
              92236.69c 1.1474E-05
              92238.69c 1.6416E-04
              13027.62c 5.1458E-02
c             total     5.4749E-02
m13           92234.69c 1.9753E-05 $ fuel plate 4
              92235.69c 3.0815E-03
              92236.69c 1.1425E-05
              92238.69c 1.6346E-04
              13027.62c 5.1480E-02
c             total     5.4757E-02
m14           92234.69c 4.8582E-05 $ fuel plate 5
             ·92235.69c 7.4422E-03
              92236.69c 8.5223E-05
              92238.69c 2.9261E-02
              42000.66c 1.0129E-02
c             total     4.6966E-02
m15           92234.69c 4.8702E-05 $ fuel plate 6
              92235.69c 7.4607E-03
              92236.69c 8.5434E-05
              92238.69c 2.9333E-02
              42000.66c 1.0154E-02
c             total     4.7082E-02·
m16           92234.69c 4.8793E-05 $ fuel plate 7
              92235.69c 7.4745E-03
              92236.69c 8.5592E-05
              92238.69c 2.9388E-02
              42000.66c 1.0173E-02
c             total     4.7170E-02
m17           92234.69c 4.8895E-05 $ fuel plate 8
              92235.69c 7.4903E-03
              92236.69c 8.5773E-05
              92238.69c 2.9450E-02
              42000.66c 1.0195E-02
c             total     4.7269E-02
m18           92234.69c 4.8972E-05 $ fuel plate 9
              92235.69c 7.5020E-03
              92236.69c 8.5907E-05
              92238.69c 2.9496E-02
              42000.66c 1.0211E-02
c             total     4.7343E-02
m19           92234.69c 4.9055E-05 $ fuel plate 10
              92235.69c 7.5147E-03
              92236.69c 8.6052E-05
              92238.69c 2.9546E-02
              42000.66c 1.0228E-02
c             total     4.7423E-02
m20           92234.69c 4.9120E-05 $ fuel plate 11
              92235.69c 7.5248E-03
              92236.69c 8.6167E-05
              92238.69c 2.9585E-02
```

```
           42000.66c 1.0242E-02
c          total     4.7487E-02
m21        92234.69c 4.9199E-05 $ fuel plate 12
           92235.69c 7.5367E-03
           92236.69c 8.6304E-05
           92238.69c 2.9632E-02
           42000.66c 1.0258E-02
c          total     4.7562E-02
m22        92234.69c 4.9255E-05 $ fuel plate 13
           92235.69c 7.5454E-03
           92236.69c 8.6404E-05
           92238.69c 2.9666E-02
           42000.66c 1.0270E-02
c          total     4.7617E-02
m23        92234.69c 4.9324E-05 $ fuel plate 14
           92235.69c 7.5559E-03
           92236.69c 8.6525E-05
           92238.69c 2.9708E-02
           42000.66c 1.0284E-02
c          total     4.7684E-02
m24        92234.69c 4.9368E-05 $ fuel plate 15
           92235.69c 7.5627E-03
           92236.69c 8.6602E-05
           92238.69c 2.9734E-02
           42000.66c 1.0293E-02
c          total     4.7726E-02
m25        92234.69c 2.0136E-05 $ fuel plate 16
           92235.69c 3.1412E-03
           92236.69c 1.1646E-05
           92238.69c 1.6663E-04
           13027.62c 5.1381E-02
c          total     5.4721E-02
m26        92234.69c 2.0136E-05 $ fuel plate 17
           92235.69c 3.1412E-03
           92236.69c 1.1646E-05
           92238.69c 1.6662E-04
           13027.62c 5.1381E-02
c          total     5.4721E-02
m27        92234.69c 1.6158E-05 $ fuel plate 18
           92235.69c 2.5207E-03
           92236.69c 9.3456E-06
           92238.69c 1.3371E-04
           13027.62c 5.2411E-02
c          total     5.5091E-02
c
*tr1     0 -10.8 0                           $ base to center
*tr2     0  7.9 0      180 90 90 90 180 90   $ down
*tr3     0 -7.9 0                            $ up
*tr4   -7.9 0 0      90 180 90 0 90 90       $ right
*tr5    7.9 0 0      90 0 90 180 90 90       $ left
*tr6   -5.6  -5.6 0 45 135 90 45 45 90       $ up/right
*tr7    5.6  -5.6 0 45 45 90 135 45 90       $ up/left
*tr8   -5.6   5.6 0 135 135 90 45 135 90     $ down/right
*tr9    5.6   5.6 0 135 45 90 135 135 90     $ down/left
c
mode   n
kcode  2500 1.0 50 250
sdef   x=d1 y=d2 z=d3
si1    -90 90
sp1    0 1
si2    -90 90
sp2    0 1
si3    -60 60
sp3    0 1
```

7.1.2 Loading of Contents - ATR Fuel or ATR U-Mo Demonstration Element Fuel Assembly

1. Remove the closure by depressing the spring-loaded pins and rotating the closure 45° to align the closure locking tabs with the mating cut-outs in the body. Remove the closure from the body.

2. Remove the fuel handling enclosure if present in the payload cavity.

3. Prior to loading, visually inspect the ATR fuel handling enclosure for damage, corrosion, and missing hardware to ensure compliance with Appendix 1.3.2, *Packaging General Arrangement Drawings*.

4. Open the ATR fuel handling enclosure lid and place a fuel element into the holder with the narrow end of the fuel element facing the bottom side of the fuel handling enclosure. As a property protection precaution, the fuel element may optionally be inserted into a polyethylene bag prior to placement in the fuel handling enclosure. Verify the total mass of polyethylene per ATR FFSC is ≤ 100 g.

    a. To open the fuel handling enclosure, release the lid by pulling on the spring plunger located at each end and rotate the lid about the hinged side.

    b. To close the fuel handling enclosure, rotate the lid to the closed position, pull the spring plunger located at each end to allow the lid to fully close, align then release the spring plungers with the receiving holes, gently lift the lid to confirm no movement and that the spring plungers are in the locked position.

5. Insert the fuel handling enclosure into the package.

6. Depress the package closure spring-loaded pins, insert closure onto package body by aligning the closure locking tabs with the mating cut-outs in the body, and rotate the closure to the locked position. Release the spring-loaded pins so that they engage with the mating holes in the package body. Observe the pins to ensure they are in the locked position as illustrated in Figure 7.1-1. The closure is fully locked when both locking pins are compressing the sleeve between the locking pin handle and the closure body.